

EXPERIMENTAL AND NUMERICAL INVESTIGATION OF
FORMATION DAMAGE CAUSED BY WATER-BASED DRILLING
FLUIDS

A THESIS SUBMITTED TO
THE GRADUATE SCHOOL OF NATURAL AND APPLIED SCIENCES
OF
MIDDLE EAST TECHNICAL UNIVERSITY

BY

ABDULLAH GÜRKAN İŞCAN

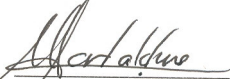
IN PARTIAL FULFILLMENT OF THE REQUIREMENTS
FOR
THE DEGREE OF DOCTOR OF PHILOSOPHY
IN
PETROLEUM AND NATURAL GAS ENGINEERING

SEPTEMBER 2006

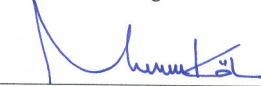
Approval of the Graduate School of Natural and Applied Sciences

Prof. Dr. Canan ÖZGEN
Director

I certify that this thesis satisfies all the requirements as a thesis for the degree of Doctor of Philosophy.


Prof. Dr. Mahmut PARLAKTUNA
Head of Department

This is to certify that we have read this thesis and that in our opinion it is fully adequate, in scope and quality, as a thesis for the degree of Doctor of Philosophy.


Prof. Dr. Mustafa Verşan KÖK
Supervisor

Examining Committee Members

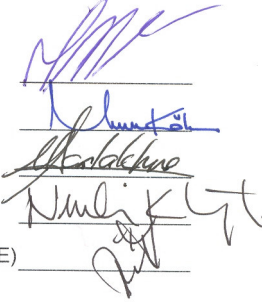
Prof. Dr. Tanju MEHMETOĞLU (METU, PETE)

Prof. Dr. Mustafa Verşan KÖK (METU, PETE)

Prof. Dr. Mahmut PARLAKTUNA (METU, PETE)

Prof. Dr. Nurkan KARAHANOĞLU (METU, GEOE)

Prof. Dr. Bülent COŞKUN (Ankara University, GEOE)



I hereby declare that all information in this document has been obtained and presented in accordance with academic rules and ethical conduct. I also declare that, as required by these rules and conduct, I have fully cited and referenced all material and results that are not original to this work.

Name, Last name : A. GÜRKAN İŞCAN

Signature :

ABSTRACT

EXPERIMENTAL AND NUMERICAL INVESTIGATION OF FORMATION DAMAGE CAUSED BY DRILLING FLUIDS

İşcan, A. Gürkan

Ph.D., Department of Petroleum and Natural Gas Engineering
Supervisor : Prof. Dr. Mustafa Verşan KÖK

September 2006, 237 pages

In this thesis, permeability impairment caused by drilling fluids and subsequent cleaning and permeability enhancement by back-flow were investigated by means of experimental and simulation studies. Permeability damage caused by three different drilling fluids was measured experimentally by core tests as a function of the filtration pressure and analyzed using a simulator describing the fines migration and retention in porous media. The pore throat plugging criteria for the three drilling fluids were determined. The particle concentration and the fraction of depositing particles were obtained simultaneously as a function of time and distance along the core length by numerical solution. Simulations were run both with experimental data in forward and backward directions along the core samples. Permeability damage ratio

was correlated with respect to drilling filtration pressure specially for each type of the drilling fluids and type curves were constructed. Simulation results accurately match the experimental data, indicating that this simulator can be used for the estimation of permeability reduction, and the permeability and porosity variation along the core samples at various filtration pressures. X-Ray digital image subtraction was applied to different sections of the core plugs before and after the circulation to visualize the fines migration into porous media. The maximum damage ratio was obtained with the CMC added drilling fluid with 81 %. In the absence of CMC and Polymer-XT, the damage ratio was found as 72.8%. It was also determined that a polymer-added drilling fluid characterized with 63.8% permeability damage ratio is the optimum drilling fluid, causing less formation damage than the water-based bentonite mud.

Keywords: Formation Damage, Damage Ratio, Fines Migration, Porosity, Permeability, Pore Throat, X-Ray

ÖZ

SU BAZLI SONDAJ SIVILARININ NEDEN OLDUĞU FORMASYON HASARININ DENEYSEL VE SAYISAL OLARAK İNCELENMESİ

İşcan, A. Gürkan

Doktora, Petrol ve Doğal Gaz Mühendisliği Bölümü

Tez Yöneticisi : Prof. Dr. Mustafa Verşan KÖK

Eylül 2006, 237 sayfa

Bu tezde, sondaj sıvılarının neden olduğu geçirgenlik azalması ve daha sonra ters yönlü akış vasıtasıyla temizleme ve geçirgenlik iyileştirilmesi deneysel ve sayısal yönden incelenmiştir. Üç farklı sondaj akışkanının neden olduğu geçirgenlik hasarı karot testleri ile deneysel olarak filtrasyon basıncının fonksiyonu şeklinde ölçülmüş ve parçacık göçünü ve gözenekli ortamdaki tutmayı açıklayan bir simulator ile analiz edilmiştir. Her üç sondaj akışkanı için gözenek boğazı tıkanma kriterleri tesbit edilmiştir. Parçacık konsantrasyonu ve biriken parçacıkların kesri eş zamanlı olarak zamanın ve karot boyunca mesafenin fonksiyonu olarak sayısal çözüm ile elde edilmiştir. Deneysel veri ile simülasyonlar karot boyunca hem ileri hem de geri yönlerde yapılmıştır. Geçirgenlik hasar oranı özel olarak her üç sondaj akışkanı türü için sondaj filtrasyon basıncı ile ilişkilendirilmiş ve tip eğrileri oluşturulmuştur. Simülasyon sonuçları

deneysel veriler ile doğru bir şekilde uygunluk sağlayarak, bu simülatörün geçirgenlik azalması, farklı filtrasyon basınçlarında karot boyunca geçirgenlik ve gözeneklilik değişimleri tahminlerinde kullanılabileceğini göstermektedir. X-Işınli dijital resim çıkartma yöntemi karot boyunca farklı kesitlere sondaj çamuru sirkülasyonundan önce ve sonra olmak üzere, parçacıkların gözenekli ortama göçünü gözlemek amacıyla uygulanmıştır. En büyük hasar oranı CMC katkıli sondaj akışkanı ile % 81 olarak elde edilmiştir. CMC ve Polymer-XT katkılarının olmadığı sondaj akışkanında % 72.8 oranında hasar oranı bulunmuştur. Polimer katkıli % 63.8 hasar oranı karakterli sondaj akışkanı formasyona daha az hasar veren optimum sondaj akışkanı olarak tesbit edilmiştir.

Anahtar Kelimeler: Formasyon Hasarı, Hasar Oranı, Parçacık Göçü, Geçirgenlik, Gözeneklilik, Gözenek Boğazı, X-Işını

To My Parents

ACKNOWLEDGEMENTS

I would like to express my deepest regards and thanks to my supervisor Prof. Dr. Mustafa Verşan KÖK for his close interest, insight and encouragements for the entire period of the study.

I would like to acknowledge Prof. Dr. Ali Suat BAĞCI for his support during the experimental parts of the thesis that were completed in Turkey.

I would like to specially acknowledge Prof. Dr. Faruk CİVAN for mentoring me both experimentally and numerically and giving me the opportunity to do research at the University of Oklahoma.

I would like to express my greatest acknowledgements to Middle East Technical University for giving me the opportunity to perform my doctoral studies and providing me the required conditions.

I would like to greatly acknowledge The Scientific and Technological Research Council of Turkey (TÜBİTAK) for the financial support during my research in the USA.

Finally, I would like to express my deepest regards, love, and thanks to my parents Nergis and Selçuk İŞCAN for their ultimate support during my studies.

TABLE OF CONTENTS

PLAGIARISM	III
ABSTRACT	IV
ÖZ	VI
ACKNOWLEDGEMENTS	IX
TABLE OF CONTENTS	XI
CHAPTER	
1. INTRODUCTION.....	1
2. MECHANISMS OF FORMATION DAMAGE	5
2.1 Mechanical Formation Damage	5
2.1.1 Fines Migration.....	6
2.1.2 External Solids Entrainment	7
2.1.3 Phase Trapping and Blocking	8
2.1.4 Glazing/Mashing.....	9
2.1.5 Geomechanics	10
2.1.6 Perforation Damage	10
2.1.7 Proppant Crushing and Embedment	10
2.2 Chemical Damage Mechanisms.....	11
2.2.1 Adverse Rock Fluid Interactions.....	11
2.2.1.1 Clay Swelling.....	11

2.2.1.2 Clay Deflocculation.....	12
2.2.1.3 Chemical Adsorption	12
2.2.1.4 Formation Dissolution.....	13
2.2.15 Paraffins and Waxes	13
2.2.2 Adverse Fluid-Fluid Interactions	14
2.2.2.1 Emulsions.....	14
2.2.3 Wettability Alterations.....	14
2.2.4 Scale Formation	15
2.3 Biological Damage	16
2.4 Thermal Damage	17
2.5 Evaluating Formation Damage.....	18
3. LITERATURE REVIEW.....	20
4. EXPERIMENTAL WORK AND SET-UP.....	45
4.1 Introduction	45
4.1.1 Saturation of The Core Sample with Brine and Measurement of Initial Porosity and Permeability Through Forward Flooding	46
4.1.1.1 Saturation of Core Sample with Brine and Measurement of Porosity and Permeability.....	47
4.2 Drilling Fluid Preparation and Dynamic Filtration	47
4.2.1 Drilling Fluid Preparation	48
4.2.2 Dynamic Circulation	52

4.3	Back Flow Through The Core Sample To Dertermine Return Permeability and Porosity.....	54
4.4	Sample Data for Each Stahe of Formation Damage Experiments.....	55
4.5	Pore Throat Plugging Procedure	57
4.6	X-Ray Procedure.....	58
4.6.1	Preparation for X-Ray Experiments.....	58
5.	MATHEMATICAL MODELING AND SIMULATION.....	59
5.1	Operation of The Fines Migration Simulator.....	59
5.2	The Governing Equations in Fines Migration Simulation.....	61
5.3	Average Particle Deposition and Overall Pressure Difference In A Core Plug.....	73
5.4	Numerical Solution	75
6.	STATEMENT OF PROBLEM.....	78
7.	RESULTS AND DISCUSSION.....	79
7.1	The Rheological Properties of The Drilling Fluids	80
7.2	The Effects of CMC	81
7.3	Polymer Based Drilling Fluids and Determination of Polymer Concentration.....	86
7.4	Pore Throat Plugging By Particles: First Stage Of Formation Damage	94
7.4.1	Analysis of the In-House Data.....	97
7.4.2	Analysis of The Data in Literature : Haynes and Gray....	108
7.4.3	Analysis of The Data in Literature : Gruesbeck and Collins.....	113

7.4.4 Practical Application of The Correlations in The Field	118
7.5 Dynamic Fluid Circulation and Formation DamageAnalysis	120
7.5.1 Analysis of Mud Invasion And Clean Up By Flow Reversal Using A Simulator and Experimental Work.....	123
7.5.1.1 Effect of Fines Invasion in Porous Media108	123
7.5.1.2 Variation of Permeability along The Core Sample	177
7.5.1.3 Investigation of Porosity and Permeability Impairment in Sandstones by X-Ray Analysis.....	193
7.5.1.4 Preparation for X-Ray Experiments.....	195
8. CONCLUSION	203
REFERENCES.....	206
APPENDICES	
A. Procedure For Permeability Measurement	213
B. Procedure For Dynamic Circulation Experiments	216
C. Procedure For Backflow Experiments	219
D.1. Procedure For Pore Throat Plugging Experiments	220
D.2. Determination of Particle Size	221
E. Procedure for X-Ray Experiments	222
F. Geological Data of Formation and The Core Samples.....	223

G.	Photographs Depicting Construction Stages of Dynamic Circulation Set-up.....	225
H.	Relative Permeability Profile For a Water Wet Core	228
I.	Numerical Stability	229
j.	Viscosity Coefficients of Exponential Pore Throat Model	232
	CURRICULUM VITAE.....	233

LIST OF FIGURES

Figure 1 The Core Holder	52
Figure 2 Schematic of Mud Circulation System	53
Figure 3 Experimental Set-up	54
Figure 4 The Plugging and non-plugging pathways along the core sample.....	70
Figure 5 Non-Plugging and plugging paths realization in a core	71
Figure 6 Fines migration and invasion into formation in vertical wells.....	71
Figure 7 Fines migration and invasion into formation in horizontal wells.....	72
Figure 8 Shear stress vs shear rate in CMC added water based drilling fluid.....	83
Figure 9 Filtration Loss vs Time in CMC added water based drilling fluids.....	84
Figure 10 Effect of CMC concentrations on filtration loss.....	85
Figure 11 Polymer XT- mixed drilling fluid shear stress shear rate	90
Figure 12 Filtration Loss vs Time in polymer added water based drilling fluids.....	91
Figure 13 Shear Stress vs Shear Rate Graphs of Drilling Fluids for Formation Damage Analysis	92
Figure 14 The filtration loss properties of Drilling Fluids for Formation Damage Analysis with respect to time	93
Figure 15 Schematic view of the particle bridging across a perforation with and without sand packing	96

Figure 16 Experimental and Calculated Results from Power Law Model (Eq.47) as a Function of Particle Reynolds Number	100
Figure 17 Coefficients of A and C for Eq.47 Power Law Model approach.....	102
Figure 18 Coefficient of B for Eq.47 Power Law Model approach	103
Figure 19 Experimental and Calculated Results from Power Law Model (Eq.47) as a Function of Particle Reynolds Number.....	104
Figure 20 Linearization of Eq.47 and Regression Coefficients for Power Law Model.....	106
Figure 21. Linearization of Eq.48 and Regression Coefficients for Exponential Law Model	107
Figure 22 Experimental and Calculated Values of Haynes and Gray Data by Power Law Model Eq.47	109
Figure 23 Experimental and Calculated Values of Haynes and Gray Data by Exponential Law Model Eq.48.....	110
Figure 24 Linearization of Eq.47 and Regression Coefficients for Power Law Model For Haynes and Gray Data.....	111
Figure 25 Linearization of Eq.48 and Regression Coefficients for Exponential Model For Haynes and Gray Data	112
Figure 26 Experimental and Calculated Values of Gruesbeck and Collins Data by Power Law Model Eq.47	114
Figure 27 Experimental and Calculated Values of Gruesbeck and Collins Data by Exponential Law Model Eq.48.....	115
Figure 28 Linearization of Eq.47 and Regression Coefficients for Power Law Model for Gruesbeck and Collins Data	116
Figure 29 Linearization of Eq.48 and Regression Coefficients for Exponential Model for Gruesbeck and Collins Data	117
Figure 30 Concentrations of particles in plugging pathways.....	125

Figure 31 Particle Concentration of non-plugging pathways.....	127
Figure 32 Fraction of plugging pathways of bulk volume occupied by the deposits.....	128
Figure 33 Fraction of non-plugging pathways of bulk volume occupied by the deposits	129
Figure 34 Variation of non- plugging porosity with respect to time	130
Figure 35 Variation of non-plugging permeability with respect to time	131
Figure 36 The fraction of plugging porosity to overall porosity (f_p) has with respect to the core length at five different times such as 4, 8, 12, 18, 24 minutes.....	132
Figure 37 The fraction of plugging porosity to overall porosity (f_p) versus core length after 22 minutes	135
Figure 38 Two different types of fluid invasion process applications available in literature	137
Figure 39 Initial and Return Permeability of Sample 1 with pressure cell (Drilling Fluid Type-1, Bentonite+Barite+Water)	140
Figure 40 . Initial and Return Permeability of Sample 2 with pressure cell (Drilling Fluid Type-1, Bentonite+Barite+Water)	141
Figure 41. Initial and Return Permeability of Sample 3 with pressure cell (Drilling Fluid Type-1, Bentonite+Barite+Water)	142
Figure 42. Initial and Return Permeability of Sample 4 with pressure cell (Drilling Fluid Type-2, Bentonite+Barite+CMC+Water)	143
Figure 43. Initial and Return Permeability of Sample 5 with pressure cell (Drilling Fluid Type-2, Bentonite+Barite+CMC+Water)...	144
Figure 44. Initial and Return Permeability of Sample 6 with pressure cell (Drilling Fluid Type-2, Bentonite+Barite+CMC+Water)	145

Figure 45. Initial and Return Permeability of Sample 7 with pressure cell (Drilling Fluid Type-3, Bentonite+Barite+ Polymer-XT+Water)	146
Figure 46 Initial and Return Permeability of Sample 8 with pressure cell (Drilling Fluid Type-3, Bentonite+Barite+ Polymer-XT+Water)	147
Figure 47 Initial and Return Permeability of Sample 9 with pressure cell (Drilling Fluid Type-3, Bentonite+Barite+Polymer-XT+Water)	148
Figure 48 Initial and Return Permeability of Sample 10 with pump (Mud Type-1, Bentonite+Barite+Water)	151
Figure 49 Initial and Return Permeability of Sample 11 with pump (Fluid Type-1, Bentonite+Barite+Water)	152
Figure 50 Initial and Return Permeability of Sample 12 with pump (Mud Type-1, Bentonite+Barite+Water)	153
Figure 51 Initial and Return Permeability of Sample 13 with pump (Fluid Type-2, Bentonite+Barite+CMC+Water).....	154
Figure 52 Initial and Return Permeability of Sample 14 with pump (Fluid Type-2, Bentonite+Barite+CMC+Water)	155
Figure 53 Initial and Return Permeability of Sample 15 with pump (Fluid Type-2, Bentonite+Barite+CMC+Water)	156
Figure 54 Initial and Return Permeability of Sample 16 with pump (Fluid Type-3, Bentonite+Barite+Polymer-XT+Water).....	157
Figure 55 Initial and Return Permeability of Sample 17 with pump (Fluid Type-3, Bentonite+Barite+Polymer-XT+Water).....	158
Figure 56 Initial and Return Permeability of Sample 18 with pump (Fluid Type-3, Bentonite+Barite+Polymer-XT+Water).....	159
Figure 57 Experimental Results of the Drilling Fluid Type-1	163
Figure 58 Experimental Results of the Drilling Fluid Type-2	164

Figure 59 Experimental Results of the Drilling Fluid Type-3	164
Figure 60 Experimental, Simulated and Formulated Results of Drilling Fluid Type-1	165
Figure 61 Linear Regression of Fluid Type-1	168
Figure 62 Experimental, Simulated and Formulated Results of Fluid Type-2	169
Figure 63 Linear Regression of Fluid Type-2	170
Figure 64 Experimental and Calculated Results of Fluid Type-3.....	171
Figure 65 Linear Regression of Fluid Type-3	172
Figure 66 Damage Ratio vs Time at Different Filtration Pressures for Drilling Fluid Type-1	174
Figure 67 Damage Ratio vs Time at Different Filtration Pressures for Drilling Fluid Type-2.....	175
Figure 68 Damage Ratio vs Time at Different Filtration Pressures for Drilling Fluid Type-3.....	176
Figure 69 Variation of Permeability along the core sample at 50 psia with Drilling Fluid Type -1	178
Figure 70 Variation of Permeability along the core sample at 100 psia with Drilling Fluid Type – 1.....	179
Figure 71 Variation of Permeability along the core sample at 200 psi with Drilling Fluid Type – 1	181
Figure 72 Variation of Permeability along the core sample at 50 psia with Drilling Fluid Type -3	182
Figure 73 Variation of Permeability along the core sample at 100 psia with Drilling Fluid Type -3	183
Figure 74 Variation of Permeability along the core sample at 200 psia with Drilling Fluid Type -3	184

Figure 75 Particle concentration variation along the core length with Drilling Fluid Type -1 at 50 psi178.....	185
Figure 76 Porosity variation along the core length with Drilling Fluid Type -1 at 50 psi.....	186
Figure 77 Porosity variation along the core length with Drilling Fluid Type -1 at 100 psi.....	187
Figure 78 Porosity variation with respect to time at different grid blocks with Drilling Fluid Type -1 at 100 psi	188
Figure 79 Particle Concentration variation along the core length with Drilling Fluid Type -2 at 100 psi.....	189
Figure 80 Particle Concentration variation along the core length with Fluid Type-3 at 100 psi.....	190
Figure 81 Digital Radiography System.....	196
Figure 82 Block Diagram of Digital Radiography System.....	197
Figure 83 Sandstone Core Sample X-Ray Scans	197
Figure 84 Porosity versus Core Length.....	199
Figure 85 Permeability versus Core Length	201
Figure 86 Areban Formation Neostratotype (TPAO Stratigraphy Lexicon)	224
Figure 87 Relative permeability vs water Saturation for a water wet rock after Kjosavik et al. 2002	228
Figure 88 Particle concentration vs time at constant distances from circulation point with drilling fluid-3 at 100 psi filtration pressure	229
Figure 89 Particle concentration vs time at constant distances from circulation point with drilling fluid-3 at 100 psi filtration pressure (on narrower time scale.....	230

LIST OF TABLES

Table 1 Drilling Fluids and Physical Properties	51
Table 2 Identification of Core Sample	55
Table 3 Data For Initial Permeability	56
Table 4 Data For Filtration Experiments.....	56
Table 5 Data For Return Permeability	57
Table 6 Representative input file for the simulation.....	68
Table 7 Fann Viscometer measurements of the Drilling Fluids	80
Table 8. Filter loss measurements of the drilling fluids.....	80
Table 9 CMC-added, water based drilling filtration loss readings	82
Table 10 Polymer XT- mixed drilling fluid shear stres readings	88
Table 11 Polymer DSHV- mixed drilling fluid shear stres readings	88
Table 12 Polymer MAC-PR- mixed drilling fluid shear stres readings	89
Table 13 Fitting Parameters of the Calculated Equations	99
Table 14 The porosity values of the core plugs used in dynamic circulation tets: For Pressure Cell Tests.....	138
Table 15 The porosity values of core plugs used in dynamic circulation tests: For Experiments with Pump	139
Table 16 The porosity values of core plugs used in dynamic circulation tests: For Experiments with Pump	139
Table 17 Experimental Results of Dynamic Circulation Tests with Drilling Fluid Type-1	160

Table 18 Experimental Results of Dynamic Circulation Tests with Drilling Fluid Type -2	161
Table 19 Experimental Results of Dynamic Circulation Tests with Drilling Fluid Type-3	162
Table 20 Fitting Parameters for Drilling Fluids-1,2, and 3	167
Table 21 Geological and physical properties of the core and the formation	223
Table 22 Pore throat coefficients of the exponential model.....	232

NOMENCLATURE

<i>A</i>	Area, cm ²
<i>d</i>	Core diameter, cm
<i>DR</i>	Damage ratio, %
<i>D_p</i>	Particle diameter, μm
<i>D_T</i>	Pore throat diameter, μm
<i>β</i>	Ratio of pore throat diameter to particle diameter
<i>k_e</i>	Entrainment rate constant, Pa ⁻¹
<i>k</i>	Uncovered deposit constant, dimensionless
<i>kⁱ</i>	Consistency index, Pa.s ⁿ
<i>nⁱ</i>	Flow behavior index, dimensionless
<i>f</i>	Fraction of porous media containing the corresponding pathways
<i>k_d</i>	Deposition rate constant, (cmxppm) ⁻¹
<i>k_p</i>	Surface deposition rate constant, (cmxppm) ⁻¹
<i>K</i>	Permeability, D
<i>L</i>	Core length, cm

N	Number of pore throats per unit bulk volume
n_1	Arbitrary constant
n_2	Arbitrary constant
A	Correlation coefficient
B	Correlation coefficient
C	Correlation coefficient
q	Filtrate flow rate, cc/sec
x	Distance along the core, cm
q_s	Superficial velocity, m/sec
t	Time, sec and min.
P	Pressure, psia and atm
u	Filtrate velocity, cm/sec
X_k	Rate constant, m ²
ε	Total fraction of depositions in the both plugging and non plugging pathways, cc/cc
σ	Particle Concentration, ppm
α	Dimensionless constant
μ	Viscosity, cp
τ	Shear Stress, Pa
η	Fraction of uncovered deposits
ϕ	Porosity

ρ	Particle density ,kg/m ³
δ	Deposition rate constant, (cmxppm) ⁻¹
c_1	Plugging side constant, (ppmxsec) ⁻¹
c_2	Plugging side constant, (ppmxsec) ⁻¹
c_3	Deposition side constant, (ppmxsec) ⁻¹
c_4	Erosion side constant, sec ⁻¹

Subscripts

cr	Critical
s	Superficial
p	Plugging
np	Non-plugging
e	Entrainment
o	Initial
f	Final
1	Fluid Type-1
2	Fluid Type-2
3	Fluid Type-3

CHAPTER 1

INTRODUCTION

Formation damage causes substantial reductions in oil and gas productivity in many reservoirs. Due to the mechanics of flow into horizontal wells and the fact that most horizontal wells remain as open hole completions, damage effects can be very severe both in horizontal wells and equivalent vertical wells. Damage can be caused by mechanical effects (fines mobilization, solids invasion, emulsion formation, water blocking), chemical effects (clay swelling, clay deflocculation, solids and wax precipitation, insoluble precipitates, acid sludges, chemical adsorption, wettability alterations), the action of bacteria or extreme temperatures associated with thermal recovery processes. Stimulation procedures required to remove formation damage in wells are costly and are often unsuccessful or marginally successful. The use of well designed laboratory programs can allow those associated with designing and conducting drilling, completion or stimulation programs to evaluate the effectiveness of specific programs, prior to their implementation in the field. Formation damage is evaluated by means of two factors: damage ratio (DR) and sectional damage ratio (SDR). The residual permeability is expressed in terms of relative values, with the initial permeability as reference.

The depth of permeability impairment is determined by measurement of the permeability various sized segmented cores. For this criterion, the SDR term is introduced. The method described here will be applied for evaluating formation damage caused by different chemicals in the drilling fluid in sandstone and limestone coreplugs in a wide range of permeability values with pressure difference, temperature, annular velocity, and time of contamination as the influencing variables. The permeability of the formation at or near the well bore may be substantially reduced as a result of the contamination by drilling fluids. There is no generally accepted method for evaluating formation damage under borehole conditions. The objective here is to describe a method that allows evaluation of formation damage caused by drilling fluids and to present results obtained from this method in terms of DR and SDR.

Formation damage in oil and gas wells is difficult to quantify in many cases. As stated by Civan (2000), a technical definition of formation damage would be, any process that causes a reduction in the natural inherent productivity of an oil or gas producing formation, or a reduction in the injectivity of a water or gas injection well“. Disappointing production or injection results from an oil or gas well can be related to a number of factors which may be difficult to diagnose. Some of these may center about poor inherent natural reservoir quality characteristics, others about mechanical considerations surrounding the condition and type of the wellbore obtained, and still others under the nebulous catch-all of “formation damage” which often absorbs the majority of the blame for poor results of many projects.

Formation damage in oil and gas wells is difficult to quantify in many cases. This is due to the inability of the reservoir engineer to retrieve exact samples and conduct detailed measurements on the area of interest, usually represented by a volume of rock surrounding the wellbore which is generally several thousand meters below the surface of the earth. However, ongoing projects over the years have allowed the development of a variety of techniques allowing the use of the available information to obtain a much better indication of the type and degree of damage which different reservoirs may be sensitive to, thereby adjusting operating practices to attempt to minimize or reduce these permeability reducing factors. This data would include information such as production and pressure data, pressure transient data, log analysis, fluid and PVT data and core, cuttings, and special core analysis data.

Formation damage can occur during drilling or coring, well completions, production, work over or subsequent injection of water or chemicals for enhanced recovery. Four types of formation damage typically encountered. One type includes the blocking of pore channels by solids introduced by drilling fluid or by completion, work-over or injection fluids. A second type of formation damage results from clay-water reaction that yields clay hydration and swelling, or clay particle dispersion and pore plugging by movement with produced or injected water. Although the hydration and dispersion mechanisms are different, both result in reduced productivity or injectivity. A third type of formation damage results from a liquid block that normally is caused by extraneous water introduced into the formation at the well bore during drilling, coring, completion, or work-over. This block results from a combination of relative-permeability and capillary-retentive properties that reduces

effective permeability to the hydrocarbon. A fourth type of permeability damage is related to the caving and subsequent flow of unconsolidated sands into the well bore. This results in well sand-up with subsequent loss of well productivity.

CHAPTER 2

MECHANISMS OF FORMATION DAMAGE

There are four primary mechanisms of formation damage:

1. Mechanical
2. Chemical
3. Biological
4. Thermal

Each of these can be further subdivided into discrete sub-mechanisms. Technology exists in numerous situations to allow an accurate determination of the types of damage to which a given reservoir is susceptible.

2.1 Mechanical Formation Damage

Mechanical damage mechanisms are related to a direct, non-chemical interaction between the equipment or fluids used to drill, complete, kill, or stimulate a well and the formation resulting in a reduction in the permeability of the formation. In some situations, some of

changes, in the properties of the reservoir fluids themselves during production operations may also cause certain types of mechanical damage. Common mechanical impairment mechanisms would include:

2.1.1 Fines Migration

This refers to the motion of naturally existing particulates in the pore system caused by high fluid shear rates. These may include various types of uncemented clays (dominantly kaolinite and detritic illite, quartz or carbonate fines and rock fragments, mica, anhydrite, pyrobitumen, etc.). Generally, fines migration tends to be more of an issue in clastic formations due to the higher concentration of potentially transportable materials (such as clays). The problem can also be present in carbonates though, so careful evaluation of the composition and degree of cementation of potentially mobile particles in the pore system is essential. Fines migration is usually only apparent when the wetting phase of the reservoir is in motion. For example, in a strongly water-wet formation which is at the irreducible water saturation, oil or gas production can occur at high rates with limited or no problem with fines migration. This is due to the fact that there is no impetus for physical migration since the phase that is encapsulating the fines is not in motion. It is only when the wetting phase saturation increases to the point where mobility occurs, that fines migration becomes problematic. If the formation is non-water wet, problems with fines migration may be apparent immediately on producing the formation. Reservoirs displaying severe fines migration problems may be treated by either: reducing production rates; increasing

flow area by high density perforating, open hole completions, horizontal wells, or fracturing to reduce interstitial velocity; or by chemical stabilizers to adhere the mobile clays to the pore surfaces to reduce the propensity for mobilization. These chemical stabilizers are often high molecular weight polymers and care must be taken in their use so they do not cause damage due to physical adsorption issues.

2.1.2 External Solids Entrainment

This refers to the invasion of particulate matter suspended in drilling or other fluids which may be injected or exposed in an overbalanced condition to the rock matrix surrounding the wellbore. This matter often may consist of a variety of suspended solids in drilling fluids (weighting agents, fluid loss control agents, bridging agents, lost circulation materials, and naturally generated rock flour or drill solids). In most formations, unless permeability is very high (large fractures and vugs) or overbalance pressures are extreme (in excess of 7-10 MPa), the majority of this damage is confined to a region generally very close to the wellbore (1-2 cm in depth). Since the majority of horizontal wells fall into this category, this damage type is often one or more primary concerns in the proper design of low damage overbalanced “drill-in” fluids. These fluids may contain a variety of sized bridging agents and other materials to assist in the rapid formation of a bridging filter cake. Considerable research has been conducted in the area of non-invasive filter cake building “drill-in” fluids in the past several years. Water injection and water

disposal operations also fall into the category of possible damage due to solids invasion because of the presence of suspended solids in many injection fluids (produced fines, corrosion products, scales and precipitates, dead and live bacteria, etc.).

2.1.3 Phase Trapping and Blocking

This is related to a combination of adverse capillary pressure and relative permeability effects. The basis of a phase trap is a transient or permanent increase in trapped fluid saturation (either water, gas or hydrocarbon) in the pore system surrounding the wellbore, causing a reduction in relative permeability to the phase which we desire to produce or inject. Frequent circumstances which may result in phase trapping may include:

1. Invasion of water-based fluids/filtrates into regions of low water saturation and resulting trapping effects on ensuing drawdown. Certain low permeability gas reservoirs and some oil wet oil reservoirs often exhibit this tendency;
2. Invasion of oil-based fluids/filtrates into zones of low or zero oil saturation and resulting trapping affects on subsequent drawdown-a common occurrence in some gas reservoirs and also in water injection projects where slugs or “skim” oil is inadvertently injected into a zone previously highly saturated with water or oil-based fluids are used in dry gas reservoir or water injection well situations;
3. Production of rich retrograde condensate type gases below the dew

point pressure resulting in the accumulation and trapping of a critical retrograde condensate saturation in the near wellbore region;

4. Production of black oils below the bubble point resulting in the release of gas from solution and the formation of a trapped critical gas saturation; and
5. Injection of free gas (aerated fluids and foams during poorly designed UBD operations, non deoxygenated brines, nitrogen energized fluids, etc.) into a fluid saturated zone resulting in the creation of a trapped critical gas saturation.

2.1.4 Glazing/Mashing

This refers to direct damage to the wellbore face caused by bit/heat interactions (glazing) or poorly centralized rotating and sliding pipe in a poor hole cleaning situation, resulting in the working fines and cuttings into the formation face. This effect is generally minimized by proper lubricity at the bit (to reduce glazing which tends to be most prevalent in pure gas/air drill operations due to heating effects associated with the poor heat transfer capacity of pure gases in comparison to liquids). Mashing is reduced by good hole cleaning to avoid large amounts of solids present in the hole (Civan 2000).

2.1.5 Geomechanics

The creation of a void space in the reservoir matrix (by the drilling of the wellbore) removes load-bearing rock and often results in the distortion of the geomechanical stress regime in a region directly adjacent to the wellbore. Although this region is generally fairly small depending on the well orientation and the reservoir stress field under consideration, either contractile or compressive stress fields can be induced which may result in a change in the pore geometry and permeability character in the near wellbore region.

2.1.6 Perforation Damage

The detonation of perforation charges may result in the creation of a crushed zone and generate mobile fines adjacent to the perforation tunnel, possibly reducing the permeability in this region. The composition of the perforating fluid, if perforating overbalanced, may also have a significant impact on damage effects.

2.1.7 Proppant Crushing and Embedment

This is a damage mechanism which can reduce the effective conductivity of an artificially generated hydraulic fracture. Normally a proppant (sand or synthetic) is placed to hold the fracture open after the fracture pressure has been released to maintain high permeability to the newly accessed portion of the reservoir. At high closure stresses,

conventional sand proppants can be mechanically crushed which releases fines, reduces fracture diameter, and may significantly reduce permeability. Embedment may be associated with high closure stresses in soft formations or with angular, rough proppants which have minimal point contact surface area. In both these situations, plastic extrusion of the proppant into the formation face occurs, once again reducing effective fracture diameter and permeability. Typically, high strength (e.g. bauxite, carbolite, etc.) based spherical proppants are used to combat these effects.

2.2 Chemical Damage Mechanisms

Chemical damage mechanisms fall into four broad classifications (Civan 2000):

- 2.2.1 Adverse rock-fluid interactions
- 2.2.2 Adverse fluid-fluid interactions
- 2.2.3 Wettability alterations in the near wellbore region.
- 2.2.4 Scale Formation

2.2.1. Adverse Rock Fluid Interactions

2.2.1.1 Clay Swelling

This is another classic mechanism of formation damage and involves the interaction and hydration of hydrophilic materials, such as

smectite or mixed layer clays, by reaction with fresh or low salinity water. The expansion and sloughing of these clays can cause severe reductions in permeability depending on the amount and location of the clay in the pore system. The problem is especially severe if the clay is lining the pore throats as only a small amount of expansion can result in a very large reduction in permeability in this configuration.

2.2.1.2 Clay Deflocculation

Less understood but often more common in occurrence than clay swelling, clay deflocculation is caused by a disruption of the electrostatic forces holding the surfaces of individual clay units that are attracted to each other as well as the walls of the pore system in a flocculated state. A rapid salinity shock, change in divalent ion concentration from high to low, or rapid transitions in pH can all induce deflocculation. Kaolinite is an example of non-water sensitive clay which can be deflocculated under certain situations.

2.2.1.3 Chemical Adsorption

Polymers and other high molecular weight materials present in some fluids may become bound or adsorbed on the surface of the formation matrix and clays, and by virtue of their large molecular size, cause restrictions in flow area and hence permeability.

2.2.1.4 Formation Dissolution

Certain formation components (halite, various shales, anhydrite, etc.) may have limited to high solubility in water-based fluids. This can result in poor gauge hole formation washouts, or collapse in certain conditions, as well as the release of mobile and potentially damaging fines.

2.2.1.5 Paraffins and Waxes

Many oils exhibit low cloud point temperatures which can result in the precipitation of crystalline in non-alkane based solid hydrocarbons, or waxes, from solution in the oil. These solids can result in the formation of bridging plugs of paraffin at or near the perforations as well as in tubing and surface equipment. Often treated with solvents, diluents, heat, or crystal inhibitors, wax deposition can be extremely damaging in many situations.

2.2.2 Adverse Fluid-Fluid Interactions

2.2.2.1 Emulsions

Emulsions often occur in oilfield operations. The most common type of problematic emulsion is the “water internal emulsion” in which small droplets of water are encapsulated in a continuous external oil phase. These types of emulsions can exhibit very high viscosity and hence may result in the formation of permeability-inhibiting “emulsion block”.

2.2.3 Wettability Alterations

Many additives to oilfield fluids, particularly many surfactants, defoamers, corrosion inhibitors, and some biocides, have polar adsorptive tendencies which may cause them to establish an oil wetting condition in the region of the reservoir in which they invade. Water wet rock, due to surface frictional drag effects associated with the motion of the water phase, tends to have fairly low endpoint relative permeability. Conversely if a rock is oil wet, the water can move easily through the central portion of the pore system, and effective endpoint relative permeability and water mobility are often much higher. If a formation is initially water wet, transition to an oil wet condition is akin to placing a semi-permeable membrane around the wellbore which tends to hold oil back and preferentially let water through. This may result in an undesirable increase in producing water-oil ratio if a mobile water saturation is present

in the matrix. Although this phenomenon is generally undesirable for a water wet producing well, there may be cases where a deliberate wettability alteration is performed to increase water injectivity in a water wet injection well. Willhite (1986) stated that wettability is the most important factor influencing the relative permeability curves. Modification of the wettability around the injection well may create a zone of enhanced water phase permeability in the near wellbore region, which may allow significantly higher water injection rates at an equivalent injection pressure level. This is a common treatment in low permeability sandstone injection wells. A representative relative permeability vs water saturation graph was drawn in Appendix H using the data from Kjosavik et al. (2002).

2.2.4 Scale Formation

Scale is a result of the abnormal behaviour of calcium carbonate. Unlike most substances, which dissolve better in hot water than in cold, calcium carbonate becomes LESS soluble as temperature increases. So, when hard water is heated, the calcium carbonate can no longer stay dissolved, and thus precipitates - or falls out of the water - as a scale. In cold water, calcium ions ($\text{Ca}^{2+}(\text{aq})$) and bicarbonate ions ($\text{HCO}_3^{-}(\text{aq})$) are surrounded by 'sheathes' or 'envelopes' of electrically-attracted water molecules, which 'insulate' against the natural tendency of the oppositely-charged ions to come together and form crystals. However, when water

is heated, the increased molecular motions cause the protections to become looser and also to break apart the fragile bicarbonate ions into carbonate ions ($\text{CO}_3^{2-}\text{aq}$). Daminov et al.(2006) declared that technology allowed to significantly reduce scaling in bottomhole equipment. However, it has been discovered that this technology has a significant disadvantage: a sharp growth of corrosion of metal downhole equipment contacting with the chemical. Taking into account that at present about 1200 wells of OAO "Yuganskftegas" fields are equipped with dosing devices, the scope of corrosion problem of downhole equipment is quite substantial. The combination of reduced 'insulation' by activated water molecules and increased attraction between ions (because the carbonate ion is doubly-charged) results in the calcium and carbonate ions being able to combine together to form crystals of calcium carbonate ($\text{CaCO}_3\text{ (s)}$)... that is, scale.

2.3 Biological Damage

This type of damage refers to problems created by the introduction of viable bacteria and nutrient streams into a reservoir. Although most commonly associated with water injection operations, bacterial contamination has the potential to occur any time a water-based fluid is introduced into a formation. Most bacteria grow best at temperatures less than 90°C . However, long-term injection of large volumes of water into deep, hot formations may result in a reduction in bottom hole temperature to the point where bacteria may survive and propagate. The three major

damage mechanisms associated with bacterial entrainment include:

1. *Plugging* – Most bacteria secrete a viscous polysaccharide polymer as a by product of their life cycle which may adsorb and gradually plug the formation.
2. *Corrosion* – Some types of bacteria set up an electrokinetic hydrogen reduction reaction which can result in pitting and hydrogen stress cracking on metallic surfaces downhole in tubing or in surface equipment.
3. *Toxicity* – A certain type of anaerobic bacteria, commonly referred to as Sulfate Reducing Bacteria (SRB), reduce elemental sulfate which may be present in formation/injection waters and create toxic hydrogen sulfide gas.

2.4 Thermal Damage

Thermal damage mechanisms refer to those associated with high temperature injection operations (steam injection, in-situ combustion, etc.) These include:

1. *Mineral Transformations* – At temperatures over approximately 180 °C, non-reactive clay species may be catalyzed and form hydratable reactive products which swell, desegregate, and reduce permeability. These reactions are most pronounced at temperatures above 250 °C.
2. *Dissolution* – Mineral solubility increases with temperature. Long-term dissolution may result in the release of encapsulated fines or

subsequent reprecipitation of the dissolved species when the hot fluids move further into the reservoir or into production wells and cool.

3. *Wettability Alternation* – Formations generally become more water wet as temperature increases. However, there are isolated circumstances of transitions to oil wet behavior on the application to formations of superheated steam.
4. *Reduction in Absolute Permeability* – This has been documented to occur under overburdened conditions at extreme temperatures. It is believed to be due to thermal induced grain expansion and subsequent pore constriction. Thermal stress cracking and manufacturing of mobile and damaging fines has also been observed at high temperatures in some isolated studies.
5. *Thermal Degradation* – Over 200 °C thermal reactions of sulfur-bearing compounds in oil and rock, as well as carbonate reactions, may result in the production of large concentrations of hydrogen sulfide, carbon dioxide, and mercaptans.

2.5 Evaluating Formation Damage

The potential areas of sensitivity to formation damage for most reservoirs can be determined by increasing the understanding of the reservoir. This is often accomplished by obtaining information from field data, fluid samples, and core analysis methods, including:

1. Wettability
2. Capillary pressure
3. Initial and irreducible fluid saturations

4. Relative permeability character
5. Matrix and clay composition and location
6. Pore size and pore throat size distribution
7. Critical velocity (fines migration testing)
8. Whole drilling fluid invasion (return permeability testing)
9. Critical filtration testing
10. Salinity and salinity shocking tests
11. Water-water, oil-water, and emulsion testing
12. Scaling and precipitate modelling via geochemical analysis of fluids
13. Proper knowledge of bubble and dewpoint of reservoir fluids
14. Evaluating cloud and pore point
15. Tests on the wetting properties of the proposed fluids on the formation
16. Bacterial content and type in injection fluids
17. Potential for thermal damage effects at high temperature

All of these issues can be evaluated by proper screening work conducted in the laboratory.

CHAPTER 3

LITERATURE SURVEY

Prevention of formation damage through fluids used for drilling and well operations provides one of the key elements for the economic success of oil- and gas field developments. To select an optimum fluid for drilling or well operations in a reservoir section, one of the most prominent criteria is potential formation damage. Using representative formation cores, service laboratories conventionally measure the permeability impairment caused by candidate fluids to benchmark formation damage potential. During recent years, a number of studies have been carried out to develop the ability to evaluate well fluids in terms of their formation damage potential.

Krueger (1963) presented results from tests of dynamic fluid-loss rates to cores from clay-gel water-base drilling fluids containing different commercial fluid-loss control agents (CMC, polyacrylate or starch), organic viscosity reducers (quebracho and complex metal lignosulfonate) and oil at several different levels of concentration. In the dynamic system the most effective individual additives to the clay-gel drilling fluid, based on cost equalized concentrations, were found to be starch and the viscosity reducers. For chemically treated clay-gel drilling fluids, both the standard and the high pressure API filter loss tests were found to be in accurate indicators of trends in dynamic fluid-loss rates under pre-defined conditions used, particularly for drilling fluids containing viscosity

reducers. Krueger (1967) studied the permeability reduction in sandstones when they are exposed to drilling fluid and the clean-up with oil at elevated pressures. The objective of their back-flush process is to displace the particle bridges. They used a drilling fluid circulating system to expose the cores for simulating the well bore conditions. Their experimental system consists of a one barrel reserve pit and a conventional fluid pump to circulate the drilling fluid through a high pressure cell. This high pressure test cell is a vessel with 12 ports for exposing core specimens to flowing drilling fluid. They varied the backflow pressure in different experiments to see the effects upon the recovery of permeability to oil in Berea cores. They obtained partial success by using oil backflush followed by low rate reverse oil flow. They concluded that low rate clean-up is better than high rate clean-up in Miocene and Pliocene producing zones. Oil back flush simulation reduced the wellbore damage from silt migration. They stated that as the solid contents in the produced oil increased, the production rate declined qualitatively.

Haynes and Gray (1974) studied the transport efficiency of suspensions through sand particles packed over a perforated casing. They proposed that a low viscosity fluid would be advantageous to minimize the channeling and would reduce the transport efficiency because of less drag applied on particles. They preferred fresh water and low viscosity brine which are less expensive to use for carrying the particles to the perforations. They concluded that the particle transport efficiency improves with increasing flow rate and varies inversely with the particle size and concentration.

Torrest and Savage (1975) studied the particle recovery as a percent of the total solids applied at different flow rates. They injected Dowex ion-exchange bead suspensions through a central tube at the top of a clear acrylic test section. The suspension concentrations were varied from 0.5 to 1.0 pound per gallon of suspension. The fluid viscosities varied from 1.0 cp to 8.0 cp. They used $\frac{1}{2}$ in and $\frac{1}{4}$ in diameter nozzles and measured the velocities of the fluid at the nozzles. They plotted the measured fractional particle recovery in the effluent versus the flow rate. The relationship between the fractional recovery and flow rate was obtained to be linear. Thus, for particles with settling velocities in the order of 10 cm/sec or less, a surprisingly simple linear correlation allows the accurate estimation of the particle recovery efficiency over a range of tube sizes and flow rates.

Gruesbeck and Collins (1982) investigated the plugging phenomenon encountered in perforations in an experimental work. They applied the particulate slurries directly over the perforations without using a sand pack. They used brines with different densities as the carrier fluids and added hydroxyethyl cellulose to attain the desired viscosity in the brines. They used five different particle sizes to prepare the suspensions of particles with these carrier fluids. They conducted the laboratory experiments concerning the transport of solids through perforations. They did not consider any drilling fluids in their study. They defined the particle transport efficiency as the mass fraction of particles that can be transported through the perforations relative to the total mass injected. Even though they mention of obtaining a good matching between the experimental and numerical data, they did not provide a correlation of the

data. They concluded that perforation diameter to average particle diameter should be at least 6/1 or greater in order to avoid the perforation plugging. They did not obtain data concerning the applications of highviscosity fluids above 40 cp. They noted that, in such circumstances, the voids can allow invasion of formation sand into the gravel pack and can lead to an early completion failure.

Marx and Rahman (1984) described a method for evaluating formation damage caused by drilling fluid in reservoirs which may have pressure considerably less than hydrostatic pressure. The method was applied to evaluate formation damage caused by KCl-Chalk fluid in two sandstones of 10 mD and 1000 mD range with pressure difference, temperature, annular velocity and time of contamination as the influencing variables. The results showed that the pressure difference did not severely damage the rock material tested. The temperature above 70 °C caused a drastic increase in damage as indicated by a sharp reduction of damage ratio. This was due to the thermal degradation of the polymer used in the drilling fluid. As expected, higher annular velocities caused higher filtration rates, thus leading to higher formation damage. The contamination period has a marked influence on the cores with low permeability.

Fordham et.al (1988) studied the variation of key parameters describing the dynamic fluid loss behaviour of two water based drilling fluids, barite- weighted and unweighted, has been systematically investigated in annular flow dynamic filtration cell designed to provide well controlled laminar flows over a wall shear rate typical of those in the wellbore during drilling. Their results can be application to the modeling of

fluid loss in drilling and well completions. Dynamic filtration of drilling fluids and other wellbore fluids is a process common to both drilling and completion operations. It also occurs with polymer gels in hydraulic fracturing, in a narrow geometry rather than an annulus. The importance of analysis of fluid loss in well completions has to be well understood in order to understand the mechanisms of dynamic filtration.

Vitthal et.al (1988) proposed a model that simulates the permeability impairment in a radial geometry. They noted that permeability impairment by fines migration produces a positive skin near the well-bore. The pressure drop across the porous medium is obtained by a relationship that correlates permeability to the mass of solid particles deposited. In their study, they analyzed the rate of release which is an important term which controls permeability impairment. They noted that the particle release from the pore walls is related with the electrostatic forces, van der Waal interactions, hydration forces and hydrodynamic forces as well as the size of the particle clays. They concluded that as the trapping length increases, the rate of capture of the suspended particles will decrease. This means that the particle is expected to move further along with the fluid before being captured at a pore throat. They stated that as there would be less reduction in permeability as the connectivity of the pore network increases. Thus, they analyzed a wide range of parameters effecting the fines migration in porous system.

Kumar and Todd (1988) studied on new approaches for mathematical modelling of formation damage due to invasion of clay suspensions. They proposed a mathematical model which is based on mass balance of particles. They applied their model on the experimental data obtained on

80 mm sandstone coreplugs. They observed that their simulation worked consistently with the experimental data.

Baghdikian et al. (1989) investigated the transient behavior of particulate plugging of porous media. They performed this study on a well-characterized system to check the validity of their theoretical predictions. For this purpose, kaolinite and bentonite suspensions were injected into 40/170-mesh Ottawa sand-packs. The pore-size distribution of the sand-pack was measured. They measured the permeability by flowing clear brine through the system. They determined the pore-size distribution in the Ottawa sand and the particle size distribution of bentonite suspensions in different molarity KCl solutions. The bentonite caused some permeability reduction. This indicates the presence of a deep bed filtration process. Kaolinite did not reduce the permeability significantly at low ionic strengths.

Dunsmuir et al. (1991) studied the application of X-Ray tomographic microscope in porous media. They made an overall interpretation in digital micro radiography overview such as x-ray source requirements, detector accuracy, detector, and lens resolution. They mentioned that optimum results are obtained when the specimen absorbs about 90% of the incident x rays. This condition is satisfied at low x-ray energies such as 5-30 keV. They employed the digital subtraction technique to highlight the differences between them. They aimed at visualizing the flow in porous media. They obtained the resulting images and called them as the volumetric projection of the accessible pores. They concluded that high-resolution porosity and flow maps can be obtained by digital subtraction radiography.

Rahman and Marx (1991) conducted laboratory experiments to study the formation damage caused by drilling fluid and cement slurry. They used two different sandstone core samples typical for gas and oil reservoirs in Germany. Core samples of 25 cm long and 2.5 cm in diameter were contaminated with commonly used four different drilling fluids and a typical class-G cement slurry. The results have shown that the current practice of using low-solid drilling fluid weighted by ground calcium carbonate can cause about 40 % reduction in permeability of the core samples extending over 20 cm. The permeability damage of the core samples caused by bentonite polymer drilling fluid was observed to be about 75 %. They concluded that this severe damage is only confined to a depth of about 5 cm which can be overcome by the perforation work. Barite as density controlling agent exhibits less formation damage than does the ground calcium carbonate. Damage is caused by the drilling fluids and subsequently by the cement slurries by two mechanisms such as invasion of solids that plug the formation and invasion of filtrate that can hydrate interstitial clay, free formation fines, precipitate solids, change formation wettability.

Einstein and Civan (1992) studied formation damage characterization by particulate processes. They estimated the rate constants using the formation damage model which was developed by Ohen and Civan. They conducted core experiments. They determined the cation exchange capacity and pore entry size distribution with respect to clay content and pore entry size, respectively. They concluded that their study verified Ohen and Civan's model by employing various particulate processes for formation damage analysis.

Chang and Civan (1992) declared that fluid introduced into petroleum-bearing formations frequently causes formation damage due to the incompatibility of the injected and indigenous fluids, and mineral constituents of the formation. The processes contributing to formation damage includes dissolution/ precipitation of minerals, fine particles release and capture and formation swelling. When the pore throats of a porous media are blocked, the porosity may remain nearly unchanged, but permeability can decrease significantly because the gates connecting the pores are shut off. This effect should be studied into permeability and porosity correlations.

Bennion et al. (1992) investigated the formation damage due to mineral alteration and wettability changes. They conducted three core flow experiments. They have seen that permeability decreased up to 95%. They focused on thermally induced formation damage. They stated that thermal stimulation processes include mineral transformations, mineral solubilization, wettability alterations and in-situ emulsion formation. They concluded that formation permeability can be reduced by up to 90% by a combination of wettability alteration, mineral dissolution and the transformation of kaolinite to clay.

Angulo et al. (1992) studied porous media by evaluation by x-rays. They presented analysis and numerical modeling of tomography data. They used a polynomial representation to express the CT numbers and attenuation coefficients. They defined attenuation coefficient to mass density of the element with a polynomial with constant coefficients. These constants on this definition are the x-ray photon energies. Density and atomic number are also involved into the approach. They obtained newer

attenuation coefficients through a second generation modified CT scanner. They concluded that polynomial model can be used for the determination of mass attenuation coefficients in CT applications for a quantitative analysis. They suggested minimizing the deviation of density and average atomic number values, improvement of raw and CT data are required.

Engler et al. (1992) studied the fluid distribution and porosity by digital radiography. They used a silica core model with holes of known size distribution and sandstone Berea. They conducted experiments both with core sample and the silica. They also simulated their data using a numerical model. They used DR mode of an industrial CT scanner. Thus, they could move the sample through an x-ray tube and a linear set of arrays which are normal to the axis of the core sample. Thus, they could measure the distributions of porosity and fluid saturations in 2 dimensions. They examined the accuracy of the fluid saturations and porosity within DR applications. They scanned a Berea sandstone sample of 63.5 mm long and 0.20 fractional porosity when it was dry. They saturated the core with decane solution before scanning. Then they displaced the solution with decane-saturated air. They insulated the cylindrical surface of the core sample to ensure that flow would be in single direction from the inlet to the outlet. They kept the core sample in horizontal position during the displacement and scanning stages. They concluded that digital radiography of the Berea sandstone core sample gave similar outputs as in CT applications.

Jiao and Sharma (1992) conducted dynamic filtration experiments on oil-based fluids show that the dynamic filtration rate is much higher

than and uncorrelated with the API filtration rates. Better external mud cakes are formed by adding the same amount of organophilic clay to the drilling fluid. Filtration loss control additives do not reduce the equilibrium filtration rate, but do reduce the spurt loss and limit the invasion rate for oil based drilling fluids is significantly smaller than water based fluids. This is caused by low relative permeability to the oil phase and by capillary pressure effects. For all the oil-based fluids tested, the dynamic filtration rate is much higher than and uncorrelated with the API static filtration tests. The filtrate loss rate more than doubles when a finite oil saturation is present in the core. This suggests that the API static filtration test is not appropriate for oil based fluids and dynamic tests on oil saturated cores need to be conducted. Oil-based mud cakes consist primarily of water droplets stabilized by colloidal particles and emulsifiers. The use of water-wet solids results in very poor quality external cakes and high fluid loss rates. Better external fluid cakes are formed by adding the same amount of organophilic clay to the fluid.

Ohen and Civan (1993) proposed that formation damage is an undesirable phenomenon encountered at any stages of well development and reservoir exploitation including oil and gas production, workover operation and hydraulic fracturing using water-based fracturing fluids. Fines migration and clay swelling have been recognized as the major causes of formation damage observed as permeability impairment. The damage is especially more severe in poorly lithified and low permeability formations with abundance of authigenic pore filling clay minerals.

Jasti et al. (1993) presented a method for imaging the microstructure of porous media by using 3D applications. They obtained the production of the 2D images using x-ray computer tomography with diverging x-ray beams. The 2-D reconstructed images can be obtained by the distribution of linear x-ray in a transaxial plane of the object. They used a glass bead pack, three Berea sandstone samples, and Texas crème chalk to test the feasibility of their system. They classified their study as consolidated porous media, sphere pack, multiphase flow, and thin section analysis. The advantage of thin section study is to visualize the sliced rock fragments under microscope and comparing the microscopic views to x-ray scans. They concluded that in all these systems, high resolution imaging system is the most advantageous for the determination of void space of the porous media representing the hydrocarbon reservoirs. They also found out that microfocal x-ray system can be used for the characterization of the two fluid phase structures in porous media.

Civan and Engler (1994) stated that fluid filtrate will invade during drilling operations the porous media developing a damaged zone around the well bore. To assess the damaged area, the filtrate concentration as a function of distance from the well bore and time of invasion must be determined. The concentration of filtrate in the porous media can be described by a convection-dispersion equation and its associated conditions. The invasion profile is assumed to be unsteady state, radial and isothermal.

Chesser, et al. (1994) described properties that are desirable in a water-based filter cake and test methods that can be used measure these properties. One method uses a dynamic filtration-loss apparatus that stirs the fluid mechanically during filtration. Tests results showed that the initial dynamic filter-cake formation is very important in controlling most of the possible filtration properties and cake quality. They discussed various factors affecting filter-cake quality and how they can be controlled to give better field performance. Filter cake compressibility and lubricity are important properties to obtain, especially where differential pressure sticking and torque-and-drag conditions prevail. Water-based fluids can be formulated to optimize desirable filter-cake properties. Water-soluble organic polymers perform effectively in this manner, but highly deflocculated systems are to be avoided.

Fraser et al. (1995) conducted laboratory project to (i) investigate the mechanisms by which filter cakes develop against sandstone faces, (ii) study the natures of the cakes produced with different types of drill-in fluids, and (iii) to investigate the implications for cake cleanup. Polymer and MMH fluids using carbonate bridging materials are capable of forming external filter cakes on sandstones. Polymer fluids using salt bridging agents form internal cakes and polymer intrusion occurs. In laboratory-prepared, carbonate weighted fluids, the size distribution of the carbonate can have a significant effect on the degree of permeability recovery, regardless of whether a polymer or MMH-based fluid is used. Polymer/carbonate, polymer/salt, and MMH/carbonate fluids give filter cakes which differ in respect to their reaction to applied back pressure (as occurs when wells are flowed back without stimulation).

Francis et al. (1995) carried out core flood tests to examine the damage arising from overbalanced drilling in operations. Results showed that the initial permeabilities to crude oil were dramatically reduced after exposure to overbalanced fluid and subsequent back production of crude oil. Thin section petrography and SEM/XRD analysis of the cores clearly showed the sources of impairment in all cases to be a thin layer fluid solids plugging pores and throats exposed to the wellbore face, forming an effective permeability barrier that was not dislodged by crude drawdown under realistic drawdown. Significant reductions in permeability occurred after fluid exposure and crude drawdown giving permeabilities in a range from 1 to 54 % of the original permeability.

Civan (1996) stated that the modeling a formation damage reservoir has been of continuing interest. Although many models have been proposed, most of them do not have general applicability. However, an examination of the various modeling approaches reveals that this types of models share a common ground and therefore , a general model can be developed, from which these models can be derived. Although modeling based on well accepted theoretical analysis is desirable and accurate, macroscopic formation damage modeling often relies on some intuition and empiricism inferred by the insight gained from experimental studies. The fundamental processing causing formation damage in petroleum bearing formations are physico-chemical, chemical, hydrodynamic, thermal and mechanical.

Hayatdavoudi and Ghalambor (1996) stated that efficient exploitation of existing petroleum reservoirs requires an understanding of nature of petroliferous formations. This makes it necessary to know the factors that

control the flow of hydrocarbon through porous media. Essentially, the flow of hydrocarbon through such formations is brought about by potential, kinetic and thermal energy in the formation.

Civan and Xinghui (1996) declared that formation damage is a very common problem encountered in almost every phase of reservoir development from drilling to production. Fine particles are always present in petroleum bearing formation and they contribute a great deal to the formation damage. During drilling and completion , fluids containing particles suspensions enter the formation. Chemical reactions can also generate particles within formation. Sedimentary rocks usually contain fines loosely attached to pore surfaces. When injection fluids are incompatible with these minerals , they can be released from pore surfaces. These particles migrate through the porous media., deposit on the surfaces, and become trapped at pore constrictions to reduce the rock porosity and permeability. Most of the similar previously studied formation damage focused primarily on single phase flow of injection fluids or filtrates. Although multiphase flow is more commonly encountered in petroleum reservoirs, the information about formation damage in multiphase flow is rather limited. The equipment and experimental setup required to study formation damage in multiphase flow are expensive and time consuming. Simulation studies give practical and less expensive alternatives.

Francis (1997) made the analysis of a large amount of data generated from reservoir conditions core flood testing has lead to an increased understanding of the dominant effects controlling the extent of drilling induced formation damage. For almost all drilling fluids tested, the

dominant form of impairment was an extremely fine layer of residual solids after removal of mud filter cake from the well bore face. The impact of this permeability barrier is dependent on initial core permeability and the reservoir fluid used in the drawdown phase (oil or gas). These results indicate that the formation damage remaining after drawdown is more dependent on the virgin reservoir properties than the drilling fluid it self. The loss of revenue caused by damaged wells producing below their potential strongly influences the profitability of any venture. A significant effort by the industry is currently being put into avoiding drilling and completion induced damage, especially in horizontal open-hole completions, where bypassing damage by perforation is not usually an option. In order to be able to avoid or remedy damage , it is first necessary to understand the underlying causes. Reservoir conditions core flood tests have been used to assess the effects of various drilling fluids and clean – up chemical on their reservoir.

Jiang et al. (1997) proposed that formation damage due to invasion of solid suspensions are of major concern from reservoir evaluation point of view. Horizontal wells are generally much more susceptible to the issue of formation damage than vertical wells because the contact area of rock immediately adjacent to the well-bore with drilling and completion fluids is substantially larger and the contact time is also much longer in horizontal wells. A method for quantitative evaluation of the formation damage caused by drilling and completion fluids in horizontal wells is investigated by skin factor, flow efficiency and production loss. In horizontal wells the flow of oil and gas from reservoir to the wellbore is the 3-dimensional flow, not only consisting of a radial flow in the horizontal plane.

Bishop (1997) identified a formation damage reaction between specific pore lining clay species and saturated salt drilling fluid with the potential for significant permeability impairment in the near wellbore region. Damage levels around 70 % were recorded in reservoir core samples. Characterization of the formation damage mechanism was carried out by scanning electron microscopy. This revealed that flocculation of the pore lining clays had occurred, due to the invasion of the very high salinity brine, producing significant pore throat bridging and plugging.

Marshall et al. (1997) designed a procedure to provide a methodology for assessing formation damage in a variety of testing situations. They set the procedure for the selection of the correct fluid for use in a reservoir is an extremely important factor for maximizing possible ultimate production of the reservoir. They centered on the measurement of return permeability are the most common evaluation tools used for determining fluid suitability and yet there has been little or no previous attempt to standardize the methods used or to quantify the significance of the results obtained. They suggested that standardization is necessary and that care should be taken when comparing results of fluid evaluation from different laboratories due to likely variations in both procedures and equipment.

Nabzar and Chauvetau (1997) studied the reduction in permeability by colloidal particles. They stated that the existence of colloidal particles in fluids flowing through porous media causes a reduction in productivity and injectivity of the wells. They described a model in terms of porous medium and particle deposition. They used SiC particles in small pyrex

cylinders. They packed the SiC into these cylinders and prepared a porous media with 41% porosity. They determined the pore volume by using a tracer injection (potassium iodide). They conducted experiments with depositing latex particles. They concluded that interactions between particles and pore surface are attractive at high ionic concentrations. They found that a reliable permeability reduction is possible by the effects of electrostatic double layers.

Longeron et.al (1998) studied the eight typical drilling fluid formulations including water-based and synthetic oil based drilling fluids. They performed static and dynamic filtration tests on the outcrop sandstone samples. They evaluated the impacts of various parameters on permeability impairment, such as initial core permeability, fluid saturations, temperature and shear rate. Porosity and permeabilities of clay-enriched sandstone samples vary with their mineralogical composition. They used 5 water-based drilling fluids, 1 oil-based mud and 2 pseudo-oil based muds. They made CT (computer tomography) tests on selected core samples to check their homogeneity. They cleaned and dried the cores. They measured the gas permeability k_g of the core samples. They measured oil permeability at connate water saturation at three flow rates and referred this permeability as the undamaged initial permeability value. They obtained return permeabilities on different sections of the core samples ranging from 4 to 24 %. They concluded that the damage took place in the first 5 cm of the core sample with water-based muds. As a summary, they concluded that static and dynamic mud tests on long core samples have accurately allowed to compare both spurt losses and filtration rates for the eight types of muds used.

Marshall et al. (1999) reported the results of a more extensive laboratory study, based on a refined recommended practice for the determination of return permeability. Several key areas have been identified in which strict control is required if results obtained are to be compared with others. By standardizing, the test materials and the testing procedures as far as possible, indications of repeatability and reproducibility of results have been obtained and, where differences have been observed, an attempt has been made to determine whether these are due to inadequacies of the procedures or to differences in the equipment being used.

Bailey et.al (1999) studied the invasion of particles from drilling fluids. They stated that particulate invasion is one of the primary mechanisms of formation damage caused by drilling fluids. They used rock samples with permeability at about 600 mD and 17% porosity. They vacuumed the cores. Then they saturated them with brine simulating connate water from the Heidrun reservoir. They measured permeability to brine at a constant flow. They used pressure transducers fitted to the inlet of the core holder to measure the pressure drop across the core. They stated that back-flushing removes near surface internal filter cake but is not sufficient to redistribute deeply invaded particles. They concluded that the permeability reduction is greatest in single phase brine conditions.

Byrne et al. (2000) conducted core flood tests to determine the clean up efficiency of a drilling mud that was applied at two different overbalance pressures. The test was designed to simulate, as closely as possible, the conditions occurring in the reservoir during the drilling operation. Relevant core material was used and the pore and overburden

pressures, mud overbalance pressures, temperature and production drawdown pressures/rates applicable to field conditions were applied in the laboratory simulation. Permeability measurements were made prior to mud application and again at the end of the flood test analysis to determine the level of any formation damage. In order to determine the nature of the formation damage mechanisms, geological techniques which include dry and cryogenic SEM and thin section analyses were undertaken. The dry SEM and thin section analyses were used to determine solid damage mechanisms such as clay fines migration, scale precipitation and drilling mud solids invasion. They concluded that higher volume losses and/or rates of losses affect the degree of fines migration.

Santos (2002) declared that no damage drilling is the ultimate goal of all well construction activities, by providing a way to explore and produce the hydrocarbon reserves with minimum reduction of the natural permeability of the reservoir rocks. Conventional drilling is conducted with an over-balanced pressure on the reservoir formation, which causes the drilling fluid to invade and damage the rock. The industry has been trying to come up with alternatives and under-balanced drilling (UBD) has grown in popularity during the last years. However, in many situations UBD is not feasible to be used, due to economical and/ or technical reasons. In cases UBD is not used, a drilling fluid with an overbalanced pressure should be used. Formation damage during drilling oil and gas wells has been very important for the oil industry. In order to overcome the problem of formation damage while drilling, the industry developed a method to drill with a bottom hole pressure below the pore pressure which is called under balanced drilling.

Civan (2002) developed a multiphase model for the estimation of filtrate during drilling and fracturing of wells. He introduced the linear and radial filter cake models. He proposed the linear model by volumetric material balance and the radial model by an appropriate transformation. He concluded that this model can be used for the evaluation of formation damage with horizontal wells. He added that this model is safe for the determination of fluid loss contents in the presence and absence of filtration control additives.

Byrne and Patey (2003) resolved some of the arguments and diversity in the procedures for laboratory formation damage test and presented clear evidence to support opinions expressed on the merits of particular tests. Through implementation of the procedures outlined in their study it is possible to simulate most formation damage mechanisms at reservoir conditions of temperature and pressure. Careful attention to sample selection, preparation and test execution is required in order to generate data which is representative of real formation damage or stimulation mechanisms.

Watson and Nelson (2003) examined the ability of the formation damage test to represent the conditions present in the wellbore in terms of filtrate loss control properties, cake development, damaging mechanisms and return permeability. They concluded that drilling fluid applications that use no or unrepresentative shear rates can provide a false classification of the damaging potential of a drilling fluid. The return permeability alone on a short core plug (whether dynamic or static filtration application) does not provide an accurate impression of the damaging potential of a drilling fluid. For the production of accurate shear

rates (and subsequently filtrate loss), the fluid must be displaced parallel to the face of the core using a scaled pump rate calculated from fluid rheology and well characteristics. Constant rate back flood may not be representative of actual production due to the faces and subsequently the regimes, being dependent on the flow rate used. Cryogenic SEM can not be used to identify fluid damaging mechanisms when using synthetic oil as the production phase.

Patino et.al (2003) analyzed the chemical formation damage. The chemical additives in both drilling and completion fluids give real damage to the formations. The alkali technique is a method which promotes the oil recovery generated in situ. High molecular naphthanic species in oil react with alkali to produce salts, which must be surface active. Mineral – alkali interactions have traditionally been of principal interest with respect to alkaline flooding operations. The objective is to maintain sufficient alkalinity in order to achieve the desired treatment efficiency.

Withjack et al. (2003) studied the role of x-ray computed tomography, which is generally known as CT. They aimed to review earlier x-ray applications in petroleum engineering into reservoir engineering categories and to present a reference of x-ray tomography for future studies. They grouped the studies in six basic items: improved recovery, hydrate studies, recovery of viscous oil, acid treatment, perforation analysis, and formation damage. In improved recovery applications, CT is used for monitoring the surfactant imbibitions for carbonate rocks. CT is used in hydrate studies to track the progression of a dissociation front in hydrate and sand mixtures. They concluded that the cost of the utilization of CT is negligible when compared to the overall project value. They

reported that application of CT for field related problems such as formation damage may be useful for remediation of problematic wells.

Ding et.al (2004) studied the near wellbore damage and natural clean-up of horizontal wells. They noted that the near-wellbore properties are altered by drilling fluid and fluid-fluid and fluid-filtrate invasion during overbalanced drilling operations. They called the degree of alteration “formation damage” which is affected by many parameters such as nature and characteristics of the drilling fluid, formation properties and operating conditions. They worked on the concept of drilling fluid invasion. They correlated permeability factor with flow rate. They concluded that a good filter cake is required to prevent filter cake. An external filter cake is preferential because of the simplicity of its removal. They resulted that a deeper particle invasion of the internal filter cake decreases the flow efficiency, although it prevents filtrate invasion. They concluded that serious loss of production can take place with damaging and non-optimized drilling fluid. They declared that the formation damage is much higher with a water based mud than an oil based mud.

Riyamy and Sharma (2004) studied the filtration properties of Oil in Water Emulsions Containing Solids. Their study focuses on factors controlling the filtration and leak-off properties of emulsions which include solid particles. They investigated the effects of percent oil, filtration pressure, core permeability, temperature, and viscosity of the continuous phase by making laboratory experiments. They conducted the experiments with Texas limestone (5mD) , Berea sandstone (175 mD) and Aloxide cores (1.5 D). They used core samples 2.5 in. in diameter and 1 in. in length. They dried the core samples in oven at 150 °F for one

day. They measured the absolute permeability with 3% NaCl brine. They concluded that increasing the oil percent from 0 to 40 vol% decreases the total filtrate volume. They observed that increasing temperature from 25 to 65°C significantly increases the fluid leak-off in limestones. Thus, they concluded that the polymer that they used is partially responsible for the damage in the cores.

Abduwani et al. (2005) studied the formation damage versus solid particles. They investigated the produced water re-injection and variation of permeability along the core surface from the interface. They conducted six standard static filtration experiments. They obtained permeability decline curve along the core sample. For image analysis, they divided the cores into ten segments. They used co-axial illumination with 2x objective lens, a 50x zoom lens and a digital camera. The captured images were obtained in shallower depths such as 10 μ m. They assume that it would be better to generate higher resolution images if a more powerful work station could be available. They concluded that a successful quantification of the deposition profile can be obtained using their technique. They noted that the permeability decline profile is mostly affected by the invasion of the solid particles.

Taud et al. (2005) studied the estimation of porosity by x-ray computer tomography. They stated that x-ray attenuation measurements taken around the object produce cross-sectional images of the object. They obtained the porosity distribution which can indicate the properties of the studied rock. They concluded that the minimum point of the curve can be used for the estimation of overall porosity.

Iskan et al. (2005) studied the effects of water based drilling fluids on permeability impairment and flow reversal. They conducted core flooding and dynamic circulation experiments with sandstones. They investigated the clean-up of pore throats due to aquifer influx which were plugged by clay particles invasion. They analyzed the variation of permeability along the length of the core samples. However, they applied core flooding and mud circulation technique, but they did not investigate the pore throat plugging by x-ray scans and image subtraction methods. They simulated their own experimental data and correlated filtration pressure and permeability damage ratio. They found out that the clean-up effect of water influx decreases as the contamination period by drilling fluids increase. They concluded that damage ratio increases exponentially with filtration pressure.

While the above-mentioned experimental studies provide valuable observations and understanding of the relevant phenomena, they do not provide a comprehensive experimental and mathematical model and specific information about the effect of the phenomenological parameters. Most of the studies considered either the experimental part or the numerical part separately. Thus, the integral structure of understanding such a complicated phenomenon becomes harder. This thesis applies a phenomenological experimental and numerical model to analyze formation damage phenomenon. First plugging criteria concept is presented to demonstrate the physical mechanisms in formation damage. Then, a set of dynamic drilling mud circulation experiments were carried out using three different drilling fluids at eleven different filtration pressures and three different circulation periods. Alteration in permeability is studied in terms of the damage ratio concept. Damage

ratio is characterized as the percentage ratio of the difference between the undamaged and damaged permeability to the undamaged permeability. The influence of filtration pressure and circulation periods are investigated both experimentally and numerically. The acquired experimental data are analyzed by means of a numerical computer simulator for fines migration and deposition in porous media. The results are correlated and an exponential model for the effect of filtration pressure on damage ratio is developed.

CHAPTER 4

EXPERIMENTAL WORK AND SET-UP

4.1 Introduction

Formation damage studies related with fines migration can be investigated by a set of professionally designed consecutive experiments. Since it is not possible to see the inside of the core samples, the drainage amount of the water at the breakthrough and reduction in porosity and permeability will give idea about the invasion of the drilling fluids into the core samples during dynamic circulations. The researcher should be ready for many failures during the experiments such as rubber sleeve leakage, confining pressure problems, overbuilding pressures, and drying of the clays inside core sample. The transportation of the core sample from saturation set-up to dynamic filtration set-up and the vice-versa should be made carefully not to damage the cake which forms on core surface.

Performing experimental studies in formation damage with drilling fluids requires a tedious and careful work. The experiment is basically divided into six sub-experiments as follows:

1. Saturation of the core sample with brine and measurement of initial permeability and porosity.
2. Drilling fluid preparation and dynamic filtration circulation.
3. Backflow through the reverse side of the core sample with brine, and measurement of final porosity and permeability
4. Sample data for each stage of the formation damage experiments
5. Pore throat plugging
6. X-ray analysis

4.1.1 Saturation of The Core Sample with Brine and Measurement of Initial Porosity and Permeability Through Forward Flooding

This section is the beginning part of the formation damage experiments. Nevertheless, a core sample cleaning by toluene extraction may be required according to the condition of the core plug. Especially core samples which were previously contaminated by hydrocarbon fluids should be subjected to toluene extraction. On the other hand for the sake of obtaining better and more observable results, uncontaminated core samples should be used in the experiments.

4.1.1.1 Saturation of Core Sample with Brine and Measurement of Porosity and Permeability

In this section, the saturation of the core sample is conducted with brine. The brine solution should be prepared prior to starting the experiment. The brine solution should not be directly pumped by the proportioning pump. A transfer cell should be used to protect the pump. Otherwise the proportioning pump is damaged due to scaling and deposition of salt particles in the cylinders of the pump. Through the use of the transfer cell, the brines or other chemicals are placed in to the transfer cell. The pump should be run with mineral oil. Because mineral oil is actually the source material for baby oils and is actually not harmful to the environment and the human health. On the other hand mineral oil is easier to clean when compared to Tellus series viscous oils. The brine volume within the transfer cell should be followed carefully. If the cell remains without water and the pump keeps running, then a specimen failure may take place. The permeability measurement procedure is given in Appendix A.

4.2 Drilling Fluid Preparation and Dynamic Filtration

After saturating the core samples with brine, the major substances that cause the formation damage are prepared. Drilling fluids include different chemicals such as bentonite, barite, CMC and some stabilizers. Lost circulation material selection can be understood best by performing filtration experiments. In this research, three different water based fluid samples were prepared: Non-treated bentonites fluid, CMC fluid and

polymer fluid (Solvadis). The fluids were prepared due to API-13E specifications. All of the fluid samples were continuously placed into the mud balance and subjected to fluid weight test. The fluid weight was set at 9 ppg. The fluid samples rested 16 hours after mixing before the applications. API filter press unit was used in the filtration experiments. Shear stress readings were made by using Fann 600 shear viscometer. Filtration experiments were made by obtaining the filtrate volume at 100 psi driving pressure and 30 minute period of 30 second intervals. Optimum CMC and polymer amounts were determined by changing their weights and repeating the filtration experiments

The cost and efficiency of drilling operations are directly related with the quality of the drilling fluid chosen. That is why the selection of the appropriate fluid additives constitutes a major role at the planning step of the drilling operation. The physical and chemical properties of the fluid should continuously be checked so that all the operation will be sustained safely. The fluid weights of all of the drilling fluids were kept as 9 ppg. The rheological parameters such as shear stress, shear rate of all of the drilling fluids were measured and apparent viscosity, plastic viscosity, yield point values were calculated.

4.2.1 Drilling Fluid Preparation

Typical water-based drilling fluids containing solid particles are used for the dynamic filtration tests. Bentonite is the major clay in most water-based drilling fluids used in the oil industry. Three types of water-based drilling fluids with different viscosities (0.10, 0.18, and 0.25 poise) were used. The major constituents of these fluids are water, bentonite, CMC

(Medium viscous Carboxy Methyl Cellulose for increasing viscosity), and Polymer XT (a fluid loss reducing polymer). 1285 g of API Bentonite and 1000 g Barite in 20 liters of water were used for each mud sample (22.5 g/350 cc) according to the API Standard RP-13B. We added 57 g of CMC for fluid type 2 and 22.8 g Polymer XT for fluid type 3 in addition to Bentonite and Barite. Caustic soda in the amount of 1 g /350 cc of slurry was also added to stabilize the mud so that the particles would not settle. The drilling fluid must be mixed for about five hours. The mud is left to rest for sixteen hours due to API standards. The mud is finally remixed for perfect homogeneous slurry conditions. The prepared drilling fluid is pumped through the core plug in the dynamic core holder (Figure 1).

The density, i.e the mud weight, of each sample was kept as 9 lb/gal (1.083 g/cc). The detailed composition of the fluids and their physical properties are given Table 1. The rheological measurements were made with CMC mud at three different CMC mass concentrations (1, 3 and 4 g weight/350 cc) and the optimum amount was chosen as 1 g weight/350 ml equivalent. The optimum condition was determined as follows: When more than 1 g weight of CMC was added in 350 cc of the slurry, there existed bubbles within the fluid. The mud became so jelly that it became almost immobile to pump by the circulation sytem (Figure 2). The Fann viscometer had real difficulty of rotating in the presence of higher CMC concentrations. It is seen that the excessively thick mud may cause not only severe damage to the wellbore and the drilling assembly but also higher pump power requirements for mud circulation result in higher costs. The rheological parameters with the polymer mud were also determined at different polymer concentrations (0.2 g weight/350 cc, 0.4 g /350 cc, 0.6 g / 350 cc, 0.8 g / 350 cc, and 1.0 g / 350 cc). The

optimum amount was determined as 0.4 g weight/350 ml. The optimum amount was determined as following. The selection of the optimum amount was made similar to that of the CMC concentration. When the polymer was added at an amount less than 0.4 g / 350 cc slurry, the fluid could not attain the rheological parameters required. Nevertheless, when higher amounts of polymer were added, the fluid became so thick that it could not be used in the thin pipe system of our experimental set-up (Figure 3). Therefore, the fluid conditions were adjusted to ensure that the fluids can flow easily from the storage tank into the test cell by gravity and under their own hydrostatic head.

Table 1 Drilling Fluids and Physical Properties

Drilling Fluids	Fluid Additives	Fluid Composition	Fluid Weight (g/cc)	* Measured Fluid Velocities (cm/sec)
Drilling Fluid-1	Bentonite+Barite+ Water Viscosity=0.10 P	Water = 350 cc Bentonite = 22.5 g Barite = 45.8 g	1.008	0.005 0.007 0.012 0.015
Drilling Fluid -2	Bentonite + Barite + CMC + Water Viscosity=0.18 P	Water = 350 cc Bentonite = 22.5 g Barite = 45.8 g CMC = 1 g	1.008	0.004 0.006 0.012 0.015
Drilling Fluid -3	Bentonite + Barite + Polymer (XT) + Water Viscosity=0.25 P	Water = 350 cc Bentonite = 22.5 g Barite = 45.8 g Polymer (XT) = 0.4 g	1.008	0.003 0.005 0.011 0.014
Corn Syrup	Pure Pure+10%Water Pure+20%Water	Corn Syrup=200 cc Water=10 cc Water=20 cc	1.366 1.243 1.053	0.002 0.004 0.008 0.012

* Measured drilling fluid Velocity values were obtained with pore throat plugging experiments with four different fluids at four different pore throat diameters 0.42, 0.32, 0.25 and 0,11 mm , respectively.

SI Unit Conversion: 1 lb/gal = 0.1198264272 g/cc

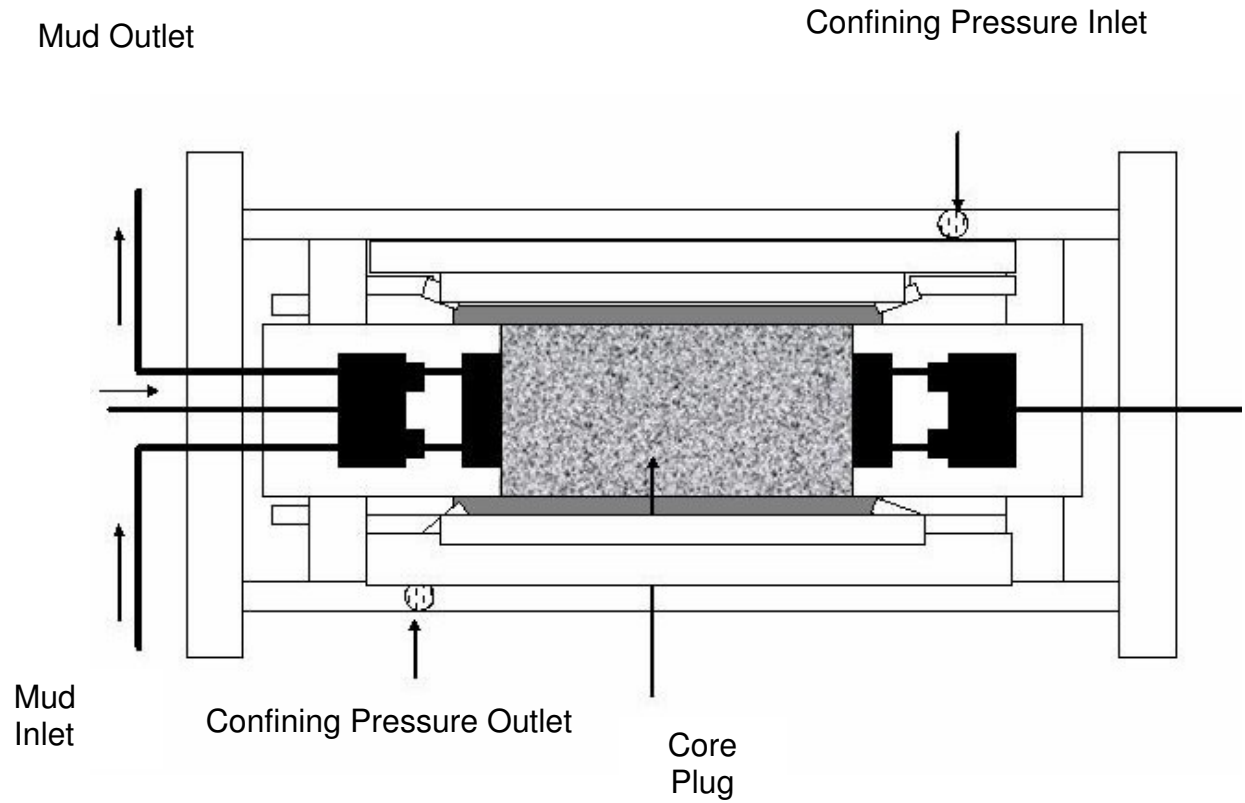


Figure 1 The Core Holder

4.2.2 Dynamic Circulation

The word dynamic emphasizes that both deposition and erosion take place at the same time. Another consideration is that if a rotating pump is used rather than the pressurized mud, then it is possible to talk about dynamic circulation.

The dynamic circulation stage is a very challenging one with respect to the other ones. The core sample should be remained wet. Installation of the core plug into core holder needs special treatment. The drilling fluid should be perfectly mixed not to cause precipitation. The dynamic filtration core holder is shown in Figure 1. The circulation path of the drilling fluid is depicted in Figure-2. The procedure for the dynamic circulation or dynamic filtration experiment is given in Appendix B.

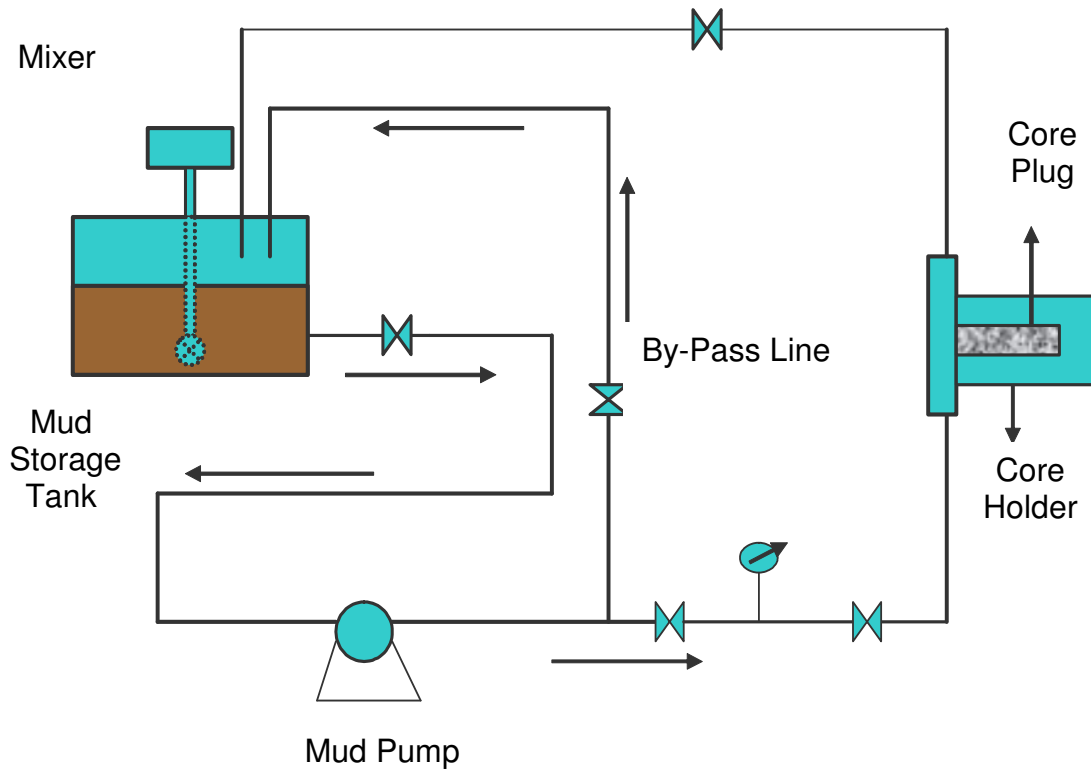


Figure 2 Schematic of Mud Circulation System

4.3 Back Flow Through The Core Sample For Return Permeability and Porosity

The damaged core samples are subjected to a final test to visualize the effects of invasion of fine particles through the set-up in Figure 3. The experimental procedure is almost the same as the initial flooding experiments that had been described in detail in section 4.1.1.1. The procedure for return flow experiments is given in Appendix C.

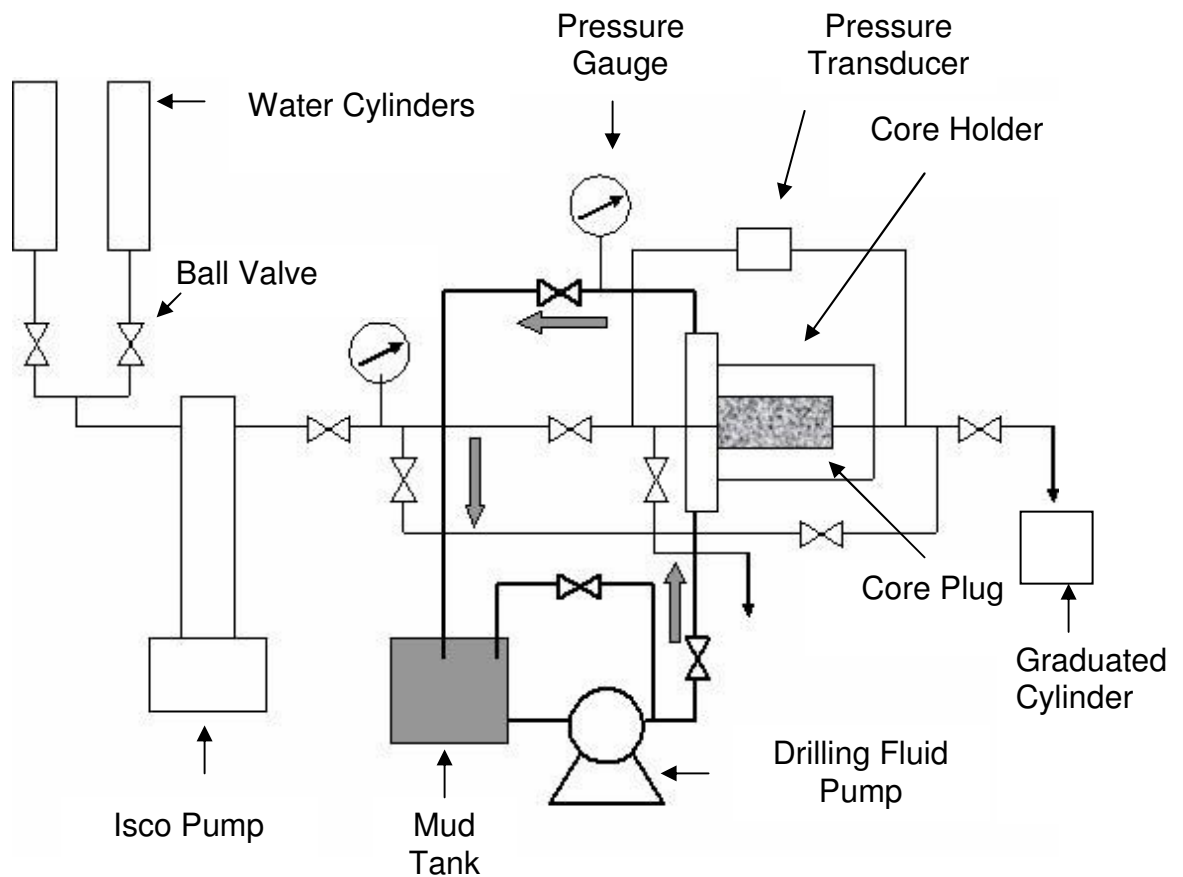


Figure 3 Experimental Set-up

4.4 Sample Data for Each Stage of the Formation Damage Experiments

In this section, a set of original experimental data obtained is presented for representative purpose. The experimental set-up shown in Figure 3 was used for obtaining the data. Identification of core sample in Table 2, data for initial permeability in Table 3, data for filtration experiments in Table 4, and data for return permeability Table 5, are presented respectively.

Table 2 Identification of Core Sample

Core Name	SST	Wet Weight (g)	148.1
Core Length (cm)	7.1	Porosity (%)	32.6
Core Diameter (in)	1.5	Cake Diameter (mm)	3.8
Mud Type	1	Initial Permeability (md)	18.4
P_f (psi)	200	Return Permeability(md)	5.9
Circulation Period (hr)	1	Ph	9.2
Dry Weight (g)	122.15	DR	67.9

Table 3 Data For Initial Permeability

Time (sec)	Pin(psia)	Pout (psia)	DP (%)
300	50.325	14.7	28.5
400	47.95	14.7	26.6
480	44.325	14.7	23.7
530	38.325	14.7	18.9
V(cc)	Qcc/sec)	ΔP (psia)	K(d)
25	0.083	35.62	0.021425
25	0.063	33.25	0.017216
25	0.052	29.62	0.016103
25	0.047	23.62	0.018287

Table 4 Data For Filtration Experiments

Time (sec)	V(dynamic filtration) (ml)	P_f (psi)	Q (l/min)
0	2.0	200	0.3
300	4.0	200	0.3
600	7.0	200	0.3
900	9.0	200	0.3
1200	11.0	200	0.3
1500	13.0	200	0.3
1800	16.0	200	0.3
2100	18.0	200	0.3

Table 5 Data For Return Permeability

Time (sec)	P_{in}(psia)	P_{out}(psia)	ΔP (%)
580	71.9	14.7	45.8
695	69.2	14.7	43.6
760	66.2	14.7	41.2
V (cc)	Q (cc/sec)	ΔP (psia)	K(d)
25	0.0431	57.2	0.00689
25	0.0359	54.5	0.00604
25	0.0328	51.5	0.00585

4.5 Pore Throat Plugging Procedure

Three drilling fluid samples of different viscosities were tested at four different driving pressures through four different outlet pipe sizes. The density of the fluids was kept constant for convenience in correlation of experimental data. The experimental procedure for pore throat plugging is given in Appendix D.1. There are basically two methods available to measure the particle size of fine materials. These are the caliper tool analysis and mesh analysis methods. In our study, a standard mesh analysis method was applied (Appendix D.2). Experimental flow velocities are given in Table-1 for determination of the Reynold's number and flow rates.

Alternatively, particles may be measured individually. Their outer diameters may be measured by a device called Calipper. Digital and analog versions of this device are available. After measuring sufficient individual sand particles, their arithmetical average is taken.

4.6 X-Ray Procedure

4.6.1 Preparation for X-Ray Experiments

Taking core scans by x-rays requires special treatment and preparation stage. It is strongly advised to take the scans while standing behind lead shields. The surface of the x-ray device tray is optically divided into squared coordinate system. For obtaining the best orientation, the core sample is placed on to a V – Channel. The central lines are drawn on the core sample just like in the rock mechanical stress tests while placing the strain gauges. The placement needs special treatment. If the correct orientation is not obtained, it can not be definite that the same sections before and after drilling fluid invasion are scanned. The x-ray images of the invading fine particles can be visualized better if some iron, magnesium or some type of radio active powder in your invading fluid system. However, no artificial substances were used not to destroy the specific heterogeneity of the drilling fluid. On the contrary, we used Barite which is commonly used in drilling industry as a weight increment agent. Barite has the chemical formula BaSO_4 and barium is radioactive. Thus, no artificial additives were mixed for better x-ray scans. Experimental procedure for X-ray experiments is given in Appendix E.

CHAPTER 5

MATHEMATICAL MODELING AND SIMULATION

5.1 Operation of The Fines Migration Simulator

Formation damage analysis is a tedious process which requires both experimental and numerical applications. Experimental work gives the basic behaviors and mechanisms in the pore throat plugging and porosity and permeability reduction. In order to complement the experimental work, a numerical fines migration simulator was developed. The in – house experimental data were run with this simulator. The simulator was basically developed to observe the fines migration into porous media. The sources of the fines were defined as basically water-based drilling fluids which include barite, bentonite, CMC and polymers. Fines migration equations (Civan and Nguyen,2005) were used in the simulation. The simulation is based on defining the porous media to be composed of two types of pathways. These pathways are defined as plugging and non-plugging pathways. This type of approach is statistically better than assuming the porous media homogeneous of single pathway. The first stage of the simulation is to decide how to relate the formation damage by drilling fluids with permeability and porosity. However, it should be noted that even though there may be particle deposition, plugging may not

occur. Hence, a criteria is required for the diagnosis of plugging. Civan (2000) has proposed a plugging criteria concept. The plugging criteria represented by Eqs. 20 and 21 is a means to determine whether bridging occurs or not with certain viscosity of fluid, certain particle size, and certain pore throat-to-particle diameter ratio. The dimensionless groups were formed from the viscosity, particle diameter, flow velocity, density, and pore throat diameter by means of the method of dimensional analysis. The particle Reynolds number and the pore throat-to-particle diameter ratio are the two important dimensionless groups involved in the proposed exponential- and power-law correlations of experimental data. The region below the correlation curve indicates the conditions for non-plugging of pore throats and perforations, and the region above the curve denotes the conditions for plugging. It should be emphasized that plugging always occurs when $0 \leq D_T / D_P \leq 1.0$, because particles having sizes equal or greater than the pore throat or perforation size will cause plugging. However, other factors, such as fluid viscosity and surface forces, may prevent a single particle to move through a pore throat even if the particle size is less than the pore throat size. Therefore, the vertical intercepts of Eqs. 20 and 21 may assume values equal or greater than 1.0. For pore throat to particle ratio greater than 1.0, the plugging correlation plots physically start by intersecting the y axis above zero. The basic aim of this simulation is to correlate the fundamental reservoir rock properties such as porosity and permeability with the invasion of fine particles. For this reason, the deposition of particles due to fines migration into the pore spaces should be determined with respect to time. However, it is more accurate to consider the deposition in two different pathways. This requires a finite difference solution of a partial differential equation at the initial condition particle deposition inside the plugging and

non plugging pathways is equal to zero at the beginning of the mud circulation process. The differential equation for plugging equation has many parameters such as pore throat plugging constant, pore filling rate, particle concentration, and flow velocity. The differential equation of particle deposition includes additionally the deposition and erosion constants, a sufficient value of shear stress to mobilize the particles. Once the particle deposition rate is determined, permeability and porosity can be correlated particle deposition. The equations used in the development of the simulator are given below:

5.2 The Governing Equations in Fines Migration Simulation

The partial differential equations were solved by the method of lines. The method can be summarized as follows: The numerical method of lines is a technique for solving partial differential equations discretizing in all but one dimension, and then integrating the semi-discrete problem as a system of ordinary differential equations or analytical equations. A significant advantage of the method is that it allows the solution to take advantage of the sophisticated general aim of methods and software that have been developed for numerical integration of ordinary differential equations or analytical equations. For the partial differential equations to which the method of lines is applicable, the method typically proves to be quite efficient. It is necessary that the partial differential equation problem be well-posed as an initial value (Cauchy) problem in at least one dimension, since the ordinary differential equation and differentially

analytical equation integrators used are initial value problem solvers. This rules out purely elliptic equations such as Laplace's equation, but leaves a large class of evolution equations that can be solved quite efficiently. Basically the solution by method of lines proposes to reduce the partial differential equations with many dependents into a single dependant problem one at a time. The programme can be operated as follows: First of all, basic parameters should be entered as input file. A sample input file is given in Table-6. The porous medium is considered as incompressible, isotropic and homogeneous. There are basically two different pathways depending on the mechanisms of fines migration retention.

The porous media is assumed to include plugging and non-plugging pathways. The simulation model is a pore scale model. No fracture or worm-hole existence is considered. Darcy flow conditions exist. The fluids are assumed incompressible. One dimensional solution is applied along the core plug. Cartesian coordinate system is used. The core plugs were simulated using 20 grid blocks.

The following equations proposed by Civan and Nguyen (2005) were considered in the mathematical model.

$$\phi_p = \phi_{po} - \varepsilon_p \quad (1)$$

$$\phi_{np} = \phi_{npo} - \varepsilon_{np} \quad (2)$$

ε_p and ε_{np} represent the fractions of the bulk volume occupied by the deposits. Thus the instantaneous porosities are given by the equations 1 and 2.

$$f_p = \phi_p / \phi \quad (3)$$

$$f_{np} = \phi_{np} / \phi \quad (4)$$

The fractions of the bulk volume containing the plugging and non plugging pathways can be approximated by the equations 3 and 4.

$$\phi = \phi_p + \phi_{np} \quad (5)$$

The total instantaneous porosities are given by equation 5.

$$\varepsilon = \varepsilon_p + \varepsilon_{np} \quad (6)$$

$$\phi = \phi_{po} + \phi_{npo} \quad (7)$$

The total deposit volume fraction and the instantaneous available porosity are given by equations 6 and 7.

$$\frac{\partial \varepsilon_p}{\partial t} = k_p u_p \sigma_p \phi_p \quad (8)$$

The rate of deposition in the plugging is given by equation 8. In this equation deposition rate constant, velocity and porosity are constant values instantaneously. The particle concentration term and rate of deposition of plugging particles are the unknown parameters. The Mathematica 4.2 uses two independent variable solver module in this type of partial differential equations by numerical iteration. The initial condition for the solution of this equation is given by equation 9.

$$\varepsilon_p = \varepsilon_{po}, t=0 \quad (9)$$

At time, $t=0$, the fraction of depositing particles are assumed as the total fraction these particles in the slurry at the first grid block. As the time ellapses, this fraction changes due to the partial differential equation given by equation 8.

$$\frac{\partial \varepsilon_{np}}{\partial t} = k_p u_{np} \sigma_{np} \phi_{np}^{2/3} - k_e \varepsilon_{np} \phi_{np}^{2/3} \eta_e (\tau_{np} - \tau_{cr}) \quad (10)$$

$$\varepsilon_{np} = \varepsilon_{npo}, t=0 \quad (11)$$

σ_{np} is the volume fraction of the particles flowing through the non-plugging pathways, k_p is the plugging constant and is assumed to be zero when $t < t_p$. t_p is the time when pore throats are blocked by forming particles bridges and jamming. Eq.11 is the initial condition for the solution of Eq.10. The rate of deposition in non-plugging tubes is given by the difference between the rates of surface deposition and sweeping of particles Eq. 10. In this equation, if the non-plugging shear stress is less than or equal to critical shear stress, the second term on the right side of equation 10 vanishes. The first term on the right side of Eq.10 is for the surface deposition and the second term is for the mobilization and sweeping of particles attached to the surface. In this equation k_d , k_e are the surface deposition and mobilization rate constants, respectively. k_e is assigned different than zero for non-plugging shear stress is greater than zero. Otherwise, k_e takes the value zero for non-plugging shear stress is

less than zero. The critical shear stress is the value for the stress above which the non plugging particle start invasion. The power `2/3` on porosity both for surface deposition and mobilization parts was determined by numerical iteration to obtain the finite result. The `NSolve D` module in Mathematica 4.2 changes the power of the equation consecutively together with the solution. Thus, several values between 0 and 1 were tried. The optimum result was obtained at 0.66 which is fractionally 2/3. For values other than this power, the solution can not be found as a finite value, and the software tries to solve the system of equation through an infinite loop. Thus, the programme is locked. However, one advantage of Mathematica is enabling variation of all constant parameters within pre-defined limits to obtain the best fit for the solution of the fraction of depositing particles. However, it should be noted that this power `2/3` is an optimized value and would be numerically found different with a much different set of input file.

$$\eta_e = \exp(-k\epsilon_{np}) \quad (12)$$

A fraction of particles attached to pore surface might be covered by a multilayer particle deposition and therefore prevented from entrainment by the following suspension. The fraction η_e of the uncovered deposits available for the sweeping from the pore surface is obtained by Eq.12. In this equation k denotes the uncovered deposition constant and the ϵ_{np} denotes the fraction of non-plugging depositing particles.

$$q = -\frac{KA\Delta P}{\mu L} \quad (13)$$

Darcy's equation was used for the determination of flow rate through the core is determined by using the filtration pressure on Darcy's equation 13.

$$\tau_{np} = k^i (8V_{np} / D_{np})^{n^i} \quad (14)$$

$$V_{np} = u_{np} / \phi_{np} \quad (15)$$

The non-plugging shear stress for the solution of Eq.10 is given by Eq.14. The velocity of the non-plugging particles per non-plugging porosity is given by Eq.15.

$$\frac{\partial \varepsilon_p}{\partial t} = (c_1 + c_2 \varepsilon_p) u_p \sigma \quad (16)$$

$$\frac{\partial \varepsilon_{np}}{\partial t} = c_3 \sigma_{np} - c_4 (u_{np} - u_c) \varepsilon_{np} \quad (17)$$

The solutions of these equations were performed by method of lines and finite difference calculus. These equations are valid for the interior points $i=1,2,3,\dots,N$ with the initial conditions. Eq.8 and Eq.10 had been earlier proposed by Gruesbeck and Collins (1982) in the forms of Eq, 16 and 17 with arbitrary constants rather than physical parameters. Civan and Nguyen (2005) improved these equations and implemented the surface deposition rate constant and the entrainment constant. Thus, the equation is physically more realistic.

$$K_p = K_{po} \exp[-\alpha(\phi_{po} - \phi_p)^{n_1}] = K_{po} \exp(-\alpha \varepsilon_p^{n_1}) \quad (18)$$

$$K_{np} = K_{npo} (\phi_{np} / \phi_{npo})^{n_2} = K_{npo} (1 - \varepsilon_{np} / \phi_{npo})^{n_2} \quad (19)$$

The permeability of the plugging and the non- plugging pathways were proposed by Eqs.18 and 19, respectively Civan and Nguyen (2005). In these equations n_1 and n_2 are empirical parameters. The rapid permeability reductions behind the prevented pore throats are expressed. Throughout these equations permeability and the fraction of depositing particles are correlated.

$$\beta_{cr} = A_1 (Re_p)^{B_1} + C_1 \quad (20)$$

$$\beta_{cr} = A_2 \{1 - \exp[-B_2 (Re_p)]\} + C_2 \quad (21)$$

The ratio of pore throat to particle size diameter and particle Reynold`s number are correlated by Eqs. 20 and 21.

Table 6 Representative input file for the simulation

Parameters	Values	Parameters	Values
Core Length, cm	7.0	$\rho_p, \text{kg/m}^3$	2825
Core Diameter, cm	3.81	μ, cp	5
ϕ_{po}	0.1	σ_{po}, ppm	0.049
ϕ_{npo}	0.2	σ_{npo}, ppm	0.0045
K_{po}, D	1.0	$\sigma_{slurry}, \text{ppm}$	9.4×10^{-7}
K_{npo}, D	16.7	$\varepsilon_{po}, \text{ppm}$	1.26×10^{-6}
$\alpha, \text{ppm-cm}^{-1}$	10	$\varepsilon_{npo}, \text{ppm}$	0.0184
$\delta, \text{ppm-cm}^{-1}$	0.0001	τ_{cr}, Pa	20
$k_d, \text{ppm-cm}^{-1}$	1.28	$U, \text{cm/sec}$	0.5

SI Conversion Factor:

$$1 \text{ Pa} = 1 \text{ N/m}^2 \quad 1 \text{ kg/m}^3 = 10^{-3} \text{ g / cc} \quad 1 \text{ cp} = 1.81\text{E} -07 \text{ g/cm-sec.}$$

The important thing is to pay attention to the precision of the programme and the significant figures. The accuracy range should be less than the precision. Otherwise, the program can give numerical error or may not run properly. The basic partial differential equation line is activated for running the program. The run-time may take 3-5 minutes according to the maximum time interval specified by the partial differential equation. There are test stages for different parameters and their plots in the control section of the program. These statements should be checked right after the program has completed running. It should be noted that

each time the program is turned on, it should be run and saved for obtaining solutions. Mathematica is a version sensitive symbolic language program. This simulator was developed using Mathematica 4.2 version. After being sure that the program is running and giving reasonable results, the output files can be constructed. The easiest way to visualize whether the program works or not is to observe the porosity and permeability test plots right under the basic partial differential equation statement. If the porosity and permeability values start declining from the input values, then it can be stated that program is running. The output files are named as out put mud files. The major output mud file command is followed by the name of the specifically varying function. It should be noted that the simulator analyses the core in 20 grid blocks. So every output file should also have a grid block name from 1 to 20. For example when, output file with a name output mud $K_{np}[E_{np5}(t)]$ is seen , K_{np} denotes non plugging permeability, as a function of the non plugging particle deposition fraction at a time t , in the 5th grid.

The advantages of these output files are their transferability to Microsoft Excel Spread Sheets and processibility. The run and saved files are opened are stored in Program Files , Wolfram, Mathematica 4.2 respectively. Then these files should be opened in .xls format. While opening these files, spaced delimited options should be chosen. Even high-tech computers are not adjusted for this much data load, so they may display `insufficient memory error`. In this case, the memory can be increased from the control panel of the computer. These files are opened for each grid for certain period of dynamic mud circulation. Thus a function such as porosity, permeability, and particle concentration can be

obtained along the core sample at various time intervals. Thus all the required data is obtained. It is possible to plot permeability vs time, porosity vs time, particle concentration vs time and permeability vs length, porosity vs length, particle concentration vs length. Damage ratio vs dynamic filtration pressure can be plotted after calculating the change in permeability with respect to its initial value. The plugging and non-plugging pathways concept is depicted in Figures 4 and 5. The fine particles accumulate in the plugging pathways which results in ultimate plugging of the throats. However, in non-plugging pathways, the cross sectional area of the open pore throat decreases as the fines deposit. This phenomenon reduces the interconnected porosity and permeability of the system. In a rock matrix or core system there may be made up of a combination of many these plugging and non plugging pathways.

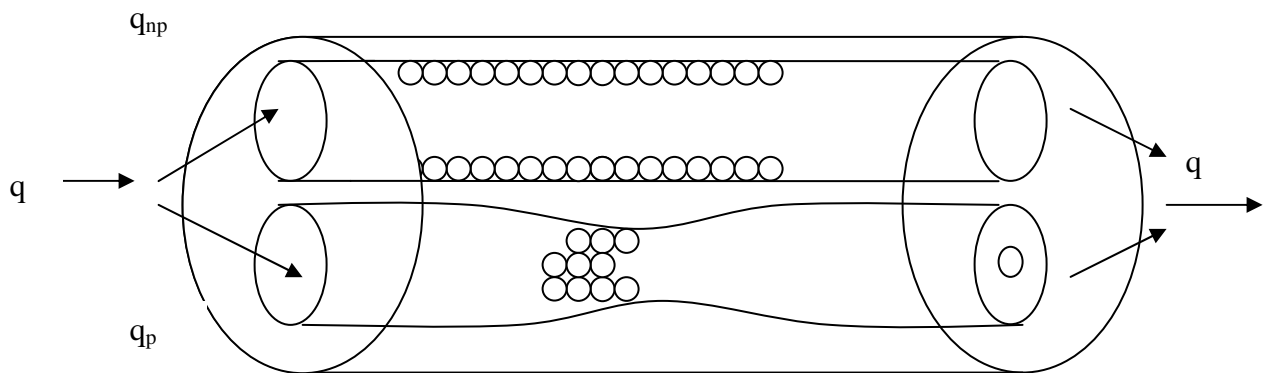


Figure 4 The Plugging and non-plugging pathways along the core sample

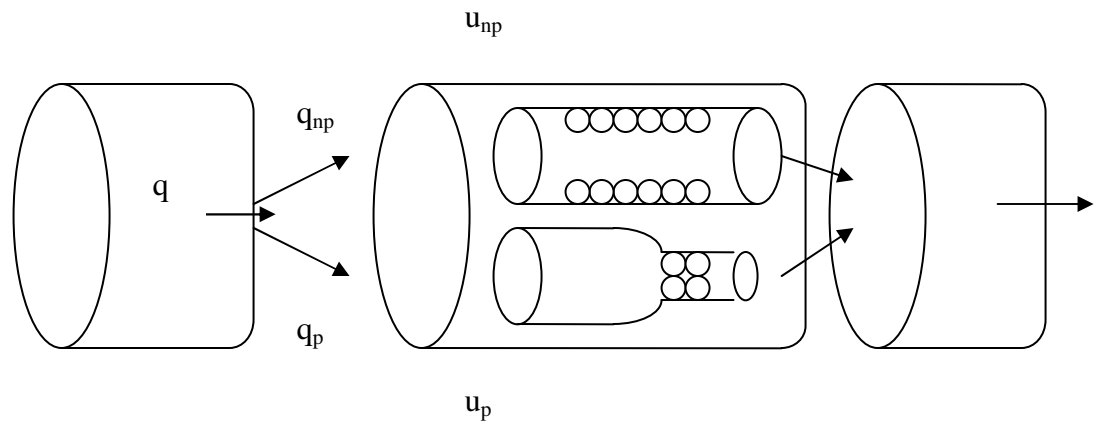


Figure 5 Non-Plugging and plugging paths realization in a core

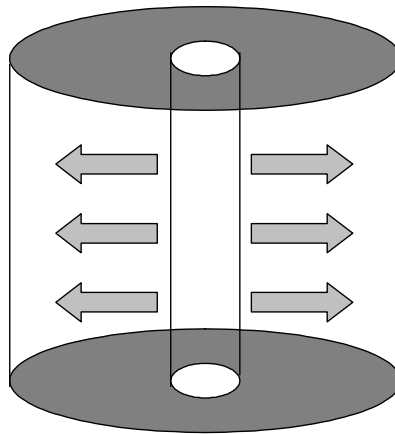


Figure 6 Fines migration and invasion into formation in vertical wells

As drilling fluid is circulated with pressure, the fine particles invade into the porous media. In vertical petroleum wells, this invasion is radially

inward towards the formation (Figure 6). The effectiveness of this invasion is higher near the well and becomes smaller as it is moved away from the well. Fines migration in horizontal wells is similar to that in vertical wells. Fines migration is maximum near the well. The migration is minimum at the end of the well (Figure 7). In the scope of this thesis, both horizontal and vertical core holder systems were used. However, the experimental results are almost same. This may be because of the scale of the experimental set-up. The major difference between the horizontal and vertical flow is the gravity effect. But since the sizes of the both horizontal and vertical core holders are really small when compared to that in the field. Thus, the gravity effect was neglected.

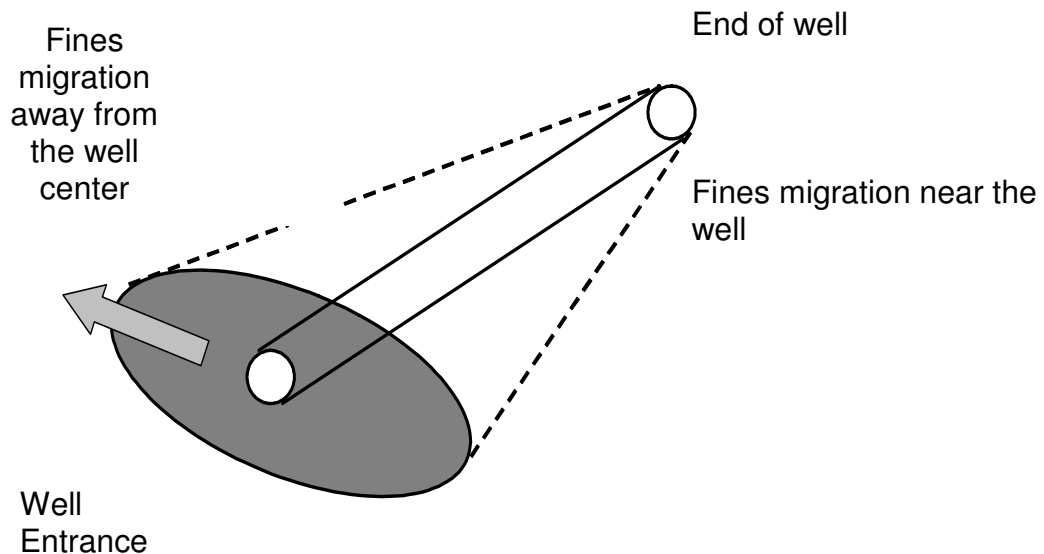


Figure 7 Fines migration and invasion into formation in horizontal wells

5.3 Average Particle Deposition and Overall Pressure Difference In A Core Plug

In the mathematical modelling of the pressure difference and particle deposition within the core sample the following equations were used. Total fraction of depositing particles are given as the sum of the plugging and non-plugging fractions. Then, the integral is applied along the core length `L` Eq.22. Darcy`s flow equation is used to correlate the instantaneous particle deposition effect on permeability and pressure Eq 26.

$$\varepsilon(t) = \varepsilon_p(t) + \varepsilon_{np}(t) = \frac{1}{L} \int_0^L [\varepsilon_p(t) + \varepsilon_{np}(t)] dx \quad (22)$$

The core length average cumulative volume of particles deposited per unit volume of porous media is defined by Eq.22. In experimental studies using core plugs, generally the total amount of particle deposition is given by the difference in particle concentrations between the injected and the effluent solutions. The overall pressure drop across a core plug is directly measured through the flooding experiments.

$$u = \frac{q}{A} = -\frac{K(x,t)}{\mu} \frac{\partial P}{\partial X} \quad (23)$$

The pressure drop across a core plug is calculated through Darcy`s law as in Eq.23. The advantage of interpreting the Darcy`s law in the above

format is the availability for defining permeability at arbitrary length and time from the start of the dynamic circulation.

$$\Delta P(t) = P_{out} - P_{in} = \int_{P_{in}}^{P_{out}} \partial P(x, t) = -\mu u \int_0^L \frac{dx}{K(x, t)} \quad (24)$$

The Eq.23 is integrated over the core length at constant flow rate. Thus Eq.24 is obtained. Eq. 24 is the integrated form of Eq.23.

$$\Delta P_0 = \Delta P(0) = -\mu u \frac{L}{K_0} \quad (25)$$

The initial or the undamaged permeability K_0 can be directly measured by core flooding. The initial pressure drop across the core plug can be measured as well. Thus, Eq.24 can be integrated between the initial inlet and outlet conditions of the core plug during flood tests. Hence, Eq.25 is obtained in terms of the measurable initial inlet conditions. So, the initial pressure difference across the core is represented in terms of viscosity, velocity, core length and the initial permeability.

$$\frac{\Delta P(t)}{\Delta P_0} = \frac{K_0}{L} \int_0^L \frac{dx}{K(x, t)} \quad (26)$$

Hence, by combining Eqs.24 and 25, Eq.26 is constructed. Thus, the overall pressure drop across the core is expressed in terms of the instantaneous permeability and distance from the drilling fluid circulation point.

5.4 Numerical Solution

For a given set of input file as in Table 6, various phenomenological parameters introduced by Eqs.8,9,10,11,26,27,28,29,30 can be solved simultaneously to obtain the quantities ε_p , ε_{np} , σ_p and σ_{np} as a function of time and distance along the core length by the equations proposed by Civan and Nguyen (2005). Cumulative particle deposition and over the core length and the total pressure drop can be obtained by the direction integration of the Eqs.22 to 25. The solutions of these partial differential equations give out the amounts of particle depositions in different pathways of the core plugs. On the hand , instantaneous fractions of the plugging and non- plugging pathways, porosity reduction and permeability impairments are obtained.

$$\frac{d\varepsilon_{p,i}}{dt} = (\delta + k_{p,i}\phi_{p,i})u_{p,i}\sigma_{p,i} \quad (27)$$

$$\phi_{p,i}\frac{d\sigma_{p,i}}{dt} + (1-\sigma_{p,i})\frac{d\varepsilon_{p,i}}{dt} = -u_{p,i} + \frac{(\sigma_{p,i+1} - \sigma_{p,i-1})}{2\Delta x} + K(\sigma_{p,i} - \sigma_{np,i}) \quad (28)$$

$$\frac{d\varepsilon_{np,i}}{dt} = k_d u_{np,i}\sigma_{np,i}\phi_{np,i}^{2/3} - k_{e,i}\varepsilon_{np,i}\phi_{np,i}^{2/3}\eta_{e,i}(\tau_{np,i} - \tau_{cr}) \quad (29)$$

$$\phi_{np,i}\frac{d\sigma_{np,i}}{dt} + (1-\sigma_{np,i})\frac{d\varepsilon_{np,i}}{dt} = -u_{np,i}\frac{\sigma_{np,i+1} - \sigma_{np,i} - 1}{2\Delta x} - K(\sigma_{p,i} - \sigma_{np,i}) \quad (30)$$

The numerical simulation of the particle migration and deposition in porous media by using the equations proposed Civan and Nguyen (2005) was conducted on a linear grid system, by considering the discretized equations. The governing equations are coupled, non-linear, first order partial differential equations. For the numerical solution, the method of lines is applied. This method is a simplification to non-linear partial

differential equations as first order ordinary differential equations. So, the central finite difference formulae are applied for the determination of the derivatives. The resulting system was solved using Runge-Kutta method. Mathematica 4.2^R was used to solve the resulting ordinary differential equations. One of the tools of this software is NDSolve which provides numerical solutions to ordinary differential equations. These equations are valid for the interior points $i=1,2,3,\dots,N$ with the initial conditions. To make the application for further researchers more convenient, the equations used in the solution scheme is simplified as suggested by Civan and Nguyen (2005).

The mathematical simplifications and boundary conditions are given by the following equations:

The initial conditions are given through Eqs.31 to 34.

$$\varepsilon_{p,i} = \varepsilon_{po}, \quad t = 0 \quad (31)$$

$$\varepsilon_{np,i} = \varepsilon_{npo}, \quad t = 0 \quad (32)$$

$$\sigma_{p,i} = \sigma_{po}, \quad t = 0 \quad (33)$$

$$\sigma_{np,i} = \sigma_{npo}, \quad t = 0 \quad (34)$$

$$\frac{d\varepsilon_{p,i}}{dt} = A_{p,i} \quad (35)$$

Eq.27 is simplified as in Eq.35. The right hand side of Eq.35 is given as in Eq.36.

$$A_{pi} = (\delta + k_{p,i} \phi_{p,i}) u_{p,i} \sigma_{p,i} \quad (36)$$

$$\frac{d\varepsilon_{np,i}}{dt} = A_{np,i} \quad (37)$$

Eq.29 is simplified as in Eq. 37. The right hand side of the Eq.37 is given as in Eq.38.

$$A_{np,i} = k_d u_{np,i} \sigma_{np,i} \phi_{np,i}^{2/3} - k_{e,i} \epsilon_{np,i} \phi_{np,i}^{2/3} \eta_{e,i} (\tau_{np,i} - \tau_{cr}) \quad (38)$$

Eq.28 is simplified by considering the right hand side in term of grouping letters as in Eq. 39 and Eq.40.

$$B_{p,i} \frac{d\sigma_{p,i}}{dt} + C_{p,i} \frac{d\epsilon_{p,i}}{dt} = D_{p,i} \quad (39)$$

The coefficients of the spatial derivatives are given in Eq.40 to 43.

$$B_{p,i} = \phi_{p,i} \quad (40)$$

$$B_{np,i} = \phi_{np,i} \quad (41)$$

$$C_{p,i} = (1 - \sigma_{p,i}) \quad (42)$$

$$C_{np,i} = (1 - \sigma_{np,i}) \quad (43)$$

The right hand side of the Eq.39 is given Eqs.44 to 45 as the results of central finite difference applications.

$$D_{p,i} = -u_{p,i} + \frac{(\sigma_{p,i+1} - \sigma_{p,i-1})}{2\Delta x} + K(\sigma_{p,i} - \sigma_{np,i}) \quad (44)$$

$$D_{np,i} = -u_{np,i} \frac{\sigma_{np,i+1} - \sigma_{np,i-1}}{2\Delta x} - K(\sigma_{p,i} - \sigma_{np,i}) \quad (45)$$

The spatial derivative of the particle concentration is obtained by the central finite difference application as in Eq.46.

$$\sigma_{np,l-1/2} = \sigma_{in} = \frac{\sigma_{np,o} + \sigma_{np,l}}{2} \quad (46)$$

CHAPTER 6

STATEMENT OF THE PROBLEM

In this thesis, estimation of the permeability damage ratio due to the differential filtration pressure and near well-bore formation damage is aimed. This type of formation damage depends upon the invasion of the fine particle into the porous media under the influence of the differential pressure that arises between the circulation drilling fluid and the interior walls of the well. There are many physical parameters such as particle concentration variation in porous media, fraction of depositing particles composition and physical properties of the drilling fluids, the type of the formation, initial permeability and the porosity of the circulation rate, reservoir longitudinal distance. In this thesis, a set of dynamic circulation experiments were conducted with three different drilling fluids and the obtained experimental data were analyzed by a numerical simulator. The damage profiles of the three drilling fluid types were obtained and plotted with respect to filtration pressure. Plugging criteria concept was introduced for these fluids using the pore throat plugging phenomena. Digital X-Ray image subtraction technique was applied on different sections of the core plugs before and after dynamic circulation to observe the invasion fines particles. The proposed damage ratio charts and correlations facilitate the estimation of permeability reduction phenomena.

CHAPTER 7

RESULTS AND DISCUSSION

Formation damage is a phenomenon which occurs in various stages of petroleum engineering such as drilling, well completion, well stimulation and production. In this study, the formation damage analysis was performed from drilling point of view. However, this is a combined discipline with both reservoir and drilling engineering. In the scope of this thesis, formation damage was analyzed from micro scale to macro scale. The micro scale deals with what is actually happening to the reservoir pore space. Thus, the analysis scheme was studied as follows:

1. Pore throat plugging and plugging criteria.
2. Dynamic drilling fluid circulation and fines migration experimentally and numerically.
3. X-Ray analysis of the core samples for formation damage analysis.

In this study three different water based drilling fluids were used (Table-1). The fluids include combinations of bentonite, water, CMC (Carboxy Methyl Cellulose), and Polymer-XT. However, it is required to know the rheological properties of the fluids and the most suitable polymer should be chosen for detailed formation damage analysis.

7.1 The Rheological Properties of The Drilling Fluids

The rheological properties of the three drilling fluids were measured and are given in Tables 7 and 8, respectively.

Table 7 Fann Viscometer measurements of the Drilling Fluids

Shear Rate (RPM)	Shear Stress Measurements (lbf/100ft ²)		
	Drilling Fluid-1	Drilling Fluid-2	Drilling Fluid-3
3	3	4	23
6	5	9	24
100	7	15	75
200	8	22	88
300	11	28	100
600	21	46	125

Table 8. Filter loss measurements of the drilling fluids

Time (minute)	Filter Loss Measurements (cc)		
	Drilling Fluid-1	Drilling Fluid-2	Drilling Fluid-3
0.5	4.5	1.0	1.0
1	4.5	1.5	2.0
3	5.5	2.0	5.4
5	6.5	3.0	6.0
7.5	8.0	4.0	7.0
10	9.5	4.2	7.9
15	12.0	5.4	8.6
30	15.5	9.2	11.6

7.2 The Effects of CMC

One other type of drilling fluid type used in the research is CMC added water based drilling fluid. For the determination of optimum CMC concentration, different amounts of CMC were added in water based drilling mud. The rheological properties, shear stress and shear rate properties were measured. 1,3 and 4 g of CMC samples were added into water based bentonite muds. It was observed that as CMC concentration increases the shear stress reached its maximum value at 4 g/350 cc. Nevertheless the bubbling and flocculation of the fluid with this concentration does not allow using this higher value. The fluid loss kept decreasing as CMC concentration increases, but the rate of decrease is too low to notice after 1 g CMC (Table 9). Shear stresses of the fluid samples were seen to increase with increasing CMC content (Figure 8). Filtration loss displayed a significant drop with increasing CMC amount. As the CMC concentration increased, the fluid concentration kept increasing with respect to time. However, at 4g /350 cc CMC concentration, the filtration loss displayed a constant trend after 15 minutes (Figure9). Although constant filtration value was obtained at 4g CMC, the mud lost its stability at this value. The fluid loss at the end of 30 minutes with 1 g CMC is very close to that of 4g CMC. Thus, optimum CMC concentration was selected as 1 g by considering the drops in filter loss. The end of horizontal segment was chosen to be the optimum stable CMC concentration (Figure 10).

Table 9 CMC-added, water based drilling filtration loss readings.

TIME (minute)	Filtration Loss Readings (Bentonite+Barite+Water+CMC mixed drilling fluids)		
	CMC concentration		
	1 g CMC	3 g CMC	4 g CMC
0.5	1.0	1.1	2.0
1	1.5	1.1	2.5
3	2.0	1.6	4.2
5	3.0	2.4	5.0
7.5	4.0	2.7	6.0
10	4.2	2.9	7.2
15	5.4	4.4	7.7
30	9.2	8.4	7.8

Fluid loss results of the CMC mud were obtained at three different concentrations (Table 9). In fact, It was observed that as the mass of CMC increased, the total fluid loss decreased at the end of 30 minutes. This is valid especially for the cumulative filter loss. It was seen that fluid loss amount doubled after the first 15 minutes. The fluid loss with 4 g of CMC after 30 minutes gives out the least fluid loss. But, the drilling fluid becomes very thick and it is not possible to circulate. 9.2 cc fluid loss after 30 minutes with the presence of 1g CMC could be used easily in the experimental set-up. 4.5 and 5g CMC concentrations were tried for the determination of the upper limit of the CMC concentration. The drilling fluid became immobile and CMC could not be mixed homogeneously with

the slurry. Thus, although high shear stresses are obtained above 4 g of CMC concentration, the practically applicability of the drilling fluid is lost. Shear stress and measurement becomes very hard. The API Fann Viscometer can not rotate at different shear rates as it has to do, due to the adhesiveness and the high viscous nature of the prepared slurry.

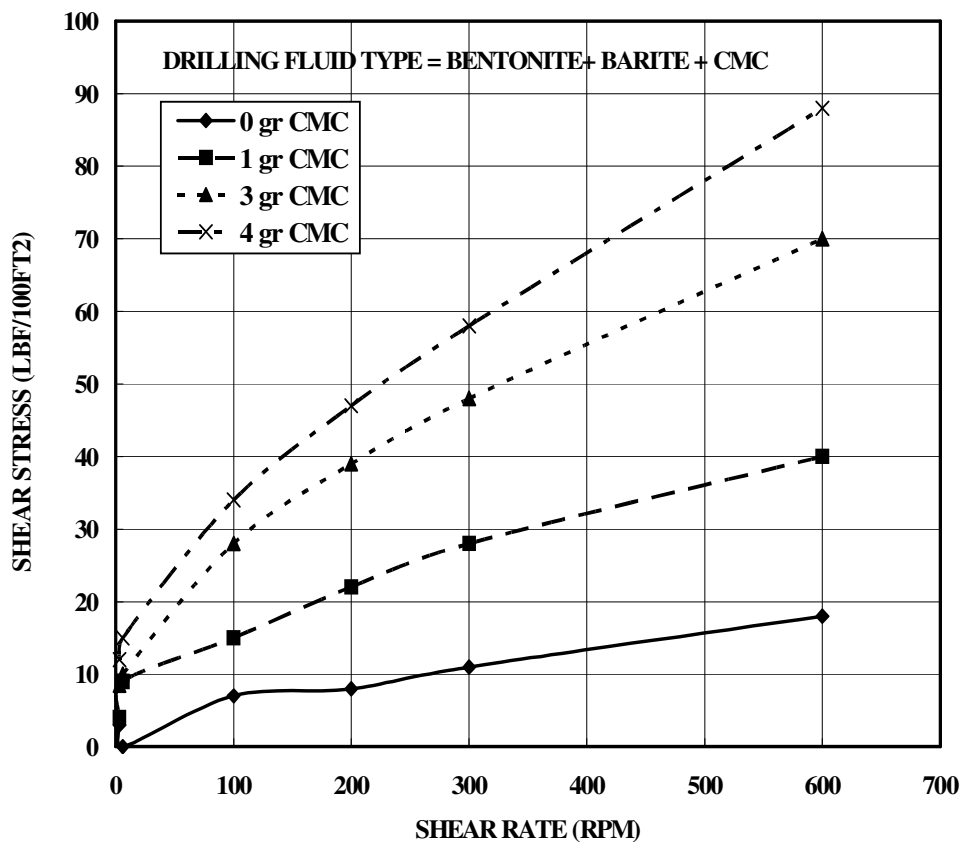


Figure 8 Shear stress vs shear rate in CMC added water based drilling fluid.

It was observed that shear stress increases as the CMC concentration increases. However, if more than 4 g of CMC is added, the

fluid loses its property and becomes almost immobile. In addition to this excess amount of CMC can not be mixed with the mud homogeneously. Experimentally, it was observed that 1g CMC /350 ml of drilling fluid slurry is sufficient for appropriate for optimum rheological efficiency.

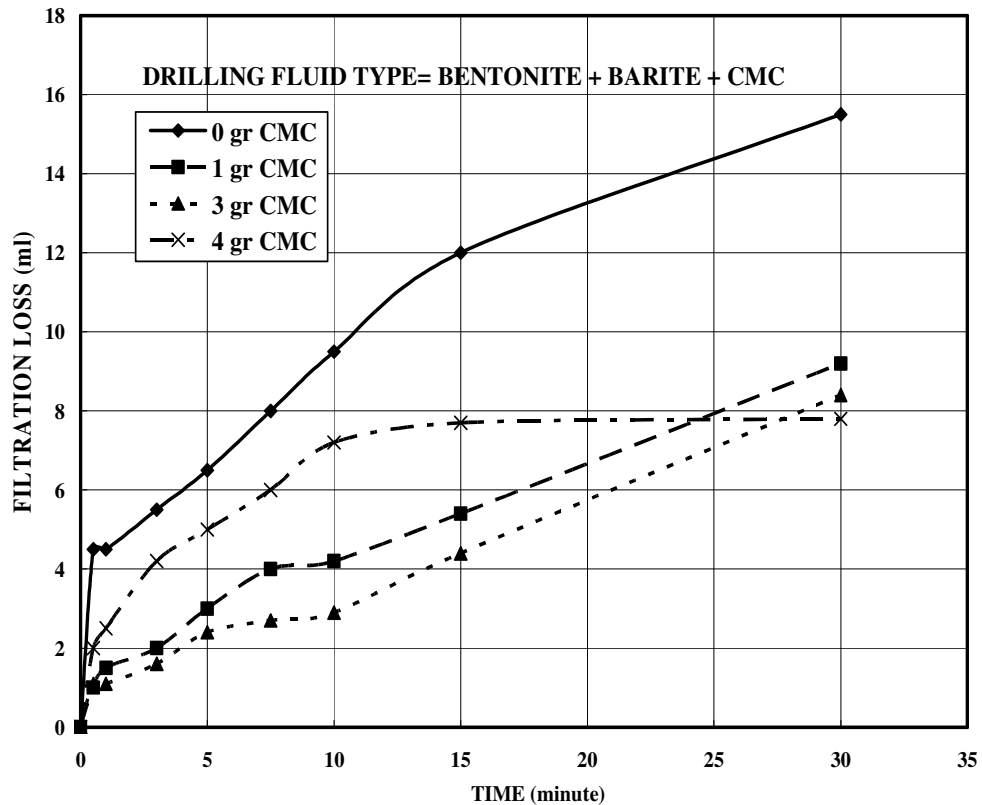


Figure 9 Filtration Loss vs Time in CMC added water based drilling fluids

Filtration loss decreases as the CMC concentration increases. From fluid loss point of view, 4 g of CMC gives a reasonable fluid loss.

However, the fluid is really thick at this concentration. 1g CMC concentration is the optimum value for both gel strength and fluid loss adjustment (Figure 10).

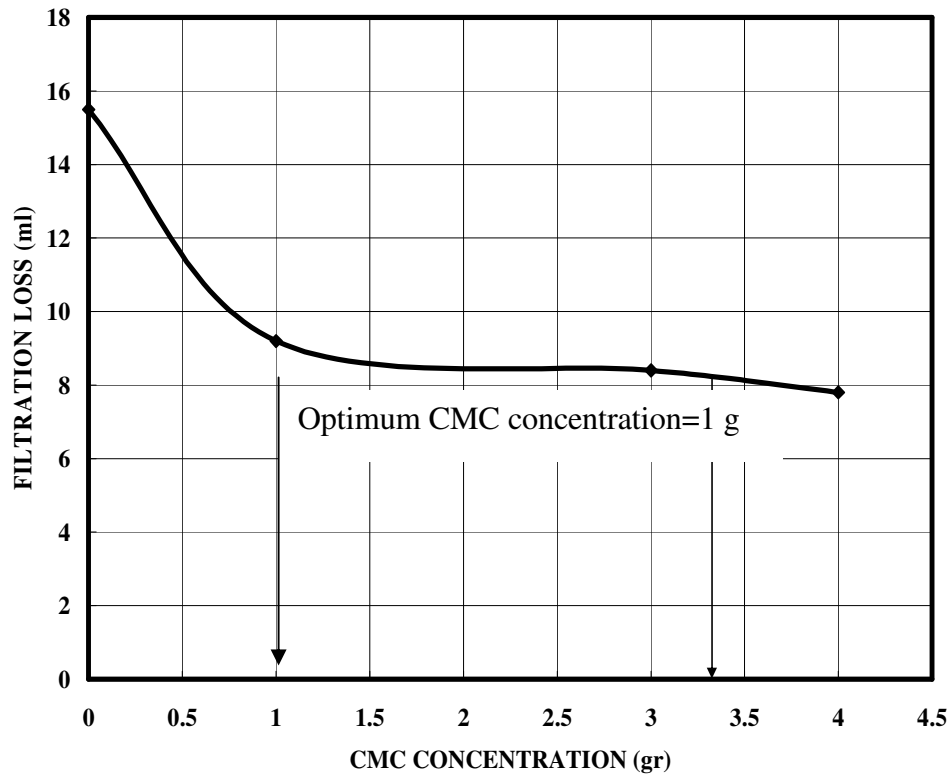


Figure 10 Effect of CMC concentrations on filtration loss

CMC is basically used for increasing the gel strength and viscosity of the drilling fluids to attain them thixotropic property to keep the cuttings suspended in case of circulation stop and carrying them to the surface efficiently. The filtration tests were conducted due to API specifications in the presence of CMC. 350 ml water 22.5g bentonite

and 45.8 g barite was used as the major additives during the preparation of the base drilling fluids. The CMC concentration was changed from 0 to 4 g (Figure 10). This plot was constructed to obtain the optimum CMC concentration for less invasive and high viscous drilling fluid preparations. API filter press apparatus was used. Static filtration was conducted at 100 psi driving force for 30 minutes. It was observed that as the CMC concentration increased from 0 to 1 g, there is a filtration reduction 15.4 ml to 9 ml. Between 1g and 3 g of CMC concentration, the filtration loss is almost constant at the filtrate value 9 ml. However, as the CMC concentration increases the drilling fluid is observed to lose its homogeneity and mobile characteristic. After 3g of CMC concentration, there is a slight reduction in the filtrate loss, but even though the filtrate loss is reduced, higher concentrations of CMC have adverse effects on the applicability of the drilling fluid circulation.

7.3 Polymer Based Drilling Fluids and Determination of Polymer Concentration

One other type of drilling fluid used in the research is Polymer added, water based drilling fluid. Different masses of different polymer types were added in to water based drilling fluid (bentonite+barite+water). The rheological properties of all of the prepared fluids were measured (Tables 10 and 11). Polymer weights of 0.2, 0.4, 0.6, 0.8 and 1 g were added to the fluids. In the determination of the polymer type, polymers

XT, DSHV and MAC PR produced by Solvadis were used. The shear rate and shear stress readings of these polymers are given in Tables 10, 11 and 12, respectively. As the polymers were added to the bentonite+barite fluids, the shear stress readings were increased, whereas the viscosity of the drilling fluids increased, too. As polymer concentration increased, apparent viscosity has also increased. Shear rate readings at different shear stresses are given in Figure 11. Optimum polymer concentration was chosen as 0.4 g. Filtration loss test results of fluids including XT, DSHV and MACPR with 0.4 g optimum polymer concentration were given in Figure 12. The polymer DSHV affects the fluid loss than the other two in the early periods. The XT polymer gave the most consistent results among the others (Kok et al. 2005). The maximum shear stress profile was obtained with the polymer added drilling fluid as it is plotted in Figure 13, whereas the other two types had closer shear stress values to each other. Figure 14 indicates that the maximum filtration loss was obtained with the conventional bentonite drilling fluid, and CMC added fluid gives the least filtration values.

Table 10 Polymer XT- mixed drilling fluid shear stress readings.

Shear Rate (RPM)	Shear Stress Readings (Bentonite+Barite+Water+Polymer (XT) mixed drilling fluids)				
	Polymer concentration				
	0.2 g	0.4 g	0.6 g	0.8 g	1.0 g
3	19	23	30	38	54
6	18	24	35	45	63
100	65	75	90	100	112
200	70	88	98	110	135
300	87	100	110	130	155
600	103	120	148	180	203

Table 11 Polymer DSHV- mixed drilling fluid shear stress readings.

Shear Rate (RPM)	Shear Stress Readings (Bentonite+Barite+Water+Polymer (DSHV) mixed drilling fluids)				
	Polymer concentration				
	0.2 g	0.4 g	0.6 g	0.8 g	1.0 g
3	11	13	15	22	30
6	14	17	20	23	30
100	25	32	40	50	62
200	40	50	58	67	83
300	45	51	60	72	99
600	72	88	100	110	138

Table 12 Polymer MAC-PR- mixed drilling fluid shear stres readings.

Shear Rate (RPM)	Shear Stress Readings (Bentonite+Barite+Water+Polymer (MAC-PR) mixed drilling fluids)				
	Polymer concentration				
	0.2 g	0.4 g	0.6 g	0.8 g	1.0 g
3	11	13	15	22	30
6	14	17	20	23	30
100	25	32	40	50	62
200	40	50	58	67	83
300	45	51	60	72	99
600	72	88	100	110	138

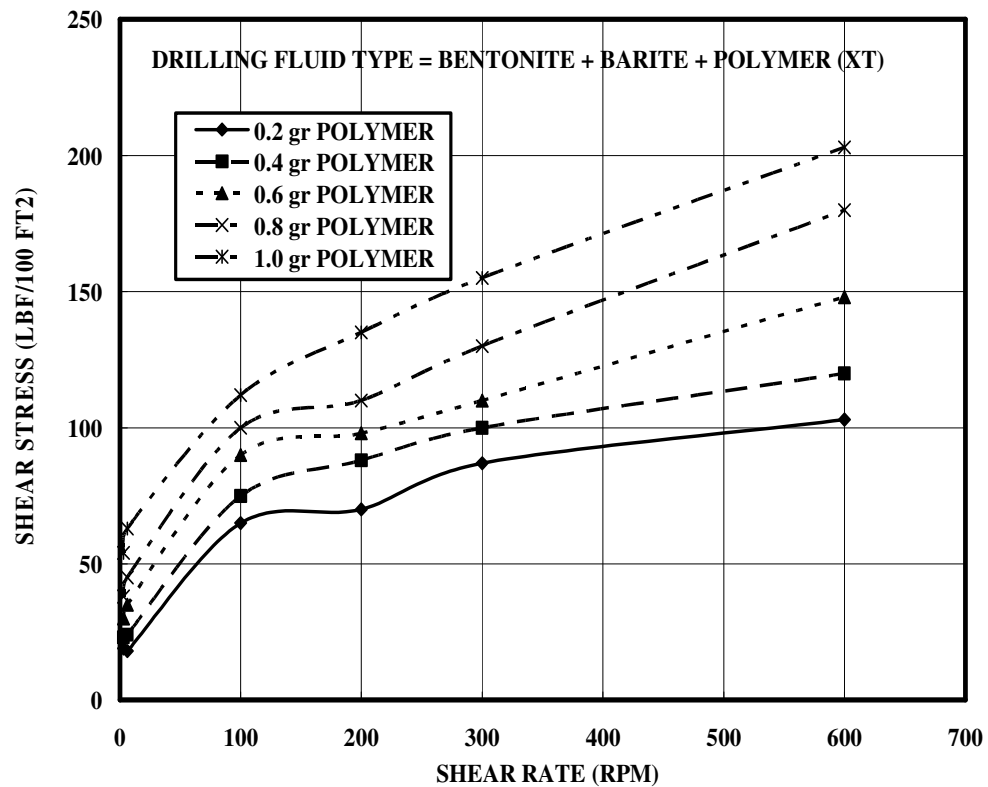


Figure 11 Polymer XT- mixed drilling fluid shear stress shear rate.

The shear stress of the drilling fluid increases as polymer concentration increases (Figure 11). Five different polymer concentrations were tested due to API specifications. It was observed that with polymer concentration less than 0.4 g, the fluid is not strong enough to attain effective gel strength. When more than 0.4 g was used, the drilling fluid became immobile in and very hard to move. Thus, 0.4 g was chosen as the optimum polymer concentration.

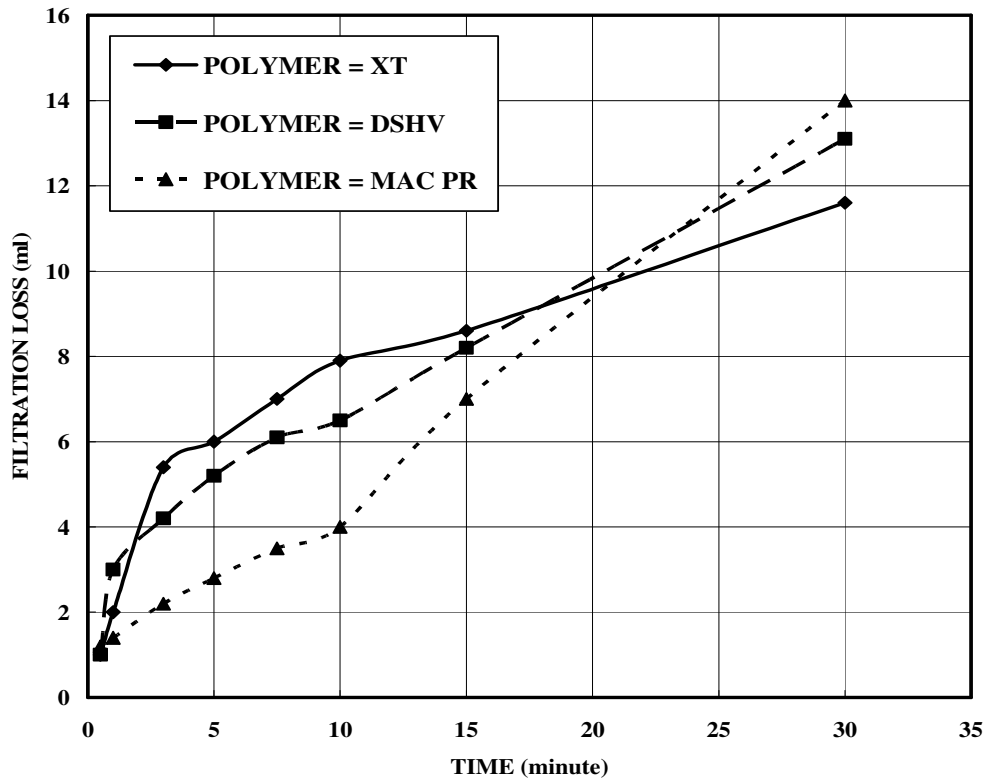


Figure 12 Filtration Loss vs Time in polymer added water based drilling fluids

Other than Polymer-XT, two more polymers supplied were tested, too. However, the minimum fluid loss was obtained with Polymer-XT (Figure 12). The other polymers displayed a sharp increase with respect to time, where the Polymer-XT displayed a smoother and less increase with respect to time. Thus, Polymer-XT mud was chosen to be used for the formation damage tests together with CMC mud and non-treated bentonite mud. A tedious rheological analysis was made for the selection

of optimum polymer type. From formation damage point of view, it is seen that if the fluid loss is high, it is more probable that the fine particles will tend to invade in to the porous media. So, the polymer which gives the least fluid loss is the best choice for detailed formation damage analysis. The general shear stress and fluid loss profiles of the major three drilling fluids selected for formation damage analysis are given in Figures 13 and 14, respectively.

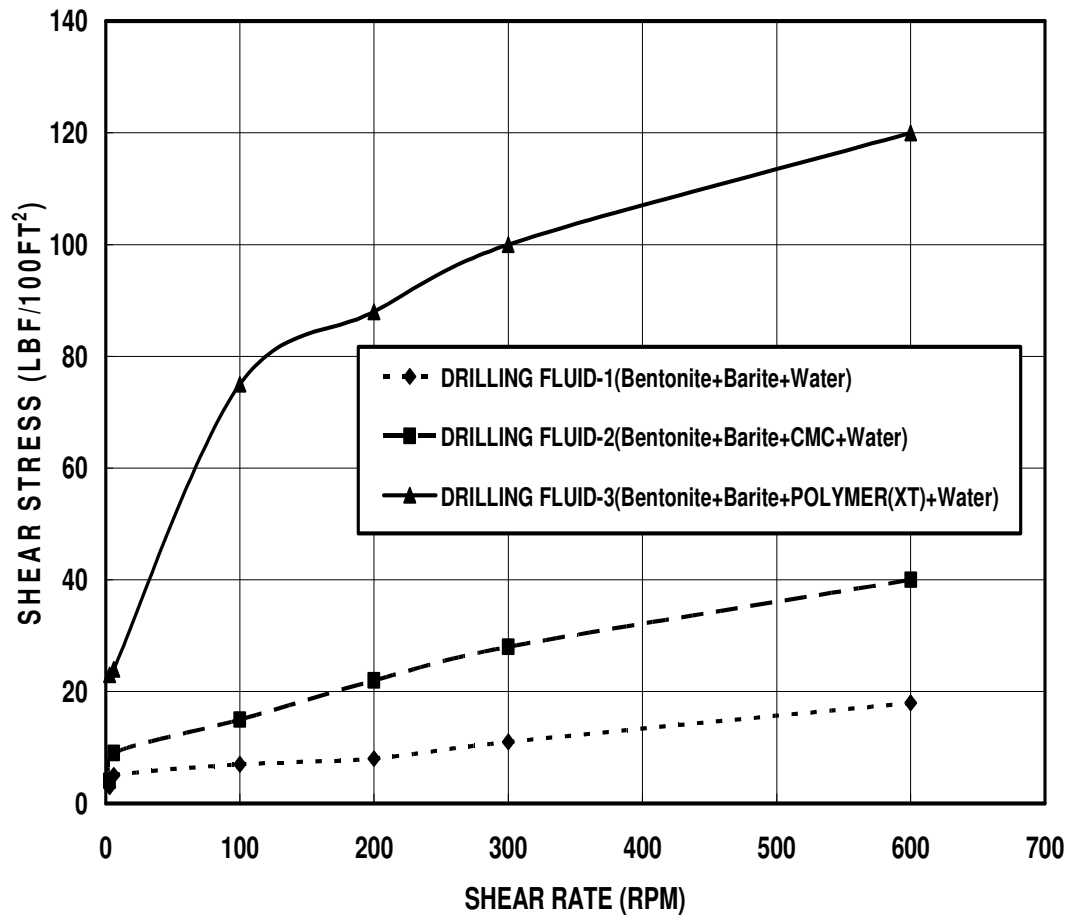


Figure 13 Shear Stress vs Shear Rate Graphs of Drilling Fluids for Formation Damage Analysis

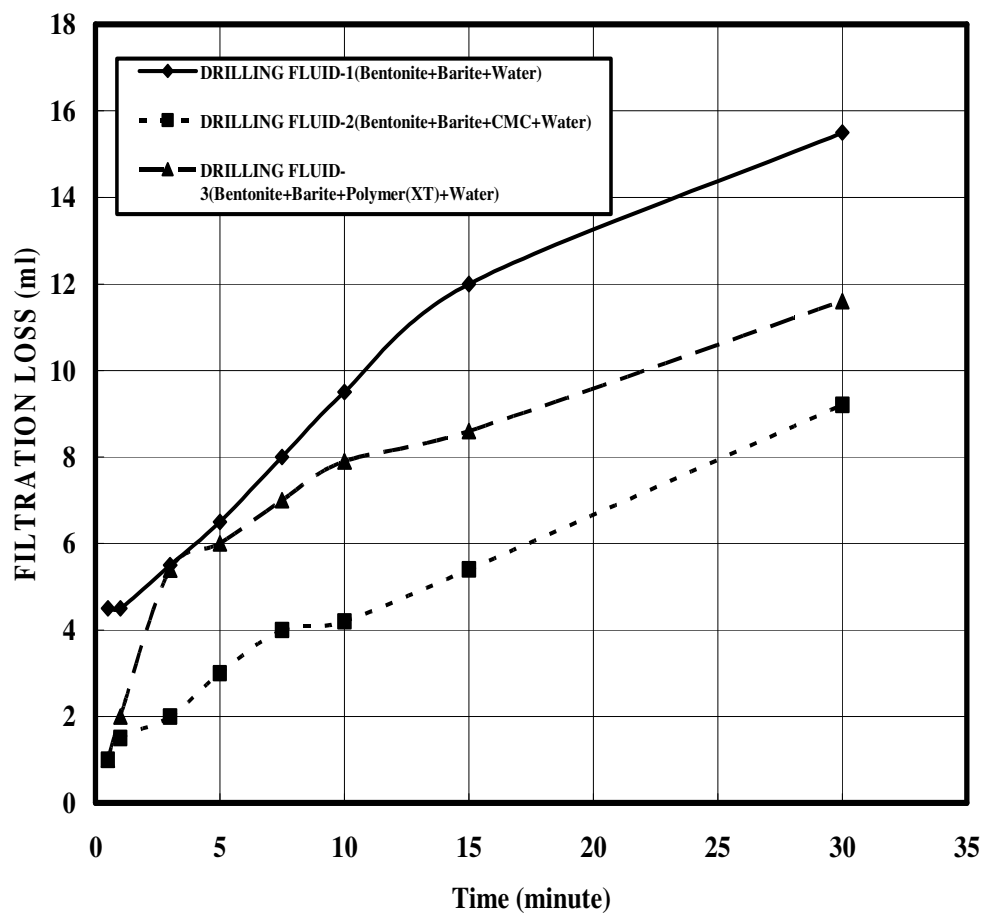


Figure 14 The filtration loss properties of Drilling Fluids for Formation Damage Analysis with respect to time

The three types of drilling fluids (bentonite+water, bentonite+water+CMC and bentonite+water+Polymer-XT) are analyzed rheologically in Figures 13 and 14. The maximum shear stress was obtained with Polymer-XT, and the minimum shear stress was obtained with the non-treated fluid.

The filter (fluid) loss profile is just the reverse of shear stress profile. That is to say, the minimum fluid loss was obtained with the Polymer-XT fluid. Thus it can be said that shear stress and fluid loss properties for a given specific type of fluid are inversely related with each other. These three different water based drilling fluid were subjected to formation damage analysis.

7.4 Pore Throat Plugging By Particles: First Stage Of Formation Damage

Particles at high concentrations and unfavorable flow conditions may plug pores and perforations by bridging across during various well operations including particle-containing water injections and workover activities. This part of the study presents an experimental determination of the conditions leading to plugging and the criteria for effective plugging conditions. The charts of the perforation or pore size to particle size ratio versus the particle Reynolds number are shown to determine the conditions leading to perforation and pore plugging. The experimental data obtained using three water-based drilling fluids and several reported experimental data are analyzed and correlated by means of the power- and exponential-law expressions. Both approaches adequately describe the conditions leading to perforation and pore plugging.

Plugging of perforations and pores of porous media with fine particles migrating within a suspension of particles is frequently encountered during various operations of oil and gas wells including water flooding, drilling, perforation, and work-over. The plugging of

perforations and the pore spaces due to the particle bridging mechanism may cause severe damage to the productivity of the oil and gas wells completed in petroleum reservoirs. Therefore, the operational conditions should be adjusted in a manner to avoid the plugging of pores and perforations by particles. The objectives of this part of the study are to investigate the conditions leading to perforation and pore plugging and develop empirical correlations for the plugging criteria. A schematic view of particle bridging across a perforation is depicted in Figure 15.

In the literature there are two extreme cases of sand packing (Haynes and Gray 1974): These are, no sand particles can be transported into the perforations at zero flow rate and nearly all particles can be transported when the viscosity and the flow rate are sufficiently high to prevent particle settling.

In this section, the second packing approach was applied. The silica flour with calcite aluminum silicates of 2.65g/cc density were used for the sand packing into a steel test tube having a cross-sectional area of 10 cm² and a height of 5 cm. The sand-packed test tube is depicted in Figure 21. An identical packing was also prepared outside the tube to measure the porosity. The packed sample was saturated with water. The dry and wet weights were measured and the porosity of the sand-pack was calculated to be 28% by the volume saturation of the water.

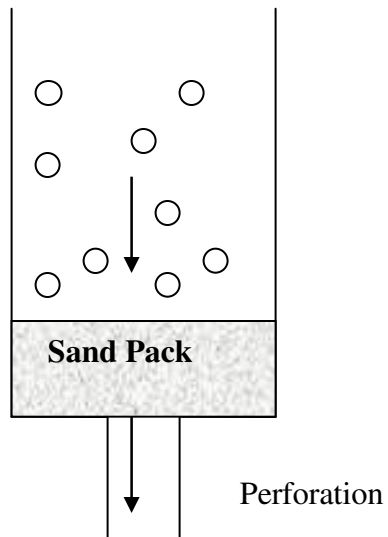


Figure 15-a

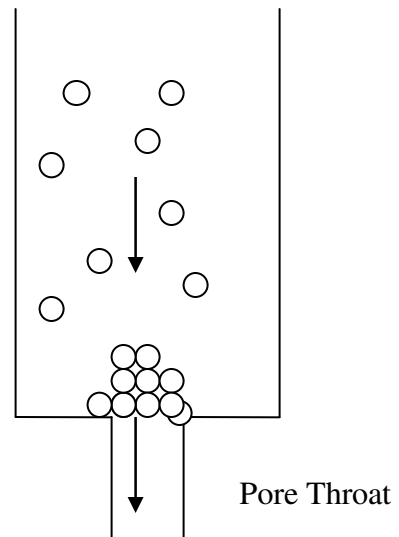


Figure 15-b

Figure 15 Schematic view of the particle bridging across a perforation (a) with and (b) without sand packing.

Figure 15 depicts the plugging phenomenon both in perforations (Figure15-a) and in pore spaces (Figure 15-b). In the scope of this thesis, pore throat plugging is more important. However, the study is applicable to perforations which may be very useful for production engineering purposes.

7.4.1 Analysis of the In-House Data

The data measured in this thesis and those reported by Haynes and Gray (1974) and Gruesbeck and Collins (1982) are correlated in this section. The data are correlated using the power-law and exponential-law equations presented by Civan (2000) as the criteria for determining the conditions leading to the plugging of pores and perforations, given respectively, as:

$$\beta_{cr} = A_1 (Re_p)^{B_1} + C_1 \quad (47)$$

$$\beta_{cr} = A_2 \{1 - \exp[-B_2 (Re_p)]\} + C_2 \quad (48)$$

The term β denotes the ratio of the pore throat diameter D_T and the particle size D_p . The results are compared for all the experimental data. The plugging criteria represented by Eqs. 47 and 48 is a means to determine whether bridging occurs or not with certain viscosity of fluid, certain particle size, and certain pore throat-to-particle diameter ratio. The dimensionless groups were formed from the viscosity, particle diameter, flow velocity, density, and pore throat diameter by means of the method of dimensional analysis. The particle Reynolds number and the pore throat-to-particle diameter ratio are the two important dimensionless groups involved in the proposed exponential- and power-law correlations of experimental data. The region below the correlation curve indicates the conditions for non-plugging of pore throats and perforations, and the region above the curve denotes the conditions for plugging.

It should be emphasized that plugging always occurs when $0 \leq D_T / D_P \leq 1.0$ (Figure 15-b) because particles having sizes equal or greater than the pore throat or perforation size will cause plugging. However, other factors, such as fluid viscosity and surface forces, may prevent a single particle to move through a pore throat even if the particle size is less than the pore throat size. Therefore, the vertical intercepts of Eqs. 47 and 48 may assume values equal or greater than 1.0; i.e. C_1 and $C_2 \geq 1.0$, as indicated by the experimental data considered in this study.

The empirical parameters A_1 , B_1 , C_1 , A_2 , B_2 , and C_2 are determined to obtain best regression of the experimental data using the linearized forms of Eqs.49 and 50, given respectively, as:

$$\log \left[\frac{\beta_{cr} - C_1}{A_1} \right] = B_1 \log(Re_p) \quad (49)$$

$$\ln \left[1 - \frac{\beta_{cr} - C_2}{A_2} \right] = -B_2 (Re_p) \quad (50)$$

The values of the fitting parameters are determined by trial-and-error to obtain the best straight-line match of the experimental data until the coefficient of regression converged as close to $R^2 = 1.0$ as possible. The present data represent the plugging of perforations during the clean-up of the near-wellbore formation from the invaded mud particles by flow back (Figure15-a). The best estimates of the fitting parameters are presented in Table 13. The straight-line plots of the experimental data are presented in Figures 20 and 21 by employing Eqs.49 and 50.

Table 13 Fitting Parameters of the Calculated Equations

	Power	Law	Model	
Suspension	A₁	B₁	C₁	R²
1	22.29	0.17	1.0	0.99
2	32.50	0.21	1.0	0.93
3	9.50	0.15	1.0	0.96
4	50.0	0.32	1.5	0.70
Suspension	A₁	B₁	C₁	R²
Gruesbeck&Collins Data Hydroxyethyl Cellulose and Tap Water With Gravels	1.87	0.26	1.52	0.89
Haynes and Gray Data Fresh Water and Brine With Angular and Ottawa Quartz	1.85	0.27	1.0	0.99
	Exponential Model			
Suspension	A₂	B₂	C₂	R²
1	4.4	3×10^{-5}	1.0	0.97
2	5.5	3×10^{-5}	1.0	0.98
3	3.0	1×10^{-7}	1.0	0.97
Suspension	A₂	B₂	C₂	R²
Gruesbeck&Collins Data Hydroxyethyl Cellulose and Tap Water With Gravels	4.6	0.18	1.52	0.91
Haynes and Gray Data Fresh Water and Brine With Angular and Ottawa Quartz	5.5	0.04	2.1	0.99

The data measured in this study and the trend-lines calculated using Eq. 47 and 48 with the determined parameter values are compared in Figure 16. The parameters of Eqs.47 and 48 are fluid-sensitive and reflect upon the characteristic of the drilling fluids. Therefore, the parameters A_1 , B_1 , and C_1 were correlated with respect to the fluid viscosity as shown in Figures 18 and 19 by Eq.47 for the power-law model. In this case, the R^2 is found to be 0.99, 0.96, and 0.93, respectively for power-law model. The parameters correlate consistently well with viscosity.

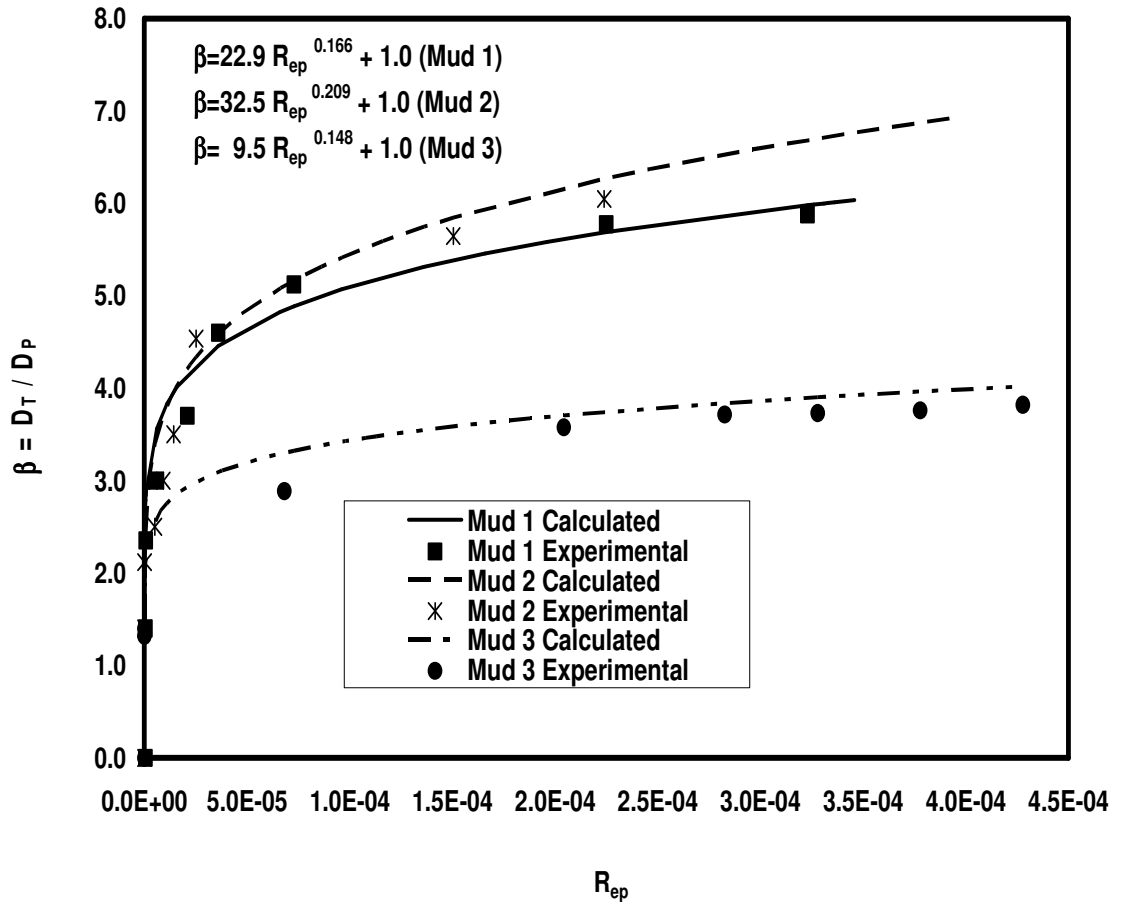


Figure 16 Experimental and Calculated Results from Power Law Model (Eq.47) as a Function of Particle Reynolds Number

In addition, a set of experiments were performed using the suspensions of 1.1 mm, 2.1 mm, and 4 mm glass beads in a viscous fluid (corn syrup) with three single-hole glass tubing, having perforation diameters of 3 mm, and 4 mm, and 7 mm, respectively (Figure 15-b). The aim of these additional experiments is to generalize the fluid type. By introducing a non-clay viscous fluid expresses that the results are valid independent of the fluid type. The viscosity of the syrup was varied by diluting with water. The viscosities of the syrup suspensions obtained this way are 63.2 cp, 50.0 cp, and 32.6 cp. The pore throat to particle diameter ratio and Reynolds number results were plotted in Figure-19. The results were correlated by the power-law model. A regression coefficient of $R^2 = 0.72$ was obtained. The viscous fluid fit with the power-law model accurately. The exponential –law model did not fit the new viscous fluid type. Thus, it can be concluded that power-law model is more general and accurate for employing various types of for the determination of the plugging criteria concept. Thus, it is confirmed that the perforation and pore plugging by particulate slurry under various conditions can be correlated by two dimensionless groups, namely the pore or perforation diameter-to-particle diameter ratio and the particle Reynolds number as suggested by Civan (2000). The plugging criteria proposed by Civan (2000) are shown to accurately represent the experimental observations. Therefore, the proposed correlations can be used for conditions encountered in other similar cases and field applications. Both models fit the experimental data of Haynes and Gray (1974) perfectly. The linearized form of the power- law model has a regression coefficient value of $R^2 = 0.99$. Both models work very well with both the in-house and Haynes and Gray (1974) data. However, the exponential-law model fits the data of Gruesbeck and Collins (1982).

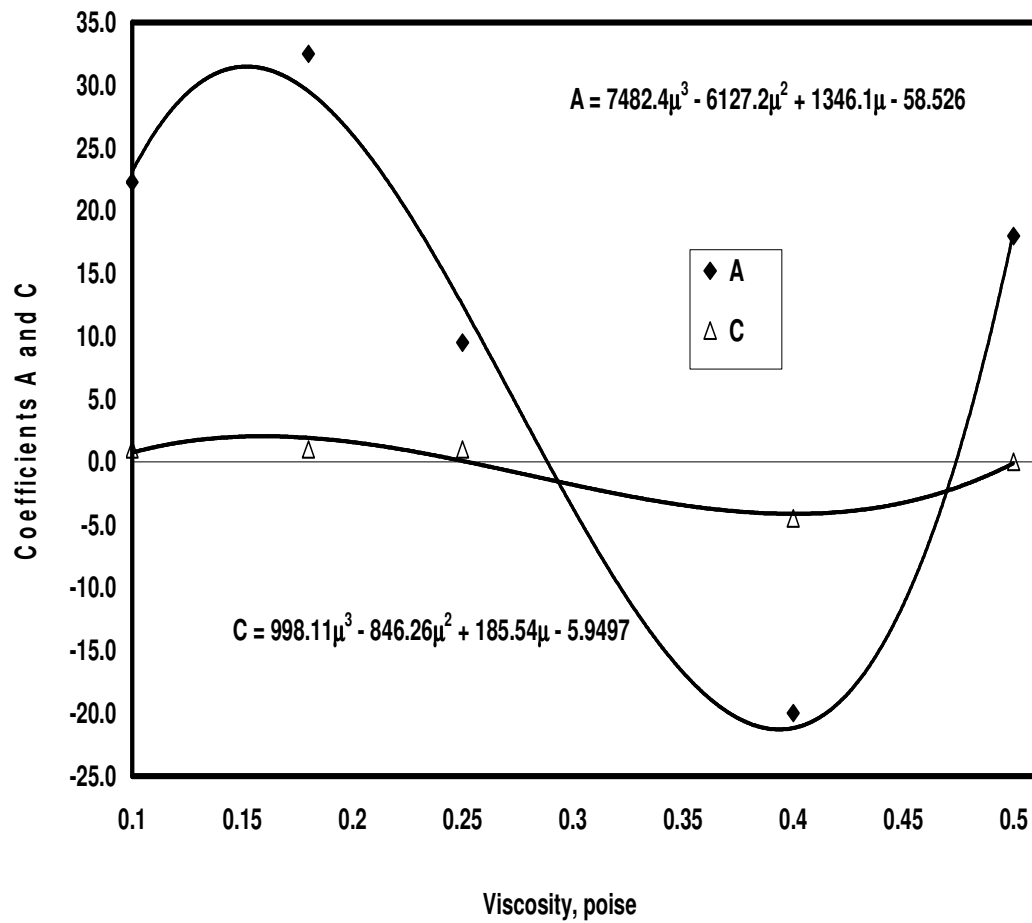


Figure 17 Vicosity coefficients of A and C for Power Law Model approach

The variation of the coefficient "A" with respect to viscosity is more sensitive than that of coefficient "C". However, it is observed that both coefficients indicate the similar profiles as the viscosities increase.

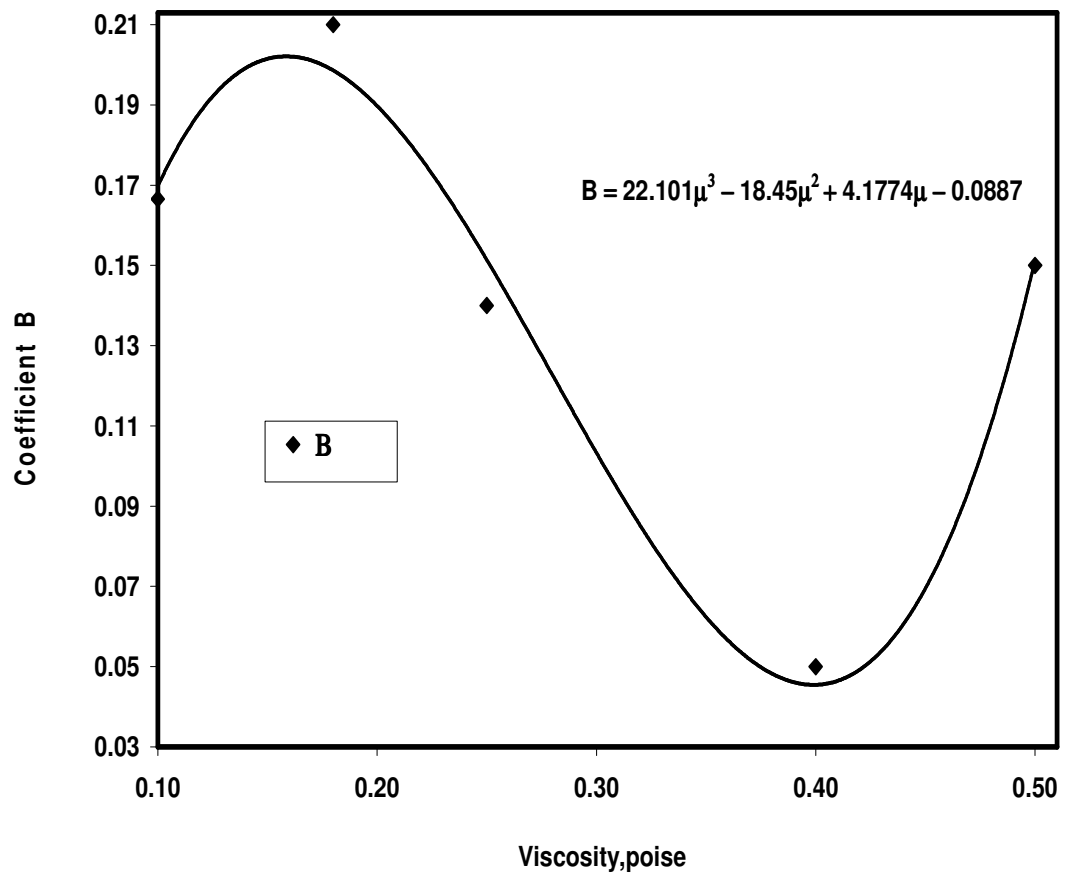


Figure 18 Viscosity coefficients of B for Power Law Model approach

It is observed that the viscosities and the correlation coefficients are related with each other. The coefficients A, B and C are of third degree functions of effective viscosity (Figures 17 and 18).

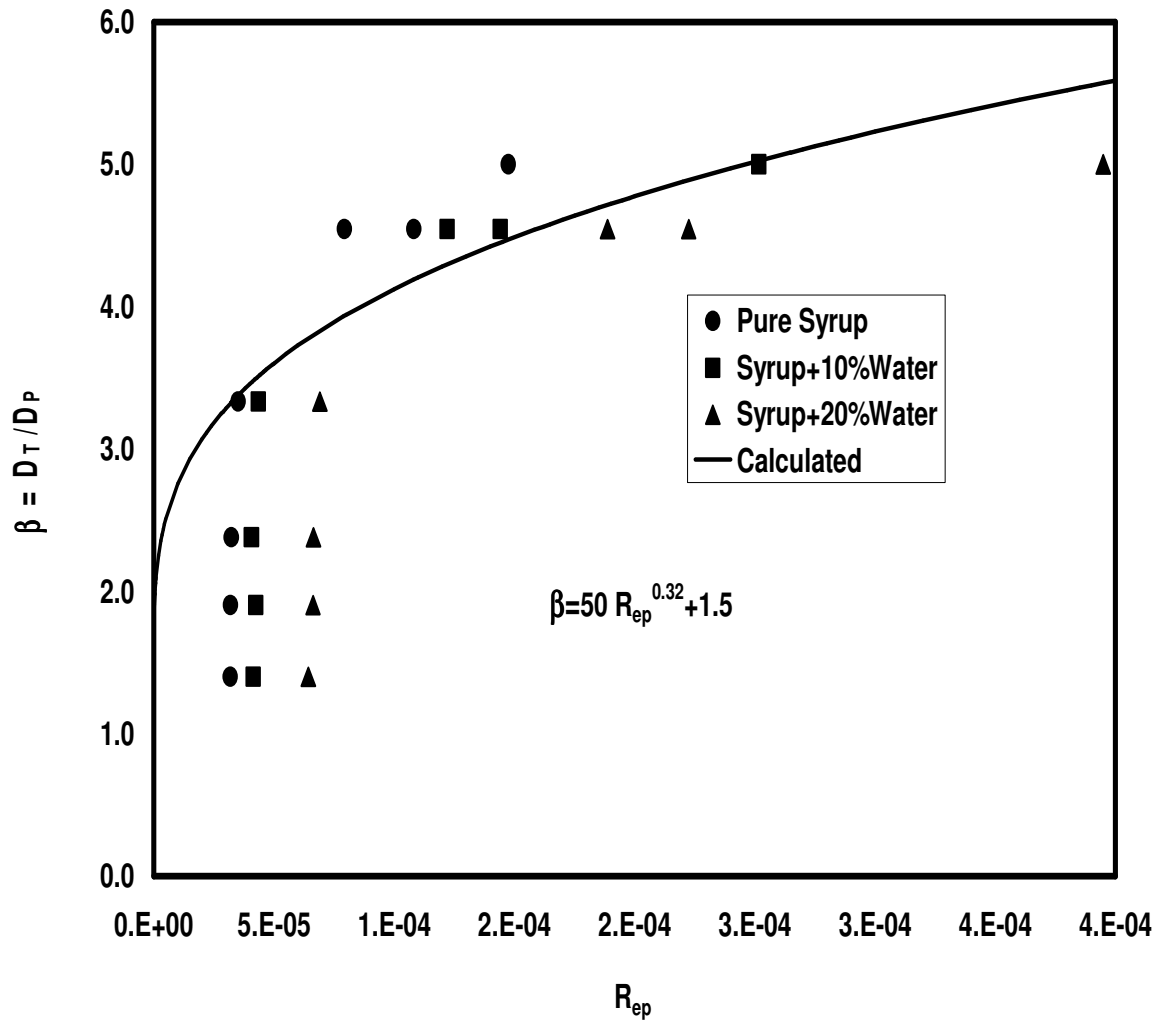


Figure 19 Experimental and Calculated Results from Power Law Model (Eq.47) as a Function of Particle Reynolds Number

Additional experiments were conducted with corn syrup (Figure 19). The coefficients of the correlation are given in Table 12 as suspension 4 for power-law model. The exponential model did not enable the data fit accurately. This fluid was used to vary and to generalize the study. Thus,

it is declared that this analysis is not only limited for drilling fluids but also for any viscous fluid. It should be emphasized that plugging always occurs when $0 \leq D_T / D_P \leq 1.0$ because particles having sizes equal or greater than the pore throat or perforation size will cause plugging. This means that pore throat diameter is less than the particle diameter. In this case there is no possibility for the particles to pass from the pore throat. Thus, particle Reynolds number can not be calculated. In some cases, even slightly higher pore throat to particle ratios than 1.0 may not be sufficient to observe the particle flow due to bridging right across the pore throat as in Figure 19. Thus, the plugging criteria line is on the pore throat to particle size axis at zero Reynolds number. Zero particle Reynolds number is obtained when there is no particle flow through the pore throat. When the particle size is greater than pore throat, it is not possible even one unique tiny particle through the pore throat.

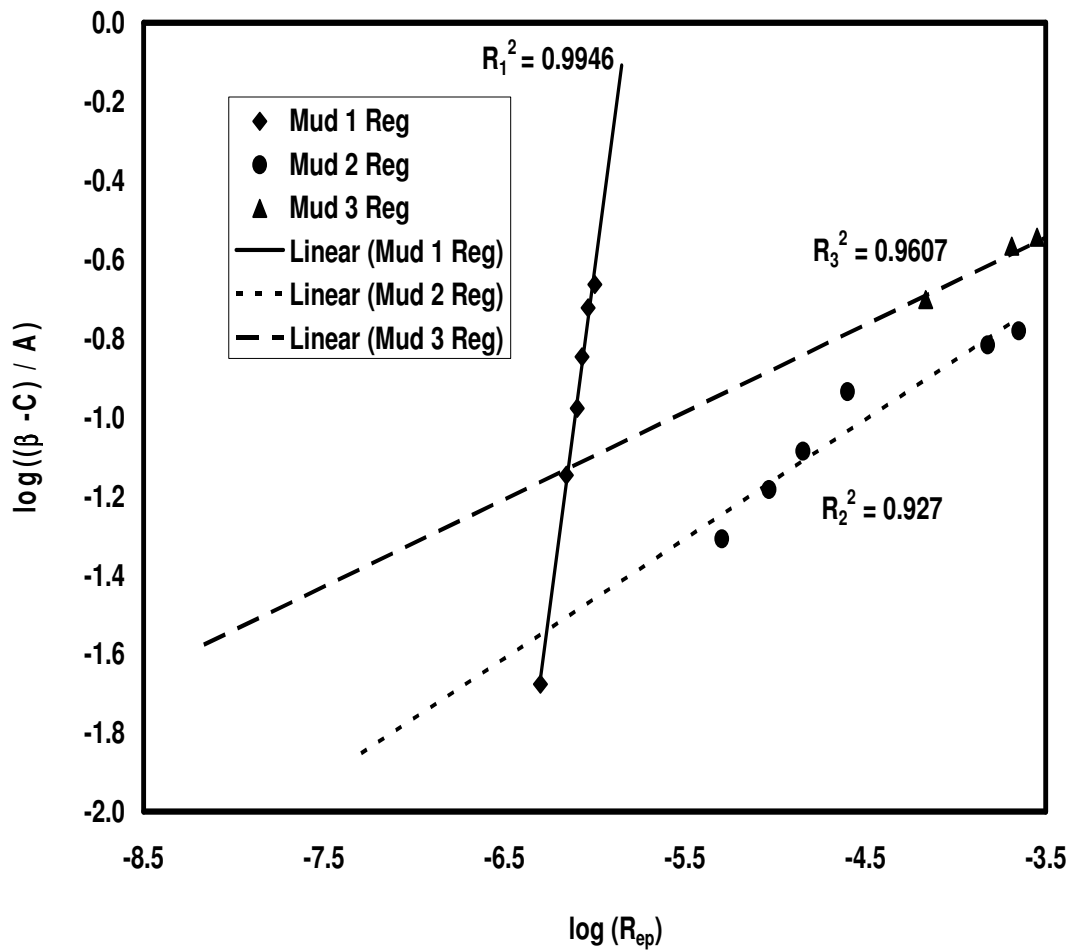


Figure 20 Linearization of Eq.47 and Regression Coefficients for Power Law Model

It is observed that the in-house experimental data gives out consistent linear plots with high R^2 values with the power-law model. The best fit was obtained with the non-treated mud. The least regression is with the polymer mud.

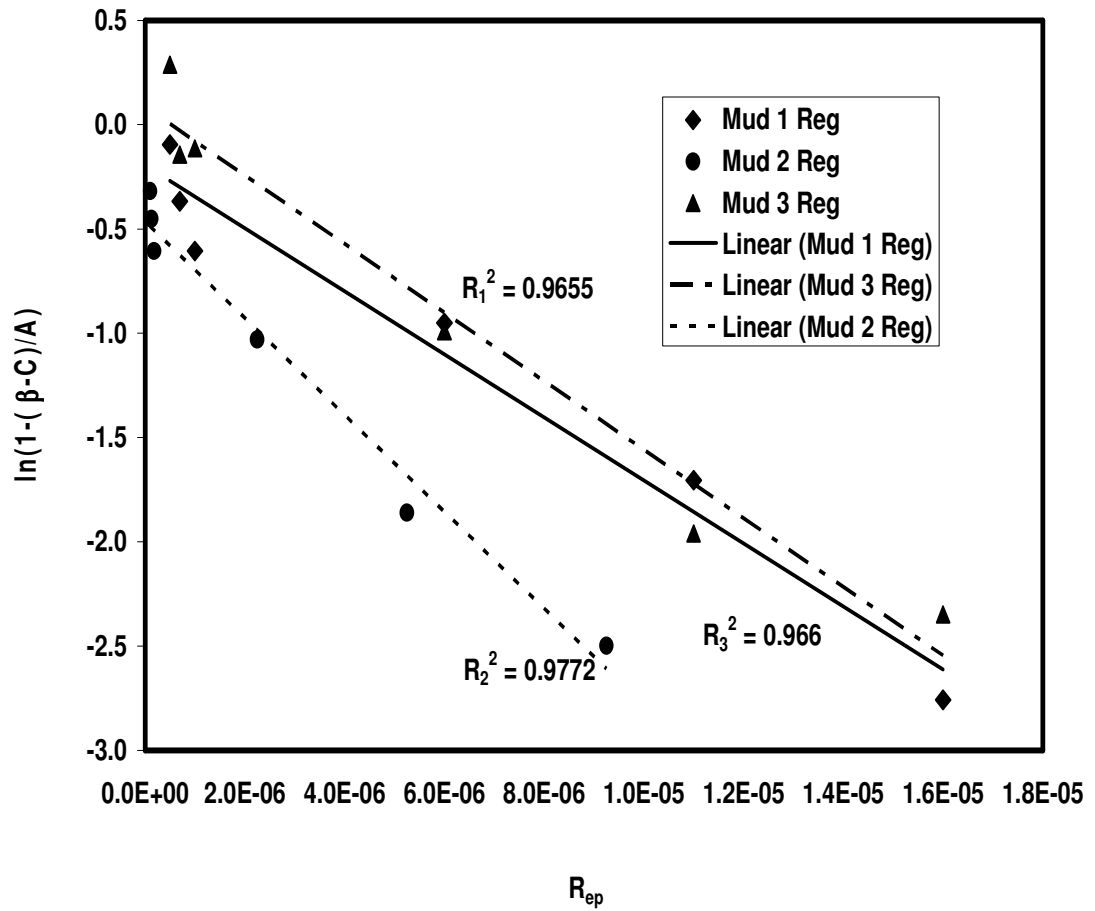


Figure 21. Linearization of Eq.48 and Regression Coefficients for Exponential Law Model

The linear regression coefficients of the exponential law model are comparatively less than the regression coefficients of the power-law model. Thus it can be stated that the power-law model works better with this experimental data.

7.4.2 Analysis of The Data in Literature : Haynes and Gray

The data of Haynes and Gray (1974) represent the plugging of pores during the sand transport from the well-bore into the perforations (Figure 15-a). The above-mentioned analysis approach has been carried out using the data of Haynes and Gray (1974). The measured and calculated data of Haynes and Gray are compared in Figures 22 and 23. Equations 49 and 50 are plotted for the data of Haynes and Gray (1974) in Figures 24 and 25. The regression coefficient of Eq.49 belonging to the power-law model is much closer to $R^2 = 1.0$ than that of Eq.50. The data of Haynes and Gray (1974) fit both models very well. Both of the power-law and exponential-law models are appropriate for their data. The regression coefficients in both models are $R^2 = 0.99$ and very close to one. Nevertheless, the power-law model fits the experimental data much better. The data used in Figures 22 and 23 belong to Haynes and Gray. The solid line curves are calculated from the present correlations. There are only a limited number of data points available in their study. In our experiments, no experimental result could be obtained below the Reynolds number value 10 even though the pore throat to particle diameter ratio has been varied. However, a rapid bridging occurs above this Reynolds number value. Thus, it can be concluded that there exists a critical Reynolds number value until which no bridging occurs for every type of slurries with particles unless the particle diameter is larger than the pore throat diameter.

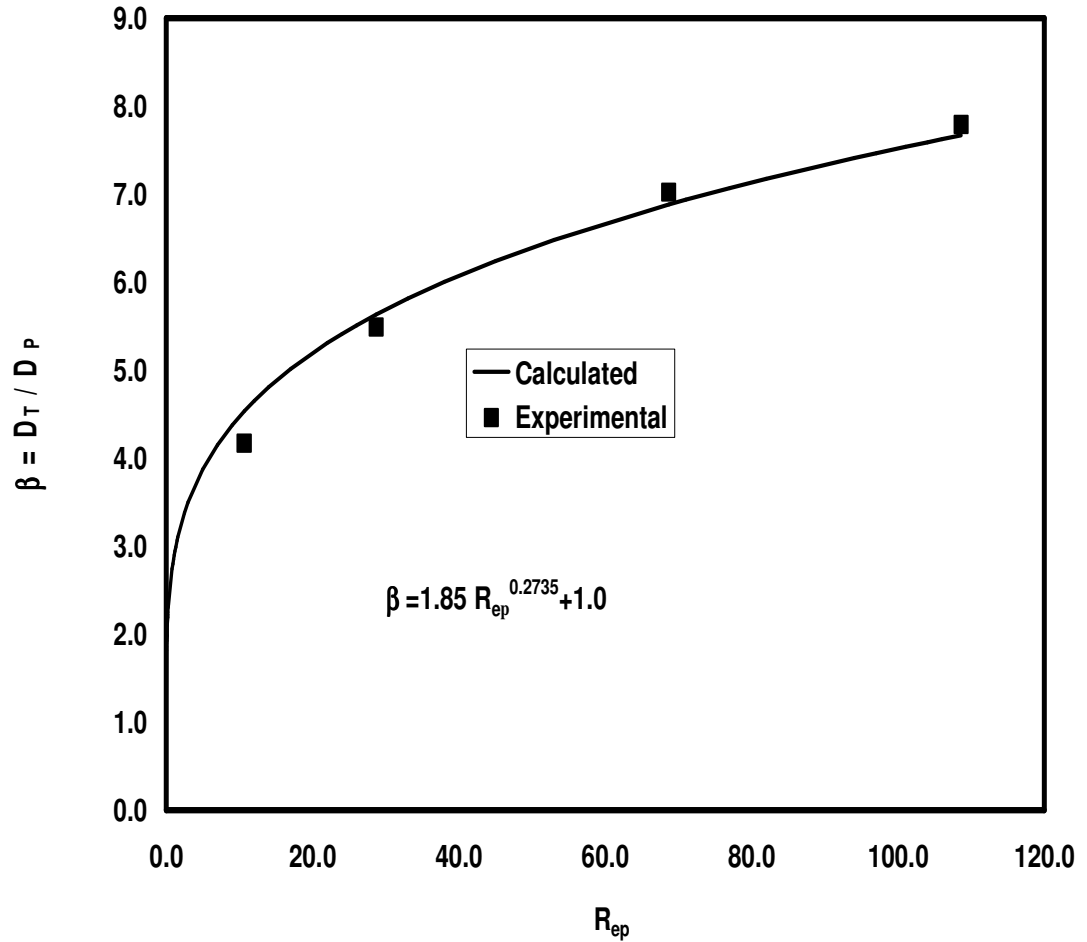


Figure 22 Experimental and Calculated Values of Haynes and Gray Data by Power Law Model Eq.47

The power-law model matches with Haynes and Gray`s data perfectly as seen in Figure 22. However, they have insufficient amount of experimental data when compared to the present study.

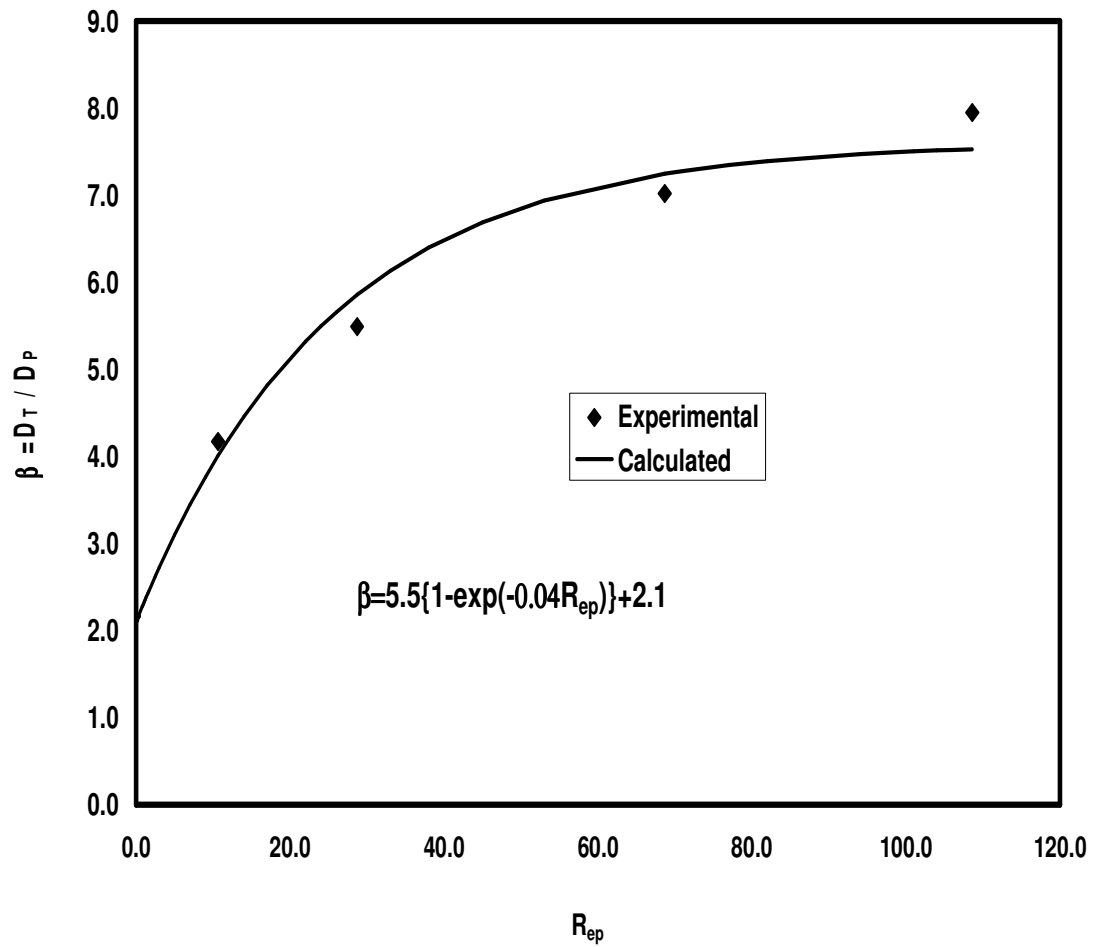


Figure 23 Experimental and Calculated Values of Haynes and Gray Data by Exponential Law Model Eq.48

The exponential-law model works better with Haynes and Gray's data than the power-law model (Figure 23). However, the insufficient number of experimental data reduces the reliability of their study.

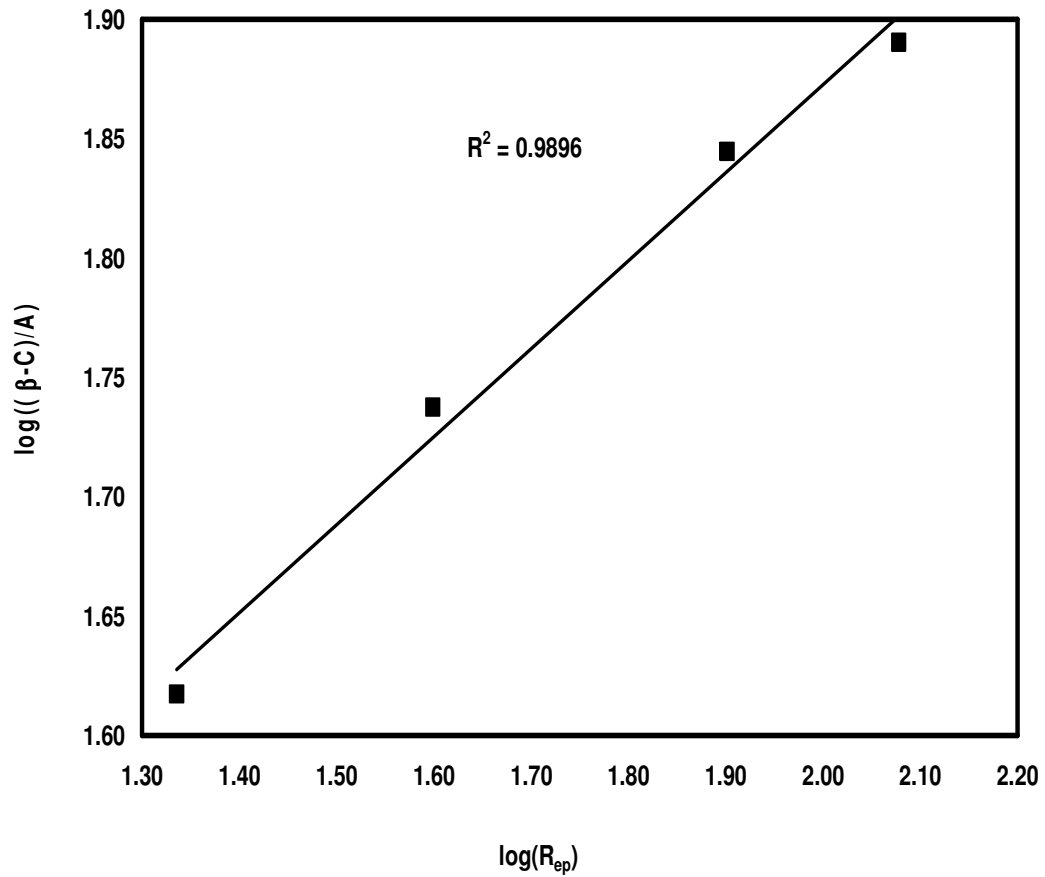


Figure 24 Linearization of Eq.47 and Regression Coefficients for Power Law Model For Haynes and Gray Data

The regression coefficients of the power-law and exponential law models applied for Haynes and Gray's experimental data are very close to each other. Both of them are in the order of 0.99. However, the linear regression of the exponential model is slightly better than that of the power-law model as depicted in Figures 24 and 25.

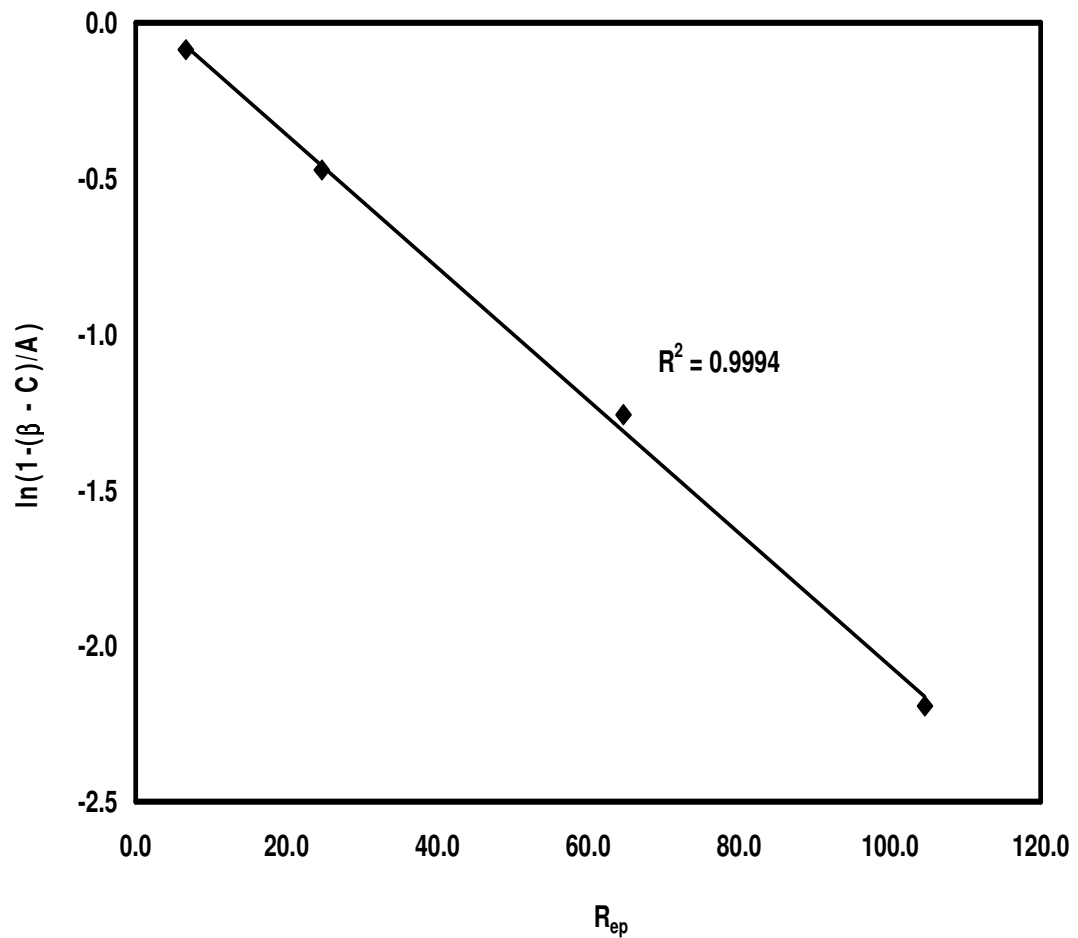


Figure 25 Linearization of Eq.48 and Regression Coefficients for Exponential Model For Haynes and Gray Data

The regression coefficient with the exponential- law model for Haynes and Gray's experimental data is 0.9994, whereas the regression coefficient with the power-law model is 0.9896. Both of them are very close to each other for these experimental data. Thus, both of the models can be applied accurately.

7.4.3 Analysis of The Data in Literature : Gruesbeck and Collins

Gruesbeck and Collins can be considered as the pioneering actual pore throat and perforation plugging studies. However, they used only glycerin as the flowing fluid in their experiments. That is why their study is a little bit far from realistically applicable field work.

The plugging of perforations during the invasion of particulate suspensions into the near-well-bore formation is depicted in Figure 15-b. The measured data and the data calculated by the correlations are compared in Figures 26 and 27. They did not provide sufficient data to allow the calculation of the Reynolds number. Therefore, the plots were simply made against the particle concentration in the suspension instead of the Reynolds number in this case. Equations 49 and 50 are plotted for the data of Gruesbeck and Collins (1982) in Figures 28 and 29. The exponential-law model has a higher regression coefficient value of $R^2 = 0.91$ than that of the power-law model which is $R^2 = 0.89$. Thus, the exponential-law model correlates the data of Gruesbeck and Collins (1982) better than the power-law model.

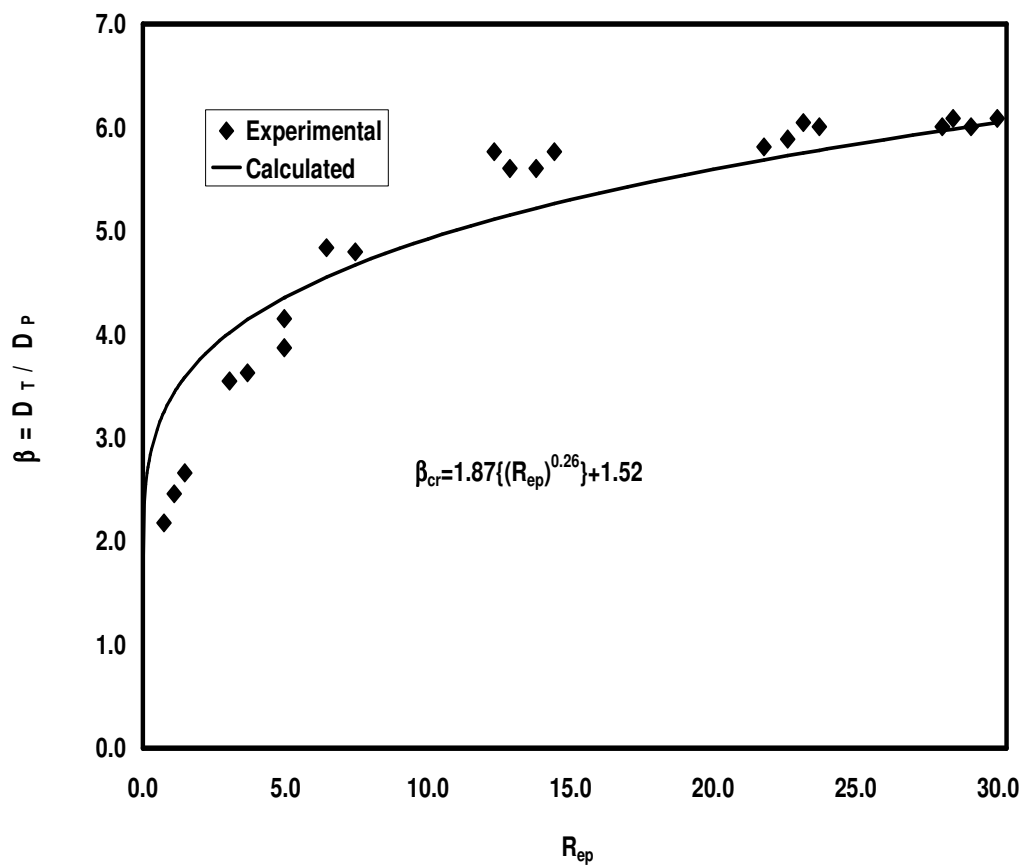


Figure 26 Experimental and Calculated Values of Gruesbeck and Collins Data by Power Law Model Eq.47

In Figure 26, the y axis intercept is the minimum pore throat to particle diameter ratio. It is interesting that the correlation catches the best fit a y axis intercept 1.52 which is different than 1.0. However the in-house data, power-law correlation of Haynes and Gray indicated the y axis intercepts as 1.0. The experiments with corn syrup had resulted in y axis different than 1.0, too. Corn syrup and glycerin are more viscous than the drilling fluids.

Thus, it can be thought that, as the viscosity of the fluid increases, the initial pore throat to particle ratio for plugging has a tendency to shift above 1.0.

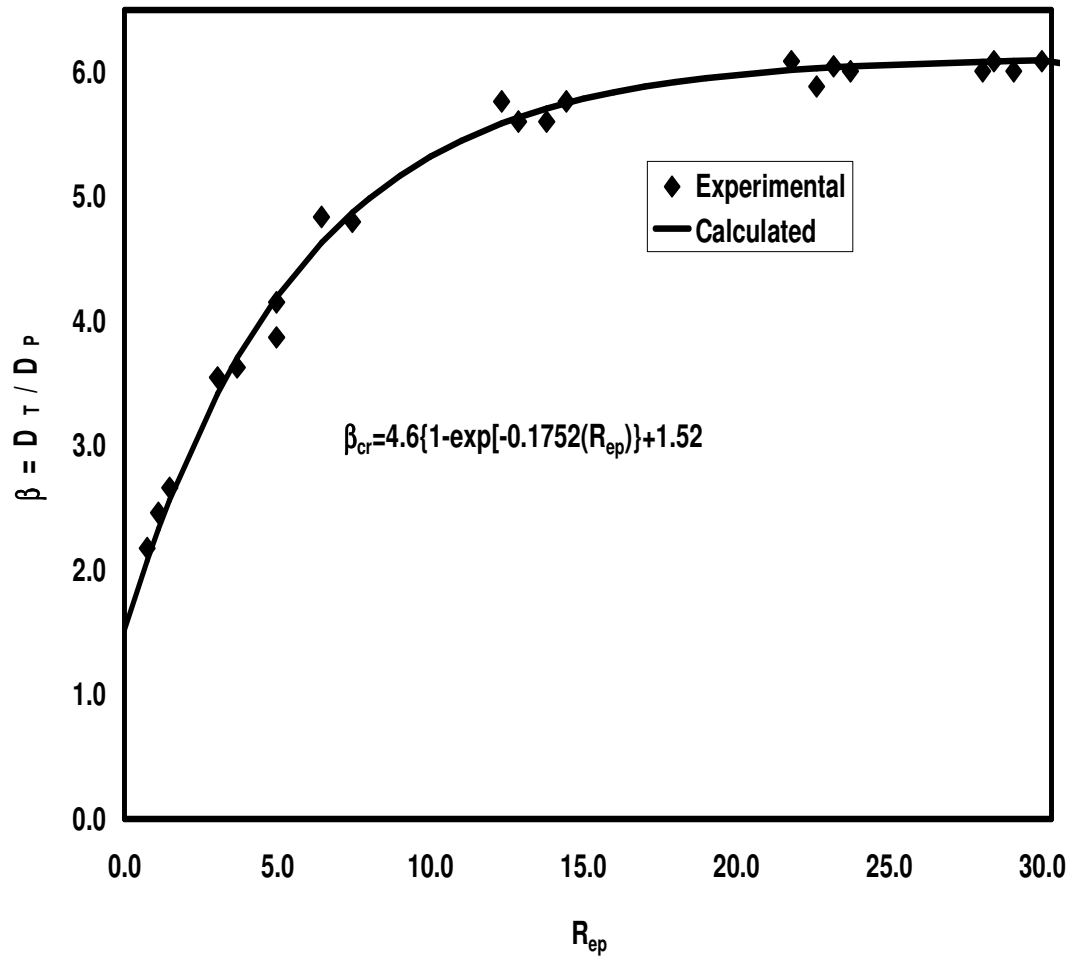


Figure 27 Experimental and Calculated Values of Gruesbeck and Collins Data by Exponential Law Model Eq.48

Exponential-law model correlation matched perfectly with the data of Gruesbeck and Collins (Figure 27). Both of the correlations were normalized. The linearized plots are given in Figures 28 and 29.

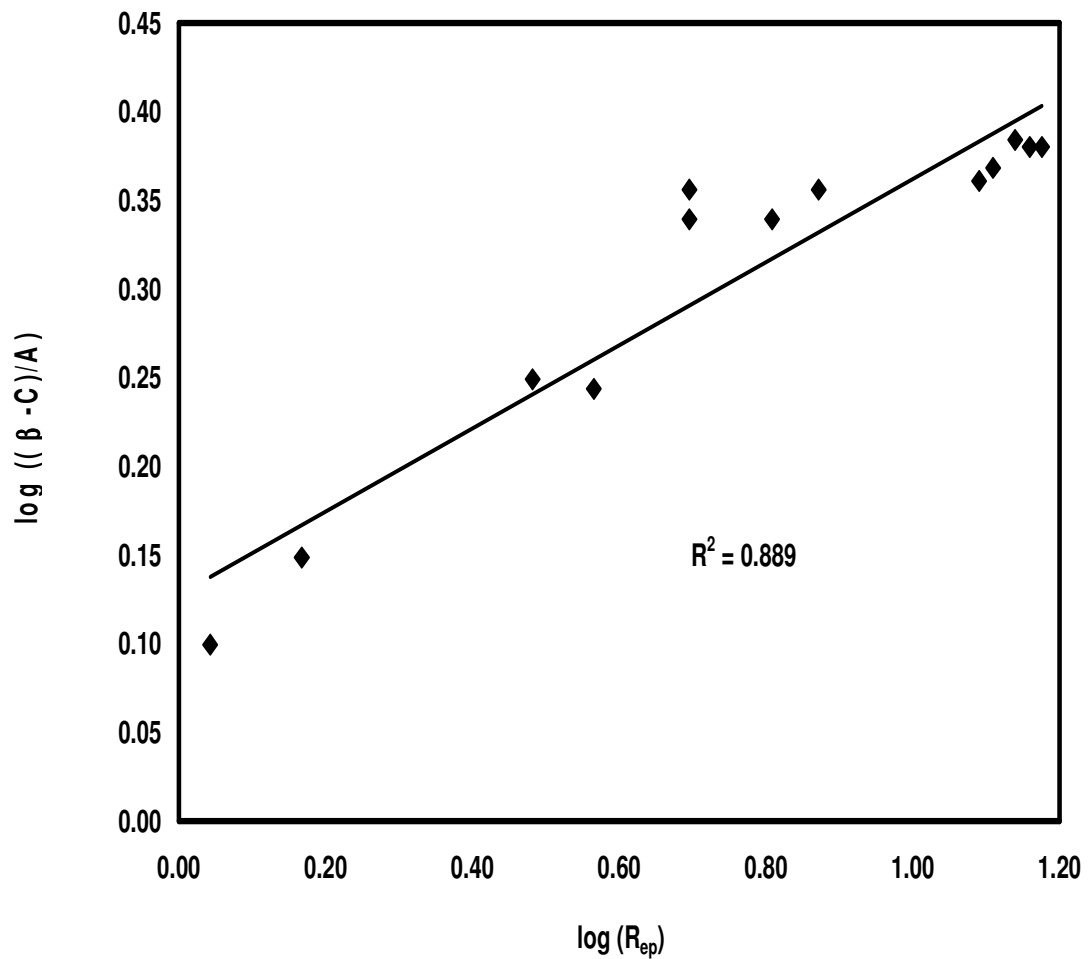


Figure 28 Linearization of Eq.47 and Regression Coefficients for Power Law Model for Gruesbeck and Collins Data

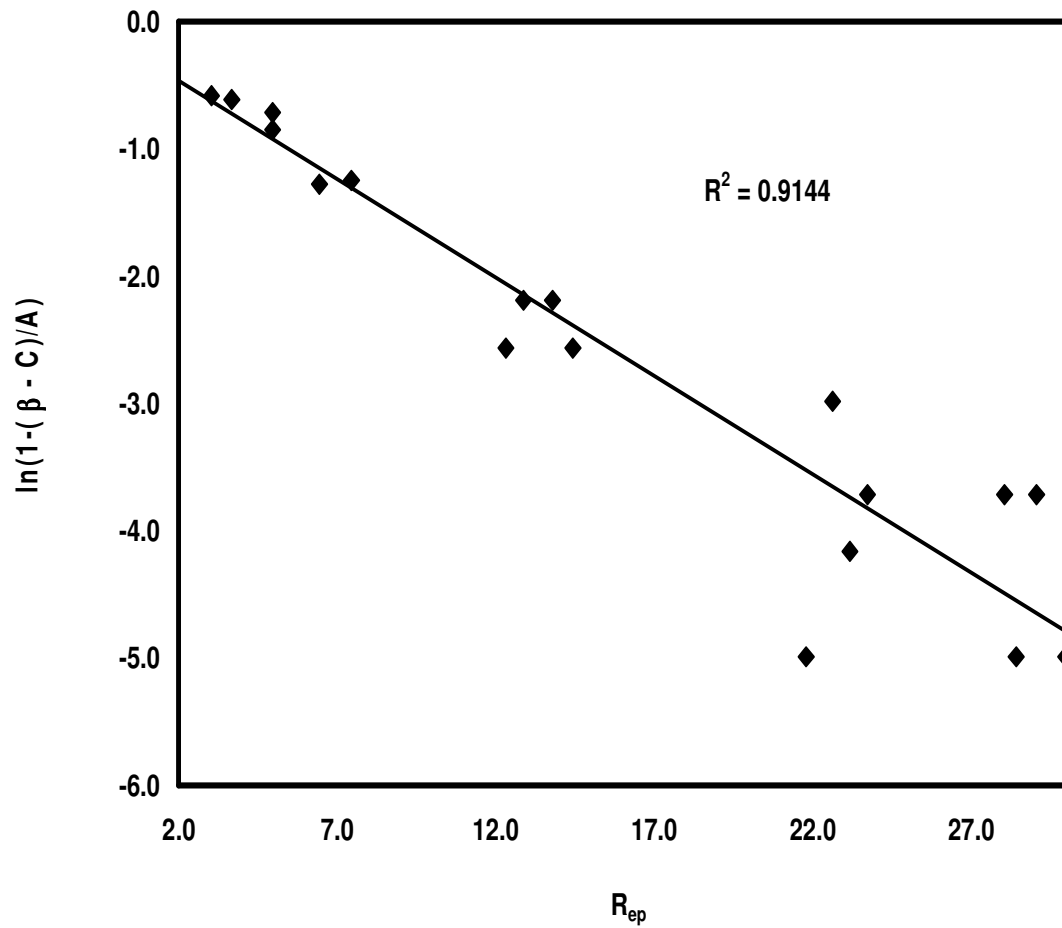


Figure 29 Linearization of Eq.48 and Regression Coefficients for Exponential Model for Gruesbeck and Collins Data.

The exponential-law model fit better than the power-law model (Figure 29). The regression coefficients are comparatively less than the correlation of Haynes and Gray's data. This may be because of the high number of experimental data in the study of Gruesbeck and Collins.

7.4.4 Practical Application of The Correlations in The Field

It is very important to have an idea about the circumstances under which the perforations or pore throats can be plugged in petroleum reservoirs. Especially during drilling and well completion operations, many types of slurries including various sizes of particles are circulated through the wells. The flow rate of the mud circulation, the viscosity of the mud, filtration rate, and the particle sizes are the basic parameters which can be measured in the field. Usually, the drilling and completion rigs contain a mud laboratory. Thus, viscosity, density, and other rheological parameters are measurable. The filtration rate can be measured by the mud engineer just by controlling the mud-pit level during circulation.

The measures that can be taken to prevent pore throat plugging can be summarized as follows. The pore throat-to-particle diameter ratio should be kept as high as possible, such as by opening larger perforations, and the particle weights in the muds and completion fluids should not be heavy. The particles should be suspended in the fluid system and homogeneously mixed. The rate of falling of particles in suspension should not be faster than the flow of the fluid through the pore throat. The filtration rate should be as small as possible. The viscosity of the fluid should be adjusted carefully so that the fluid should have both the thixotropic property and the easier ability to flow. A proper optimal set of the parameter values can be selected with the help of the correlations developed in this study so that pore and perforation plugging problems can be avoided in the field.

The plugging criteria confirms that the perforation and pore plugging by particulate slurry under various conditions can be correlated by two dimensionless groups, namely the pore or perforation diameter-to-particle diameter ratio and the particle Reynolds number as suggested by Civan (2000). The plugging criteria proposed by Civan (2000) are shown to accurately represent the experimental observations. Both the power-law and exponential-law correlations of the plugging criteria perform satisfactorily with the coefficients of regressions very close to $R^2 = 1.0$ for all the data analyzed in this study. Therefore, the proposed correlations can be used for conditions encountered in other similar cases and field applications. Both models fit the experimental data of Haynes and Gray (1974) perfectly. The linearized form of the power-law model has a regression coefficient value of $R^2 = 0.99$. Both models work very well with both the in-house and Haynes and Gray (1974) data. However, the exponential-law model fits the data of Gruesbeck and Collins (1982) better.

The importance of the Reynolds number and filtration rate for determining the plugging criteria has been demonstrated by analyzing various experimental data. As the rate of filtration increases, the Reynolds number increases also. Consequently, as the Reynolds number increases for a given pore throat to particle diameter ratio, the plugging criteria determines that the suspension is approaching the plugging condition. Therefore, an increase in the rate of filtration shifts the conditions from non-bridging towards bridging.

7.5 Dynamic Fluid Circulation and Formation Damage Analysis

In this part of the study, dynamic fluid circulation experiments, reduction in permeability due to fines particles migration, correlation of the permeability reduction with filtration pressure, back-flow simulations and the clean up effects are discussed.

Many petroleum engineering operations, such as drilling, well completions, and work-over may cause an alteration in the properties of hydrocarbon bearing formations, such as porosity and permeability. In this study, the impairment in permeability by drilling fluids and the enhancement of the reduced permeability by backflow cleaning up are analyzed. The damage ratios as functions of the filtration pressure caused by two different drilling fluids are measured experimentally by core tests and analyzed using a simulator. Simulations were run for both in forward and backward directions along the core sample at different volumetric flux rates. The flow-paths through the core sample were classified as plugging and non-plugging types. The fraction of depositional volume to bulk volume of the core sample, particle concentration, ratio of plugging porosity to bulk porosity were considered by relevant mechanisms. The rates of particle deposition and mobilization were determined. Permeability was correlated and represented in terms of the depositional volume fractions of fine particles. The clean-up time was determined after back-flush with fresh water. The improvement in both porosity and permeability was observed. The simulation results accurately matched the experimental observations, thus allowing the estimation of the relevant phenomenological parameter values.

Permeability alteration by fines migration is a very important problem in petroleum engineering applications. Clay particles intrude into reservoir formations during drilling operations with water-based drilling fluids. This intrusion causes plugging and bridging across the pore throats within the pore spaces. Thus, permeability decreases. However, many hydrocarbon reservoirs have aquifer boundaries. Water influx takes place in many cases. The cleaning effect of aquifers can be simulated by injecting water to the mud invaded core samples. In this study, the cleaning effect of the aquifers and the change in permeability are studied in terms of the damage ratio, both experimentally and numerically.

While the experimental studies mentioned in Literature Review part provide valuable observations and understanding of the relevant phenomena, they do not provide a comprehensive mathematical model and specific information about the effect of the phenomenological parameters. This study applies a phenomenological model to analyze the available data. First a synthetic case study is presented to demonstrate the capability of the present model and simulator. Then, a set of dynamic drilling mud circulation experiments were carried out using three different drilling fluids at eleven different filtration pressures and three different circulation periods. Alteration in permeability is studied in terms of the damage ratio concept. Damage ratio is characterized as the percentage ratio of the difference between the undamaged and damaged permeability to the undamaged permeability. The influence of filtration pressure and circulation periods are analyzed both experimentally and numerically. The acquired experimental data are analyzed by means of the numerical computer simulator. The results are correlated and an exponential model for the effect of filtration pressure on damage ratio is introduced.

The fine particle invasion and clean up processes are modelled by using a set of equations that correlate the particle concentration and fraction of depositing particles to permeability according to Civan and Vinh (2005). This model facilitates a plugging and nonplugging pathways concept. A sensitivity analysis with the simulator has been carried out to determine the contribution of plugging pathways to permeability reduction. The permeability changes in the plugging sections were found negligible with respect to the non-plugging permeability. However, both the plugging and non-plugging pathways participated in fine particle transport. The core samples used in this study have significantly less plugging pathways than the non-plugging ones. Civan (2000) defined permeability as a function of fraction of depositing particles in both plugging and non plugging pathways. In our case, the permeability is more sensitive to non-plugging pathways deposition than the plugging ones. After the calculation of the non-plugging permeability, the damage ratio is calculated as the reduction percentage ratio of the initial permeability of the core sample with respect to filtration pressure and time.

$$DR = \frac{K_o - K_f}{K_o} \quad (51)$$

These percentage reduction calculations are performed before and after the fluid circulation process (Eq.51). As the drilling fluids are circulated, the fines particles tend to invade into the porous media by the help of the differential pressure occurring on the core surface. This differential pressure is the driving force for the fines particles to be transported in the porous media. If these fines particles cause bridging across the pore throats, plugging occurs. Thus, permeability decreases.

7.5.1 Analysis of Mud Invasion And Clean Up By Flow Reversal Using A Simulator and Experimental Work

In this section, fines invasion and cleanup processes are simulated.

7.5.1.1 Effect of Fines Invasion in Porous Media

A finite-difference simulator implemented in Mathematica was used. The aim of this application is to simulate the effect of constant rate circulation of drilling fluids on invasion of fine particles into porous media and plugging of the pore pathways. The reduction of porosity and permeability was simulated in terms of the plugging and non-plugging deposition fractions. A sandstone core sample has been subjected to drilling fluid circulation for approximately 106 minutes. The particle concentration variation was observed as the circulation continued across the porous media. The plugging and non-plugging core sample pathways initial fine particle concentrations were assumed zero. The volumetric particle concentration of the fluid was considered as $9.4 \times 10^{-4} \text{ cm}^3 / \text{cm}^3$. As the circulation took place, the solid concentration increased in both plugging and non plugging paths through the core sample (Figure-30 and Figure-31). The deposition rate was determined by the change of the fractions of plugging and non-plugging pathways of bulk volume occupied by the deposits (Figure-32 and Figure 33). The average plugging deposition rate is $8.49 \times 10^{-9} \text{ min}^{-1}$. The average non-plugging deposition rate is $1.72 \times 10^{-4} \text{ min}^{-1}$. Both the plugging and non-plugging porosity and permeability of the core sample decreased as the particles in the suspension deposited. Figure 34 indicates that the plugging fraction of deposits continue to increase until the end of minute 102 and reaches the

maximum value of $1.2 \times 10^{-6} \text{ cm}^3/\text{cm}^3$. From that time on the data look constant for two more minutes. In Figure 33, the non-plugging fraction of deposits keep increasing until the minute 80 and slightly decreases its increase trend and reaches 0.0184 at the end of the total time 106 minutes. The concentration of plugging particles displays a very sharp increase between the 15th and 30th minutes. After this moment, there is a reasonable reduction in the plugging concentration for about ten minutes. This may be due the pushing effect of the depositing particles behind this point. The plugging concentration increases almost linearly after this point until the end of the core sample and reaches the value of 0.6 ppm (Figure 35). The non-plugging concentration increases sharper between the 20th and 40th minutes. This increase may be due to a sudden plugging and then relief by jet action of deposited particles. From 40th minute on, the non-plugging particle concentrations keep increasing in their normal trend and reach the value of 0.02 ppm (Figure 36). The non-plugging porosity decreases as the concentration of the fluids increased in time. There is more reduction in non-plugging porosity with respect to plugging porosity. The non-plugging porosity decreases linearly from 0.2 to 0.183. This means a 8.5% reduction in non-plugging porosity (Figure 34). The reduction in non-plugging permeability is about 35% in 106 minutes. This reduction means that permeability has dropped from 25 D to 16.25 D. The reduction is less in the first 13 minutes of the circulation, but from that moment on the non-plugging permeability reduction is sharper (Figure 35). However, the reduction in plugging permeability is much less than that of non-plugging permeability as percentage. Nevertheless, a small change in the plugging permeability may influence the flow of fluids because of the low initial value of the plugging permeability. The fraction of plugging porosity to overall porosity (f_p) has been drawn along the core

sample at five different times such as 4, 8, 12, 18, 24 minutes (Figure 36). It is seen that the as the contamination period increases, the starting values of f_p increase. The f_p values keep decreasing along the core sample significantly in the first five grids of the core sample. After the fifth grid, the f_p remains constant at 0.48.

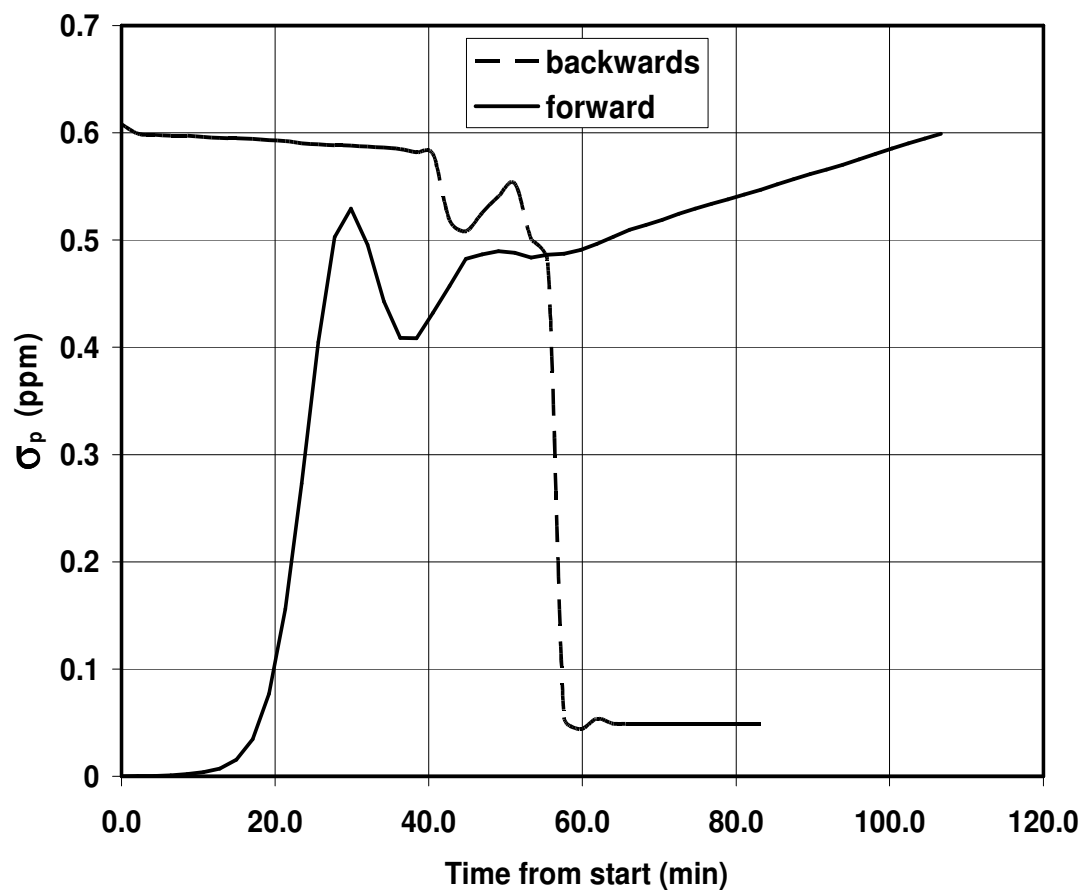


Figure 30 Concentrations of particles in plugging pathways

The particle deposition with in the porous media due to fines migration by drilling fluids and the clean-up effect due to the existence of an aquifer

are depicted in Figure 30. It is seen that the particle concentration increases sharply within the first 30 minutes of the circulation. This may be due to sudden bridging of particles across the pore throat. However, even though the bridging has formed, the particle source keeps bringing additional particles. This causes deposition behind the bridge and exerts pressure across the pore bridging. Then the bridging is deformed due to this pressure effect. Thus, a slight reduction is observed with the deformation of the bridging and until the formation of the new bridging. From this moment on, particle concentration through the porous media keeps increasing.

The pore pathways had been classified as plugging and non-plugging. It is seen that bridging occurs majorly in the plugging pathways in Figure 30. However, the increase of the particle concentrations in the non-plugging pathway is reasonably smoother (Figure 31). It is observed that the particle concentration values on the vertical axis of the non-plugging pathways are much smaller than the plugging ones.

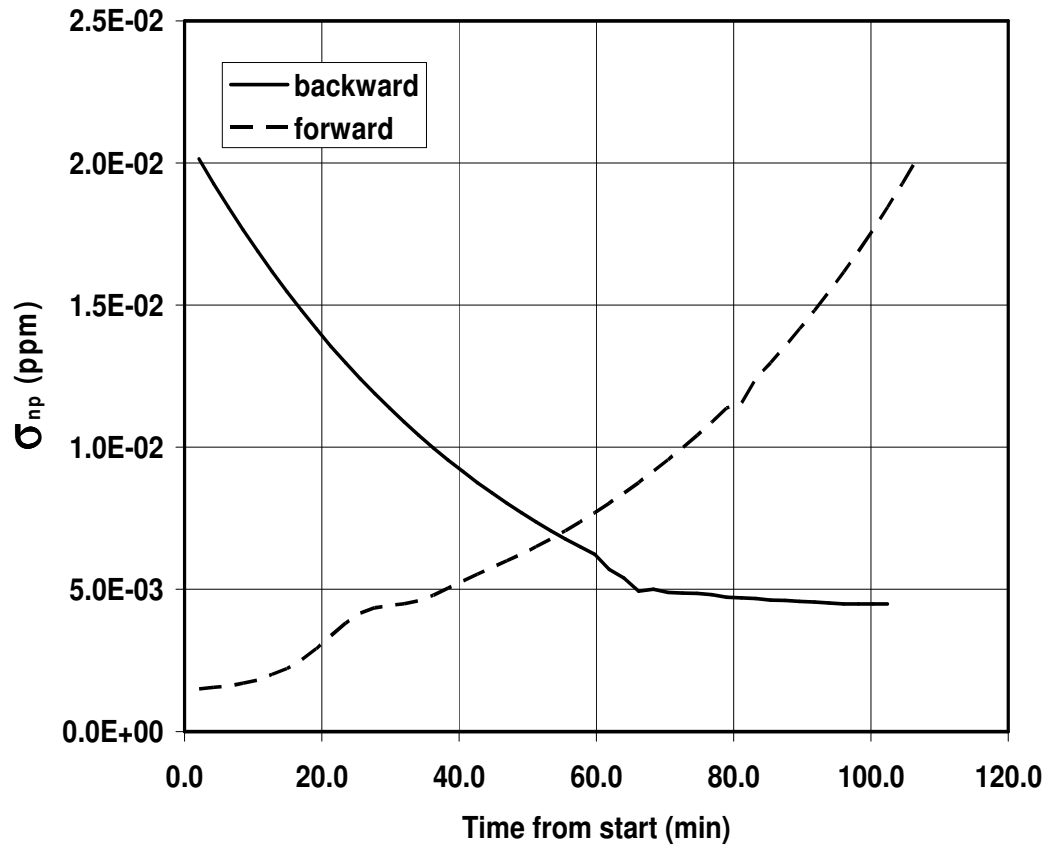


Figure 31 Particle Concentration of non-plugging pathways

The deposition of the particles in non-plugging pathways increases as the circulation time increases. However, the cleaning of the deposited particles can be achieved under limited circumstances. The major clean-up results in the first 62 minutes of the backflow by the aquifer boundary (Figure 31).

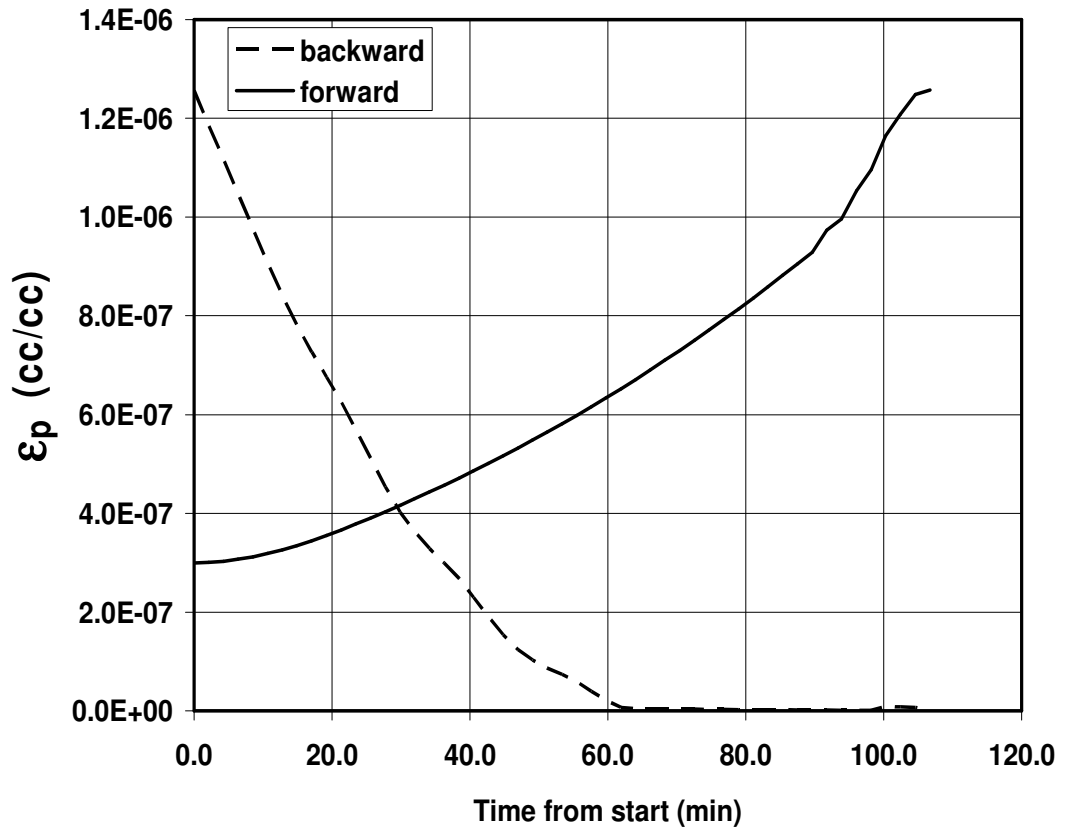


Figure 32 Fraction of plugging pathways of bulk volume occupied by the deposits

The deposition rate was determined by the change of the fractions of plugging and non-plugging pathways of bulk volume occupied by the deposits (Figure 32 and Figure 33). The average plugging deposition rate is $8.49 \times 10^{-9} \text{ min}^{-1}$. The average non-plugging deposition rate is $1.72 \times 10^{-4} \text{ min}^{-1}$. Both the plugging and non-plugging porosity and permeability of the core sample decreased as the particles in the suspension deposited. These rates were calculated on average basis. The difference

between the final and initial values of the plugging concentration is divided by the total drilling fluid circulation time.

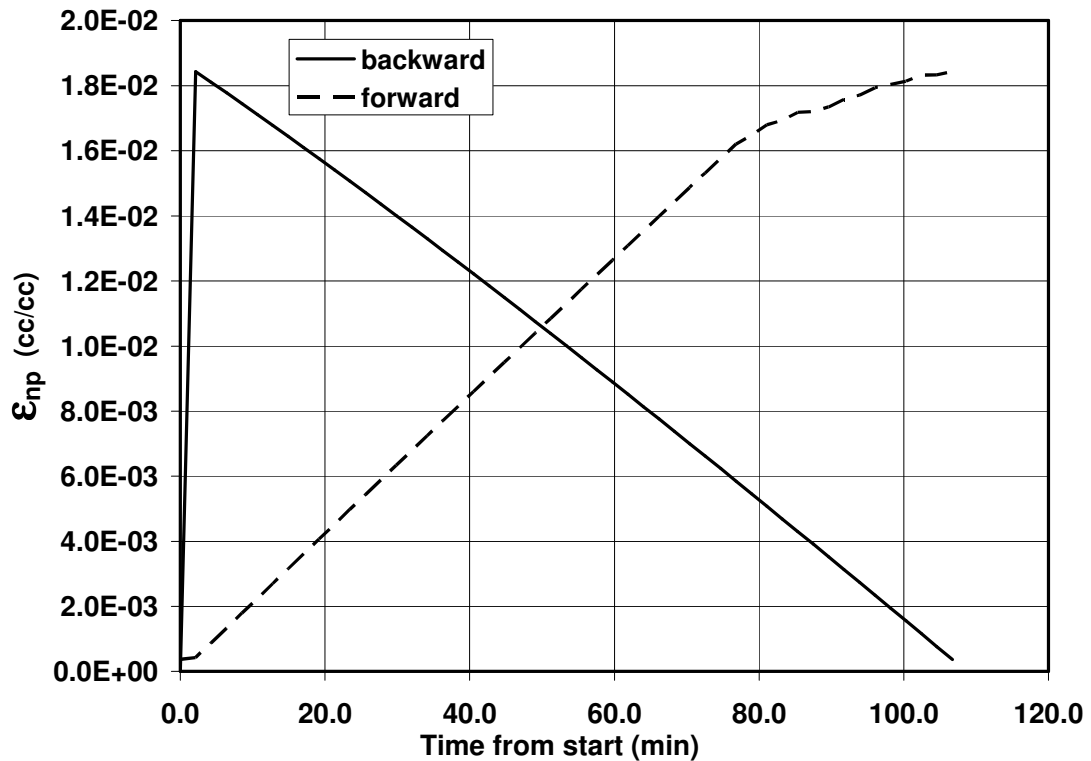


Figure 33 Fraction of non-plugging pathways of bulk volume occupied by the deposits

The fractions of non-plugging pathways which were occupied by the deposits increase in the first 80 minutes sharply. However, the slope decreases after 80 minutes. This indicates that the accumulating particles are moved by some of the next coming fines particles (Figure 33). The concentration of plugging particles displays a very sharp increase between the 15th and 30th minutes. (Figure 32) After this moment, there is

a reasonable reduction in the plugging concentration for about ten minutes. This may be due the pushing effect of the depositing particles behind this point.

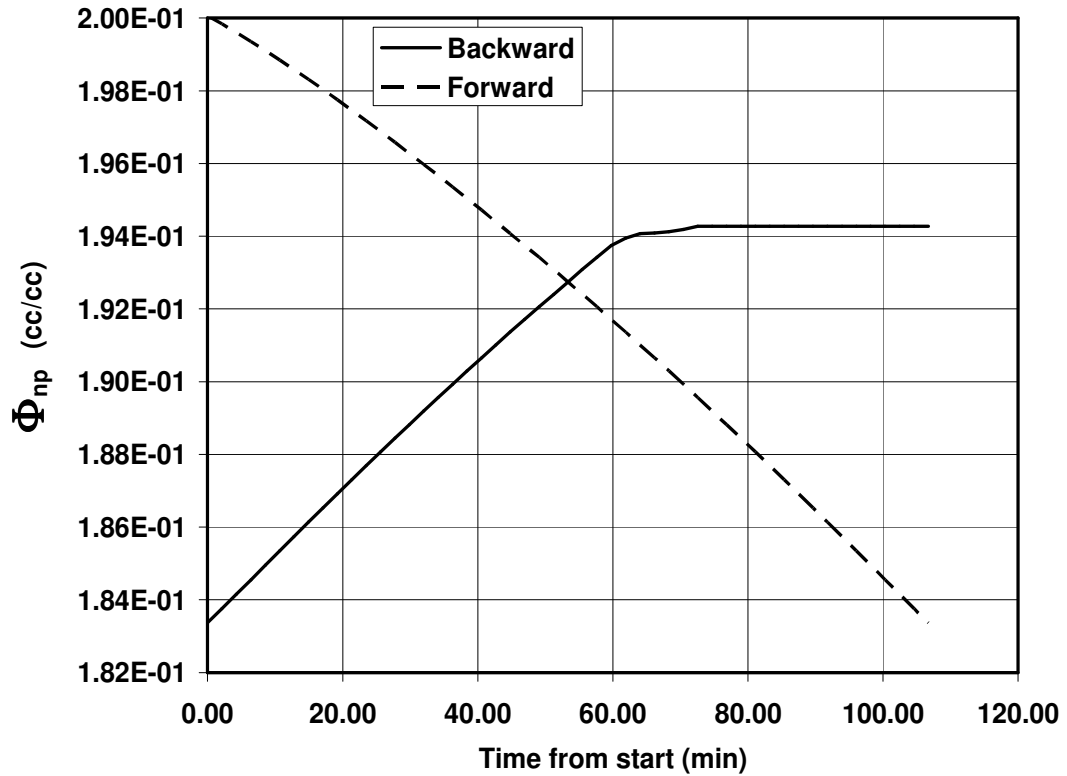


Figure 34 Variation of non- plugging porosity with respect to time

The non-plugging porosity decreases almost linearly with time for the complete circulation period. If Figure 34 is observed carefully, there is a slight bending in the porosity decline, but it may be assumed to be linear. It is seen that the porosity decreased by 8.5% at the end of minute 106.

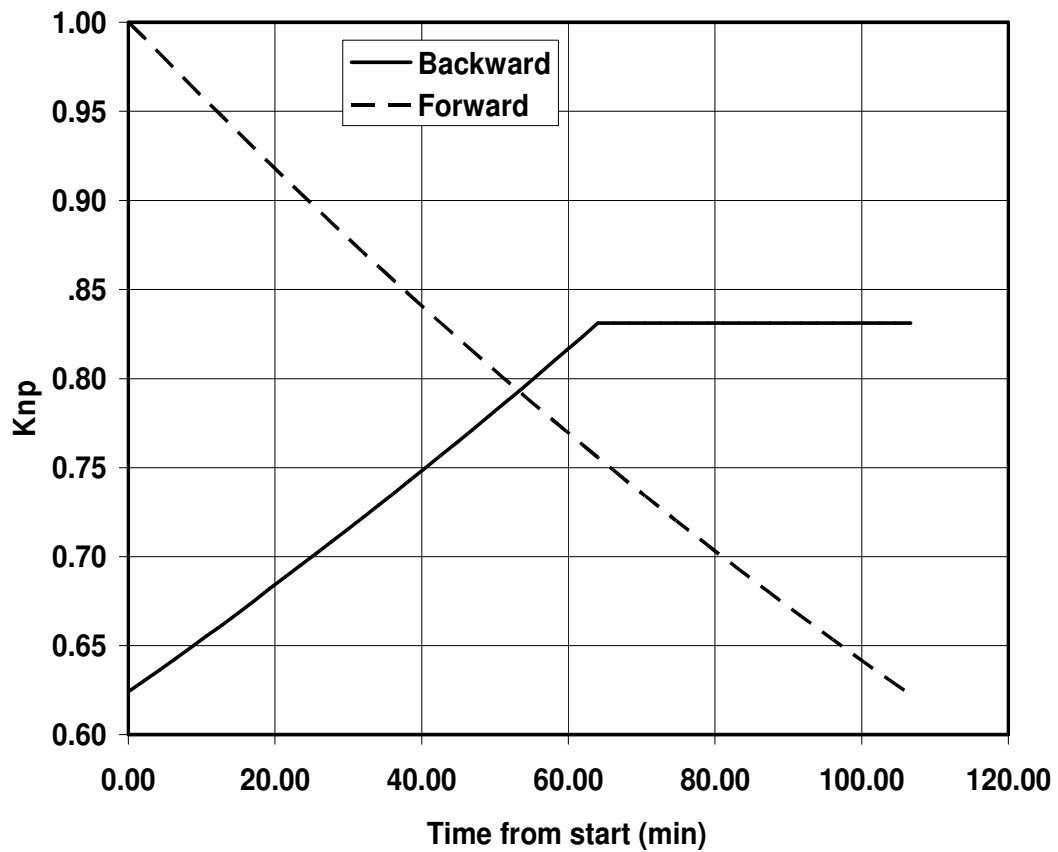


Figure 35 Variation of non-plugging permeability with respect to time

The permeability reduction is significant. The reduction percentage is 35%. For the sake of simplicity the permeability is normalized and represented as a fraction of 1.0. The reduction in non-plugging permeability is about 35% in 106 minutes (Figure 35). This reduction means that permeability has dropped from 25 D to 16.25 D.

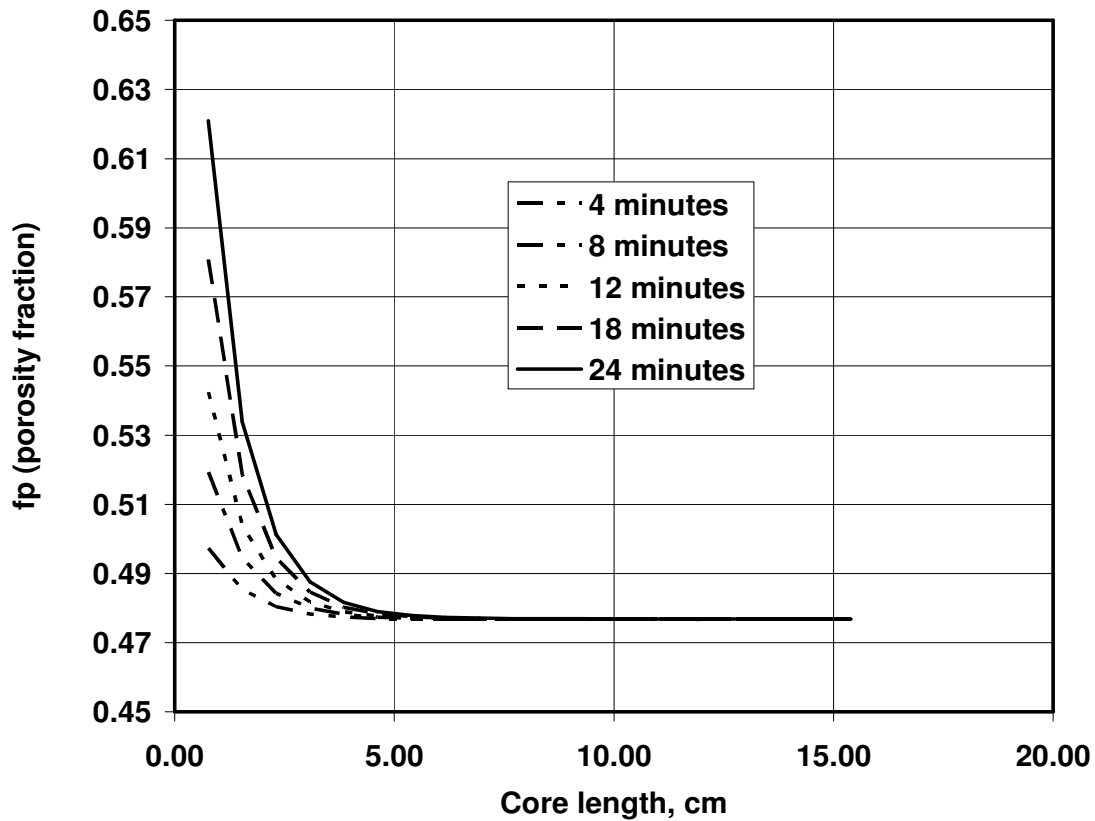


Figure 36 The fraction of plugging porosity to overall porosity (f_p) with respect to the core length at five different times.

The porosity fraction is different than the effective porosity. Because, it is defined as the ratio of the instantaneous porosity of the relevant core point to the instantaneous overall porosity of the core plug. It is seen that the as the contamination period increases, the starting values of f_p increase (Figure 36). The f_p values keep decreasing along the core sample significantly in the first five grids of the core sample. After the fifth grid, the f_p remains constant at 0.48.

The endpoints of the forward run described in the previous section are placed as the new initial conditions. The simulation is carried out by injecting water from the reverse side of the core. Thus, the cleaning effect by backflow is studied. The backflow rate is the same as the forward injection rate. Only the initial concentration of the back-flushing fluid is reduced. The time axis in the graphs is from the starting point. The back-flush simulation starts after the completion of the forward run after 106 minutes. The cleaning period takes 60 minutes. Thus, the complete process including the back and forth is completed in 166 minutes. The removal rate was determined by looking at the change of the fractions of plugging and non-plugging pathways of bulk volume occupied by the deposits (Figure 32 and Figure 33). Both the plugging and non-plugging fractions of bulk volume occupied by deposits have been cleaned efficiently. The clean-up rate for the plugging fraction is $2.0 \times 10^{-8} \text{ min}^{-1}$ (Figure 32). The clean up rate is almost fifty times faster than the forward contamination scheme. The clean-up time is 60 minutes. In the non-plugging fraction of bulk volume, the clean-up rate is constant. There is no turning point in contrast to the forward run. The clean-up rate is 1.74×10^{-4} and slightly faster than the deposition rate of the non-plugging deposits fraction in forward run (Figure 33). The particle concentration decreased both in plugging and non-plugging pathways. The plugging particle concentration decreased from 0.60 to 0.56 linearly for 81 minutes. After this moment, there is a sharp reduction followed by an increase. This increase may be because of the movement of the dislodged plugging particles towards another pore-throat location and re-plugging the media at that point. However, after the increase, plugging particles concentration kept decreasing sharply down to 0.054 ppm at the end of 60 minutes. Then, the plugging particles concentration remained constant

for the rest of the time until the outer end of the core sample. The clean-up time for the plugging particles is 60 minutes (Figure 30). The non-plugging particles were cleaned at about 62 minutes. After that time, the reduction continued, but did not provide a perfect cleaning of the non-plugging particles (Figure 31). The non-plugging porosity starts from 0.183 and appraises up to 0.193 in 60 minutes. Then it follows almost a constant trend. The non-plugging porosity is given in its real values, not by the normalized ones, because the reduction in numbers is obvious (Figure 34). The improvement in the non-plugging permeability is linear and cannot attain the initial value of 0.2 even though the particles concentration has reduced significantly. The non-plugging permeability improves from 0.62 to 0.83 as normalized values in 64 minutes (Figure-35). The actual value of the final non-plugging permeability becomes 20.75 D.

A sketch of the fraction of bulk volume containing the plugging and non-plugging pathways along the core sample is given for both contamination and cleaning cycles in Figure 37. There is an improvement in f_p from 0.476 to 0.526 throughout the core sample. However, the reduction in plugging permeability is much less than that of non-plugging permeability as percentage. Nevertheless, a small change in the plugging permeability may influence the flow of fluids because of the low initial value of the plugging permeability. The fraction of plugging porosity to overall porosity (f_p) has been drawn along the core sample at five different times such as 4, 8, 12, 18, 24 minutes (Figure 36).

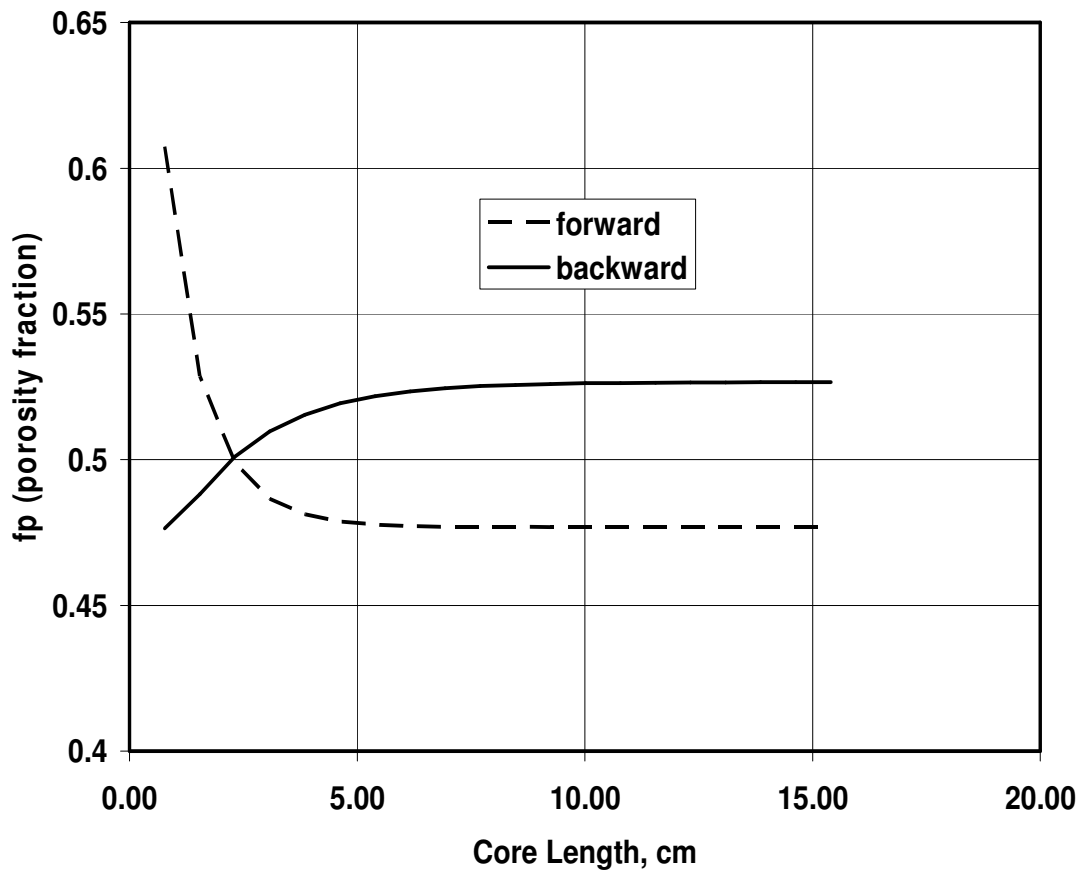


Figure 37 The fraction of plugging porosity to overall porosity (f_p) versus core length after 22 minutes.

The variation of instantaneous in-situ porosity with respect to the overall instantaneous porosity is given in Figure 37. It is seen that the dashed lines representing the forward reaction case reduce significantly within the first 5 cm of the core length. This is an indicator that porosity reduction due to fines migration occurs dominantly in the reservoir closer to the well. The recovery by the aquifer influx is insufficient to compensate this reduction, but however, there is a 10.5% porosity recovery.

The experimental work for formation damage analysis started with the determination of the porosity, permeability of the sandstone core samples (Table 14). The determination of filtration loss properties were both performed due to API RP-13 B specifications and the dynamic fluid circulation principles. Although API tests are very common in petroleum industry, they do not reflect the accurate phenomenological data. This is because, the API tests are performed under static conditions, at constant driving force 100 psia and for 30 minutes. One other disadvantage of the API tests is allowing the filtration in vertical direction. However, in most of the oil and gas wells the invasion of the fines particles and fluid loss is radially outward from the well towards the formation. On the other hand, the fluid is dynamically being circulated during drilling operations. So, API filtration test may only give limited information for static conditions, and no information for dynamic conditions.

In the literature, there are two types of dynamic fluid circulation processes. These are, the confining the pressurized fluid across the core plug for constant and short periods. The drilling fluid is kept over the core and then replaced with the next portion. In this type of application, the permeability of the core plug is initially measured. The drilling fluid is applied. Then the return permeability is measured. Thus, the reduction in permeability is obtained, and the The second type of application is circulating the fluid with nitrogen pressure continuously across the core sample. This application looks more realistic. However, the disadvantage is not using a pump. Because, in field conditions, drilling fluids are circulated using strong pumps.

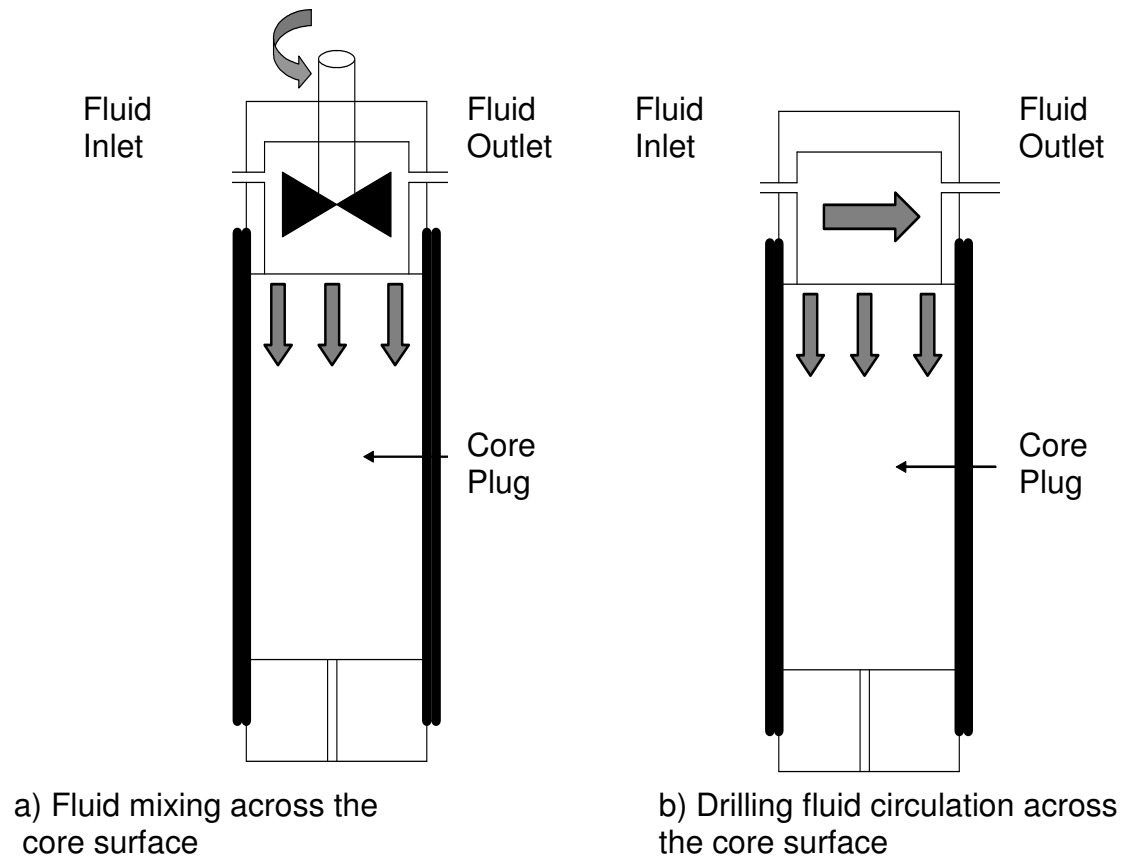


Figure 38 Two different types of fluid invasion process applications available in literature.

Drilling fluid is mixed across the core sample and there is a continuous circulation of the fluid with the driving force of the pressure exerted by nitrogen gas (Figure 38-a). Drilling fluid is confined across the surface of the core plug and subjected to pressure for 10 minute intervals. In this

case fluid is not being circulated continuously. However, fluid is kept confined temporarily. In the experiments performed in this thesis, the set-up Figure 38-b was established. Moreover, a real case field model was developed. The real case circulation system enables researchers operate with real pump and core holder system. Thus, it reflects the formation damage phenomenon better. The real case dynamic circulation is the latest of the attempts of this type of research. The porosity values of the core plugs are given in Tables14, 15, and 16 respectively.

Table 14. The porosity values of the core plugs used in dynamic circulation tests: For Pressure Cell Tests

Core Name	Dry Weight (g)	Wet Weight (g)	Ø (%)
SST1	117.63	144.25	22.63
SST2	118.28	143.80	21.58
SST3	120.80	145.13	20.14
SST4	117.22	136.13	16.13
SST5	115.09	138.50	20.34
SST6	120.38	145.23	20.64
SST7	120.89	141.82	17.31
SST8	125.25	145.48	16.15
SST9	116.80	146.40	25.34

Table 15. The porosity values of core plugs used in dynamic circulation tests: For Experiments with Pump

Core Name	Dry Weight (g)	Wet Weight (g)	Ø (%)
SST10	118.08	140.20	27.73
SST11	121.90	144.20	27.95
SST12	122.15	148.10	32.57
SST13	119.80	146.20	32.60
SST14	120.60	146.50	32.50
SST15	122.20	147.30	31.50
SST16	122.19	145.20	28.86
SST17	122.20	145.30	28.96
SST18	121.20	146.30	31.54

Table 16. The porosity values of core plugs used in dynamic circulation tests: For Experiments with Pump

Core Name	Dry Weight (g)	Wet Weight (g)	Ø (%)
SST19	182.30	205.60	26.59
SST20	118.88	145.75	30.67
SST21	186.27	207.45	24.17
SST22	177.10	183.45	7.25
SST23	116.75	141.17	27.87
SST24	185.20	203.35	20.70
SST25	183.65	196.42	14.57
SST26	118.75	142.15	26.71
SST27	181.30	208.40	30.91

The initial and return permeabilities of the core samples were calculated at different filtration pressures.

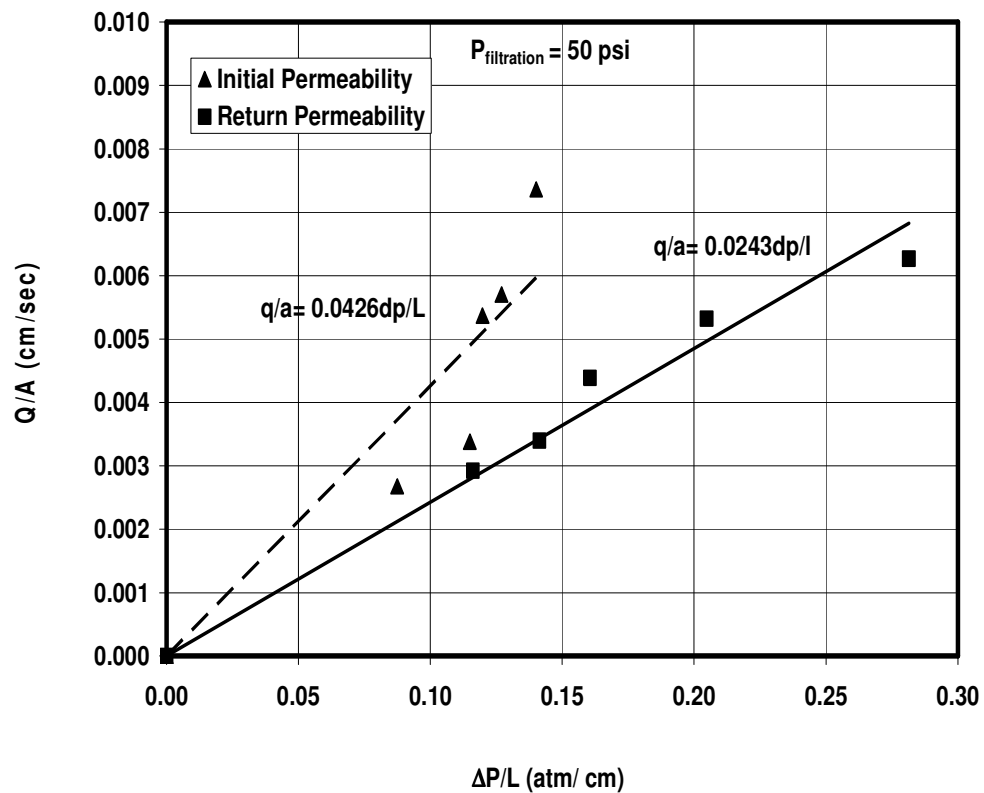


Figure 39 Initial and Return Permeability of Sample 1 with pressure cell (Drilling Fluid Type-1, Bentonite+Barite+Water).

The filtration pressure was set at 50 psi (Figure 39). This pressure is even less than the API (American Petroleum Institute) specifications. However, it is certain that permeability reduction due to fines migration exists even at low pressures. The reduction is significant. The permeability decreases from 42.6 md to 24.3 md. This indicates a 43% reduction in permeability.

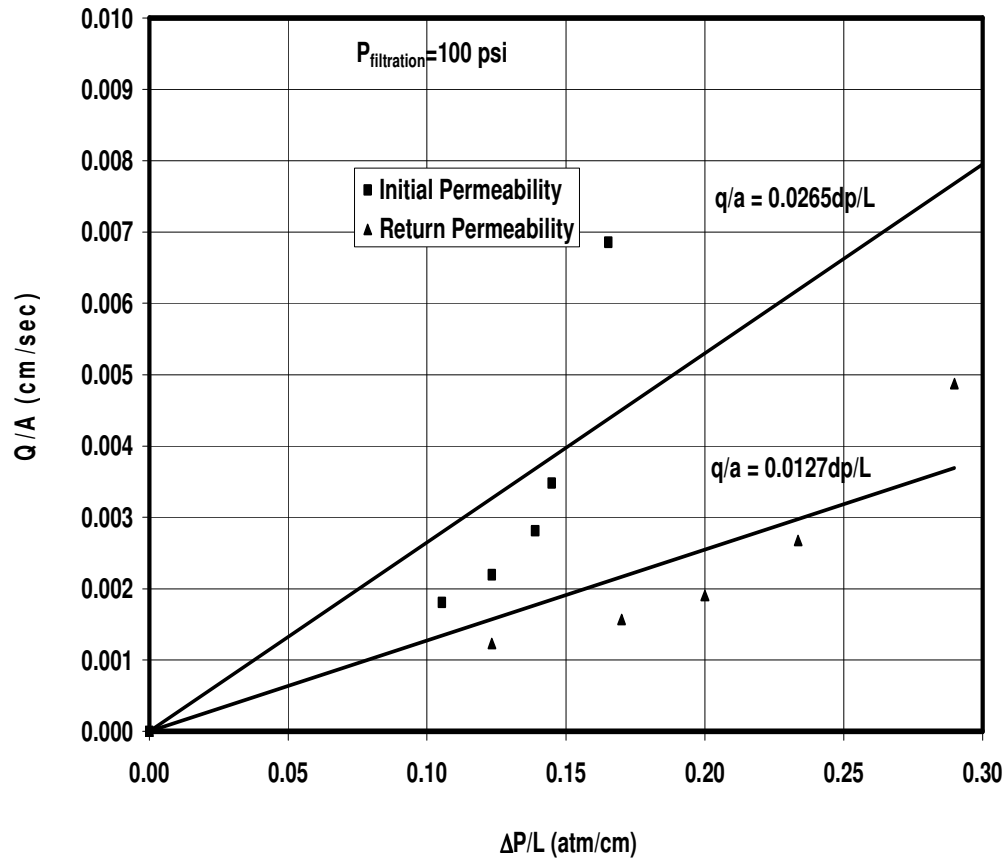


Figure 40 . Initial and Return Permeability of Sample 2 with pressure cell (Drilling Fluid Type-1, Bentonite+Barite+Water).

The filtration pressure was set at 100 psi (Figure 40). This pressure is the value specified by API. However, it is certain that permeability reduction due to fines migration exists even at 100 pressure. The reduction is significant. The permeability decreases from 26.5 md to 12.7 md. This

indicates a 52% reduction in permeability. Doubling the filtration caused a 9% increase in permeability reduction.

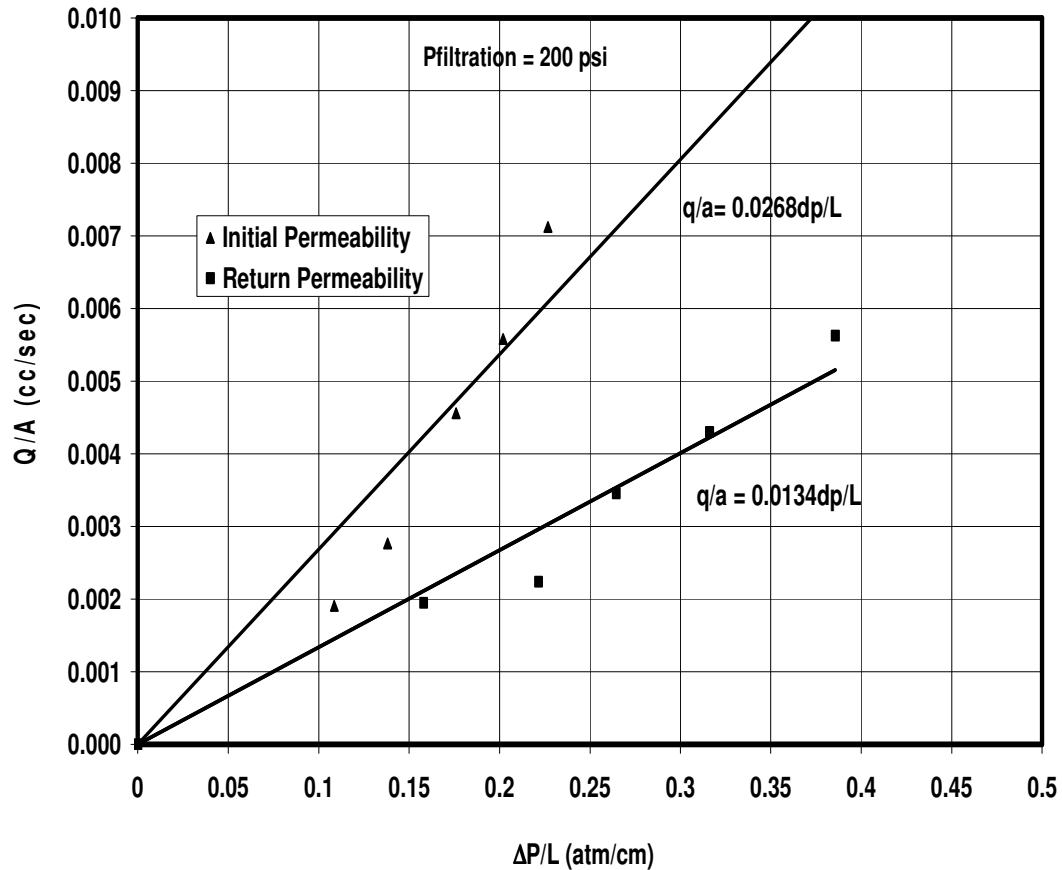


Figure 41. Initial and Return Permeability of Sample 3 with pressure cell (Drilling Fluid Type-1, Bentonite+Barite+Water).

It is seen that even the filtration pressure was increased up to 200 psi, the reduction in permeability did not increase (Figure 41). On the contrary,

the permeability reduction percentage is at the level of 50 %. Thus permeability reduction is reduced. This may be due to the high-pressure effect. The previously plugged pore throats and bridging might be cleaned slightly. Higher pressure might expose a jet effect on the nozzles. Thus a comparatively permeability improvement can be obtained.

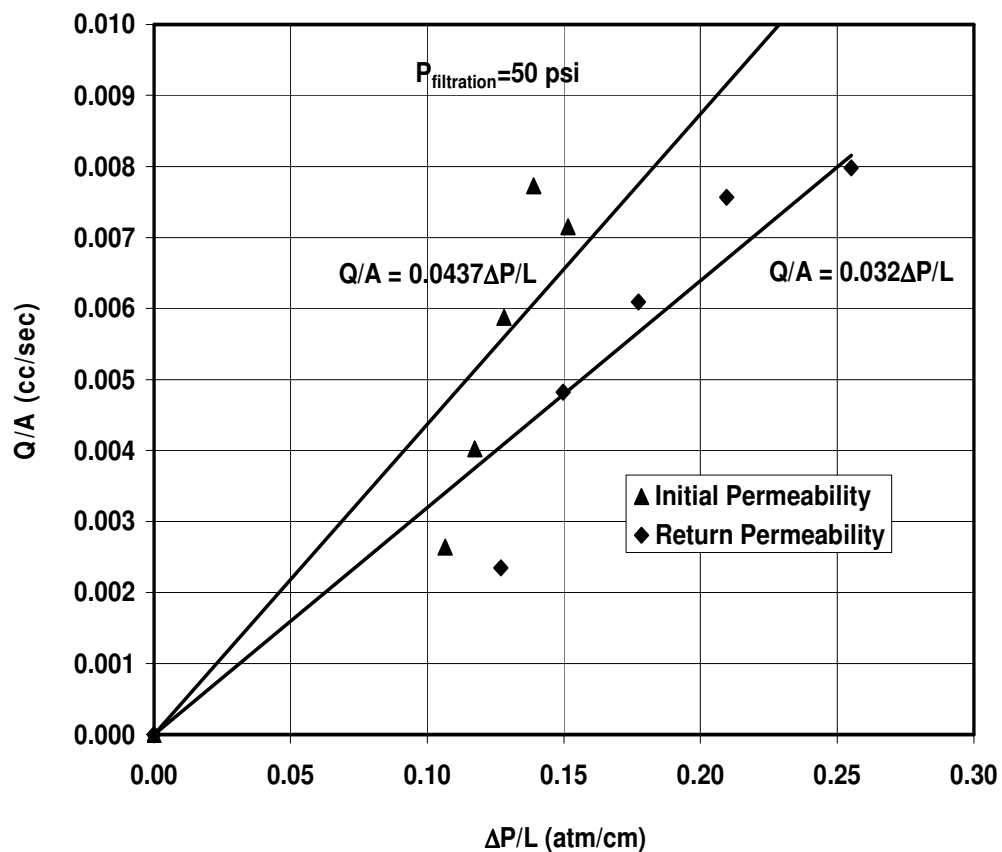


Figure 42. Initial and Return Permeability of Sample 4 with pressure cell (Drilling Fluid Type-2, Bentonite+Barite+CMC+Water)

The initial and return permeability measurements were performed using the CMC mud (Figure 42). The permeability reduction is 26.7%. This reduction percentage is less than the mud type-1 at a filtration pressure of 50 psi. The existence of CMC reduced the damage. However, 50 psi is not sufficient for making decision. So, further filtration pressures are tested with the same mud type.

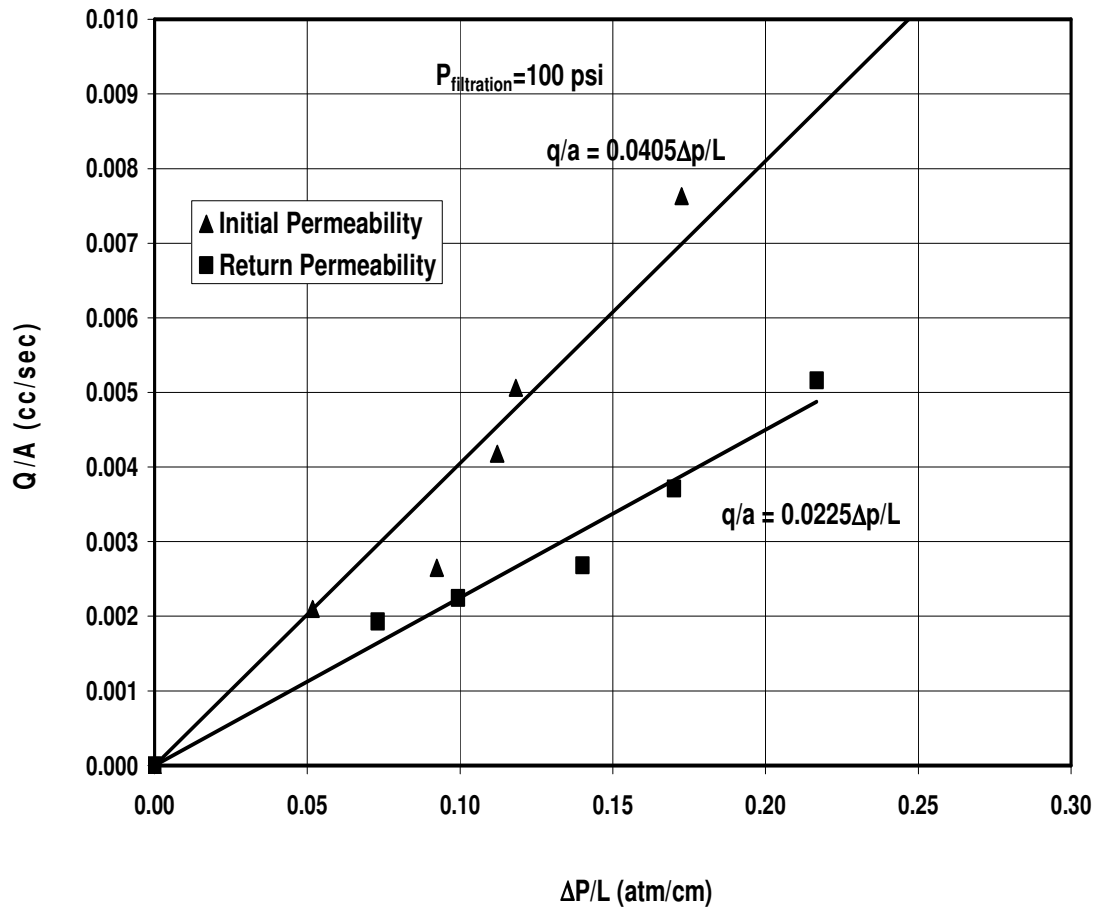


Figure 43. Initial and Return Permeability of Sample 5 with pressure cell (Drilling Fluid Type-2, Bentonite+Barite+CMC+Water).

The filtration pressure is set at 100 psi. The permeability damage ratio increased from 26.7% to 44.4 % (Figure 43). 50 psi pressure increment resulted in 17.7% increase in permeability reduction. 44% overall damage ratio with CMC mud is even less than the damage ratio 52% obtained mud type-1 at 100 psi.

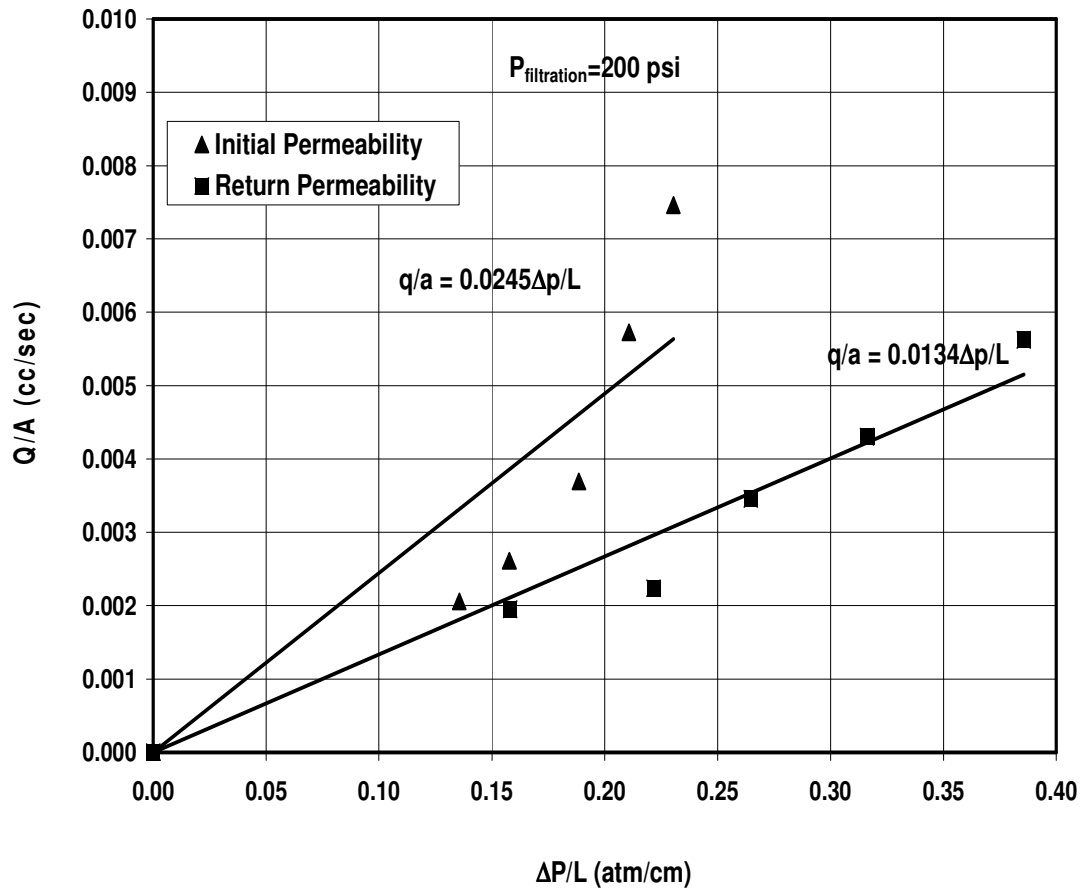


Figure 44. Initial and Return Permeability of Sample 6 with pressure cell (Drilling Fluid Type-2, Bentonite+Barite+CMC+Water).

The damage ratio at 200 psi filtration pressure is in the order of 45.3% (Figure 44). This damage ratio is slightly higher than the ratio obtained at 100 psi. Thus, it can be said that the permeability damage ratio is almost constant from 100 psi to 200 psi filtration pressure. The trends of the permeability reductions in both fluid type-1 and fluid type-2 are very similar. There is a sharp increase up to 100 psi. Then an almost constant trend is followed.

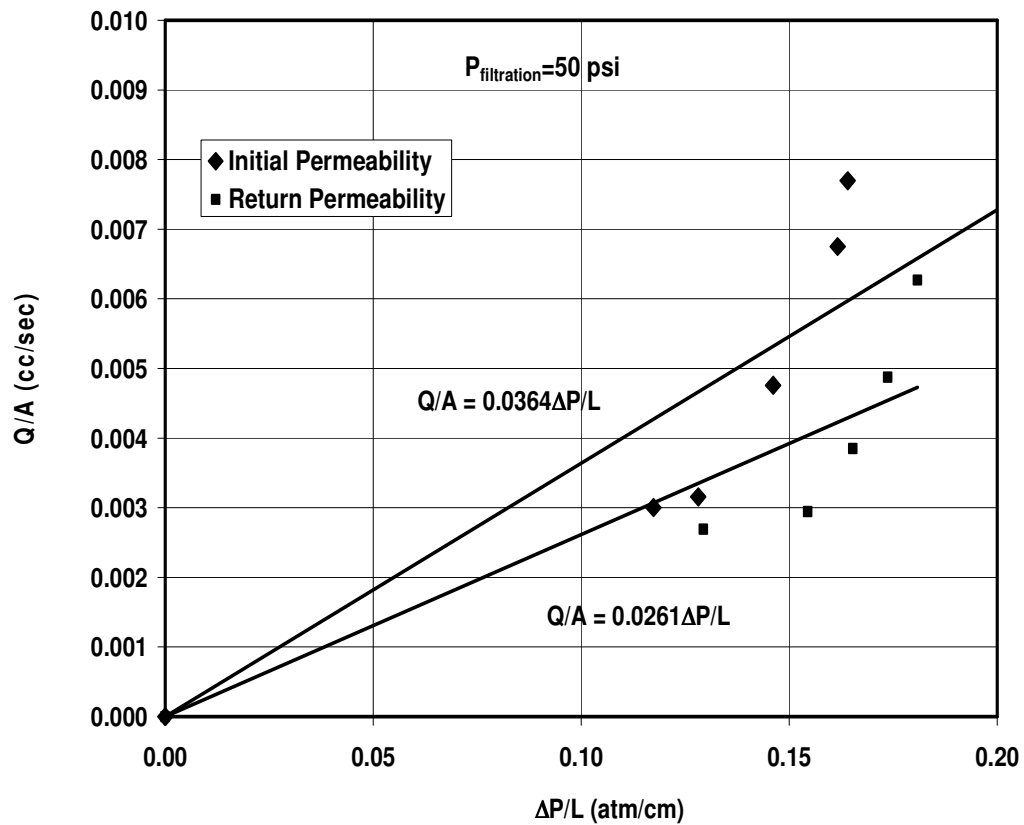


Figure 45. Initial and Return Permeability of Sample 7 with pressure cell (Drilling Fluid Type-3, Bentonite+Barite+Polymer-XT+Water).

The permeability reduction percentage is 28.2 % (Figure 45). This value is less than the non-treated bentonite mud which is fluid type -1. However, it is almost equal as the damage ratio of CMC mud (Fluid Type -2). Thus, the 50 psi value is not sufficient for making comparison between the fluid type-2 and 3. The damage ratios at 100 psi and 200 psi filtration pressure are required.

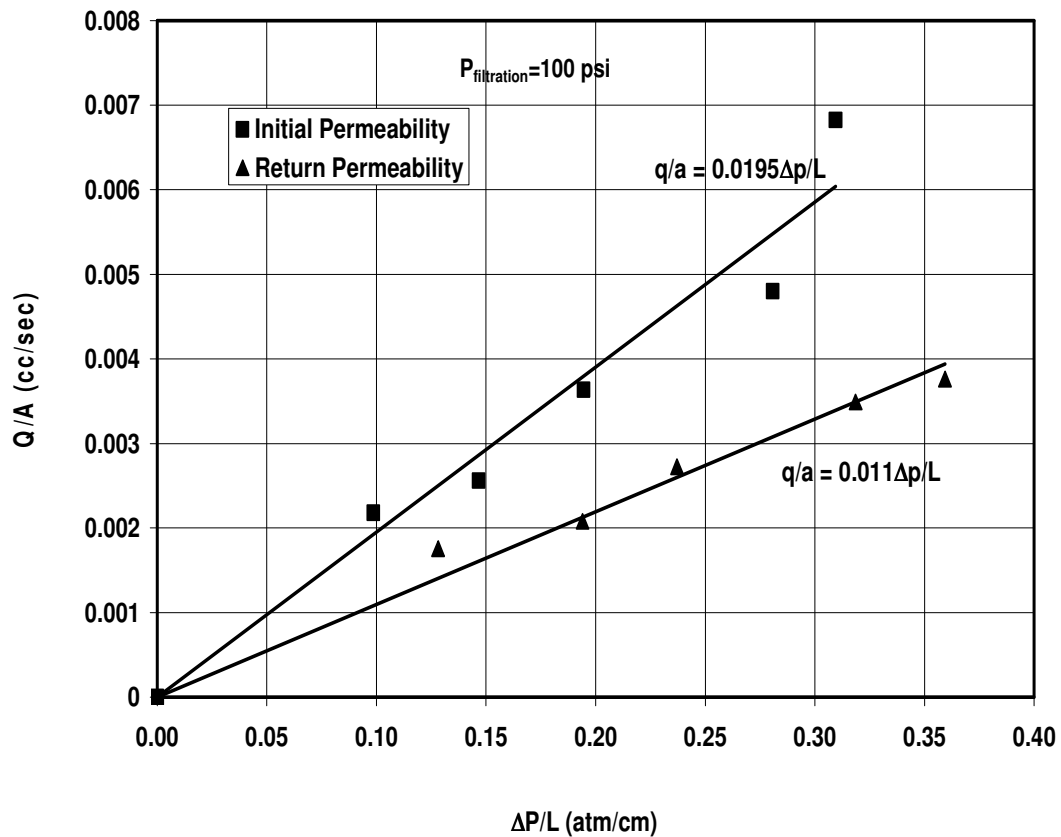


Figure 46 Initial and Return Permeability of Sample 8 with pressure cell (Drilling Fluid Type-3, Bentonite+Barite+Polymer-XT+Water).

The damage ratio with mud type-3 at 100 psi is 43.5 % (Figure 46). This value is very close to the damage ratio with fluid type -2 at 100 psi. Thus, it is not possible to compare mud type 2 and 3. It is observed that the damage ratio is reduced with respect to non-treated mud. Thus, a final attempt was made at 200 psi.

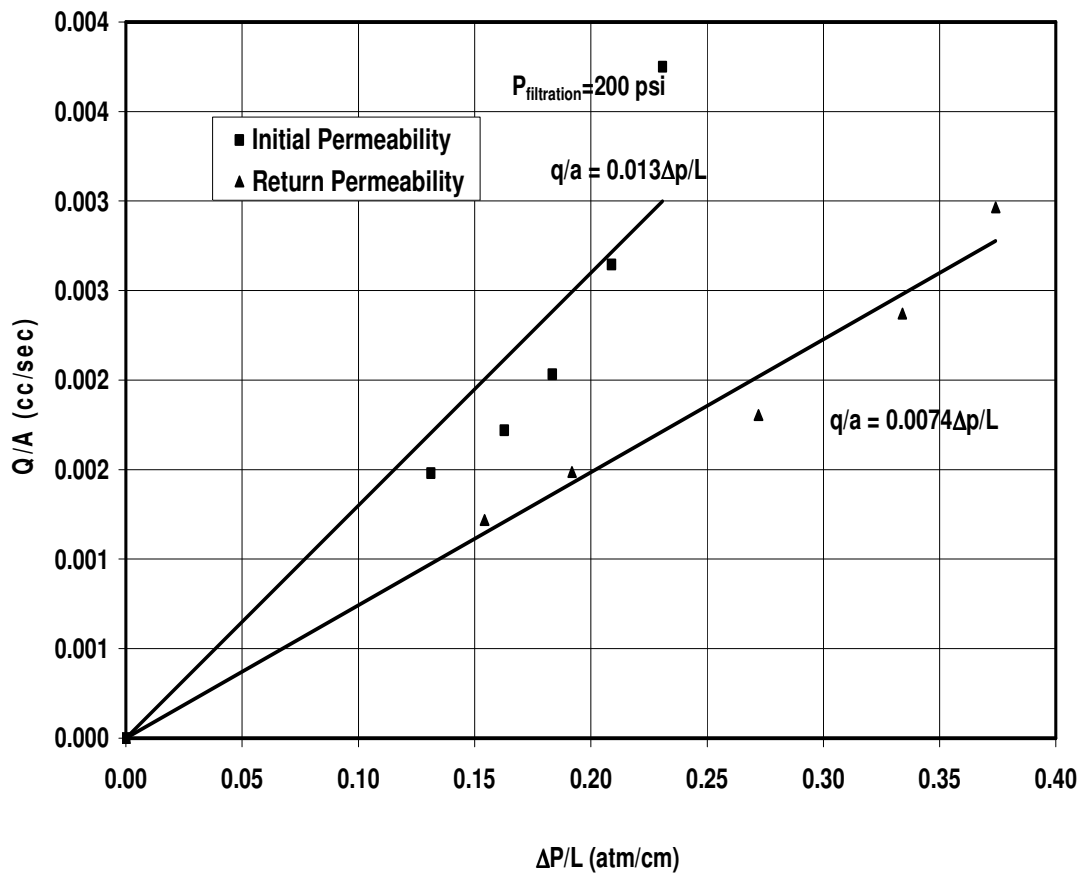


Figure 47 Initial and Return Permeability of Sample 9 with pressure cell (Drilling Fluid Type-3, Bentonite+Barite+Polymer-XT+Water).

The damage ratio at 200 psi is 41% (Figure 47). This damage ratio value is less than that of CMC mud at 200 psi. When the over all values are considered, it is seen that the minimum damage ratio can be obtained with the polymer mud which is mud type-3. However, it should be noted that the experimental results depicted above were obtained with the pressurized experimental set-up (Figure 38). Although, these experiments are representative for the fines invasion phenomenon, they may not reflect the reality, completely. The reason is the absence of pump and lack of the continuous dynamic circulation in the systems. The pressurized unit in Figure 38 is good for understanding the behavior, However, drilling mud is circulated at constant time periods consecutively. This application is dynamic, too. In field conditions, the drilling mud is circulated continuous by mud pumps. Thus, a new experimental set-up with continuous mud flow was constructed in Figures 1,2, and 3. This set-up enables the continuous flow of the drilling mud over the core plug surface. There are no waiting sessions, or unrealistic assumptions. The set-up makes it possible to make initial permeability measurement, dynamic mud circulation and return permeability measurement consecutively, without even touching or changing the position of the core plug. This is an advantage for obtaining better results. Because as the core plug is artificially moved by the researchers, the mud cake may be deformed, the invaded particles may change position in the porous media due to vibrations. The core plug is vacuumed initially. Then the core plug is saturated with brine. The drilling muds are circulated. The fines particles invade into porous media. This can be understood when the breakthrough at the outlet end of the core plug flows with clays. However, this may not be always possible. In some cases the pore throats may be 100% plugged. This phenomenon depends upon the type of the drilling

mud, the chemical additives, the formation and the differential filtration pressure. A correlation between the permeability damage ratio and the filtration pressure is very useful for making further predictions. On the other hand, the selection of appropriate drilling mud with as less invasive characteristics as possible is important for formation damage analysis. Thus, the clay particle may not move towards the breakthrough. The results of the dynamic experiments with pump are given below in figures and tables.

All of the flooding and dynamic circulation tests were conducted twice. Core plugs were taken from closer sections of the same rock fragments to have better results in reproducibility. Even though the core plugs were taken from closer sections, the rocks do not display the same characteristic throughout the whole matrix. However, the permeability and the return permeability measurements were very close to each other as in the order of 10%. One other reason of this variation in the measurements is the homogeneity of the drilling fluids. Although they are continuously mixed in the mixing tank, some clay particles stick on the walls of the tank and some clay loss is observed. However, it was seen that the experiments are reproducible, under the identical conditions as noted in the procedures given in the Appendices A,B,C,D. The x-Ray tests were conducted for only once due to the availability of the limited time in the USA.

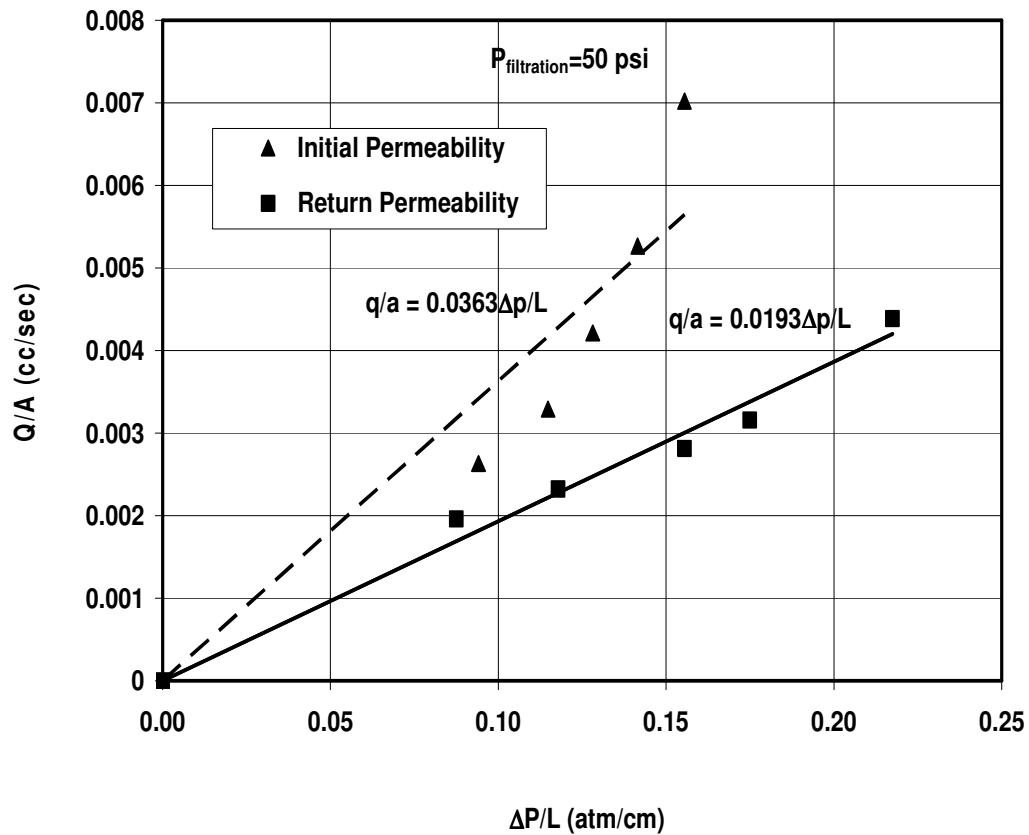


Figure 48 Initial and Return Permeability of Sample 10 with pump (Mud Type-1, Bentonite+Barite+Water).

The damage ratio increased by 4% and was observed as 47% in the presence of mud pump (Figure 48). The damage ratio was calculated as 43% with the same mud type at the same filtration pressure 50 psi with the presence of pressure cell. This 4% increment is the continuous circulation effect of the dynamic mud motion across the core plug surface. One important factor is the erosion on the core surface. The core plug starts being eroded as the time elapses. Thus, core surface is softened.

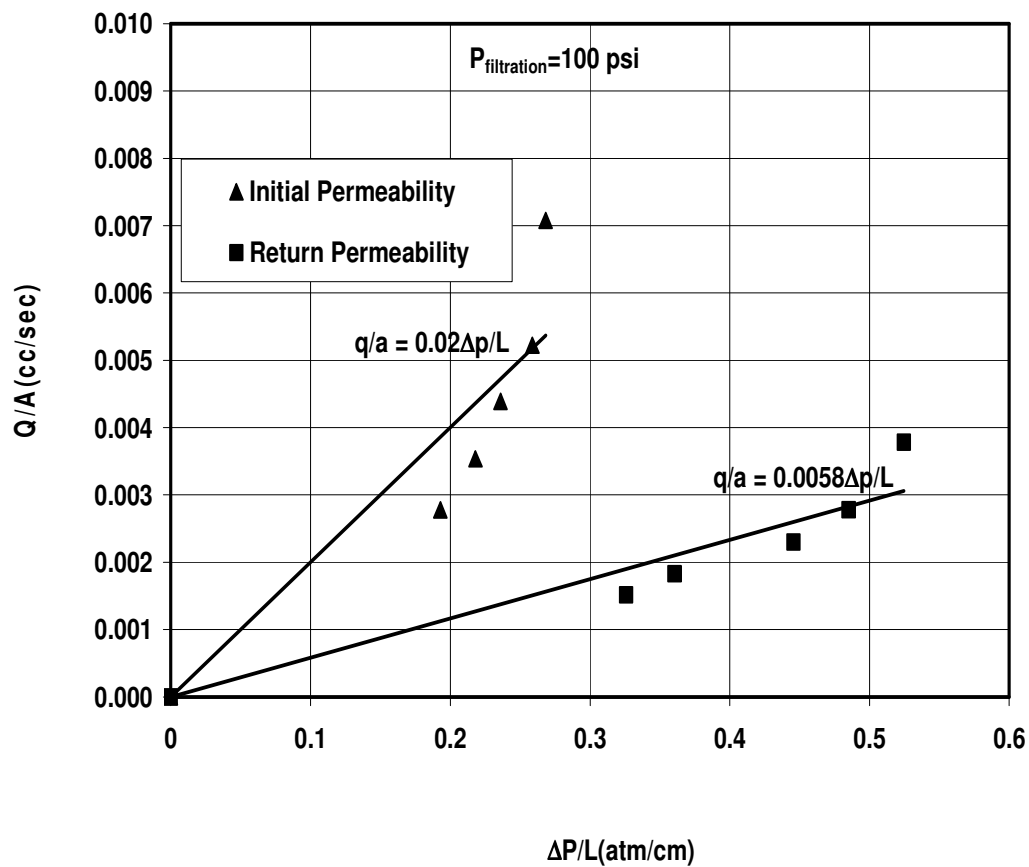


Figure 49 Initial and Return Permeability of Sample 11 with pump (Fluid Type-1, Bentonite+Barite+Water).

The damage ratio increased by 19% and was observed as 71% in the presence of mud pump (Figure 49). The damage ratio was calculated as 52% with the same mud type at the same filtration pressure 100 psi with the presence of pressure cell. This 19% increment is the continuous circulation effect of the dynamic mud motion across the core plug surface. It is really interesting that the existence of pump triggered the damage

ratio and caused a sudden jump. At 50 psi, the increment was comparatively less with respect to damage ratio at 100 psi with mud pump.

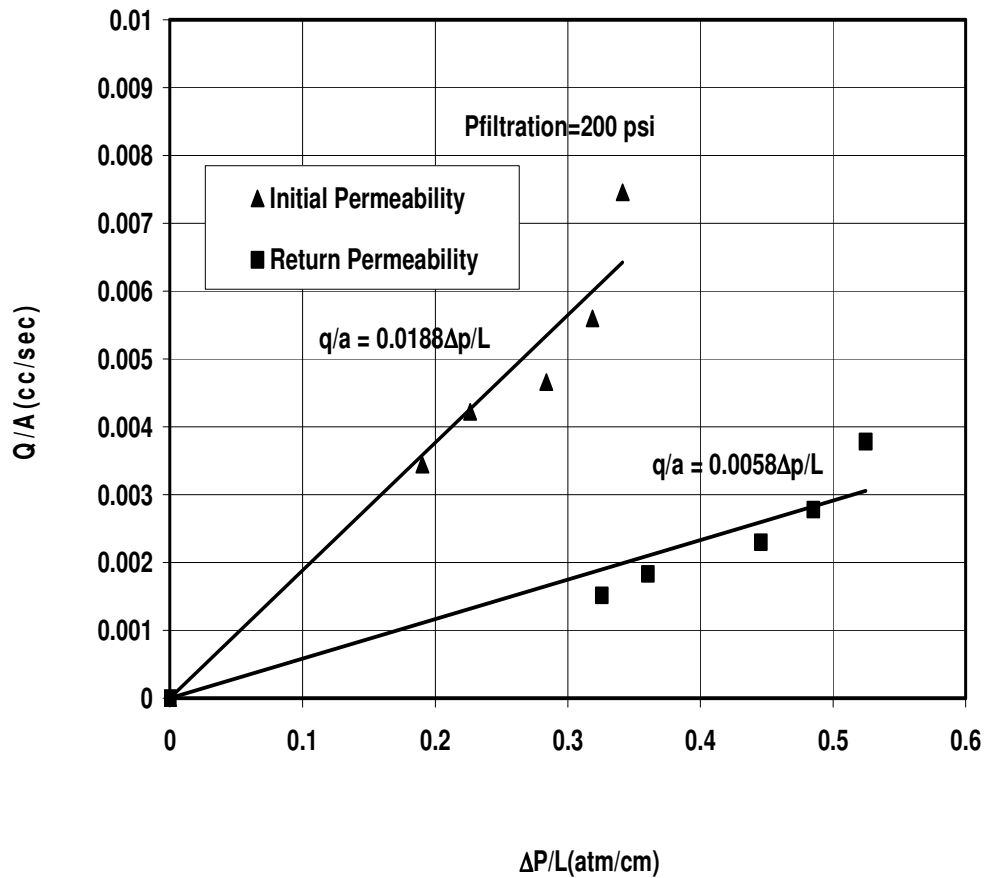


Figure 50 Initial and Return Permeability of Sample 12 with pump (Fluid Type-1, Bentonite+Barite+Water).

The permeability reduction at 200 psi filtration pressure is 69% (Figure 50). This value is 19% more than the damage ratio with the same fluid at 200 pressure with the conventional pressure cell set-up. The overall profile of the damage ratio with fluid type-1 at three different pressures as

50 psi, 100 psi and 200 psi are 47%, 71% and 69 %. It can be observed that the rapid damage ratio build up takes place with until 100 psi filtration pressure is reached. The slight reductions in damage ratio such as 1% or 2 % are because of deformation of the previously formed bridges across the pore throats.

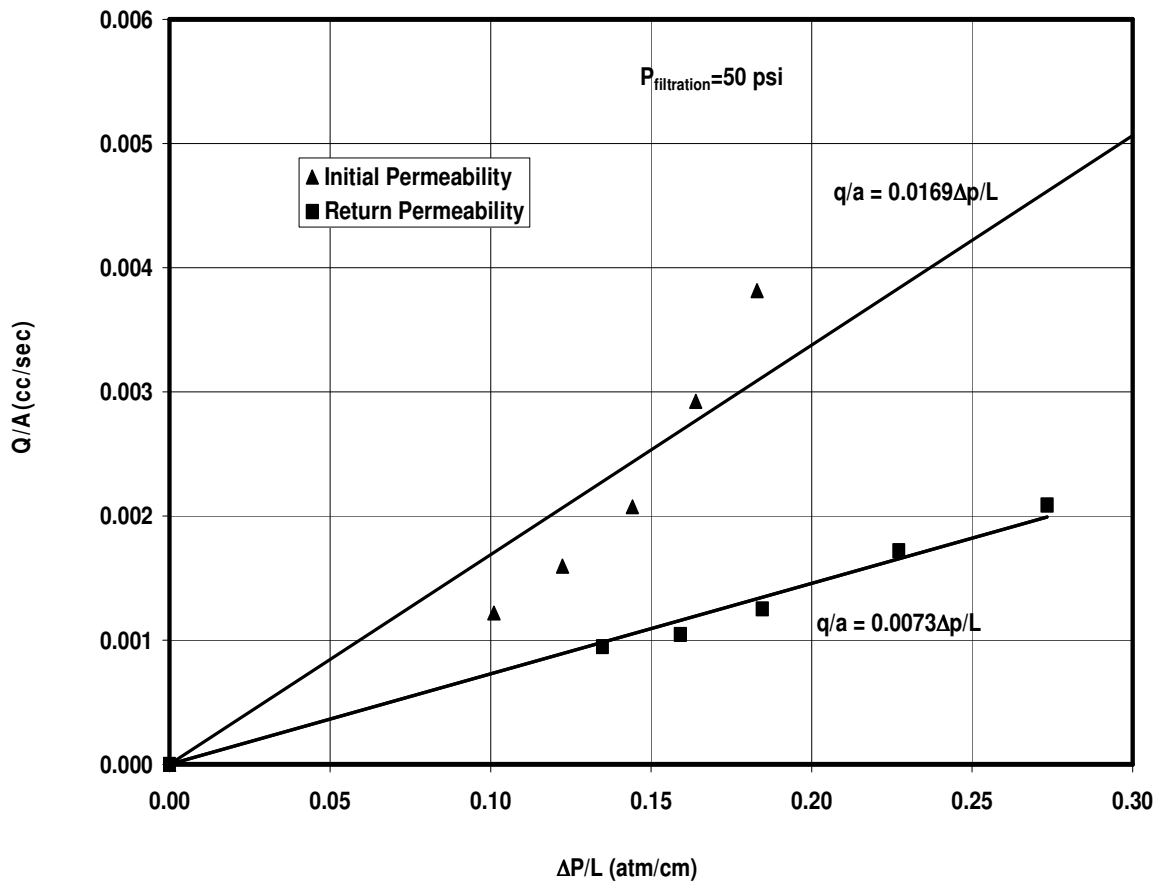


Figure 51 Initial and Return Permeability of Sample 13 with pump (Fluid Type-2, Bentonite+Barite+CMC+Water).

The second type drilling mud gives out a permeability damage ratio of 57% (Figure 51). This value is more than twice the damage ratio at the same pressure with the same drilling mud with pressure cell set-up. The damage ratio increased by 30% and was observed as 57% in the presence of mud pump. The damage ratio was calculated as 26.7% with the same mud type at the same filtration pressure 50 psi with the presence of pressure cell. This 30% increment is because of the continuous circulation effect of the dynamic mud motion across the core plug surface.

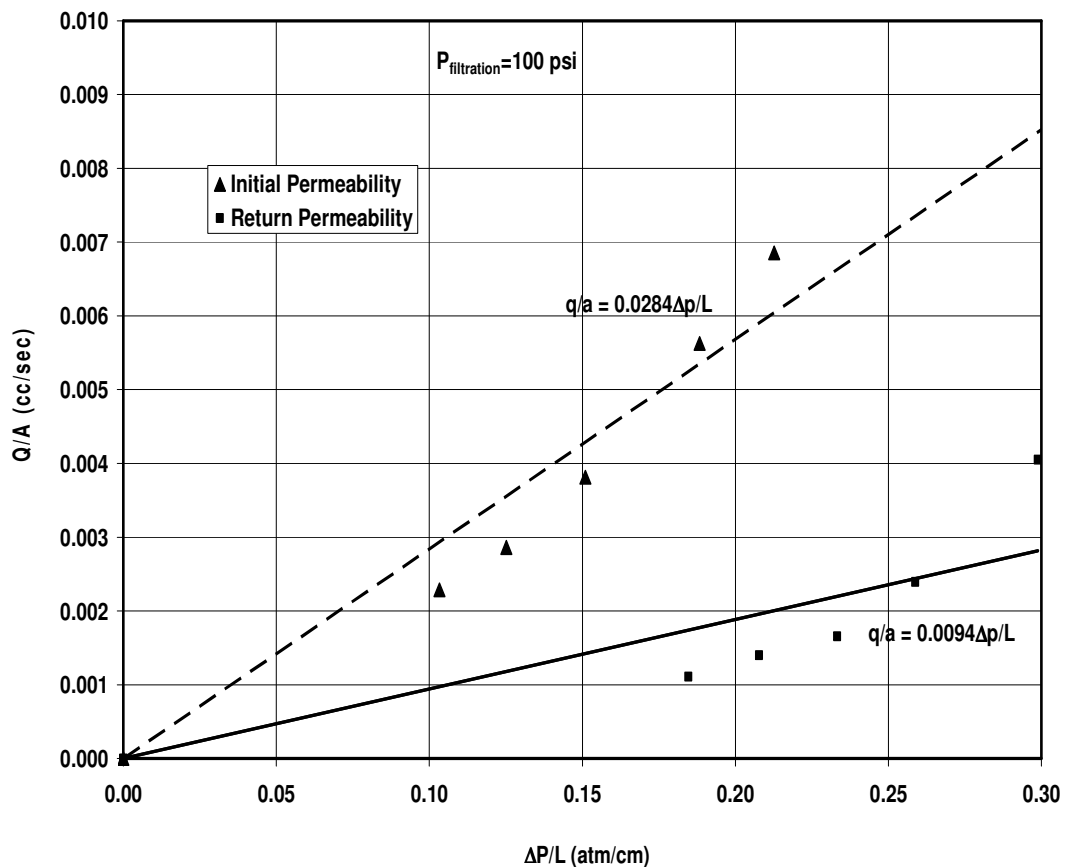


Figure 52. Initial and Return Permeability of Sample 14 with pump (FluidType-2, Bentonite+Barite+CMC+Water).

The second type drilling mud gives out a permeability damage ratio of 67% (Figure 52). This value is 23% more than the damage ratio at the same pressure with the same drilling mud with pressure cell set-up. The damage ratio increased by 23% and was observed as 67% in the presence of mud pump. The damage ratio was calculated as 44% with the same mud type at the same filtration pressure 100 psi with the presence of pressure cell. This 23% increment is due to the continuous circulation effect of the dynamic mud motion across the core plug surface.

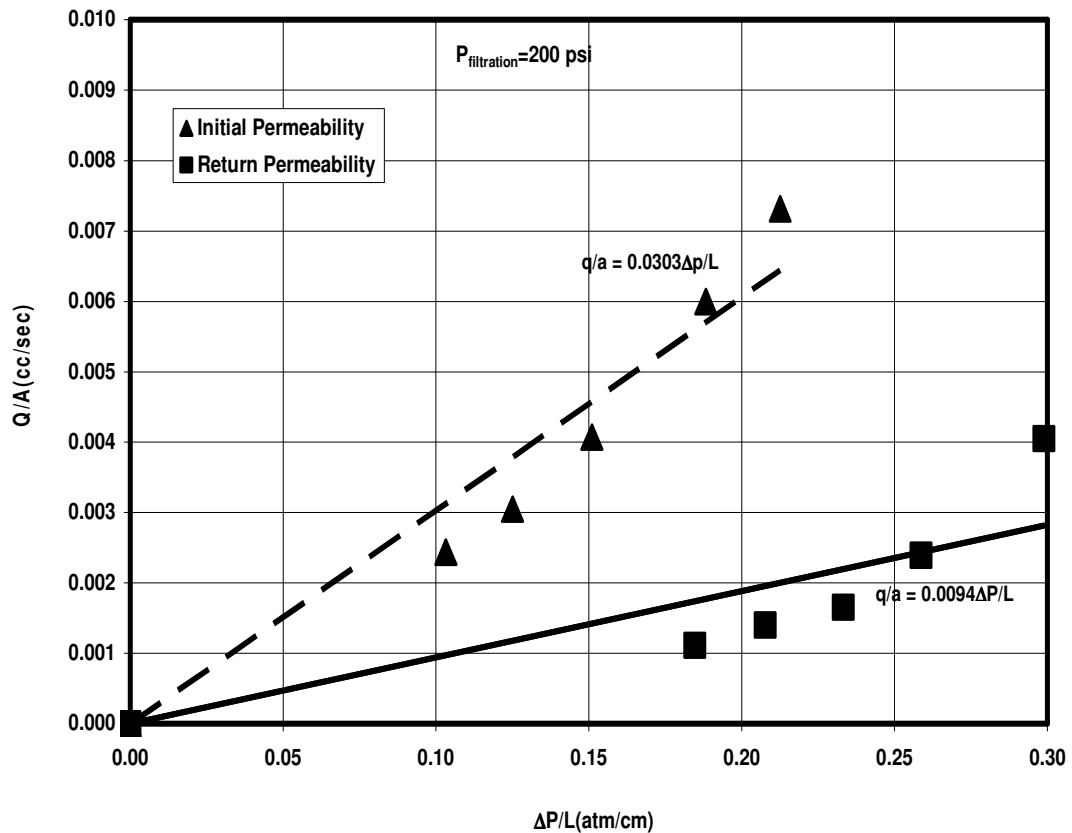


Figure 53 Initial and Return Permeability of Sample 15 with pump (Fluid Type-2, Bentonite+Barite+CMC+Water).

The damage ratio at 200 psi filtration pressure in the presence of mud pump is 67% (Figure 53). This value is close to the value obtained at 100 psi. All of the permeability plots exhibit that the damage ratio does not change significantly after 100 psi. The damage ratio increases until 100 psi very sharply. From this pressure value on the trend is almost constant.

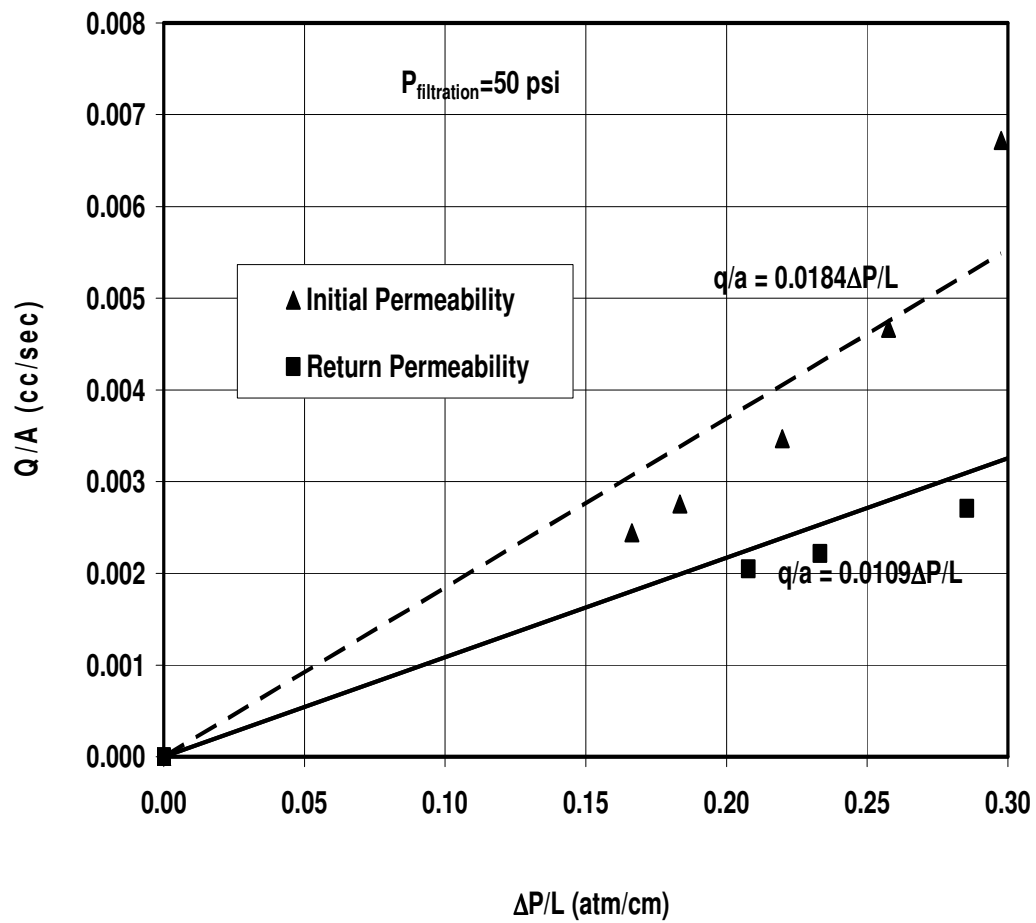


Figure 54 Initial and Return Permeability of Sample 16 with pump (Fluid Type-3, Bentonite+Barite+Polymer-XT+Water).

The permeability damage ratio is 41% at 50 psi filtration pressure (Figure 54). The damage ratio increase with respect to pressure cell is about 13%. It is seen that even at lower pressures, mud type-3 has qualified the minimum damage ratio. Polymer mud looks like a good candidate for the optimum damaging drilling mud.

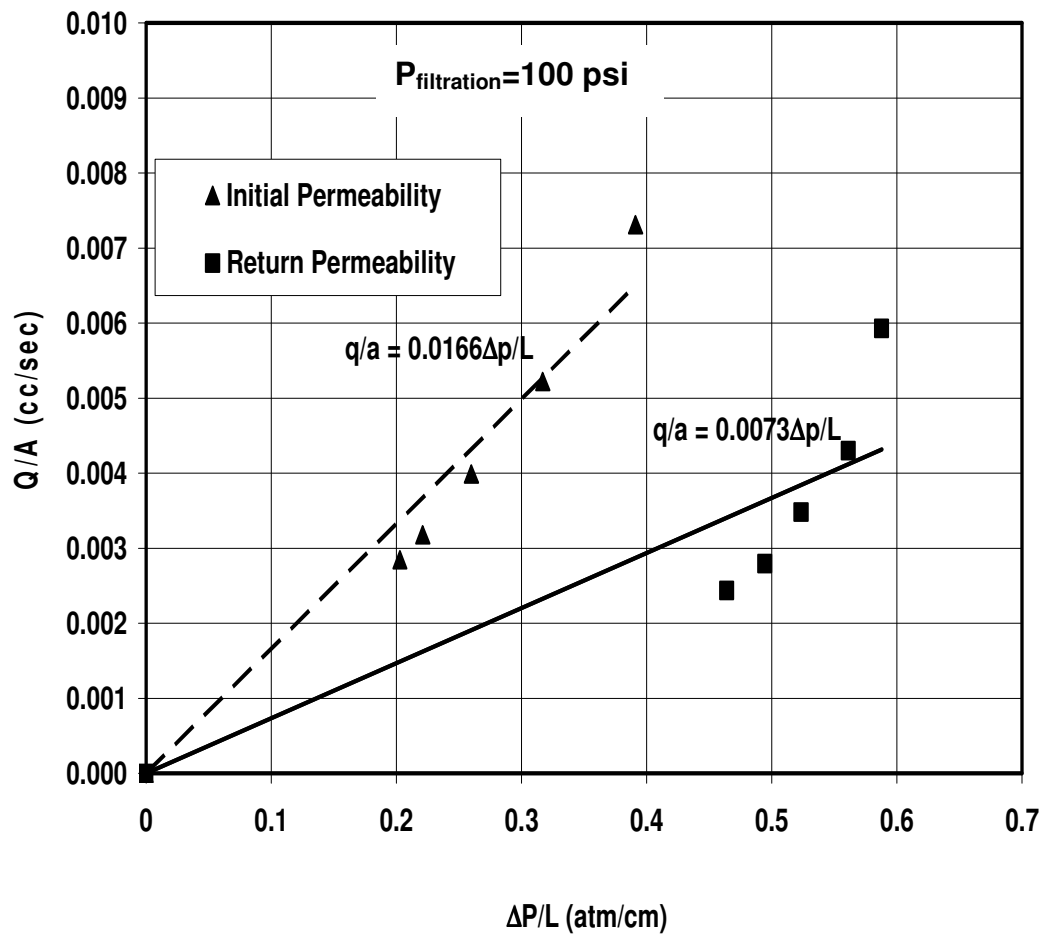


Figure 55 Initial and Return Permeability of Sample 17 with pump (Fluid Type-3, Bentonite+Barite+Polymer-XT+Water).

The damage ratio with fluid type-3 at 100 psi filtration pressure is 56% in the presence (Figure 55). This value is 12.5 % more than the pressure cell experiment performed at the same conditions. However, a damage ratio of 56% is less than the damage ratios of the other mud types at 100 psi. Thus, minimum damage ratio is obtained with mud type-3 at 100 psi, too as well as at 50 psi.

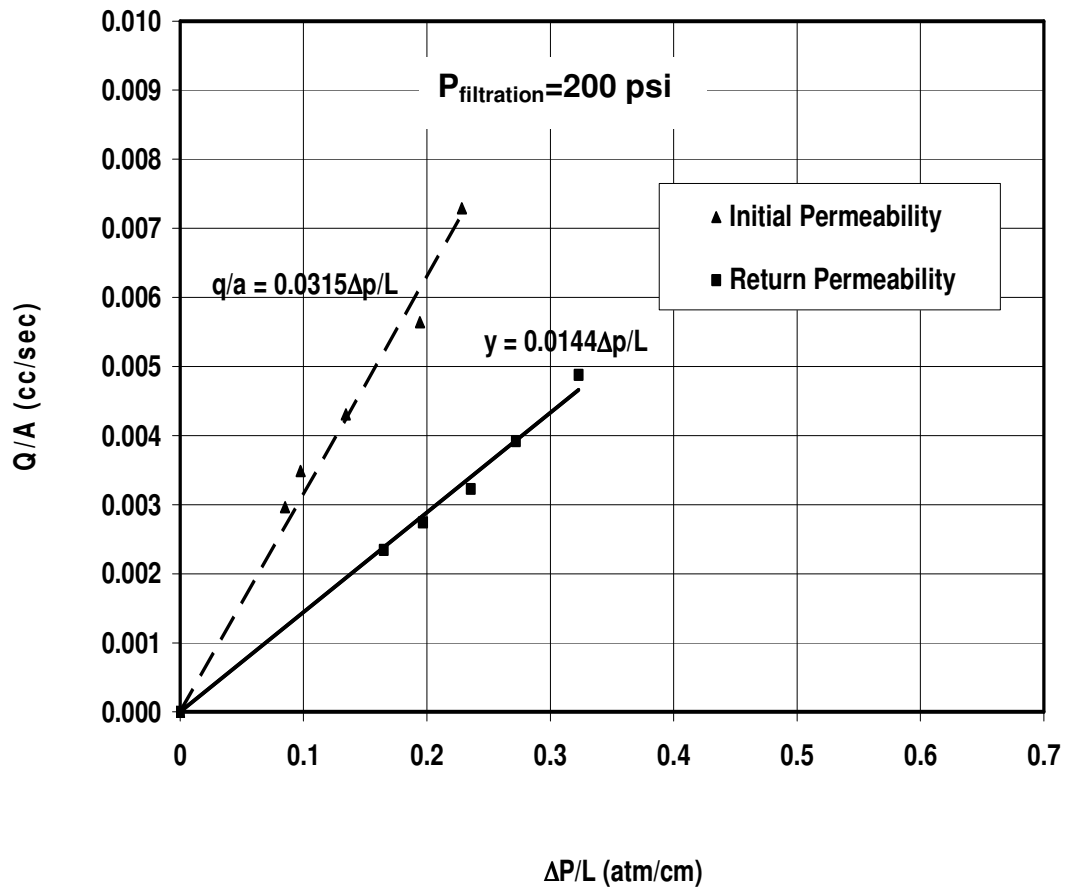


Figure 56 Initial and Return Permeability of Sample 18 with pump (Fluid Type-3, Bentonite+Barite+Polymer-XT+Water).

The damage ratio with mud type-3 at 200 psi filtration pressure is 54% in the presence (Figure 56). This value is 13 % more than the pressure cell experiment performed at the same conditions. However, a damage ratio of 54% is less than the damage ratios of the other mud types at 200 psi. Thus, minimum damage ratio is obtained with mud type-3 at 200 psi, too as well as at 50 psi, and 100 psi filtration pressures. The experiments conducted with both pressure cell and mud pump, indicate that mud typ-3 (bentonite + barite+ Polymer-XT+ water) is the least damaging fluid among the three mud samples.

Table 17 Experimental Results of Dynamic Circulation Tests with Drilling Fluid Type-1

Filtration Pressure, P_f (psi)	Damage Ratio, DR(%) after 30 minutes	Damage Ratio, DR(%) after 60 minutes	Damage Ratio, DR(%) after 90 minutes
0	0.0	0.0	0.0
20	18.9	26.0	29.9
30	26.5	37.0	40.6
40	33.2	43.0	47.4
50	36.1	47.0	51.7
75	54.8	64.0	68.1
100	65.1	71.5	76.2
110	65.9	72.5	77.1
125	63.8	71.7	75.6
150	61.1	70.8	74.1
175	60.7	69.8	73.2
200	59.8	69.0	72.8

The experimental results of the dynamic circulation experiments are summarized in Tables 17, 18 and 19. It is observed that the damage ratio increases as the mud circulation period increases. Experiments were run at eleven different filtration pressures and three different circulation periods. The maximum permeability damage ratios were obtained with the CMC mud which is referred as fluid type-2. The minimum damage ratio was obtained with the polymer mud which is referred as fluid type-3. The simulation of the fines migration and damage ratio is applied on the experimental data. The experimental and simulated data are compared, too.

Table 18 Experimental Results of Dynamic Circulation Tests with Drilling Fluid Type -2

Filtration Pressure, P_f (psi)	Damage Ratio, DR(%) after 30 minutes	Damage Ratio, DR(%) after 60 minutes	Damage Ratio, DR(%) after 90 minutes
0	0.0	0.0	0.0
20	32.0	35.5	37.2
30	36.0	40.0	41.4
40	42.0	46.5	48.8
50	49.0	55.3	64.4
75	65.0	68.5	70.2
100	71.0	73.2	79.3
110	71.5	74.8	79.6
125	71.9	75.7	79.8
150	72.6	76.2	79.9
175	72.8	76.4	79.9
200	73.0	76.7	81.0

Table 19 Experimental Results of Dynamic Circulation Tests with Drilling Fluid Type-3

Filtration Pressure, P_f (psi)	Damage Ratio, DR(%) after 30 minutes	Damage Ratio, DR(%) after 60 minutes	Damage Ratio, DR(%) after 90 minutes
0	0.0	0.0	0.0
20	21.5	32.4	37.4
30	23.8	36.5	39.7
40	26.5	38.3	44.2
50	29.3	41.0	48.1
75	35.8	48.2	56.3
100	38.3	56.2	60.7
110	38.9	56.6	63.7
125	42.2	56.3	63.3
150	42.8	54.5	63.8
175	43.3	54.4	63.8
200	43.8	54.2	63.8

The experimental results of the dynamic circulation tests are depicted in Figures 57, 58, and 59, respectively. Three different water based drilling fluids at three different circulation periods are plotted. The damage ratio profiles for the three fluid samples are similar. They display a quick increase upto 100 psi. Then, they exhibit a small reduction and have almost a constant value. The reason for the sudden increase of the damage ratio until 100 psi is, continuous deposition of the particles until that pressure value. From this point, the pore-throat pluggings come to a saturation point and they can not be plugged further more. Moreover, some of the previously deposited are moved from their places due to the jet impact caused by the increasing of the pressure. Thus, a small reduction in damage ratio occurs.

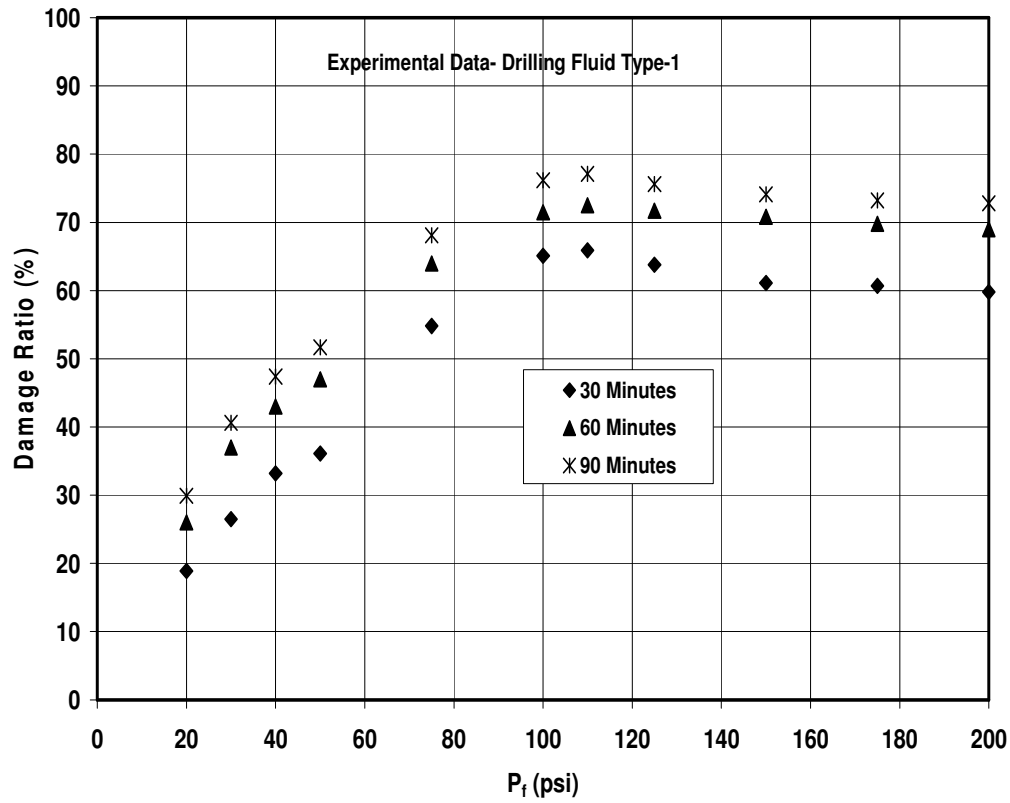


Figure 57 Experimental Results of the Drilling Fluid Type-1

It can be extracted through Figures 57, 58, and 59 that, the maximum permeability damage ratio was obtained with drilling fluid type-2. The minimum damage ratio was obtained with drilling fluid type-1. The damage ratios of the three mud samples increase with increasing circulation periods. However, it should be noted that the major permeability reduction or the major damage ratio increase takes place until the filtration pressure is reached up to 100 psi. The damage ratio exhibits a constant trend from 100 psi on. It is understood that the drilling fluid with Polymer –XT is the least damaging type. Thus, it can be interpreted as the least invading and optimum mud for having the minimum formation damage.

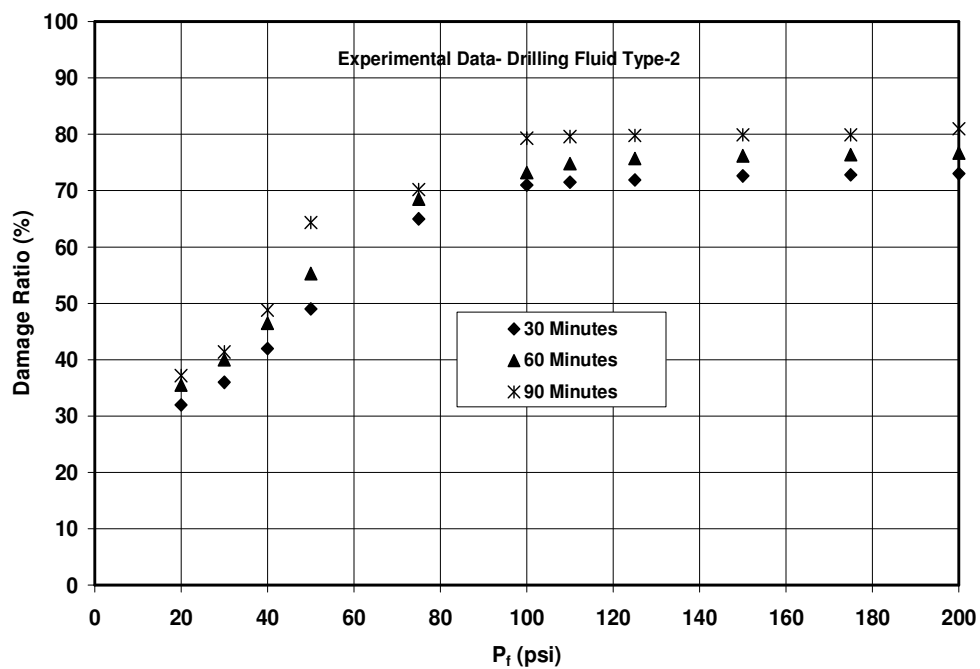


Figure 58 Experimental Results of the Drilling Fluid Type-2

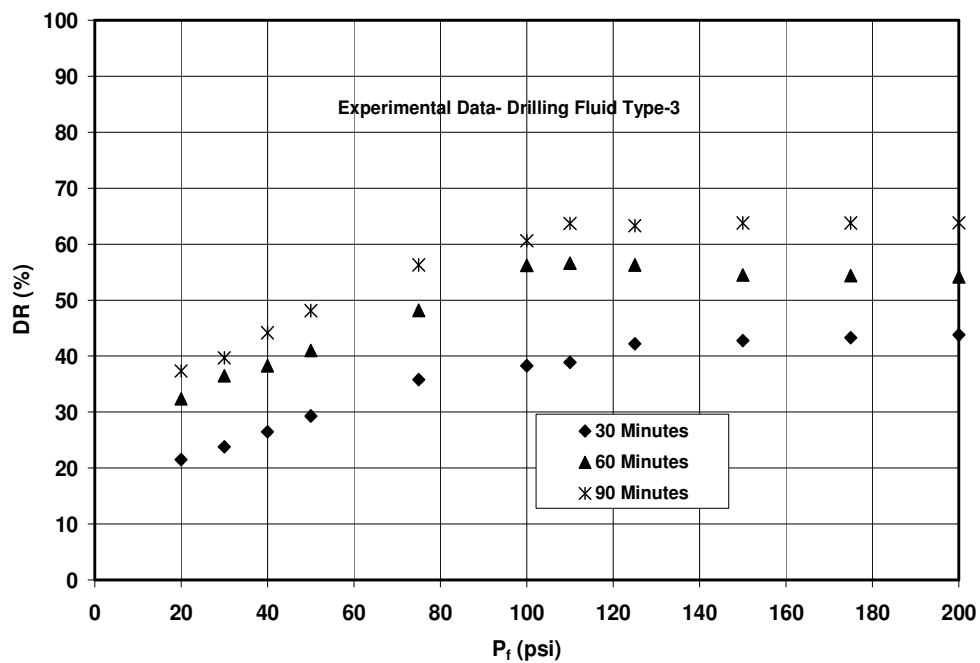


Figure 59 Experimental Results of the Drilling Fluid Type-3

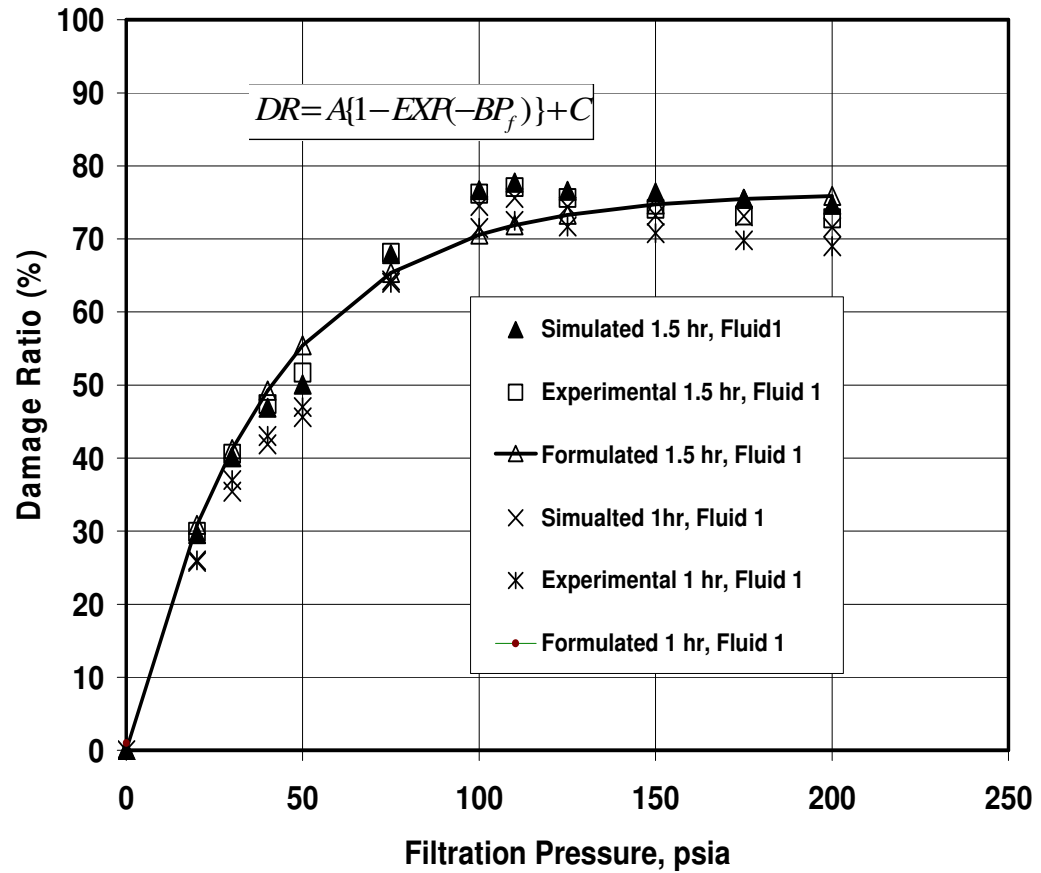


Figure 60 Experimental, Simulated and Formulated Results of Drilling Fluid Type-1

In Figure 60, the experimentally obtained damage ratio values are plotted together with the simulated and the formulated values. The formulated values were calculated by Eq.52. This equation relates filtration pressure directly with the damage ratio by considering the viscosity effects through the arbitrary constants A, B, and C. The damage ratios versus filtration pressure were plotted for the both drilling fluids.

After that the results were analyzed by using both Microsoft™ Excel Goal Seek tool and linear regression, a parametric curve fitting study was made. The modeling parameters for drilling fluid-1 A_1 , B_1 , C_1 , for drilling fluid-2 A_2 , B_2 , and C_2 and for drilling fluid-3 A_3 , B_3 , and C_3 are summarized in Table 20. Then a correlation between filtration pressure and damage ratio was proposed as follows:

$$DR = A\{1 - \exp(-BP_f)\} + C \quad (52)$$

The linearized form of this equation is derived as follows:

$$\ln[(A - DR + C)/A] = -BP_f \quad (53)$$

The experimental, simulated and formulated data match very accurately. A linear regression plot for drilling fluid type-1 is drawn in Figure 61. Permeability damage ratio is high at higher coefficients. The vertical intercept of the correlation function should be set at zero. Fines migration, invasion of particles and consequent reduction of permeability can not take place at zero filtration pressure. The experimental and simulation damage ratio results with drilling fluid type-1 are very close to each other. Drilling fluid type-1 is the conventional, non-treated mud sample without any chemicals. This type of mud is very commonly used frequently in various reservoir fields. The only difference may be the density of the mud which is adjusted due to the considerations of the formation pressure.

Table 20 Fitting Parameters for Drilling Fluids-1,2, and 3

Drilling Fluid-1	A₁	B₁	C₁	R²
30 Minutes	67.7	0.018	0	0.90
60 Minutes	73.8	0.023	0	0.99
90 Minutes	76.3	0.026	0	0.94
Drilling Fluid-2	A₂	B₂	C₂	R²
30 minutes	78.5	0.190	0	0.98
60 minutes	80.0	0.195	0	0.86
90 minutes	82.2	0.212	0	0.92
Drilling Fluid-3	A₃	B₃	C₃	R²
30 Minutes	45.7	0.021	0	0.94
60 Minutes	55.2	0.033	0	0.94
90 Minutes	63.8	0.032	0	0.98

The parameters in Table 20 are viscosity and circulation period related values. The coefficients increase as the viscosity and circulation period increase. The maximum coefficients were obtained with the CMC mud. The minimum coefficients were obtained with the Polymer-XT fluid. This trend is completely consistent with the damaging characteristics of the drilling fluids that were used. Thus, it can be interpreted that the minimum coefficients correspond to the mud which is the least invasive.

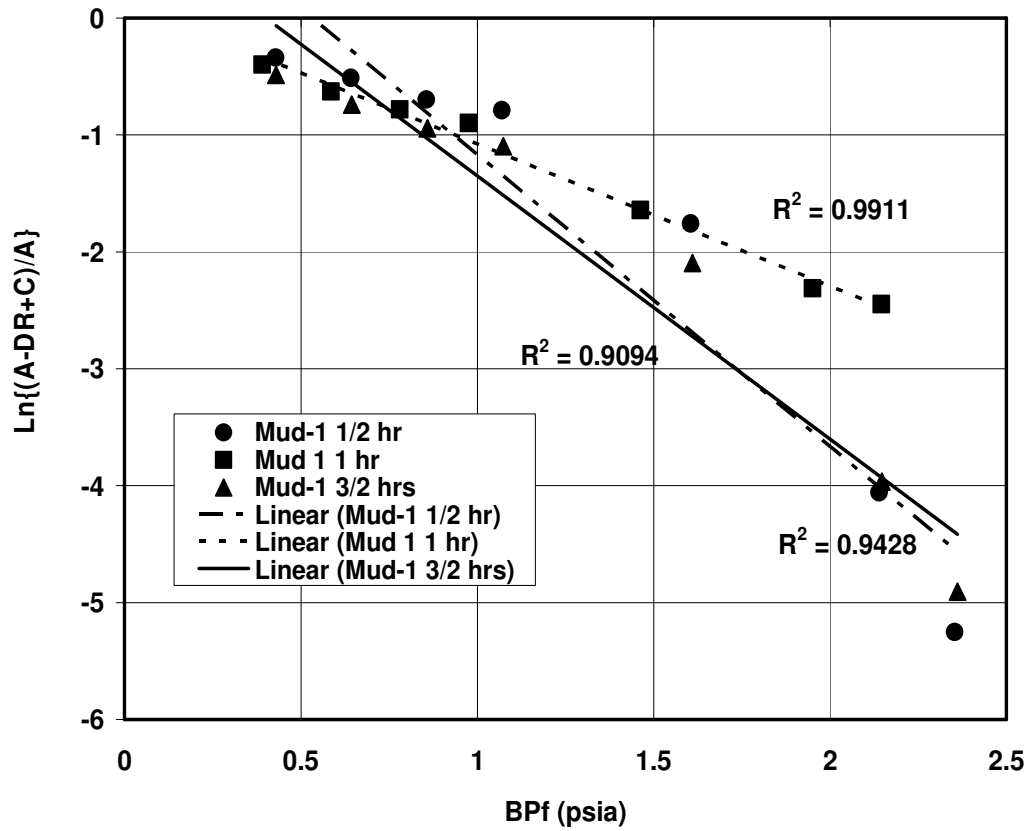


Figure 61 Linear Regression of Fluid Type-1

Equation 52 is linearized as in Equation 53. Then Equation 53 is plotted in Figure 61. The regression coefficients are all above 0.90. The linear regression was made by considering the experimental and formulated results. Thus, it can be stated that the proposed correlation works very well and outcomes consistently matching results with the experimental values.

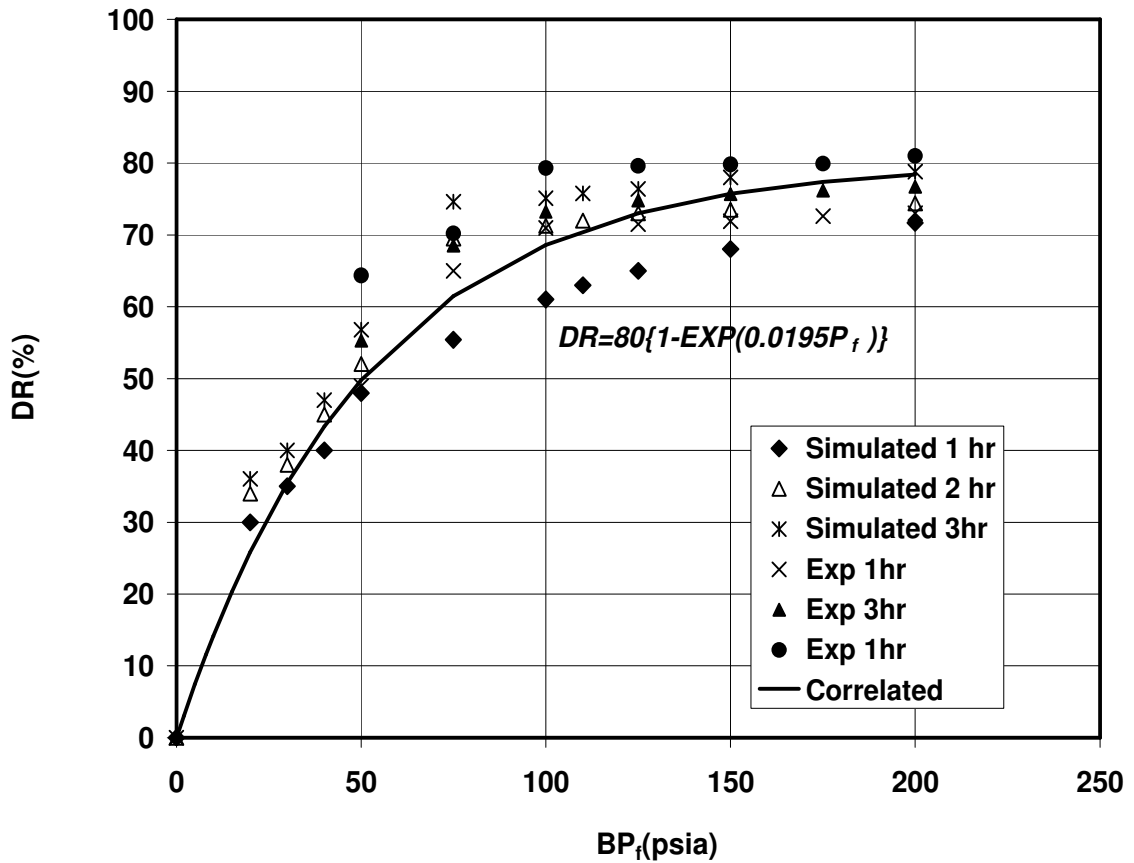


Figure 62 Experimental, Simulated and Formulated Results of Fluid Type-2

The damage ratio is in the order of 80 percent by the experimental, simulated and correlated results of the fluid type-2. Equation 53 was employed with the appropriate coefficients. The proposed correlation fits very well together with the experimental and simulated data. The damage ratio with fluid type-1 was found in the order of 75%. Thus, it is observed that addition of CMC into the drilling mud system affected permeability adversely.

The damage ratio increased in the presence of the CMC in the mud sample. Although CMC is suitable for viscosity and gel strength control of the drilling muds, it is more invasive and permeability reducing.

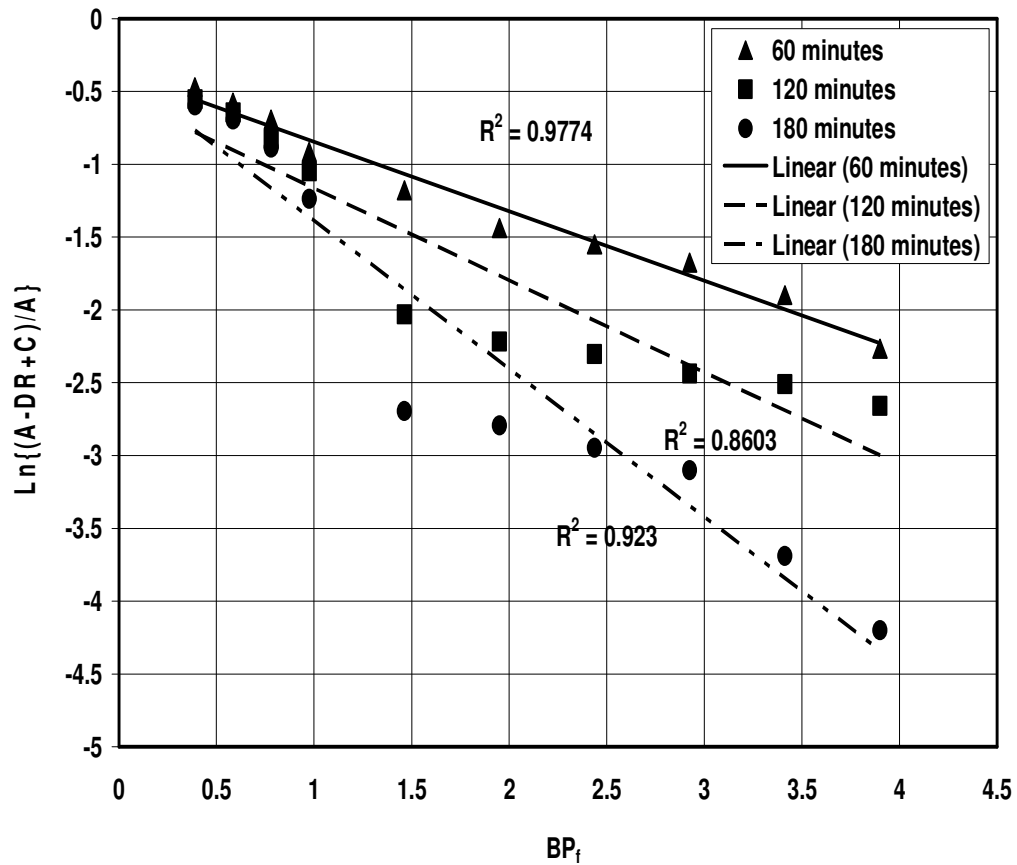


Figure 63 Linear Regression of Fluid Type-2

The linear regression plots of mud type-2 are depicted in Figure 63. It is seen that there is a good match within the data. The regression coefficients are high. However, the regression coefficient for circulation period of 120 minutes is comparatively less than the others. 0.86 is not

very low. However the reason for this slight reduction may be due the fluctuation in the final experimental data of fluid type-2. The experimental damage ratios depict a very slight reduction at 175 psi.

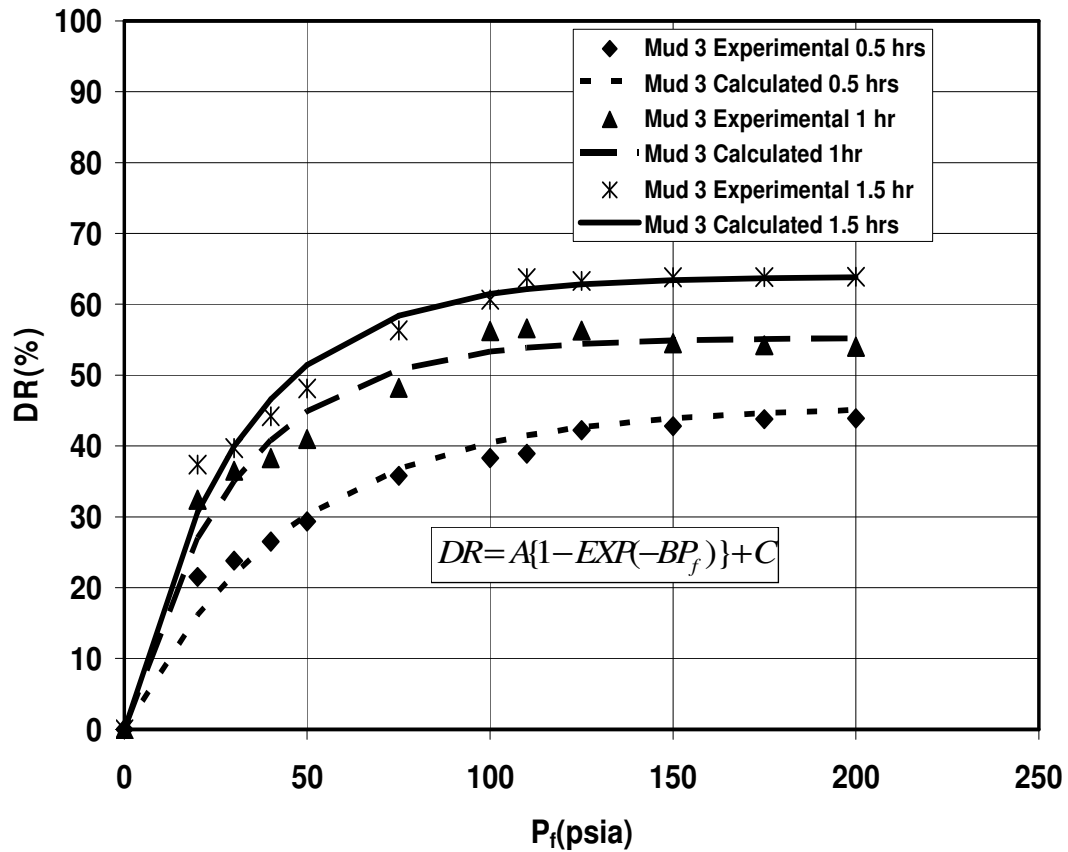


Figure 64 Experimental and Calculated Results of Fluid Type-3

It is observed seen that the permeability damage ratio decreased down to 63% after 90 minutes. The reduction in permeability is much less at early

circulation periods. The proposed model fits the experimental data very accurately. The Eq. 52 catches the experimental data almost right on the line. It should be noted that the damage ratio changes more significantly during drilling circulation with fluid type-3. However, the damage ratio was reasonably less than that of the two other mud types. Thus, mud type-3 with Polymer-XT is the best candidate for applications and obtaining as minimum formation damage as possible.

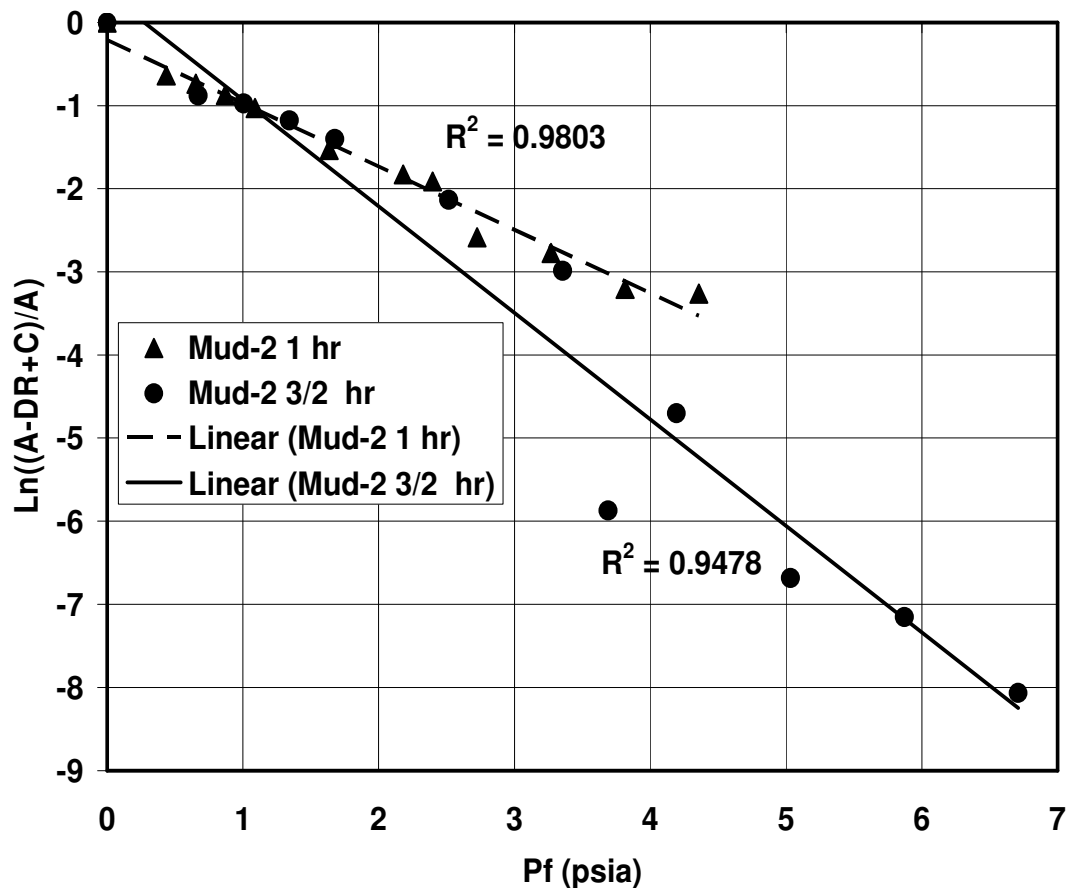


Figure 65 Linear Regression of Fluid Type-3

The regression line for $\frac{1}{2}$ hour data almost overlaps with the 1 hr data, so it was not drawn to avoid a crowded figure (Figure 65). The correlation coefficients are close to 1.0 and the proposed model is satisfied. Thus, an accurate approach is obtained to estimate the reduction in permeability in terms of filtration pressure. This correlation (Eq.52) enables an accurate estimation of the near wellbore formation damage as a function of pressure. The simplicity of the correlation makes it more attractive for field uses. One very common way of representing formation damage is the concept of damage ratio (DR). In this part of the study, the experimental results of permeability impairment due to mud circulation were analyzed. The experimental data of the two different mud samples at eleven different filtration pressures were plotted at three different circulation periods 30, 60, and 90 minutes (Figures 66,67,and 68). The damage ratio keeps an increasing trend until 110 psia filtration pressure for fluid type 1 slightly reduces until 130 psia and then becomes almost constant (Figure 66). As the circulation period increases from 30 to 90 minutes, the damage ratio increases. The maximum damage ratio 77% is reached with fluid type-1. The maximum damage ratio with polymer added mud-3 is about 65 % at the end of the 90 minute circulation period (Figure 68). The damage ratio is less with the polymer added mud than the damage ratio with the conventional bentonite mud. The damage ratio increases as the filtration pressure increases until 125 psia. From this pressure on the trend is almost horizontal for the three different circulation periods (Figure 68). After plotting the experimental data for the three different mud types at three different circulation pressures, an exponential function was proposed (Eq.52). In this model, the damage was expressed as an exponential function of the filtration pressure. The calculated damage ratio values were drawn together with

experimental data (Figures 60, 62, and 64). The proposed exponential model fits the experimental data very well. The regression coefficients of the linearized form of Eq.52 for fluid 1 are 0.90, 0.99, and 0.94 for $\frac{1}{2}$, 1, and 1.5 hour-periods, respectively (Figure 63). The regression coefficients of the linearized form of Eq.52 for mud 3 are 0.94 and 0.98 for 1.0 and 1.5 hour periods, respectively (Figure 65).

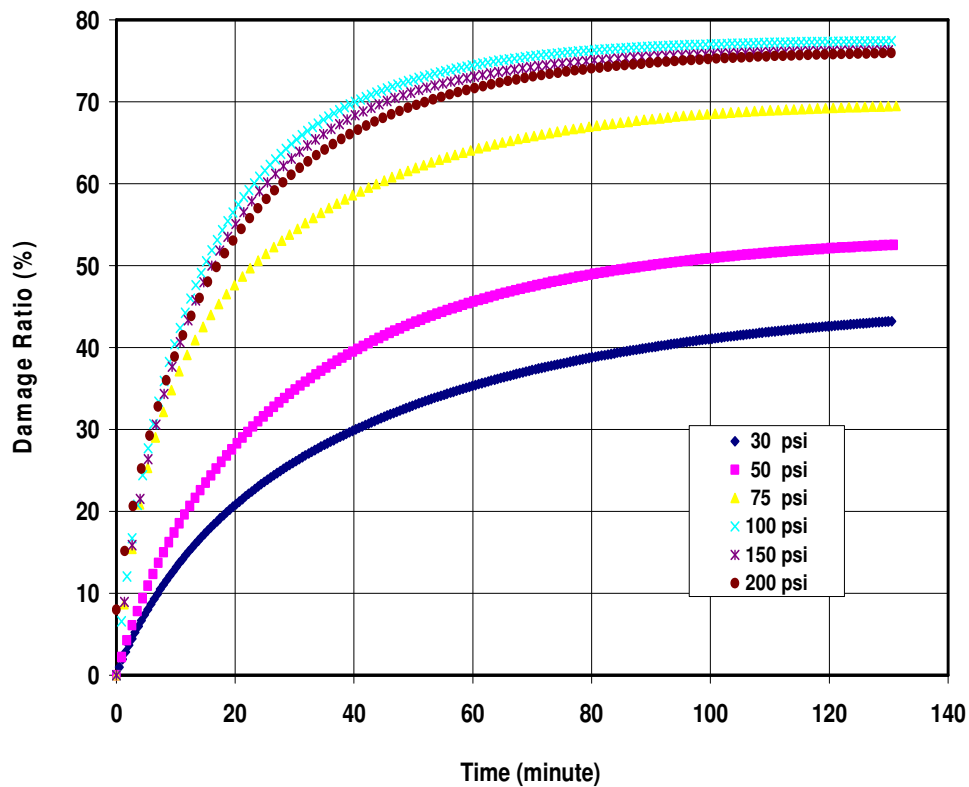


Figure 66 Damage Ratio vs Time at Different Filtration Pressures for Drilling Fluid Type-1

The damage ratio increases as the circulation period increases. The trend of the damage ratio versus circulation time profile looks similar to the profile of damage ratio versus filtration pressure. The major increase in damage ratio takes place until the pressure goes up to 100 psi. The damage ratio decreases slightly between the interval of 100 psi and 200 psi (Figure 66). The reason for this slight reduction is the cleaning of the previously formed bridgings by the increasing pressure effect. It should be noted that higher filtration pressure may hatch out the formation and may cause near well bore fracturing.

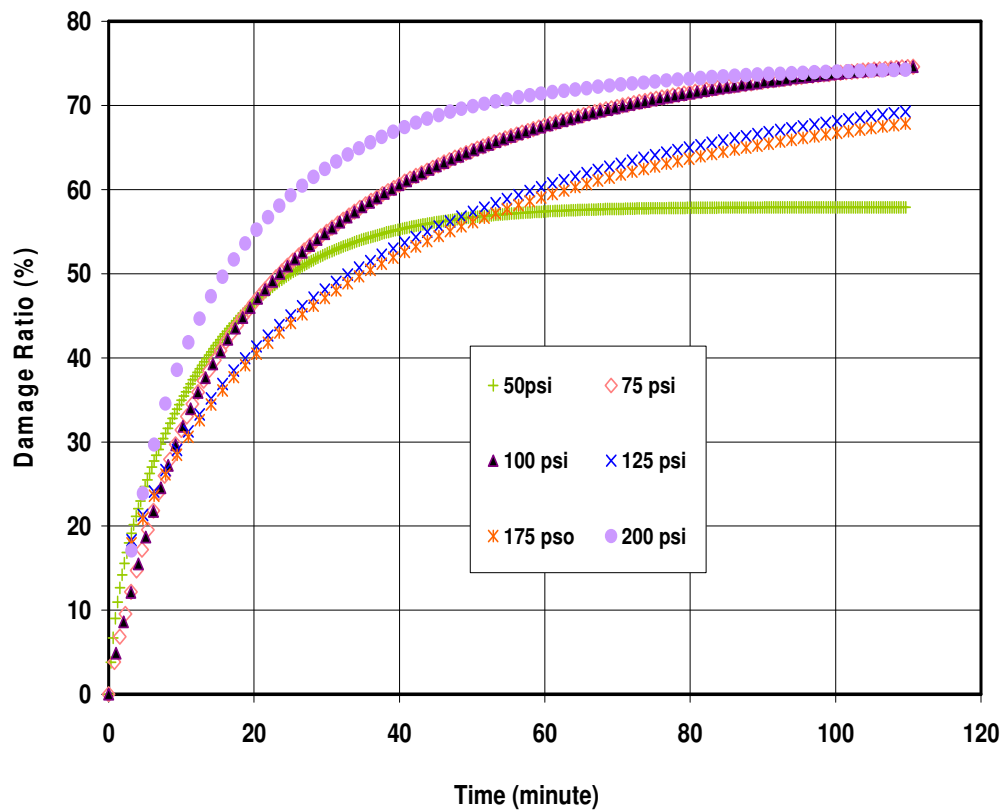


Figure 67 Damage Ratio vs Time at Different Filtration Pressures for Drilling Fluid Type-2

The CMC fluid is the more damaging than fluid type-1. The damage ratio at 50 psi has a smoother trend. After 50 psi, the damage ratio profile becomes sharper. They come to a limiting value towards 200 psi. The damage ratio increases as the circulation period increases. However, fluid type-2 is not recommended, because with the addition of CMC, the damage ratio increased. The damage ratios at 100 psi and 125 psi are almost on top of each other. They come to a steady value around damage ratio of 73%. The reason for changing increase trend in the profiles after 50 psi is sudden deposition of fines particles and forming of bridging.

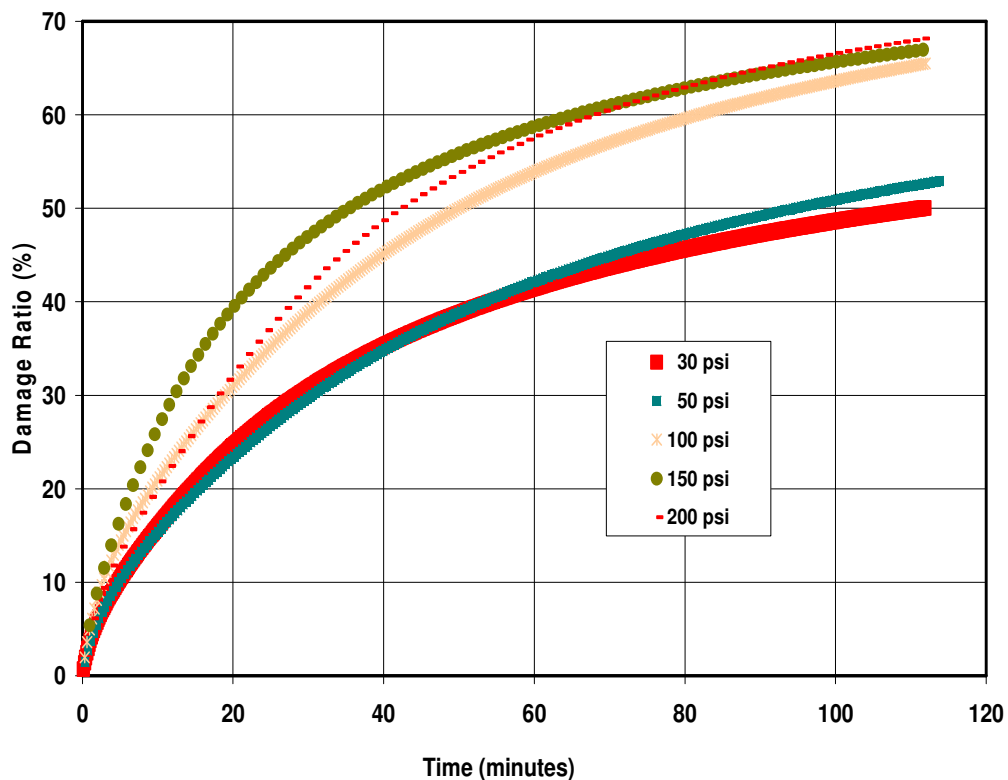


Figure 68 Damage Ratio vs Time at Different Filtration Pressures for Drilling Fluid Type-3

The minimum damage ratios were obtained in the presence of mud type-3. The damage ratio increases as the filtration pressure increases. The damage ratio profiles after 100 psi are almost on top of each other. Thus, the plots in Figure 68 are mostly on top of each other. However, the profiles unite and become steady at 200 psi.

7.5.1.2 Variation of Permeability along The Core Sample

The numerical simulator divides the core sample into grid blocks. The permeability of the core sample is calculated along the core length. The outputs are obtained for each grid block at different time intervals starting from 0 minute to 90 minutes. Simulation results were obtained for two different drilling fluids at three different filtration pressures such as 50, 100, and 200 psi and nine specific time intervals ranging from 10 minutes to 90 minutes. Then, for every time interval, the variation of non-plugging permeability with respect to core length was plotted (Figures 69 - 74).

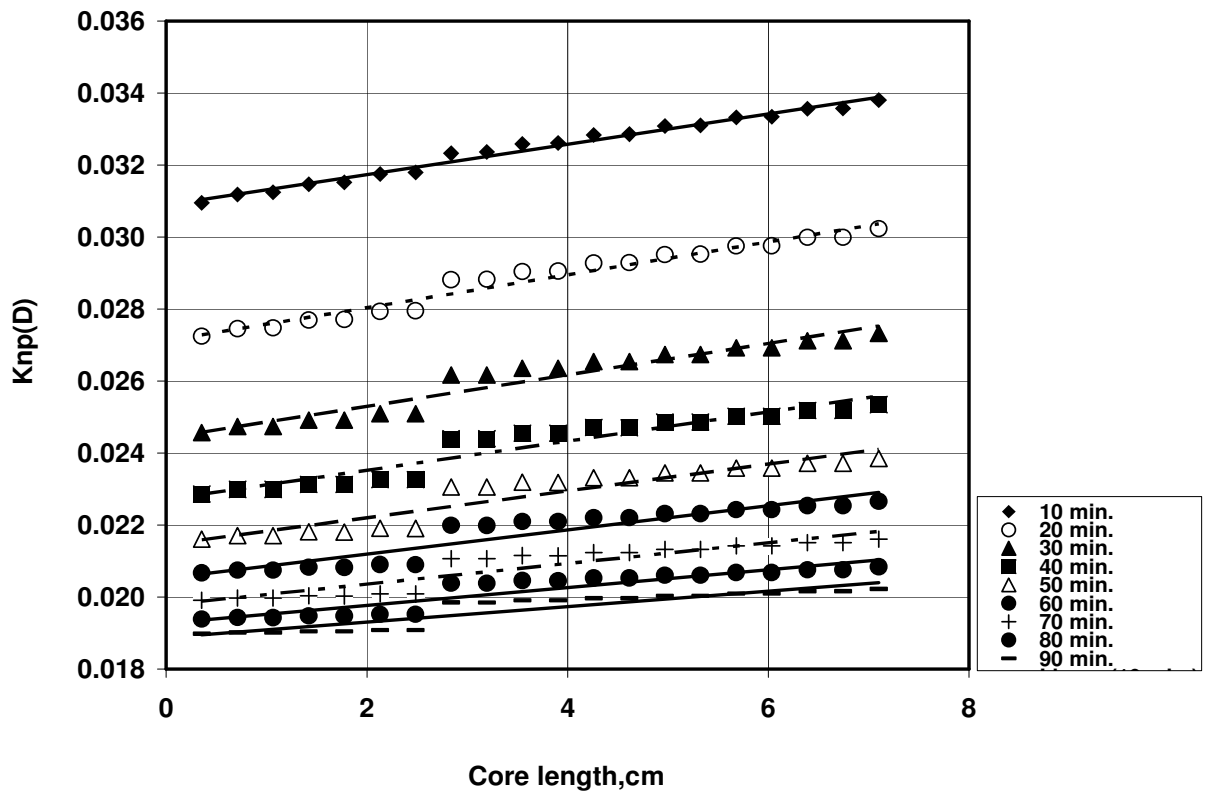


Figure 69 Variation of Permeability along the core sample at 50 psia with Drilling Fluid Type -1.

In Figure 69, the variation of the non-plugging permeability of the core sample during the circulation of Mud-1 at 50 psia circulation pressure is shown along the core sample. There is a sharp slope linear trend within the first half hour of the circulation. Then, the rate of increase decreases. On the other hand, there is a slight jump in the increase of permeability after 6.2 cm away from the circulation end of the core sample. But this jump does not disturb the linear increase of non plugging permeability along the core sample. The reason of the discontinuity may

be the non-homogeneity within the core sample or pushing the bridging particles with nozzle effect rapidly at a specific point of the core from the circulation end at lower pressures. When the filtration pressure is increased, the jump in the increase of the permeability is not observed. The maximum variation in permeability took place at the end of the first ten minute period. At the end of the ninth ten minute period, the variation in permeability along the core sample is almost zero.

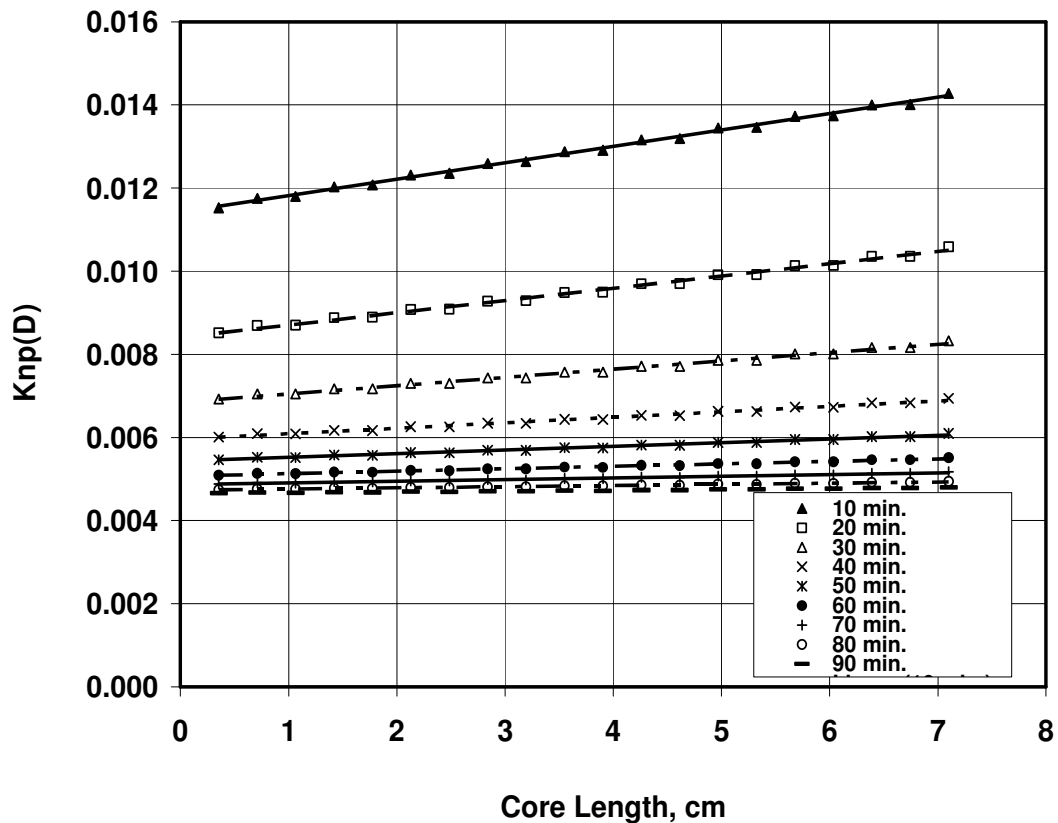


Figure 70 Variation of Permeability along the core sample at 100 psia with Drilling Fluid Type - 1

In Figures 71 and 72, the variation permeability along the core sample is drawn when the core sample is subjected to the circulation of mud- 1 at 100 psi and 200 psi filtration pressures, respectively. There is no jump in the permeability value along the core sample at these pressures. Considering the initial 10 minutes for Figures 69, 70, and 71, the permeability increased from 0.0310 D to 0.0335 at 50 psi circulation amounting to an 8% increase along the core sample. However, the increases in permeability at 100 and 200 psia are found as 26% and 18 %, respectively. The increase in permeability along the core sample is very meaningful, because the maximum deposition of the particles takes place close to the well bore during drilling circulations. However, the increase along the core is neither a stimulation nor improvement in permeability. It is just a relative increase as it is moved away from the circulation point. Even the most far point of the core sample has a reduced permeability than the initial undamaged permeability.

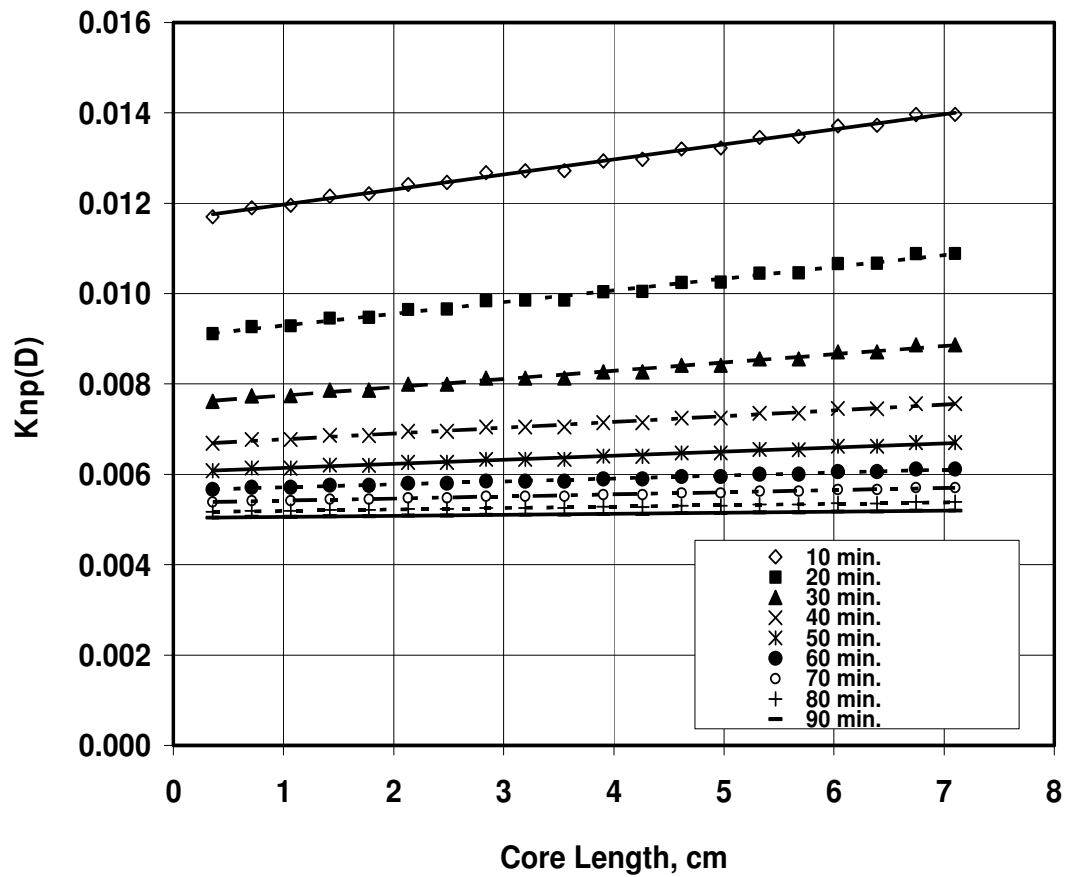


Figure 71 Variation of Permeability along the core sample at 200 psi with Drilling Fluid Type - 1.

In Figures 70 and 71, the permeability change becomes almost zero after fifty and sixty minutes, respectively. Even though the filtration pressure is doubled, the permeability of the core may no longer be altered significantly. The variation of permeability of fluid-3 along the core samples is drawn in Figures 72-74.

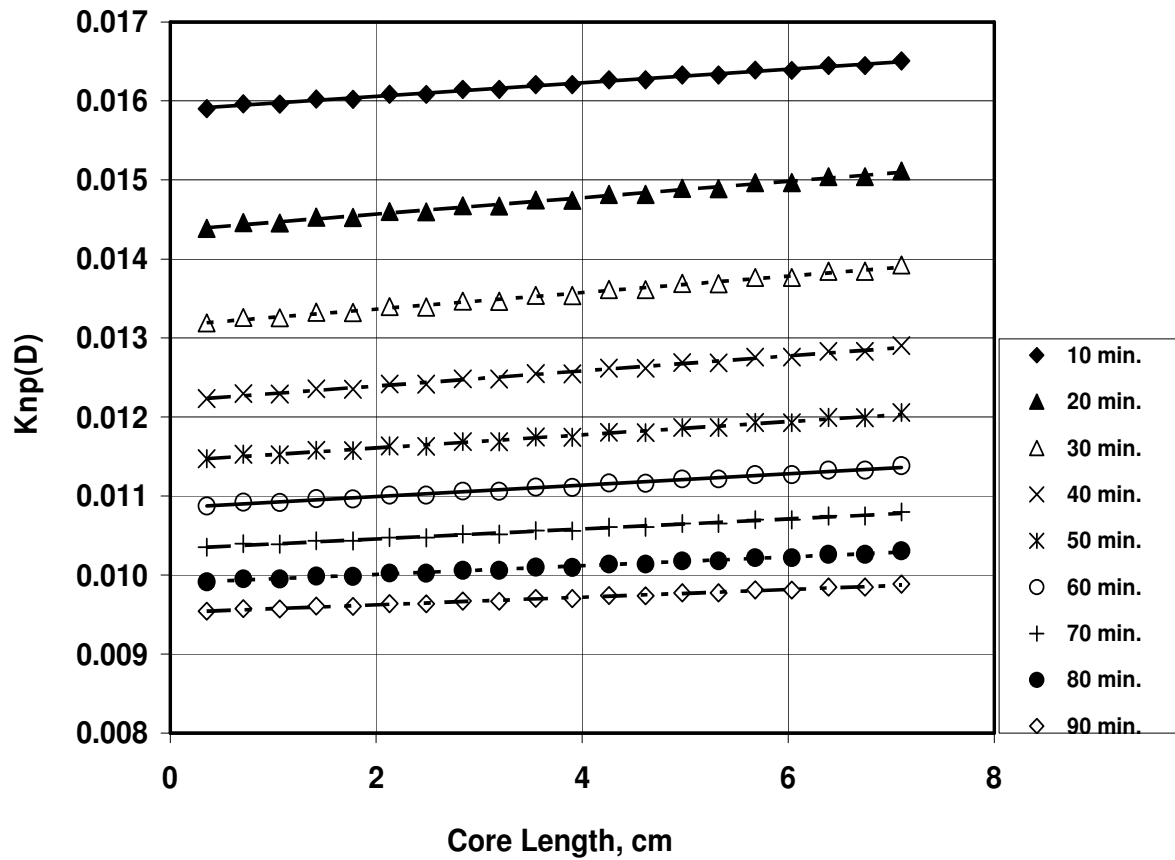


Figure 72 Variation of Permeability along the core sample at 50 psia with Drilling Fluid Type -3.

When water-based polymer mud is used during circulation, the increase in permeability is also linear. Nevertheless, unlike mud-1, the variation of permeability with core length does not have a discontinuity point even at lower pressures such as 50 psia (Figure 72).

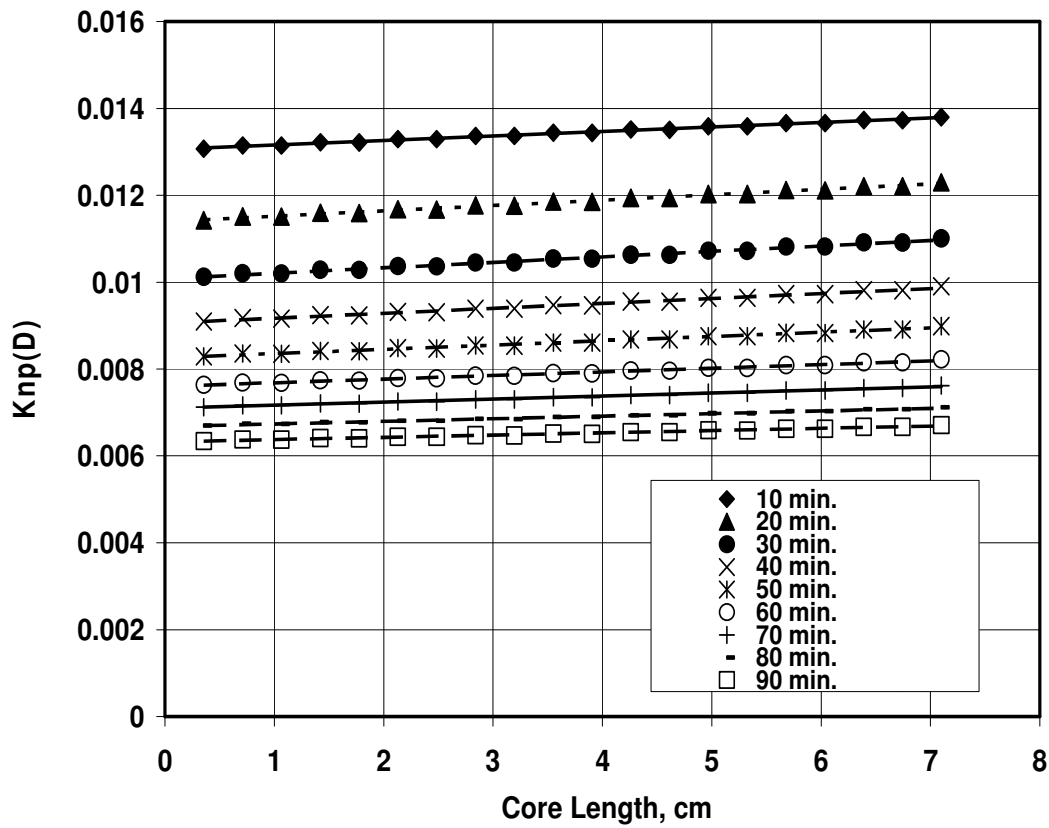


Figure 73 Variation of Permeability along the core sample at 100 psia with Drilling Fluid Type -3.

The slopes of the lines in the first thirty minutes are almost the same with mud-3 at 50 psia. However, at later times, even though the rate of increase in permeability has decreased, it did not vanish even at higher pressures unlike mud-1 (Figure 73). On the other hand, the rates of increase in mud- 3 simulations are less than that of mud-1. This may be because of the higher viscosity and thixotropic property of the mud with Polymer XT. As the circulation period elapsed, the linear lines

approached each other in the three application pressures. As the filtration pressure increased from 50 to 100 psi, the permeability difference between the circulation end and the far most end of the core sample increased (Figures 72 and 73). This difference is higher at 200 psi than at 50 psi, but slightly less than the difference with 100 psi circulation (Figure 74).

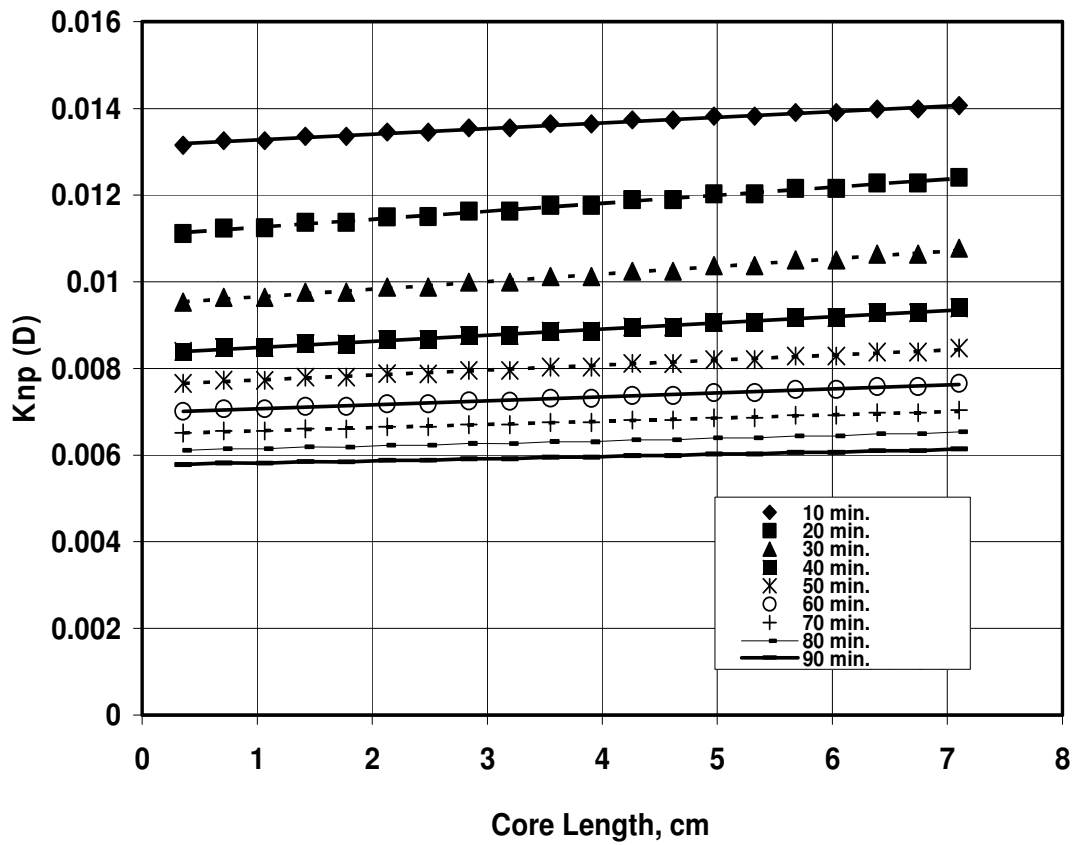


Figure 74 Variation of Permeability along the core sample at 200 psia with Drilling Fluid Type -3

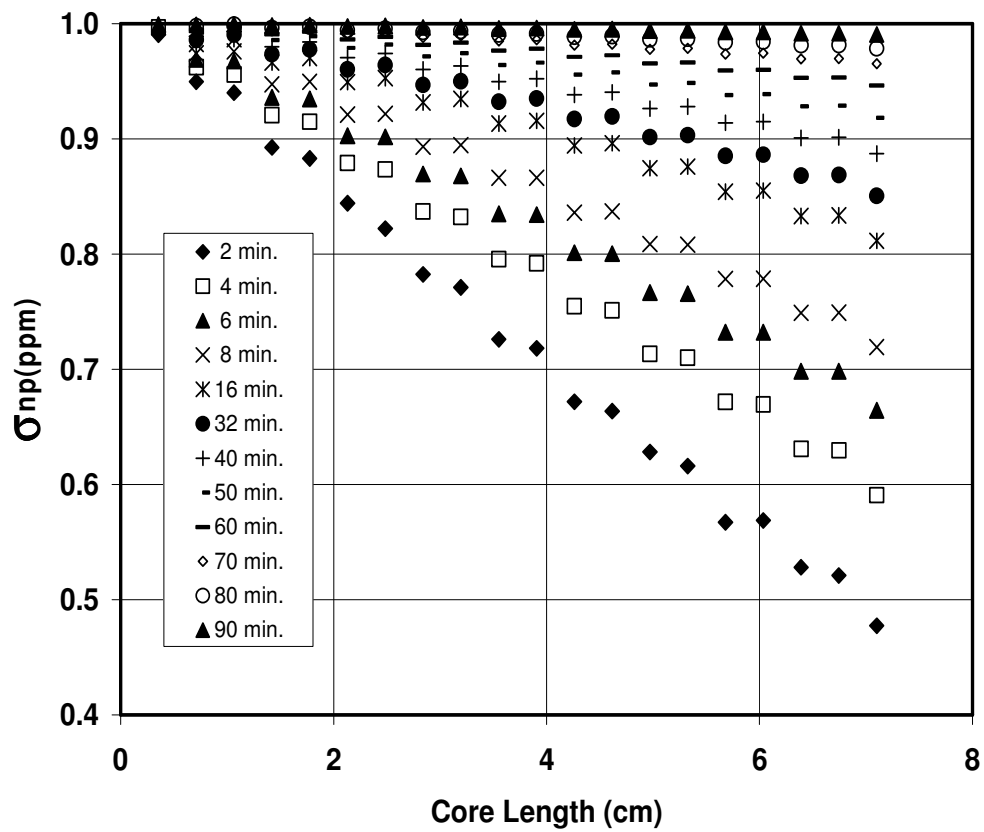


Figure 75 Particle concentration variation along the core length with Drilling Fluid Type -1 at 50 psi.

The maximum variation of particle concentration takes place in the early periods of dynamic circulation (Figure 75). As the circulation time proceeds, the variation in particle concentration becomes almost constant. The variation of particle concentration is almost linear. The maximum particle deposition takes place in the early 32 minutes of the circulation. The particle concentration is higher at the side of the core sample over which circulation is performed. As it is moved away from the

dynamic circulation point, the concentration of the particles reduces along the length of the core sample.

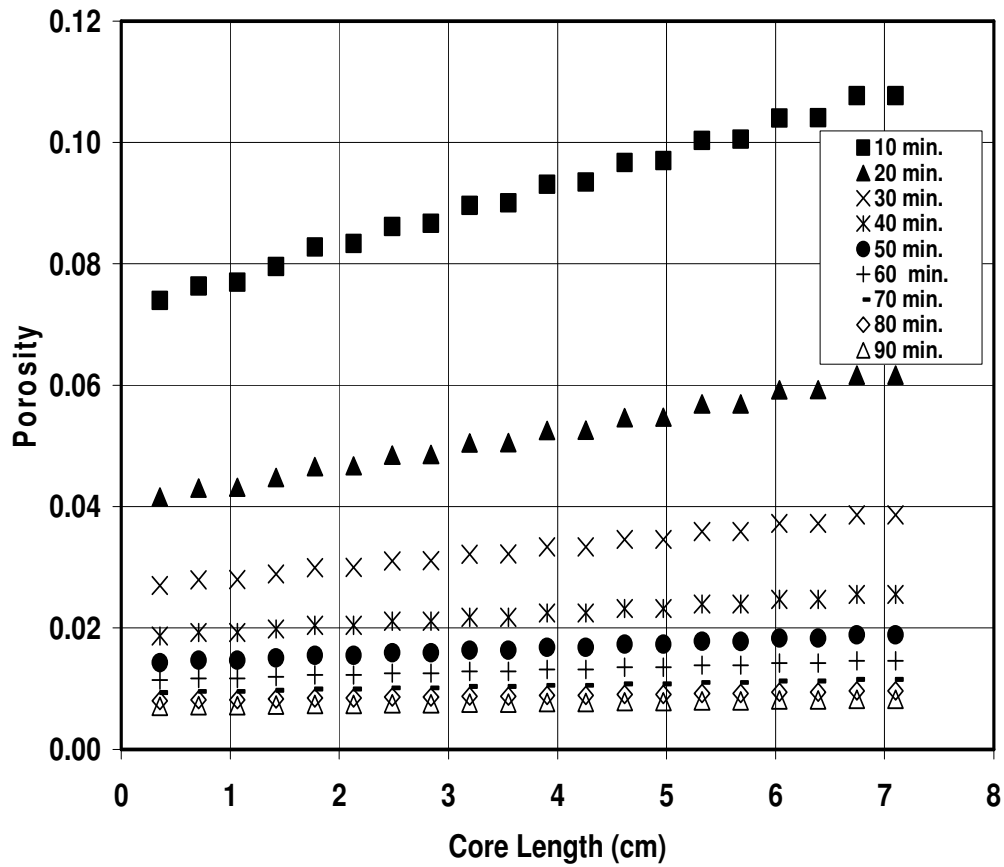


Figure 76 Porosity variation along the core length with Drilling Fluid Type -1 at 50 psi.

The porosity variation along the core sample was simulated for 90 minutes at 50 psi filtration pressure. It is seen that the porosity increases from the application point of the drilling fluid towards the end of the core

plug (Figure-76). The maximum porosity variation takes place in the first ten minutes of the circulation. The variation of porosity along the core sample becomes almost zero after 40 minutes. It should be noted that the porosity decreases as the drilling fluid is circulated. However, the porosity increase along the core sample is a relative increase with respect to the porosity of the application point. Briefly this phenomenon proposes that the closer grid blocks to the drilling mud application point are more affected when compared to the further grid blocks of the sample.

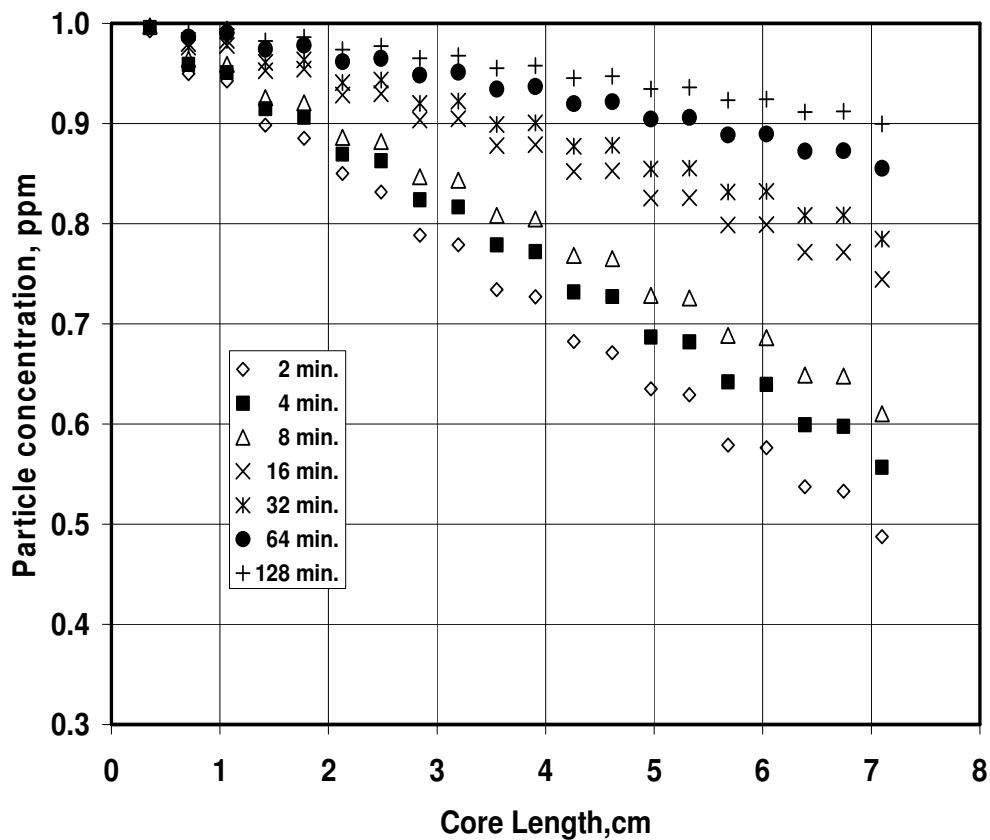


Figure 77 Particle concentration variation along the core length with Drilling Fluid Type -1 at 100 psi.

The particle concentration varies more severely at 100 psi (Figure 77). At 50 psi filtration pressure , the particle concentration variation is more horizontal than at 100 psi. The concentration at the first grid at 50 psi is 0.47 99m whereas the concentration at the same grid at 100 psi after the same circulation period 2 minutes is 0.49 ppm. On the other hand, the major particle concentration variation is spread over the whole circulation period at 100 psi while, this period is majorly limited within the first 32 minutes at 50 psi

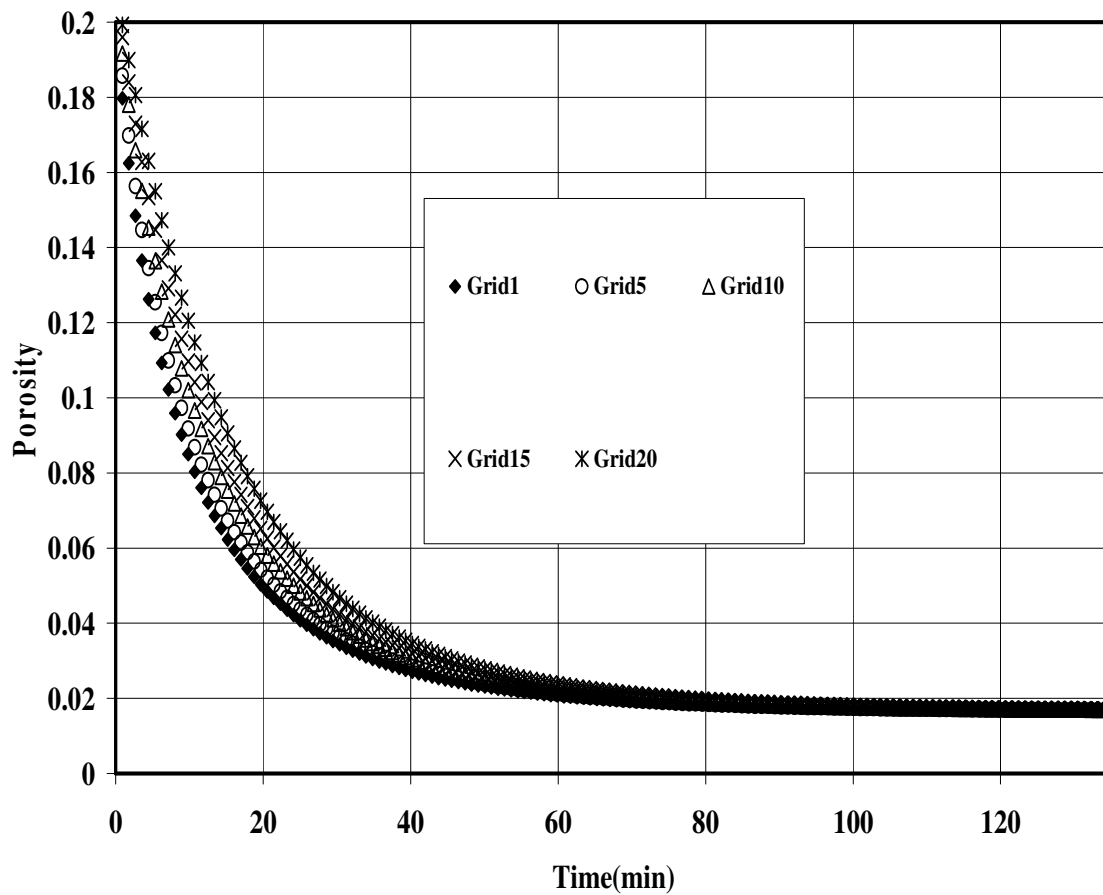


Figure 78 Porosity variation with respect to time at different grid blocks with Drilling Fluid Type -1 at 100 psi.

The porosity variation is observed in the first hour of the drilling mud circulation. The reduction in porosity decreases as it is moved away from the circulation point. The variation of porosity after 60 minutes displays a horizontally asymptotic behavior at 0.018 porosity fraction (Figure 78).

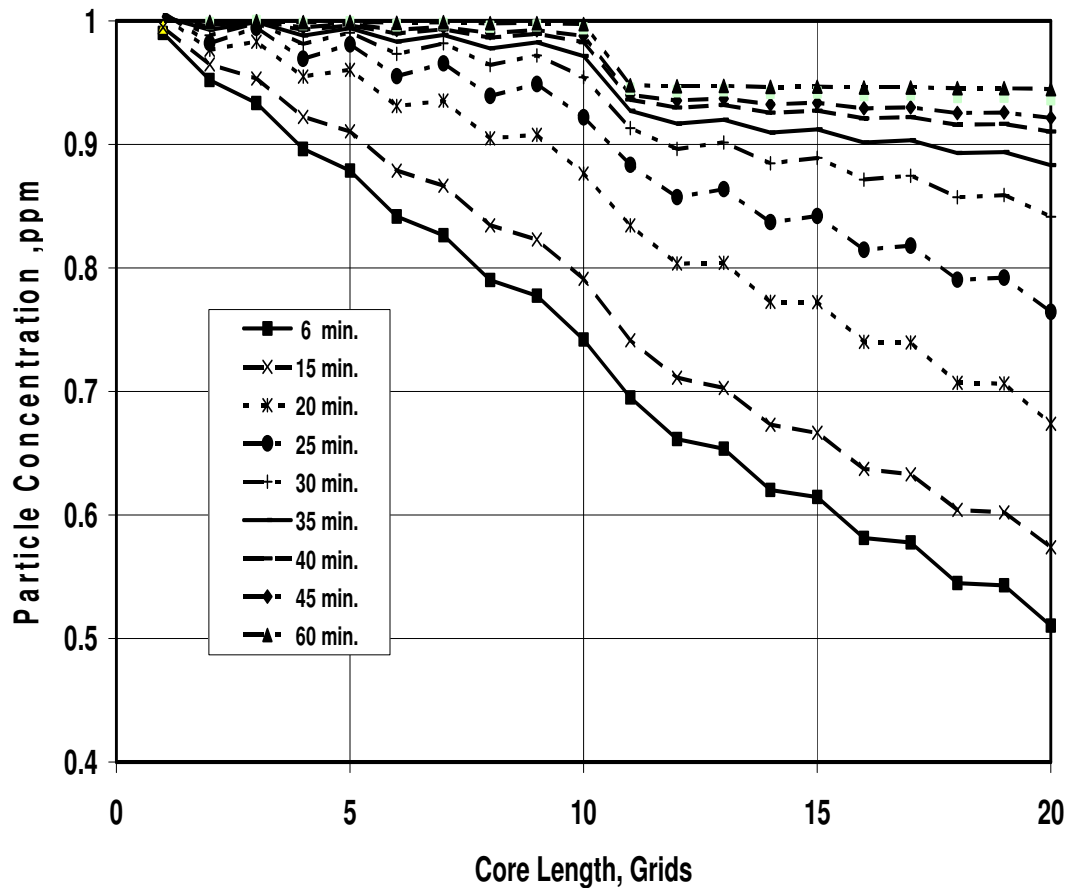


Figure 79 Particle Concentration variation along the core length with Drilling Fluid Type -2 at 100 psi.

The ultimate particle concentration remained above 0.5 ppm. This concentration was below 0.5 with fluid type-1. Moreover fluid type-2 makes fluctuations at later stages of the circulation. This phenomenon causes a sudden reduction in particle concentration between the frid blocks 10 and 12 (Figure 79). After the completion of early half an hour period, the particle concentration profile behaves almost constant due to the forming of the bridgings.

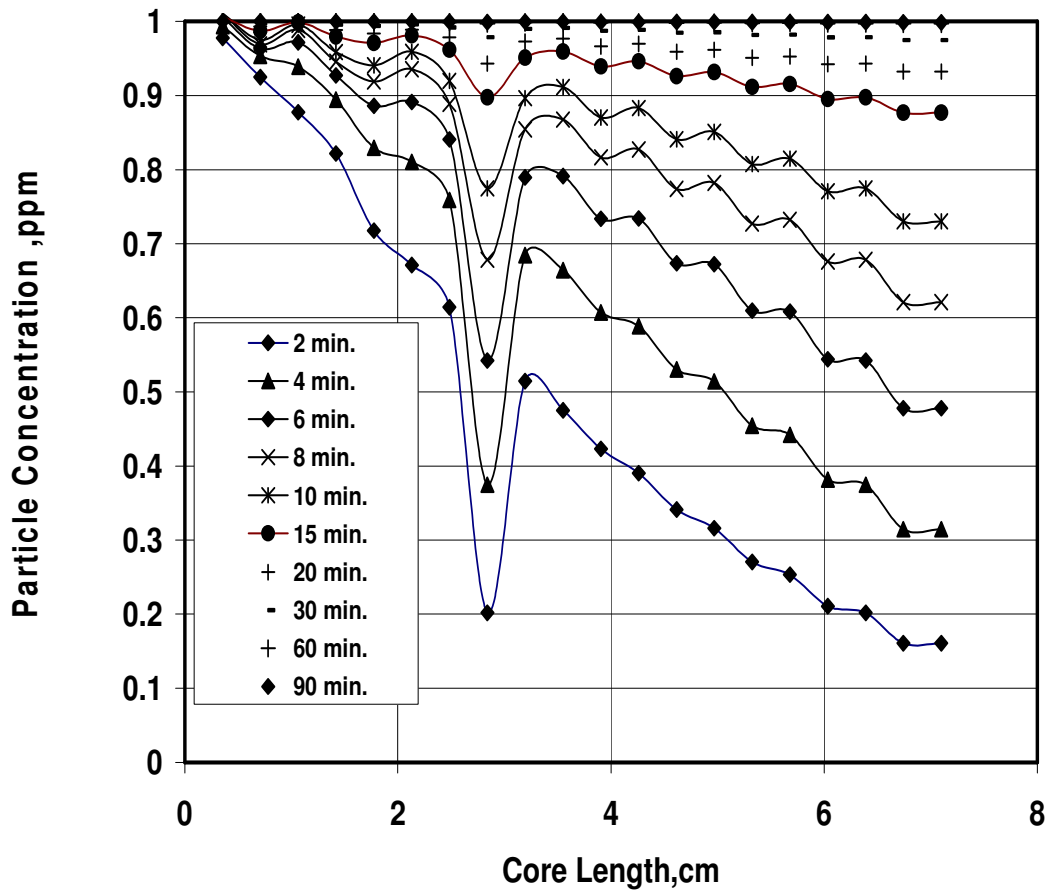


Figure 80 Particle Concentration variation along the core length with Fluid Type-3 at 100 psi.

The particle concentration profile with fluid type-3 is rather different. There exists a sudden reduction in particle concentration at the 2.84th cm of the core plug. This sudden reduction is because of the early formed deposition. This oscillation is due to the increase of the viscosity. The particle concentration variations with fluid 1 and 2 are rather more linear and the oscillation can not be seen apparently (Figures 77 and 79). As the viscosity increased, the oscillation in the early parts of the core plug becomes more significant. The viscosities of three fluid types are 10 cp, 18 cp and 25 cp, respectively. In Figure 79, the oscillation is slightly seen towards the middle section of core plug with the increase of viscosity from 10 to 18 cp. The addition of the polymer-XT increased the viscosity to 25 cp. Thus the oscillation became very significant. The particle concentration was plotted with respect to time at constant distances from the fluid circulation point in Figure 86. The oscillatory trend is seen throughout this plot, too. The particle concentration depicts a sudden reduction at the 2.84th cm of the core plug. The early formed deposition can not resist the overflowing fines and pressure. Thus, the plugged pore throat opens suddenly. The particle concentration increases quickly back to the expected drop profile. It is interesting that the concentration at the end of the circulation profile at final grid is about 0.16 ppm. This value is much lower than the two other mud types where the concentration was in the order of 0.5. Thus, less particle concentration indicates less formation damage. It is confirmed that the fluid type -3 with Polymer-XT is recommended for less formation damage. The permeability damage ratios of the three mud types have been experimentally and numerically evaluated with respect to the filtration pressure. It is seen that the least damage ratio has been obtained with fluid type -3. The particle concentration profiles and damage ratios at different circulation periods

confirm that mud type-3 is a good and optimum choice for drilling operations with least formation damage potential. Mud type-1 is a very conventional mud without any ingredients except Barite. This mud type is easy to treat, but it is very invasive. The porosity and permeability of the formations are damaged severely. Fluid type-2 includes CMC to increase gel strength and viscosity. However, while attaining the required gel strength, the CMC mud is severely damaging the porous media. Thus, an ultimate reduction in permeability takes place. Mud type -3 with Polymer-XT optimizes the formation damage, viscosity and gel strength at lower concentrations. The optimum CMC concentration to obtain API specified mud was 3 g. The polymer-XT mud achieved all the requirements at an optimum concentration of 0.4g giving much less damage to the formation. The obtained numerical experimental and formulated results were plotted in Figures 60,62 and 64 respectively. The major aim of this study is to correlate the permeability damage ratio with the differential filtration pressure. This aim was achieved. The sensitivity plots were drawn for experimental and calculated values of damage ratio in Figures 61,63 and 65. Regression coefficients of 0.94-0.98 were obtained. The experimental data were obtained at eleven different filtration pressures and the sensitivity plots were drawn with 8 to 10 data points of the experimental and the calculated values. Thus, the sensitivity of the results vary between 0.94 to 0.98 with linear regression coefficients and 73-91% from number of data point of view.

7.5.1.3 Investigation of Porosity and Permeability Impairment in Sandstones by X-Ray Analysis

Both porosity and permeability constitute the major parameters in core analysis. In this study, the variation of these two parameters along a sandstone core sample was investigated during formation damage.

A water based drilling fluid was dynamically circulated through the core sample for three different time intervals of 15minutes, 45 minutes, and 60 minutes at 100 psi circulation pressure. The core sample was analyzed using x-ray digital radiography by sectional image approach. The differences in the porous media due to fines migration by drilling fluid were examined. Digital image subtraction method was applied by using an in-house simulator developed to run with MATLAB[®] to determine porosity. The experimental results obtained by dynamic circulation and x-ray imaging were compared with the results obtained by using a numerical fines migration simulator. Consistent matches between the experimental and numerical results were observed indicating that porosity and permeability impairments with distance can be described accurately. For prediction of production wells it is important to consider effect of permeability and porosity impairment as a function of distance at various times. Most studies determined the impairment as an average over the core length. However, for many practical applications, prediction of permeability and porosity distribution along the core are needed.

In this part of the study, formation damage due to fines migration was analyzed using a simulator and conducting x-ray experiments. The experimental work includes dynamic mud circulation tests through the cores and x-ray scans of the core samples before and after fine particles invasion. The experimental and simulation results were compared and their consistencies with each other were seen. The application simplicity of x-ray scans and image subtraction technique is expressed when compared to that of computer tomography applications. Formation damage application is emphasized in our study.

Generally computer tomography applications are used in core analysis. However x-Ray radiography is used widely used in core analysis, because the x-ray radiography is much faster and convenient compared to CT. The device is a high Frequency Radiographic X-Ray generator with anatomical programming cm measurement, auto tube calibration, 40 - 125kV in 1 kVp increments, 10 - 400 mA, 0.001-6.3 sec. timing. Display of kVp, mA, Time, mAs and cm. Automatic line compensation, Tube protection with heat unit calculator is also available. The experimental preparation and the procedure are as follows:

7.5.1.4 Preparation for X-Ray Experiments

Taking core scans by x-rays requires special treatment and preparation stage. It is strongly advised to take the scans while standing behind lead shields. The surface of the x-ray device tray is optically divided into squared coordinate system. For obtaining the best orientation, the core sample is placed on to a V – Channel. The central lines are drawn on the core sample just like in the rock mechanical stress tests while placing the strain gauges. The placement needs special treatment. If the correct orientation is not obtained, we can not make sure that we are scanning the same sections before and after drilling fluid invasion. The x-ray images of the invading fine particles can be visualized better if some iron, magnesium or some type of radio active powder in your invading fluid system. However, we did not use any artificial substances not to destroy the specific heterogeneity of the drilling fluid. On the contrary, we used Barite which is commonly used in drilling industry as a weight increment agent. Barite has the chemical formula BaSO_4 and barium is radioactive. Thus, we did not need any artificial additives for better x-ray scans. The x-ray apparatus is displayed in Figure 81.

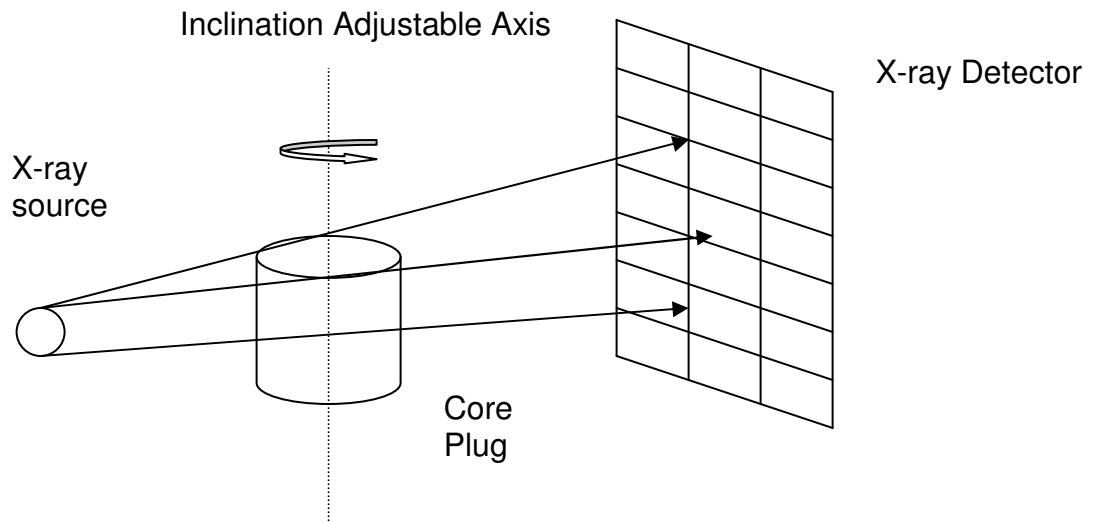


Figure 81 Digital Radiography System

Scans were performed both on clean core sample and after 15 minute. 45 minute and 60 minute contamination of the core sample. The block diagram of the digital x-ray system is depicted in Figure 82. The bulk scanned core samples before and after fines migration is shown in Figure-83. It is observed that the scanned image has more darker color after drilling fluid circulation which is the indication of the invasion of the fines particles.

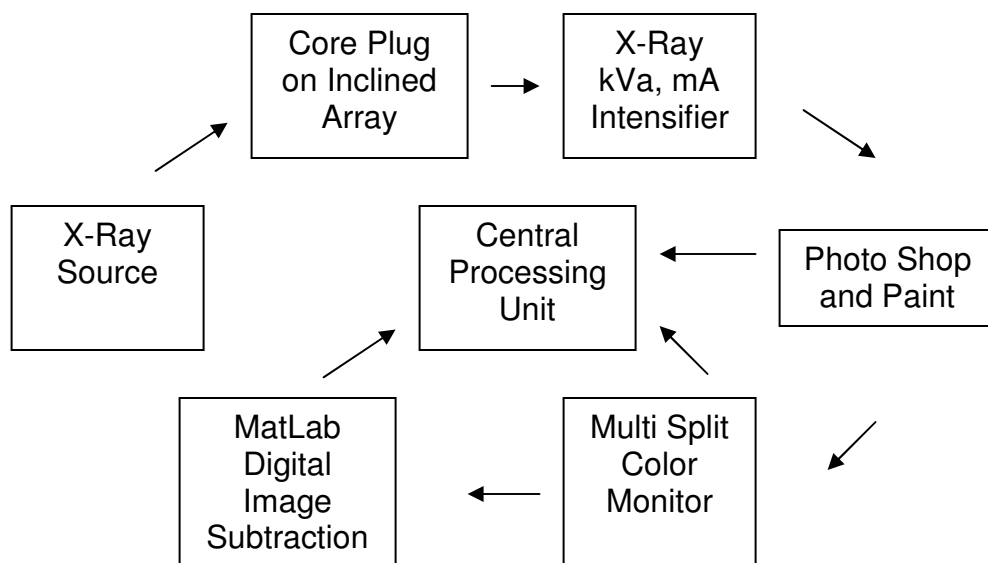


Figure 82 Block Diagram of Digital Radiography System

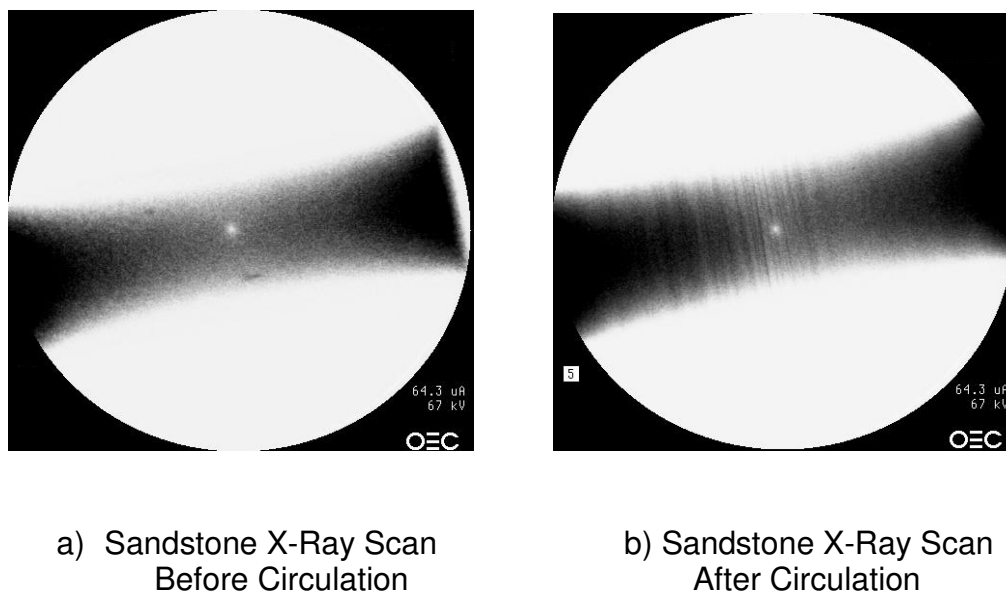


Figure 83 Sandstone Core Sample X-Ray Scans

The processing method of the scanned images is applied and discussed here. The aim of this analysis is comparing the sectional images of a core sample before and after fines particles invasion due to drilling fluid invasion. The images scanned by the X-Ray fluoroscope were stored in the hard disk of the fluoroscope. The images were originally stored in bitmap file format (bmp) which is a non-preferred format due its high hard space requirement. Those file should be converted to jpeg files for easier processing. The important thing while doing this is not to destroy the resolution quality of the images. Microsoft[®] Photo Shop is suggested for image file conversions. The core scans made after successive drilling fluid circulations are opened on Microsoft[®] Paint program as jpeg files. The images were divided into coordinate systems. 50 x 50 pixel size captures are extracted along the length of the core sample. This process was applied on the scans of the same core sample before and after the drilling fluid circulations. A computer code was written in MATLAB[®] software. Digital image subtraction technique is applied through the program. The image segments of the clean and contaminated scans are introduced to the code that was written. The program recognizes the captured image segments in (i,j) coordinated matrix columns. It is also possible to adjust color intensity affect by the program so that differences between the clean and contaminated core images can be visualized better. The program subtracts the digitized image sections and divides the subtraction to the uncontaminated initial image of the core sample. If this application is repeated on successive scans along the core sample, the porosity variation can be obtained. The advantage of this application is that the researcher need not make an assumption of homogeneous porosity distribution along the core sample, because all of the subtraction and divisions are made on individual sectional images. It was seen that

the normalized porosity increases along the core sample and becomes constant towards the last 2 cm of the core sample. It is also observed that as the circulation period increases the porosity decreases due to more invasion of fine particles.

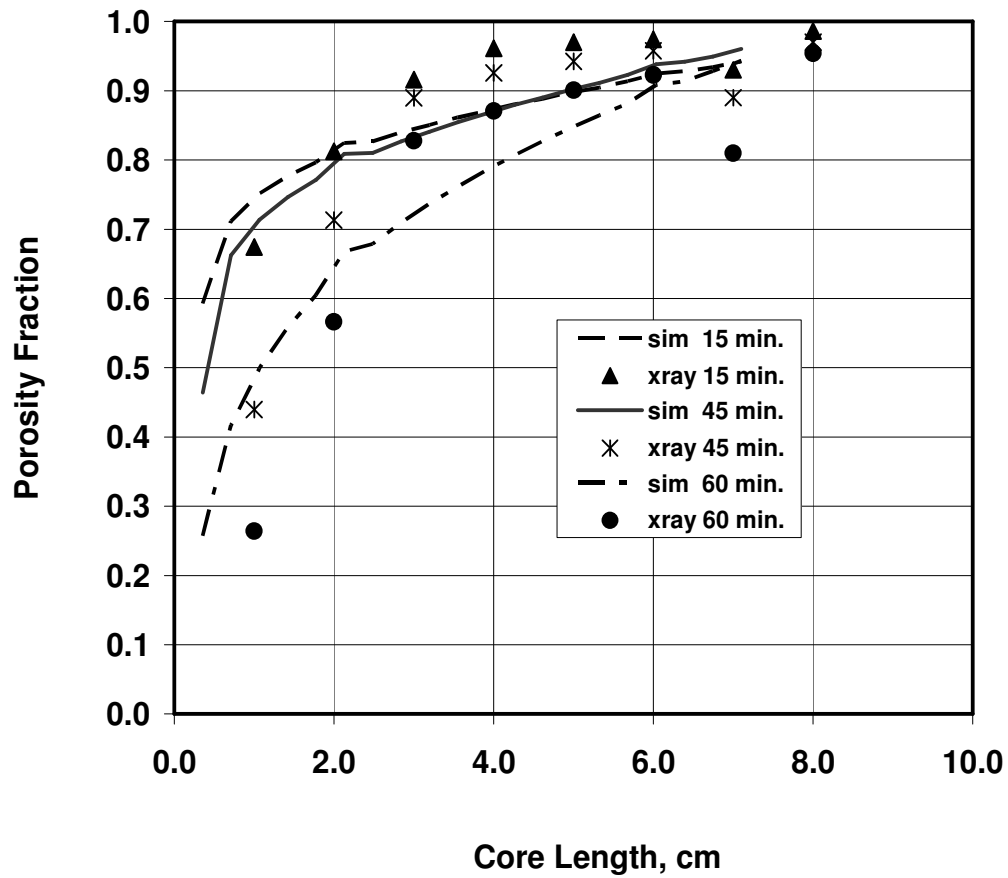


Figure 84 Porosity versus Core Length

After obtaining the porosity profile along the core sample, we tried to simulate our in-house data with our numerical fines migration simulator. The simulations were made for 15 minutes 45 minutes and 60 minutes periods under 100 psi drilling fluid circulation pressures. The porosity simulation results and the experimental x-ray results were plotted on the same graph (Figure 84). It is seen that there is a reasonable matching. This verifies that our fines migration model works well on porosity variation along the core sample.

The flooding of the core sample was measured by brine injection as mentioned in experimental procedure. The dynamic circulation pressure was set at 100 psi. The special feature of our core holder with different transducer ports along the rubber sleeve enabled us to observe the pressure profile after drilling fluid circulations at different time intervals. The pressure profile decreased along the core sample.

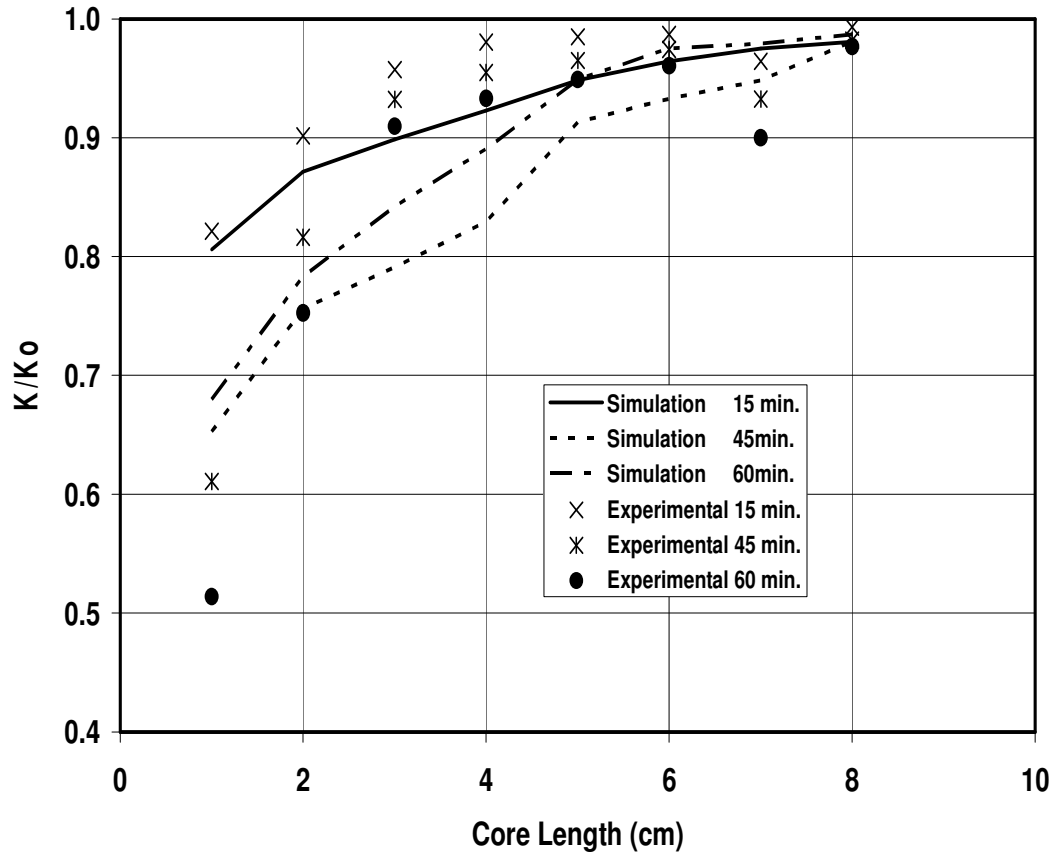


Figure 85 Permeability versus Core Length

The permeability was calculated according to this pressure profile. The absolute permeability of the core sample was 0.25 D. It is seen that the permeability approaches this value as it is moved along the core sample. The flooding data was also simulated by the fines migration simulator. The simulated and the experimental permeability were plotted in Figure 85. It is observed that the permeability reduction effect is higher

at the sections of the core sample which are close to the drilling fluid circulation point. The experimental and simulated permeability values display similar trends.

CHAPTER 8

CONCLUSION

This study confirms that the perforation and pore plugging by particulate slurry under various conditions can be correlated by two dimensionless groups, namely the pore or perforation diameter-to-particle diameter ratio and the particle Reynolds number. The permeability damage ratio was correlated with drilling fluid filtration pressure. A drilling fluid type sensitive empirical correlation was introduced for user-friendly applications. The particle concentration, permeability and porosity variation along sandstone core samples were analyzed. The clean-up effect due to presence of an aquifer was studied. The study was complemented through an X-Ray image analysis with clean and contaminated core plugs. An overall formation damage analysis was conducted in porous media with different mechanisms. The following conclusions were obtained :

1. Damage Ratio and filtration pressure relation was modelled and correlated.
2. Application of plugging and non-plugging pathways increases the accuracy of the porosity and permeability analyses in porous media. The plugging particle concentration increases in each grid with time. They display a fluctuation during the circulation for about twenty minutes due to the unplugging of formerly deposited bridging by jet nozzle effect.

3. The overall permeability of the core samples reduces as expected. The permeability increase along the core sample increases with the increasing pressure. The major increase in permeability takes place in the early thirty minutes of the circulation along the core sample. The increase becomes almost zero with the fluid-1 where as the increase keeps with fluid-2 and mud-3 even at later circulation periods. Damage ratio increases with increasing filtration pressure. The increase slows down and becomes almost constant between 100- 150 psia.

4. The maximum damage ratio is 75% with drilling fluid-1 and is higher than fluid-3 which is 65% under identical experimental conditions. The maximum damage ratio is 79% with the fluid with CMC. Water based Polymer XT mud is less damaging than the conventional bentonite drilling fluid. Fluid-2 is more damaging than fluid -1 and fluid-3.

5. The average plugging deposition rate is $8.49 \times 10^{-9} \text{ min}^{-1}$. The average non-plugging deposition rate is $1.72 \times 10^{-4} \text{ min}^{-1}$

6. The clean-up time during the backflow is about 60 minutes. Even after this period there is no perfect cleaning. The non-plugging porosity decreases linearly by 8.5% through out the whole circulation period. The recovery in non-plugging porosity is about 6% during the back flow with water from the aquifer. The change in plugging porosity is numerically very low and negligible. The non-plugging permeability decreases linearly in 106 minutes by 35%.

7. Digital image subtraction method prevents the researchers making homogeneous porous media assumptions.

8. Finally, it was understood that, the bridging and pore throat plugging due to fines clay particles accumulation cause the reduction in permeability and porosity.

REFERENCES

Al-Abduwani, F.A.H., Shirzadi, A., and Curie, P.K.: "Formation Damage vs. Solid Particles Deposition Profile During Laboratory-Simulated Produced-Water Reinjection", SPE paper 82235, *SPE Journal*, June, 2005., pp.138-151.

Al-Riyami, K., and Sharma, M.M.: "Filtration Properties of Oil-in-Water Emulsions Containing Solids," SPE paper 73769, Sept. 2004, pp.164-172.

Angulo, R., and Ortiz, N.: "X-Ray Tomography Application In Porous Media", SPE paper 23670, paper presented at *Second Latin American Petroleum Engineering Conference*, March 8-11, 1992, pp.187-193.

Baghdikian, S.Y., Sharma, M.M., and Handy, L.L.: "Flow of Clay Suspensions Through Porous Media", *SPE Reservoir Engineering*, May, 1989, pp. 213-220.

Bailey, L., Boek, E., Boassen, T., Selle, O., Argillier, and Longeron, D.: "Particulate Invasion from Drilling Fluids," SPE paper 54762, May 1999, pp. 1-10.

Bennion, D.B., Thomas, D.W., Bietz, R.F.: "Fluid Design to Minimize Invasive Damage in Horizontal Wells", *Journal of Canadian Petroleum Technology*, November, 1996, 45-52.

Bishop, S.R. "The experimental investigation of formation damage due to the induced flocculation of clays within a sandstone pore structure by a high salinity brine", SPE Paper 38156, presented at 1997 SPE European Formation Damage Conference, The Hague, The Netherlands, 2-3 June 1997.

Byrne, M.T. and Patey, I. "Formation damage laboratory testing – A discussion of key parameters, pitfalls and potential", SPE Paper 82250, presented at SPE European Formation Damage Conference, The Hague, The Netherlands, 13-14 May 2003.

Byrne, M.T., Spark, I.S.C., Patey, I.T.M. and Twynam, A.J. "A laboratory drilling mud overbalance formation damage study utilizing cryogenic SEM techniques", SPE Paper 58738, presented at 2000 SPE International Symposium on Formation Damage Control, Lafayette, Louisiana, 23-24 February 2000.

Chang, F.F. and Civan, F.: "Predictability of Formation Damage by Modelling Chemical and Mechanical Processes", paper SPE 23793, *SPEJ*, 1992, pp.293-312.

Chesser, B.G., Clark, D.E. and Wise, W.V. "Dynamic and static filtrate-loss techniques for monitoring filter-cake quality improves drilling-fluid performance", SPE Drilling & Completion, September, 1994, 189-192.

Civan, F. and Nguyen, V., "Modeling Particle Migration and Deposition in Porous Media by Parallel Pathways with Exchange," Chapter 11, Handbook of Porous Media, Second Edition, Vafai, K. (Ed.), CRC Press, Taylor and Francis Group, Boca Raton, FL, pp. 457-484, 2005.

Civan, F., ve Xinghui, L.: "Formation Damage and Filter Cake Buildup in Laboratory Core Tests: Modelling and Model Assisted Analysis," paper SPE 25215 presented at the SPE International Symposium on Oilfield Chemistry, 1993, 26-30.

Civan, F.: "A Multiphase Model For Evaluation of Filtration During Drilling and Fracturing of Wells" paper SPE 77599 presented at the 2002 SPE Annual Technical Conference and Exhibition, Texas, September, 2002.

Civan, F.: "A Multi-Purpose Formation Damage Model" paper SPE 31101, *SPEJ*, 1996. pp. 311-326

Civan, F. ve Engler, T.: "Drilling Mud Filtrate Invasion- Improved Model Solution," *Journal of Petroleum Science and Engineering*, 1994, 183-193.

Ding, Y., Longeron, D., and Audibert, A.: "Modeling of Near-Wellbore Damage and Natural Clean up of Horizontal Wells Drilled With Water - Based Drilling Fluids ," paper SPE 73733, *SPEJ* ,Sept. 2004, pp. 252-264.

Dunsmuir, J.H., Ferguson, S.R., D'Amico, K.L., and Stokes, J.P.: " X-Ray Microtomography: A New Tool For The Characterization of Porous Media", SPE paper 22860, paper presented at the 66th *Annual Technical Conference and Exhibition of SPE*, October, 1991, pp.423-430.

Einstein, M. And Civan, F.: "Characterization of Formation Damage By Particulate Processes" , *The Journal of Canadian Petroleum Technology* ,March 1992, v. 31, no.3, pp.27-33.

Engler, P., Santana, M.W., and Narayanan, K.R.: " Determination of Two-Dimensional Fluid Distribution and Porosity by Digital Radiography", SPE paper 25817, September, 1992, 19 pages.

Fordham, E.J., Ladva, H.K.J., Hall, C.: " Dynamic Filtration of Bentonite Muds Under Different Flow Conditions" paper SPE 18038 presented at the 63rd *Annual Technical Conference and Exhibition of SPE*, Oct.2-5, pp 215-226.

Francis, P.A., Eigner, M.R.P., Patey, I.T.M. and Spark, I.S.C. "Visualization of drilling-induced formation damage mechanisms using reservoir conditions core flood testing", SPE Paper 30088, presented at European Formation Damage Conference, The Hague, The Netherlands, 15-16 May 1995, 101-115.

Francis,P.A.:”Dominating Effects Controlling the Extent of Drilling Induced Formation Damage”,paper SPE 38182 presented at the SPE European Formation Damage Conference, Netherlands,2-3, June 1997, pp.365-373.

Fraser, L.J., Reid, D.P., Williamson, D. and Enriquez, F. “Mechanistic investigation of the formation damaging characteristics of mixed metal hydroxide drill-in fluids and comparison with polymer-base fluids”, SPE Paper 30501, presented at the SPE Annual Technical Conference and Exhibition, Dallas, Texas, 22-25 October 1995, 521-531.

Gruesbeck, C. and Collins, R.E.: “ Particle Transport Through Perforations,” *SPE AIME*, paper SPE 7006 (Dec. 1982), Vol.22, No.11, pp. 857-865.

Hayatdavoudi, A.and Ghalambor A.: “ A Study of Formation Damage of Selective Clay and Other Minerals By Bacterial Plugging”, SPE Drilling and Completion , September 1996, pp. 160-167.

Haynes, C.D. and Gray, K.E.: “Sand Particle Transport in Perforated Casing,” *J.Pet.Tech.* (Jan.1974) Vol.26, No.1, pp. 80-84.

Iskan, A.G., Civan, F., Bagci,A.S., Kok,M.V.: ”Alteration of Permeability by Drilling Fluid Invasion and Flow Reversal ” submitted to Journal of Petroleum Science and Engineering, May 19,2005. (under revision)

Jasti,J.K., Jeslon,J., and Feldkamp, L.: ”Microscopic Imaging of Porous Media With X-Ray Computer Tomography”, SPE paper 20495, *SPE Formation Evaluation*, September,1993, pp.189-197.

Jiang, G., Yan, J., Wu,X.: “Evaluation of Formation Damage Caused by Drilling and Completion Fluids in Horizontal Wells,” *The Journal of Canadian Petroleum Technology* May 1997, v.35, no. 5, 36-42.

Jiao, D. and Sharma M.M. "Dynamic filtration of inert-emulsion muds", SPE Paper 24759, presented at the 67 th SPE Annual Technical Conference and Exhibition, Washington, DC, October 4-7, 1992, 999-1012.

Kjosavik,A., Ringen,J.K., Skaeveland, S.M. "Relative Permeability Correlations for Mixed Wet Reservoirs" SPE Journal, March,2002, pp.49-58.

Kok M.V.,İscan A.G, Ülker B.:"Effects of Axial Stress on Reservoir Rocks" ,Energy Sources, 2002, Vol. 24, pp.915-920.

Krueger, R.F.:"Effect of Pressure Drawdown on Clean-Up of Clay- or Silt-Blocked Sandstone," SPE paper 1605, *JPT*, March, 1967, pp. 397-403.

Krueger, R.F. "Evaluation of drilling-fluid filter-loss additives under dynamic conditions", Journal of Petroleum Technology, January 1963, 90-98.

Kumar, T., Todd, A.C.: "A New Approach for Mathematical Modeling of Formation Damage Due to Invasion of Solid Suspensions" paper SPE 6905 presented at the 1988 Annual Technical Conference and Exhibition of SPE, Houston, October, 1988.

Longeron, D.G., Alfenore, J., Poux-Guillaume.: "Drilling Fluids Filtration and Permeability Impairment: Performance Evaluation of Various Mud Formulations," SPE paper 48988, Sept. 1998, pp. 237-251.

Marshall, D.S., Gray, R. and Byrne, M.T. "Development of a recommended practice for formation damage testing", SPE Paper 38154, presented at 1997 SPE European Formation Damage Conference, The Hague, The Netherlands, 2-3 June 1997, 103-113.

Marshall, D.S., Gray, R. and Byrne, M.T. "Return permeability: A detailed comparative study", SPE Paper 54763, presented at 1999 SPE European Formation Damage Conference, The Hague, The Netherlands, 31 May-1 June, 1999.

Marx, C. and Rahman, S.S. "Evaluation of formation damage caused by drilling fluids, specially in pressure-reduced formation", SPE Paper 12494, presented at the Formation Damage Symposium, Bakersfield, Ca, February 13-14, 1984, 209-214.

Mathematica^R Software by Wolfram Research Inc.

Nabzar, L. and Chauveteau, G.: "Permeability Damage by Deposition of Colloidal Particles", paper SPE 38160, SPEJ, 1997, pp. 161-191.

Ohen, H.A. and Civan, F.: "Simulation of Formation Damage in Petroleum Reservoirs", SPE Advanced Technology Series SPE paper 19420-PA, v.1, pp. 27-35.

Patino, O., Civan, F., Shah, S.: "Identification of Mechanisms and Parameters of Formation Damage Associated with Chemical Flooding", SPE paper 80271-MS presented at International Symposium on Oilfield Chemistry, Houston, Texas, 2003.

Rahman, S.S. ve Marx, C.: "Laboratory Evaluation of Formation Damage Caused by Drilling Fluids and Cement Slurry," The Journal of Canadian Petroleum and Technology, Aralık 1991, v.30, no. 6, 40-46.

Santos, H.: "No Damage Drilling: How to Achieve this Challenging Goal" paper SPE 77189 presented at the Asia Pacific Drilling Technology, Jakarta, Sept.9-11.2002.

Taud, H., Martinez-Angeles, R., Parrot, J.F., and Hernandez-Escobedo, L.: "Porosity Estimation by X-Ray Computed Tomography", *Journal of Petroleum Science and Engineering*, v.47, 2005, pp.209-217.

Torrest,R.S.and Savage,R.W.: "Particle Collection from Vertical Suspension Flows Through Small Side Ports- A Correlation," *Canadian Journal of Chemistry*, (Dec.1975), Vol. 53, No.6, pp. 699-701

Vitthal, S., Sharma, M.M., and Sepehrnoori, K.: "One- Dimensional Formation Damage Simulator for Damage Due to Fines Migration," SPE paper 17146 presented at the 1988 SPE Formation Damage Control Symposium, California, Feb.8-9, pp. 29-42.

Watson, R.B., Nelson, A.C.: "Representative Laboratory Testing Procedures for Selecting Drilling Fluids" paper SPE 82300 presented at the 2003 SPE European Formation Damage Conference , Hollanda, May. 13-14.

Willhite, G.P. : "Waterflooding", SPE Textbook Series, Vol.3, 1986.

Withjack, E.M., Devier, C., and Michael,G.: "The Role of X-Ray Computed Tomography in Core Analysis", SPE paper 83467, presented at the *SPE Western Regional/AAPG Pacific Section Joint Meeting, California, USA*, pp.1-12, 2003.

Yilmaz, E., Duran,O.: "TPAO South East Anatolia Otocstone and Alloctone Units Stratigraphhy Dictiniory, Lexicon", TPAO Directorate of Research Group Education Publications, No.31, 1988.

APPENDIX A

Procedure For Permeability Measurement

1. Fill a beaker of two liters with water. Weigh 40 g of KCl. Pour the KCl gently into the water. Stir until the salt completely dissolves with in water. The solution is desired to be 20000 ppm for the sake of simplicity. The aim of using brine solution is to prevent swelling within the core. Using higher concentration may cause undesired plugging during saturation. That is why 20000 ppm was determined as an optimum concentration value.
2. There is a plastic piston inside the transfer cell. Push it back to its starting point by using pressurized air supplied by the experiment tables. Fill the transfer cell with brine. Do not fill the cell completely. Just fill it up to the line at the cover inlet of the cell. Thus, brine overflow is prevented while closing the cover. Close the cover gently. Turn it with your hand until it stops rotating. Meanwhile always check the condition the o-rings inside the covers. If the o-rings are ruined. They should be replaced. Otherwise, leakage will occur.
3. Bring the pump scale to zero point. Be sure that adequate volume of mineral oil exists in the inventory of the pump. Connect the inlet hose of the transfer cell to the pump outlet.
4. Take a rubber sleeve suitable for your core holder. It should have ports for transducer connections. Place the rubber sleeve gently into the core holder.

5. Measure the dry weight of the core plug sample. Place the core plug sample inside core holder. Make sure that the core is placed on equal spaces from each end of the core holder. Select appropriate lengths of spacers to fill the gaps between the ends of the core plug and the core holder (Figure-1). The important thing which should be noted that is the consideration of the lengths of the covers of the core holder.
6. Connect the core holder inlet to the outlet of the transfer cell
7. The unused transducer ports on the core holder should be sealed with caps.
8. A hand pump is connected to the core holder from the point close to the outlet. Insert the rubber hose of the pump into a beaker full of water. This pump is used to set the confining pressure. The confining port close to the inlet should be remained while pumping the water with hand pump until a steady flow comes out of the port. Then this port is closed with a cap. The pressure is set at 800 psig. It should be noted that the confining pressure should be always at least 200 psi above the maximum differential pressure across the core plug. Otherwise, leakage will occur.
9. A transducer is connected to the inlet to measure the absolute inlet pressure. A transducer is placed between the inlet and the outlet of the core holder. It is wise to use a back pressure transducer which is ready to open at 138 psig.
10. The Ruska proportioning pump is turned on. It is adjusted to “feed-in” position. The rate of the pump is adjusted by a dual system. There are three letters A, B, and C. There are five speeds at each letter thus a fifteen combination speed variation is available.
11. The brine solution is run through the core sample until

breakthrough. Then the constant volume brine accumulation is observed at different pump flow rates. Then permeability is calculated by using Darcy's law.

12. At the end of the permeability measurement, stop the pump. Bring the needle to neutral position. Release the confining pressure. Take the core sample out of the core holder. Measure the wet weight of the core sample.

APPENDIX B

Procedure For Dynamic Circulation Experiments

1. The vertical circulation core holder is cleaned with toluene. Then a rubber sleeve is placed inside the core holder. The ports on the sleeve are carried on top of the vertical core holder by 1/8 in pipes. These pipes are each pumped with water and thus they are checked whether they are plugged or not. The ports are chosen for transducer connection. The most left side pipe corresponds to the lowest port on the core sleeve.
2. The core plug is inserted into the core holder. While doing this, it is important to move bottom assembly downwards very slowly. The sign on the bottom of the bottom assembly should face the flow meter side for flow to occur.
3. Hand pump is connected to the core holder. The confining pressure is set at 800 psia. The hand pump should always be fed by a water supply. Air should not be pumped for confining purposes due to its compressibility.
4. The transducers are mounted to the relevant ports. One transducer is mounted to the inlet to see the absolute pressure in the entrance.
5. Fill the mud tank with drilling fluid. Close the top cover carefully. Connect the gas tube to the top of the mud tank. Pressurize the mud tank at different pressure values. Circulate the pressurized mud with centrifugal pump. The centrifugal pump is a rate

controlled device. The flow rate can be adjusted by the electric control unit. The experimental set-up is drawn in Figure-3.

6. The pressurized gas is drawn through the mud storage tank and the pump is run. The flow control valve is opened to see a continuous flow is assured. The flow rate is seen on Halliburton Flow Meter. This device measures the flow in gallons per minute. The top scale displays the total volumetric flow while the bottom scale indicates the instantaneous flow. The flow control valve is closed.
7. A beaker is placed on to the top of the core holder which is open to the atmosphere.
8. It should be remembered that the core sample was saturated with brine during the flooding stage. As the drilling fluid flows through the surface of the core sample. The fine particles start invading into the porous media by displacing the brine from the end which is open to the atmosphere. The drainage is accumulated in a graduated cylinder. The filtration volume is recorded in 5 minute or 10 minute intervals.
9. The Halliburton flowmeter should be calibrated periodically after 3 or 4 experiments by following the guidelines given by Halliburton Flowmeter Manual.
10. The filter cake thickness is measured on the surface of the core sample. Ph of the filter fluid and the cake are measured.
11. Drilling fluids include bentonite, barite, CMC and some other chemicals. These materials have tendency to solidify when they are dried. It is really important to flush the entire system with fresh water. Before flushing, the core sample is taken out. The mud tank is filled water. The water is pressurized and circulated through the

system. Flow control valve is opened until clean water comes out of the system. If the system is not cleaned right after the experiment, the pipes would need to be replaced.

APPENDIX C

Procedure For Backflow Experiments

1. Place the contaminated core sample into a helium porosimeter. Measure the porosity by helium confinement. Saturation method would not be suitable to determine the porosity of a contaminated sample due to the mobility of the fines during flooding.
2. Insert the contaminated core sample into the core flooding unit.
3. The fluid injection side is the contaminated surface. The injection pressures will be much higher than the pressures that had been obtained during the initial saturation period.
4. Start injection at lower flow rates of Ruska Portioning Pump. Record the volume accumulated the breakthrough and the flow period.
5. Determine the return permeability.
6. This return flow experiments should be completed without mistake. Because after injecting sufficient amount of water, clean water may start coming through the other end. From this time on, return permeability measurement loses its validity.

APPENDIX D

D.1 Procedure For Pore Throat Plugging Experiments

1. Install the perforation pipes (0.21cm to 0.42 cm) to the bottom of the pressure resistant cell.
2. Close the mud tank drainage valve. Fill about 500 ml of fluid. Adjust the nitrogen tube at 50 psig. Open the bottom valve of the mud tank to allow flow into the pressure cell.
3. Place a graduated cylinder at the open end of the variable diameter pipes at the very bottom of the pressure resistant cell.
4. As soon as the pressure in nitrogen tube is applied on the fluid, open the bottom valve of the pipe. Measure the fluid volume collected for about 30 minutes.
5. Close the nitrogen tube at the end of the 30 minute period. Release the inlet pressure. Remove the pipe at the bottom of the cell.
6. Mud particles will accumulate along the circumference of the perforation pipes. Measure the accumulation of particles on the circumference of the perforation pipe by a compass.
7. Repeat steps 1 to 6 for three different fluid types and four different pipe sizes at four different driving pressures.

D.2 Determination of Particle Size

1. 500g of the sample is weighed.
2. Several mesh size screens such as 10, 20, 50, and 100 are used.
3. Screens are placed on a shaker. The largest mesh, size 10, is placed at the top. The 20, 50, and 100 meshes are placed consecutively below the 10 mesh screen.
4. The 500g sample is placed on the 10 mesh screen.
5. The screens placed on the shaker are shaken for 8 hours until the flow of particles from one top screen to the lower one stops.
6. The largest particles are accumulated over the 10 mesh screen and almost a powder type residue is obtained on the 100 mesh screen. The particles from each screen is collected and weighed.
7. The mass of particles remaining above each screen is weighed. The weight of particles above each screen is divided by the total mass of the particles used in the mesh analysis.
8. The largest percentage generally determines the particle size of the mud.

APPENDIX E

Procedure for X-Ray Experiments

1. In our analysis, an 8 inch sandstone core sample was used. The core sample was cleaned in a toluene extractor prior to the experiments. Then, it was heated at 100 °C. The core sample is placed onto the tray of the device.
2. Because most of the x-ray devices are manufactured for live tissues such as human bones, etc, the adjustment of the system is required to the rock samples. Thus, some trial and error applications at different intensity varying from 40-70 kVa have been made. The best resolutions were obtained at 65 and 67 kVa values and 53.3 and 64.3 mA currents. If the correct values for these parameters are not obtained, the images can not be visualized correctly. The x-ray scans were captured at three consecutive time intervals of 15 minutes, 45 minutes and 60 minutes. An x-ray fluoroscope device was used for the experiments.
3. Once the accurate orientation and the intensity parameters are set, the x-ray scans can be made by pressing the scan button. It should be noted that the parameters should be stored in the device under a specified folder, because there is a time gap between each scan. The x-ray apparatus is displayed in Figure-86.
4. Scans were performed both on clean core sample and after 15 minute. 45 minute and 60 minute contamination of the core sample. The bulk scanned core samples are observed, before and after fines migration.

APPENDIX F

GEOLOGICAL DATA OF FORMATION AND CORE SAMPLES

Table 21 Geological and physical properties of the core and the formation

Rock Type	Average Porosity (%)	Average Permeability (mD)	Average Core Length (cm)	Core Depth (ft)
Sandstone	18	20	7	5200
Orogenic Event	Eon	Era	Period	Formation
Early Alpine	Phanerozoic	Mesozoic	Cretaceous	Areban

SI Conversion: 1 in = 2.54 cm
1 ft = 12 in

Type Locality: The river at the north east of Areban Village at 16 km southeast of Mardin – Derik. Detailed geological description is given in Figure 86 adapted from TPAO Stratigraphy Lexicon, 1988.

Order: It is the lowest formation of Mardin Group

Stratotype : The thickness of the formation is measured at the neostatotype as 273 m. Bottom sections of the formation are wine coloured sandstones. Thin, middle, and large quartz particles, and greenish marl samples are seen. Basically sandstone forms the major characteristic of the formation.

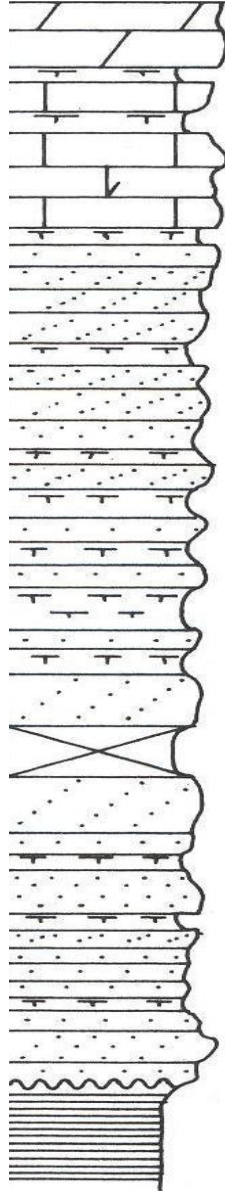
AGE	GROUP	FORMATION	THICKNESS (m)	LITHOLOGY	EXPLANATIONS
CENOMANIAN	M A R D I N	SABUNSUYU			<p>Dolomite : Semi-thick layered, dusty white coloured</p> <p>Limestone: Yellowish, light brown coloured Semi marled.</p> <p>Sandstone: Dark coloured, Very thick layered.</p> <p>Sandstone: White- yellow coloured, thin particles as gravel. Brittle.</p> <p>Sandstone-Marl Sedimentation</p> <p>Soil Layer</p> <p>Sandstone: Dirty yellow and dirty white, blue green marl mid-layered.</p> <p>Clay</p>
APTENE-ALPINE		A R E B A N	273		
UPPER-MID ORDOVICIAN		BEDINAN			
HABUR					

Figure 86 Areban Formation Neostatotype (TPAO Stratigraphy Lexicon)

APPENDIX G

PHOTOGRAPHS DEPICTING CONSTRUCTION STAGES OF THE DYNAMIC FILTRATION SET-UP



1. Mud Tank



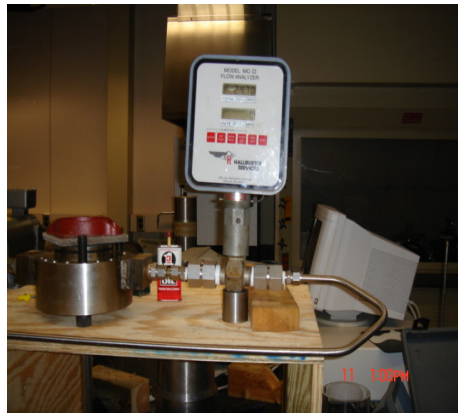
2. Pressure Gauge



3. Vertical Core Holder Lift



4. Mud Circulation Regulator



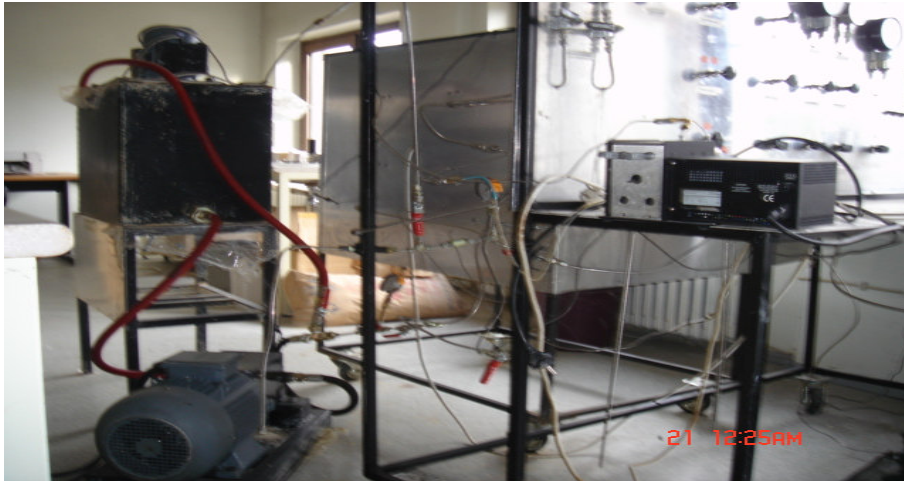
5.Flowmeter



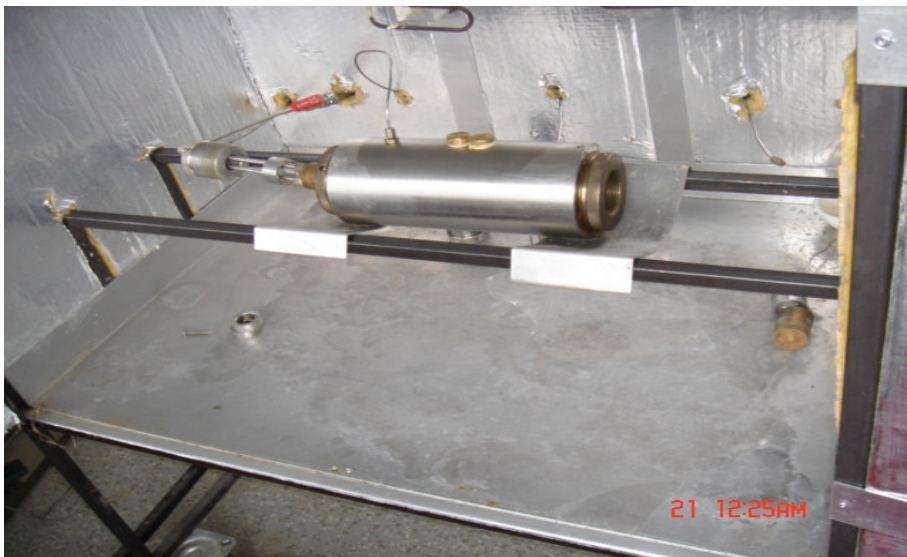
6. Parts Connected



7. Complete Dynamic Circulation Set-up Constructed at The University of Oklahoma in the USA



8.Dynamic Circulation Set-Up Constructed at Middle East Technical University.



9. Dynamic Circulation Core Holder Constructed Middle East Technical University.

APPENDIX H

RELATIVE PERMEABILITY PROFILE FOR A WATER WET CORE

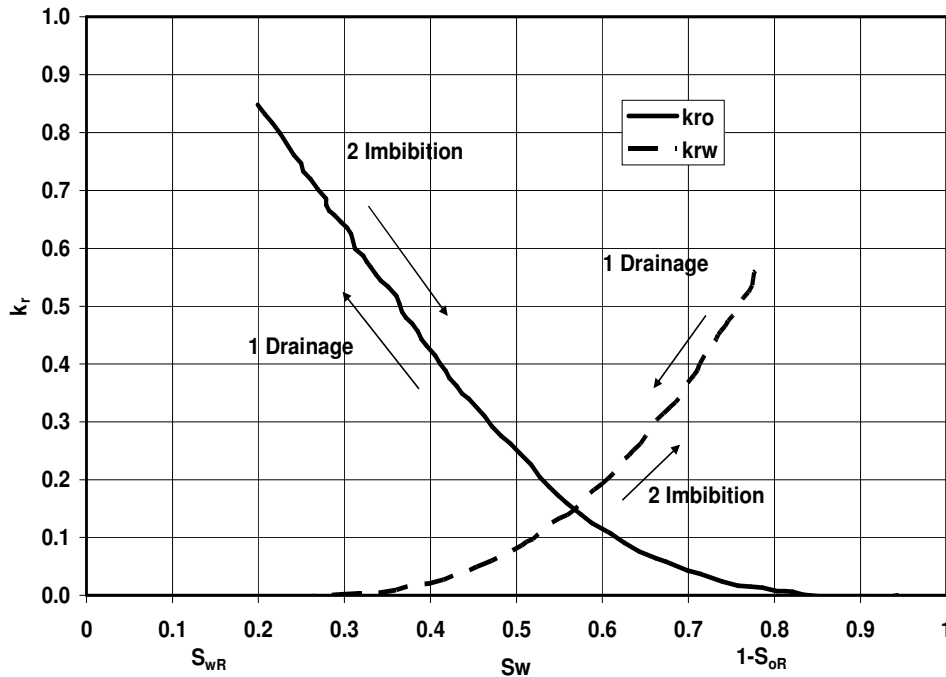


Figure 87 Relative permeability vs water Saturation for a water wet rock after Kjosavik et al. 2002

Modification of the wettability around the injection well may create a zone of enhanced water phase permeability in the near wellbore region, which may allow significantly higher water injection rates at an equivalent injection pressure level. This is a common treatment in low permeability sandstone injection wells. A representative relative permeability vs water saturation graph was drawn in Appendix H using the data from Kjosavik et al. (2002).

APPENDIX I

NUMERICAL STABILITY

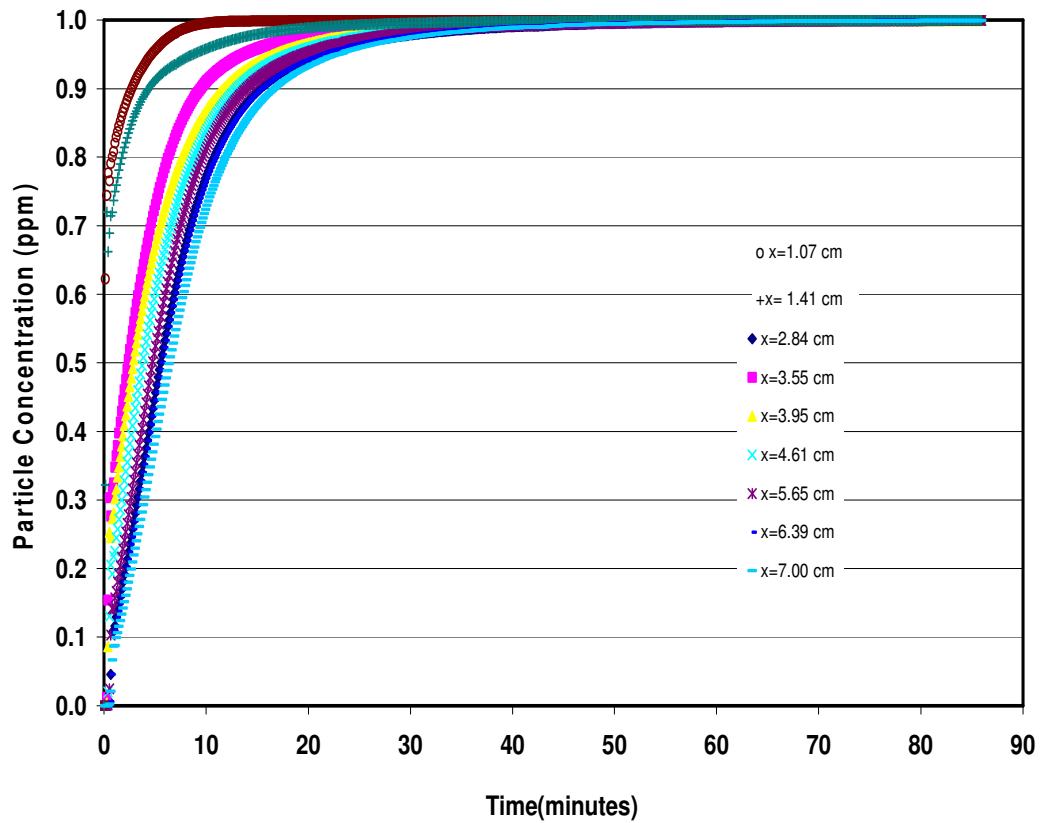


Figure 88 Particle concentration vs time at constant distances from circulation point with drilling fluid-3 at 100 psi filtration pressure

The significant change in particle concentration is seen in the early thirty minutes. However, when the particle concentration is plotted for the whole circulation period 90 minutes, the bending section is hard to distinguish,

so the plot was redrawn for the early 30 minutes to see the change with respect to time at constant distances from the circulation point.

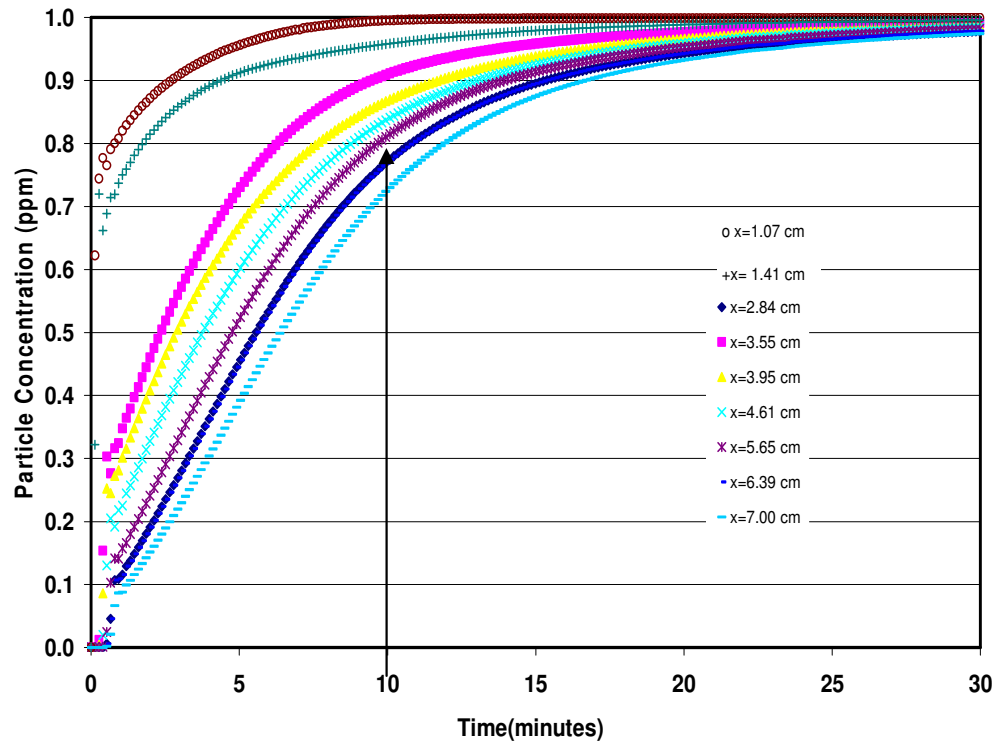


Figure-89 Particle concentration vs time at constant distances from circulation point with drilling fluid-3 at 100 psi filtration pressure

The particle concentration increases as the circulation period increases and becomes constant through the end of the early thirty minutes for the Polymer-XT drilling fluid at 100 psi filtration pressure. The upper most curve was obtained at a distance 1.07 cm from the fluid circulation point. When the curve is plotted for 1.41 cm, it is observed that particle concentration slightly decrease as in Figure 80. When the curve is plotted at 2.84 cm (blue coloured diamonds) where the oscillation took its minimum values in Figure 80, the particle concentration decreases

dramatically as well. As the curves are plotted for consecutive constant distances, the same oscillatory trend of the particle concentration is observed. Another evidence of the numerical stability is trying to see the particle concentration values in both graphs (Figure-80 and 91). For example, the particle concentration at distance 5.65 cm for 10 minute profile in Figure-80 is read as 0.814 ppm. If the particle concentration is read from Figure 91 after 10 minutes at the constant distance profile 5.65 cm, this concentration value is 0.814 ppm. Thus, both for each point and as general behavior trend, the numerical solution is thought to be stable. Hence, both sets of curves in Figures 80 and 91 are correspondingly consistent with each other. To visualize the numerical stability of the study the particle concentration vs core length of fluid type-3 at 100 psi (Figure 80) is re-plotted.

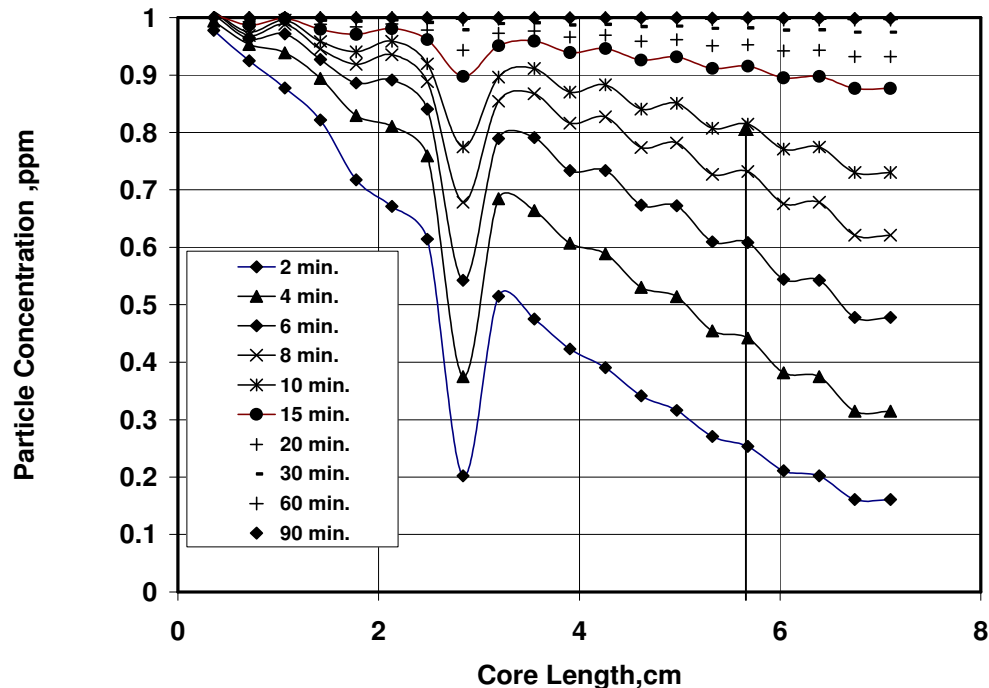


Figure 80 Particle Concentration variation along the core length with Fluid Type-3 at 100 psi. (Re-plotted for convenience)

APPENDIX J

VISCOSITY COEFFICIENTS OF EXPONENTIAL PORE THROAT MODEL

Table 22 Pore throat coefficients of the exponential model

Viscosity, cp	A	B	C
0.10	4.4	3×10^5	1.0
0.20	5.5	3×10^5	1.0
0.25	3.0	1×10^7	1.0
0.40	4.6	0.18	1.52
0.48	5.5	0.04	2.1

CURRICULUM VITAE

Palace and Date of Birth: Ankara / 06.08.1977

Contact Adresse : Middle East Technical University
Department of Petroleum and Natural Gas Engineering Inonu Bulvari
06531/Ankara

Phone : 312-2104884

Fax : 312-2104883

e-mail : iscan@metu.edu.tr /iscan@ou.edu

EDUCATION

Country	University	Faculty	Department	Degree	Graduation Year
Turkey	Middle East Technical University	Faculty of Engineering	Department of Petroleum and Natural Gas Engineering	Ph.D	2006
Turkey	Middle East Technical University	Faculty of Engineering	Department of Petroleum and Natural Gas Engineering	M.Sc.	2001
Turkey	Middle East Technical University	Faculty of Engineering	Department of Petroleum and Natural Gas Engineering	BSc.	2000

WORK EXPERIENCE

Organization	Country	City	Department	Occupation	Period
Middle East Technical University	Turkey	Ankara	Department of Petroleum and Natural Gas Engineering	Research Assistant	2000-2006
University of Oklahoma	USA	Oklahoma City	Mewborne School of Petroleum and Geological Engineering	Research Assistant	2005-2005

AWARDS

Name of Award	Organization	Year
DAAD Research Scholarship	DAAD/ Germany	2006
NATO A-2 Research Scholarship	TÜBİTAK	2005
Research Scholarship	Phillips-Conoco Company	2005
Assitanship and Research Scholarship	University of Oklahoma	2005
Rank#1 BSc Graduation Award	Middle East Technical University	2000
Rank#1 BSc Graduation Money Award	Turkish Chamber of Petroleum Engineers	2000

PUBLICATIONS

PARTICIPATED SCIENTIFIC CONGRESSES AND PUBLICATIONS IN REFEREED PROCEEDINGS

KOK, M.V., BAGCI. A.S., **ISCAN, A.G.**, 2003. Thin Section Analysis and Effects of Geothermal Gradient to Determine Porosity and Permeability in Sandstone and Limestone Reservoir Rocks, EGC 2003, European Geothermal Conference Proc. CD., Szeged, Hungary

ISCAN, A.G., KOK, M.V, and BAGCI A.S Determination of Porosity and Permeability of Sandstone and Limestone Reservoir Rocks by Thin Section Analysis and CMS Applications, 14th International Petroleum Congress and Exhibition of Turkey, 2003, (International Proceeding)

KOK, M.V, **ISCAN, A.G.**, and BAGCI A.S.: "Relative Permeability and Pore Size Distribution Trough Image Analysis of Thin Sections Under Capillary Pressure Approach" 5th International Symposium on Eastern Mediterranean Geology, Thessaloniki, Greece, 14-20 April 2004, (International Proceeding)

KOK, M.V, **ISCAN, A.G.**, and BAGCI A.S "Liquid and Gas Pemeability Determination of Limestone Rocks to Determine Gas Slippage Effect by Different Gas Samples" 5th International Symposium on Eastern Mediterranean Geology, Thessaloniki, Greece, 14-20 April 2004, (International Proceeding)

BAGCI A.S, KOK, M.V., and, **ISCAN, A.G.**: "Drilling Fluid Loss Circulation Additive: Evaluation of Walnut Shells", 15th International Petroleum and Natural Gas Congress and Exhibition, May 11-13, 2005, Ankara/Turkey.

BAGCI A.S, KOK,M.V., and, **ISCAN,A.G.**: "Investigation of Formation Damage Caused to Drilling Fluids in Porous Medium / Gözenekli Ortamda Sondaj Sıvılarının Neden Olduğu Formasyon Hasarının İncelenmesi", 15th International Petroleum and Natural Gas Congress and Exhibition, May 11-13,2005, Ankara/Turkey.

ISCAN, A.G., and KOK, M.V.: " Oil Shale Kinetics by Differential Methods", European Symposium on Thermal Analysis and Calorimetry, August 27-31,2006, Krakow, Poland.

ISCAN, A.G., KOK,M.V.,and BAGCI, A.S.: " Kinetic Analysis of Central Anatolia Oil Shales by Combustion Cell Experiments", European Symposium on Thermal Analysis and Calorimetry, August 27-31,2006, Krakow, Poland.

INTERNATIONAL REFEREED JOURNAL PAPERS

KÖK M.V. and **İŞCAN A.G.**: "Catalytic Effects of Metallic Additives on the Crude Oil Combustion" *Journal of Thermal Analysis and Calorimetry*,2001, Vol. 64 , pp. 1311-1318.(SCI)

KÖK M.V.,**İŞCAN A.G.**, Ülker B.: "Effects of Axial Stress on Reservoir Rocks" ,*Energy Sources*, 2002, Vol. 24, pp.915-920. (SCI)

OZBAYOGLU,E., GUNES, C., Esat C. APAK, E.,KOK,M.V and **ISCAN, A.G.**: "Empirical Correlations for Estimating Filtrate Volume of Water Based Drilling Fluids *Petroleum Science and Technology*, V.23 , March 2005, 423-436 (*Science Citation Index Expanded, SCI-Exp.*)

ISCAN,A.G.,and CIVAN,F.:“ Correlation of Criteria For Perforation and Pore Plugging By Particles ,” Journal of Porous Media, March 3, 2005. (ACCEPTED FOR PUBLICATION), (SCI)

ISCAN,A.G., CIVAN,F., KOK,M.V., BAGCI,A.S.:,”Alteration of Permeability by Drilling Fluid Invasion and Flow Reversal ” submitted to Journal of Petroleum Science and Engineering, May 19,2005. (REVIEW), (SCI)

ISCAN,A.G.,and ,CIVAN,F.: ” Investigation of Porosity and Permeability of Sandstones by X-Ray Analysis, Dynamic Circulation, and Numerical Simulation”, submitted to Journal of Petroleum Science and Engineering, Sept 23,2005.(SCI)

ISCAN A,G., KOK,M.V.,AND BAGCI, A.S.:”Estimation Permeability and Rock Mechanical Properties of Limestone Reservoir Rocks Under Stress Conditions by Strain Gauge" Journal of Petroleum Science and Engineering, v.53, 2006, pp. 13-24.

ISCAN A,G., KOK,M.V., AND BAGCI, A.S.: “Effects of Walnut Shells on the Properties of Water Based Drilling Fluids",Energy Sources, Dec 17,2005. . (ACCEPTED FOR PUBLICATION), (SCI)

ISCAN A,G., KOK,M.V., AND BAGCI, A.S.: “Permeability Reduction Due To Formation Damage By Drilling Fluids" , Energy Sources, Dec 16,2005. (ACCEPTED FOR PUBLICATION), (SCI)

ISCAN A,G., KOK,M.V., AND BAGCI, A.S.: “Effects of Polymers and CMC Concentration on Rheological and Fluid Loss Properties of Water Based Drilling Fluids" ,Energy Sources, Dec 15,2005. (ACCEPTED FOR PUBLICATION), (SCI)

HOBBIES

Tennis, squash, chess, fitness, running, cycling.